U. S. Department of Energy
1000 Independence Avenue, S.W.
Washington, D.C. 20585

Fiscal Year 2019: Fourth Quarter

Progress Reports:
Advanced Battery Materials Research (BMR) Program
&
Battery500 Consortium

Released December 2019
for the period of July – September 2019

Approved by

Tien Q. Duong, Program Manager
Advanced Battery Materials Research Program & Battery500 Consortium
Vehicle Technologies and Electrification Program
Energy Efficiency and Renewable Energy

TABLE OF CONTENTS

Advanced Battery Materials Research Program

Battery500 Consortium Program

TABLE OF FIGURES

TABLE OF TABLES

A MESSAGE FROM THE MANAGER: ADVANCED BATTERY MATERIALS RESEARCH PROGRAM AND BATTERY500 CONSORTIUM

This is a proud moment for the battery community. Three of our own, M. Stanley Whittingham (Binghamton University), John B. Goodenough (University of Texas at Austin), and Akira Yoshino (Asahi Kasei Corporation, Meijo University) received the most prestigious award that can be bestowed on a scientist or engineer, the Nobel Prize (https://www.nobelprize.org/prizes/chemistry/2019/summary/). Their combined contributions in developing lithium-ion batteries have revolutionized the world in which we live. Congratulations to the new Nobel laureates!

The BMR and Battery500 Team members continue to make advancements in next-generation battery materials. This document summarizes the efforts conducted from July 1, 2019, through September 30, 2019. A few notable achievements from the BMR investigators this quarter are summarized below:

- **Lawrence Berkeley National Laboratory.** Chen's group investigated the effect of surface treatment and found that NH_4F improves discharge capacity and capacity retention as well as average voltage retention in cation-disordered rocksalt cathodes. The results suggest that chemical treatment may be an effective mitigation approach to surface-initiated performance degradation in this class of cathode materials.
- **Pacific Northwest National Laboratory (PNNL).** Wang's group used cryo-TEM imaging, EDS elemental analysis, and EELS electronic structure analysis to investigate the role of additives and obtain design insights on electrolytes. Their results show that in the presence of vinylene carbonate, electrochemically deposited lithium metal is slightly oxidized and the SEI adopts a mosaic-like structure, leading to significantly enhanced Coulombic efficiency.
- **University of California at Berkeley.** McCloskey's group screened a range of potential additives to improve conductivity of a Li^+-neutralized, sulfonated polymer and found that 15-crown-5 ether is able to increase the polyelectrolyte conductivity by over an order of magnitude. They also showed that the optimized 15-crown-5 ether-containing solution enables operation of a battery composed of commercial electrodes. This study provided clear proof of concept for the idea of polyelectrolyte solutions as battery electrolytes.
- **Stanford University.** Cui's group investigated sulfur morphology change on nickel, carbon, and aluminum substrates during charging and discharging. The researchers found that the presence of a thin, dense oxidation layer (Al_2O_3) on aluminum surface weakens the adsorption of sulfur species on the interface, rendering the surface inert to sulfur conversion, and that the thin layer of insulating sulfur/Li_2S on the inactive interface passivates the electrode. This terminates further accumulation of sulfur species and leads to negligible capacity in charging/discharging processes. On the other hand, nickel substrates favor reversible polysulfide conversion, yielding high area capacity. This finding provides important understanding of the various substrates in Li-S batteries.
- **Pennsylvania State University.** Wang's group developed a functional porous sponge sulfur (FSS) electrode using cross-linked polymers with Li-ion-affinity to eliminate self-discharge and enable high performance of a Li-S battery. At an electrolyte/sulfur (E/S) ratio of 5 µl/mg, the FSS electrode with a sulfur mass loading of ~ 11.7 mg cm^{-2} exhibits a high energy density of 412 Wh/kg and good cycling stability for 100 cycles. When the E/S ratio is further reduced to 3.5 µl/mg, the FSS electrode shows an initial energy density of 432 Wh/kg, with highest energy density reaching 460 Wh/kg. These results show an important influence of the cross-linked polymers on sulfur loading, cycling response, and energy density in the Li-S system.

- **Texas A&M University.** Balbuena's group has been examining various kinds of deposits that occur on lithium metal, including mossy deposition and dendritic growth, and are developing models that can help explain why these transitions occur. These meso-scale models are showing that temperature and charging rates are critically important in determining the nature of the deposit. While higher temperature favors uniform deposition, decreasing temperature could lead to a transition from uniform lithium deposits, to mossy deposits, to lithium dendrite formation. These changes are connected to the temperature dependence of the electrolyte transport and the surface diffusion rates.

Highlights from the Battery500 consortium team include the following:

- **Keystone Project 1 (Materials and Interfaces).** Team members from PNNL developed a localized high-concentration electrolyte based on hydrofluoroorthoformate, which leads to a highly homogenous SEI structure and stable cycling of Li||NMC-811 cells. Brookhaven National Laboratory in collaboration with University of Texas at Austin identified an anomalously large d-spacing peak for NMC-622 cathode at highly charged state (> 4.5 V), providing new structural insight for high-voltage charging.
- **Keystone Project 2 (Electrode Architectures).** The University of California at San Diego team made significant advancement in understanding the form of inactive lithium with two different morphologies at nanoscale using Cryo-TEM. The Stanford team developed an effective artificial SEI for Li-metal batteries using polymer with self-healability and single-ion conductivity.
- **Keystone Project 3 (Cell Fabrication and Testing, and Diagnosis).** University of Washington team members achieved higher stability at a 4.6 V cutoff voltage for prototype cells containing LiF/$LiBO_2$-coated NMC-811 cathode. Cells displayed reduced polarization and high capacity. The Idaho National Laboratory team developed a novel electrochemical analytical diagnosis technique that can help identify failure modes.

We encourage you to follow our progress as we proceed. Our next report is expected to be available in March 2020.

Sincerely,

Tien Q. Duong

Tien Q. Duong

Manager, Advanced Battery Materials Research Program & Battery500 Consortium
Vehicle Technologies and Electrification Program
Energy Efficiency and Renewable Energy
U. S. Department of Energy

TASK 1 – Liquid/Polymer Solid-State Electrolytes

Summary and Highlights

The BMR Program goal is to develop long-life batteries superior to commercial Li-ion systems in terms of cost, vehicle range, and safety. The BMR Program addresses the fundamental problems of electrode chemical and mechanical instabilities that have slowed development of affordable, high-performance, automotive batteries. The aim is to identify electrode/electrolyte materials that yield enhanced battery performance and lead to greater acceptance of electric vehicles (EVs). Currently, the U. S. Department of Energy (DOE) Vehicle Technologies Office (VTO) supports ten projects in the BMR Program under this Electrolytes Task. These projects can be categorized into three general topics:

- **Liquid.** The projects for liquid electrolyte aim to develop electrolyte formulations, based on fluoro-chemistries, to achieve significantly improved operating voltage, increased durability, and increased energy density of Li-ion batteries at a reasonable cost. Nonaqueous polyelectrolyte solutions with high Li^+ transference numbers will be developed to achieve high rate capabilities at room temperature. In addition, electrolytes with new polymer binders bearing a pentafluorophenyl group on the backbone will be designed, synthesized, and tested.
- **Polymer.** The targets of polymer electrolyte (PE) projects include inorganic/polymer and polymer/gel hybrid electrolytes that have flexibility, mechanical strength, thermal stability, high ionic conductivity, stable interfaces against lithium metal, and polysulfide-trapping capability enabling energy density Li-S batteries, with comparable cycle life.
- **Self-Forming & Self-Healing.** The self-forming, self-healing electrolyte projects are focused on developing and implementing Li-metal-based metal fluorite and metal iodide batteries, capable of energy densities > 400-500 Wh/kg and 1000 Wh/L.

Highlights

The Daikin group (Sunstrom, Hendershot, and Falzone) investigated transition metal (TM) dissolution in cells using NMC-622 cathodes as a function of electrolyte and voltage. Data were collected using 200 mAh NMC-622 cells following 200 symmetric charge/discharge cycles at 0.7C. They found that the amount of dissolved cobalt shows little variance as a function of cathode/electrolyte/voltage. When cycled at 4.2 V, cells with the 1,3-(1,1,2,2-tetrafluoroethoxy)propane (HFE) electrolyte contain more dissolved metals than those with the HFE / fluoroethylene carbonate (FEC) electrolyte, consistent with observations in NMC-532 cells (Q3, FY 2019). For cells cycled at 4.5 V, the HFE/FEC electrolyte resulted in the highest concentration of nickel, in addition to the largest amount of total dissolved metals. For 4.6 V, the cells containing HFE/FEC electrolyte have higher concentrations of all TMs (nickel, manganese, and cobalt), in addition to a higher overall concentration. These findings are critical for identifying electrolyte formulations, based on fluoro chemistries, to significantly improve operating voltage, increase durability, and increase energy density of Li-ion batteries.

The University of California (UC) at Berkeley group (McCloskey) screened a range of potential additives to improve conductivity of a Li^+-neutralized, sulfonated polymer and found that 15-crown-5 ether is able to increase the polyelectrolyte conductivity by over an order of magnitude. They also showed that the optimized 15-crown-5 ether-containing solution enables operation of a battery composed of commercial electrodes. This study provided clear proof of concept for the idea of polyelectrolyte solutions as battery electrolytes.

At Argonne National Laboratory (ANL – Zhang, Curtiss, and Ngo), the group studied using hexafluorobenzene (HFB) as an additive for Li-S battery electrolyte by electrochemical testing and density functional theory (DFT) calculations. In addition, 0.1 M $LiNO_3$ was added to the 1,3-dioxolane (DOL)/dimethoxyethane (DME)/1.0 M LiTFSI electrolyte in the presence of various amount of HFB. They found that the 3% HFB cell showed much improved capacity retention, and in a DOL/TTE/1.0 M LiTFSI cell, and the same effect was observed with high concentration HFB. The DFT calculations confirm the mechanism by which HFB acts as an additive to activate the low order polysulfide and mitigate the loss of the active material. These results demonstrate the beneficial role of HFB additive in Li-S batteries.

At University of Maryland (UMD – Wachsman, Hu, and Mo), coin cells were assembled to demonstrate high capacity Li-S battery using a hybrid solid electrolyte. The group found that capacity has been continuously increasing for the first 100 cycles, almost doubles after 100 cycles, then starts to fade slowly. The battery maintains 95% capacity for 300 cycles. Overall, the battery shows high reversible cycling capacities with Coulombic efficiency (CE) above 98%, exhibiting good electrochemical stability over 300 cycles. A high volumetric energy density of 776 Wh/L was achieved, and the gravimetric energy density was 195 Wh/kg (affected by the thick lithium anode). The progress last quarter meets the milestone of achieving 10-mAh full cell.

The University of Washington group (UW – Jen and Yang) has attempted to cast cathode films with 4-5 mgS/cm^2 loading at only ~ 400-500 μm thickness, using ionomer gels. However, the casted cathode films were not mechanically robust and did not survive the die-cutting process without significant crumbling and/or delamination from the carbon-coated aluminum substrate, due to the reduced amount of poly(ethylene glycol) dimethacrylate (PEGDMA) crosslinker relative to solids content. They are adjusting the ratio of liquid components in slurry to produce a robust cathode with high loading and reduced thickness, as well as attempting to introduce the self-healing polymers into the slurry for additional robustness and electrochemical performance enhancement. In addition, they have replaced polyvinylidene difluoride (PVDF) with polyethylene glycol (PEO) to form a polymer blend of PENDI-350, Pyrene units, and PEO as a binder for S/C cathode, with sulfur loading of 2.91 mgS/cm^2. The capacity remains around 918 mAh/g after 30 cycles with relative capacity retention of 97%. This study helps to eliminate the possible interference of PVDF with the interactions between PENDI-350 chains or between PENDI-350 and S/C composite.

At West Virginia University (WVU – Wu and Zhang), the group has developed a plastic-crystal-added solid polymer electrolyte based on PEGDMA and pentaerythritol tetraacrylate (PETA) cross-linked polymer with addition of puccinonitrile (SN) plasticizer PETA/PEGDMA-SN80, showing ionic conductivity of 8.3×10^{-4} Scm^{-1} at room temperature, and an electrochemical stability window of 4.7 V versus Li/Li$^+$. With 20 wt% LLAZO nanofibers, the composite electrolyte demonstrated ionic conductivity of 8.5×10^{-4} Scm^{-1} at room temperature, and an electrochemical stability window of 5.0 V versus Li/Li+. Full cell performance with different composite electrolytes was investigated, to corroborate the effectiveness of the polyelectrolytes.

The Stanford University (Bao and Cui) group used a model liquid system to investigate the effect of Li-ion solvation on lithium deposition. They designed a nonpolar:polar electrolyte mixture, where nonpolar alkanes can limit the accessibility of the polar solvent to the electrode surface. They show that the addition of hexane and cyclohexane to ether solvents (1,3-dioxolane and 1,2-dimethoxyethane) reduces the Li-ion solvation, halves the nucleation and growth overpotentials for lithium deposition, increases the cell CE, improves the lithium deposition morphology, increases the electrolyte oxidative stability (> 0.2 V), and doubles the cycle life, even when compared to a widely used fluorinated ether.

The Lawrence Berkeley National Laboratory (LBNL – Balsara) group studied the parametric range over which stable lithium electrodeposition is obtained. They showed that stable electrodeposition was observed in an all-organic poly(ethylene oxide)-based rigid block copolymer electrolyte at a low current density: 0.04 mA cm^{-2}. In addition, they have measured higher limiting currents in hybrid-inorganic-organic block copolymer electrolytes than in all-organic block copolymer electrolytes. This suggests that one may achieve stable electrodeposition at higher current density in hybrid inorganic-organic electrolytes: if the limiting current ratio is proportional to the ratio of critical current densities at which stable electrodeposition is achieved.

At Stony Brook University (SBU – Takeuchi), *in situ* and *operando* measurements of lithium iodide (LiI) cells, with decreasing electrolyte particle size, were carried out. Their data show that the new electrolyte processing method significantly lowers the resistance of the cell in both the pristine and charged states. In addition, modified processing of the electrolyte material facilitates the formation of a distinct plateau, and increased processing allows the cell to deliver the largest capacity and ultimately improve CE to 100%. Furthermore, 100% CE while cycling at 40ºC for 60 cycles was achieved.

At Rutgers (Amatucci), the group investigated effect of hybrid electrolyte inclusion in the cell structure. This hybrid electrolyte comprised their standard solid-state electrolyte (SSE) and a small amount of ionic liquid, which was applied to the surface prior to cell formation. Four different hybrid electrolytes were evaluated with the new orientation/cell structure for the single-cell configuration, but with a 90-micron electrode spacing. Several chemistries were explored, revealing that electrolyte D yielded the best results, improving electrode utilization from 45% for the standard solid electrolyte to 85%. These advances were attributed to enhanced ionic mobility. The group is carrying out measurements for optimized cell structure with 60-micron electrode spacing.

Task 1.1 – Advanced Lithium-Ion Battery Technology: High-Voltage Electrolyte (Joe Sunstrom, Ron Hendershot, and Alec Falzone, Daikin)

Project Objective. The project objective is to identify electrolyte formulations, based on fluoro-chemistries, that will allow significantly improved operating voltage, increased durability, and increased energy density of Li-ion batteries at a reasonable cost. The project seeks to understand the conditions under which the electrolyte degrades, the effect on battery performance, and solutions that can overcome current limitations of the electrolyte. Gassing in Li-ion batteries is one of the most common failure mechanisms and poses the greatest safety risk in consumer devices. This project aims to investigate gas composition as a function of cathode material, electrolyte formulation, and operating voltage, and proposes optimal cell compositions at decomposition voltages.

Project Impact. Developing an understanding of the operating conditions in which gasses form in Li-ion batteries enables the project to propose optimized cell compositions that operate at higher voltages for a longer period. Different fluorinated electrolyte components and additives may suppress and/or eliminate gas generation at or above hypothesized decomposition voltages. To investigate these topics, it is imperative that the project utilize multiple approaches, including, but not limited to: cathode material, electrolyte composition, operating voltage, and cycle number.

Approach. The evolving composition of the electrolyte in the battery will be examined by various analytical instruments to study volatiles [gas chromatography – mass spectrometry (GC-MS)/thermal conductivity detector (TCD)], liquid [liquid chromatography MS (LC-MS)], and solid [time-of-flight secondary ion mass spectrometry (TOF-SIMS), thermogravimetric analysis MS (TGA-MS), X-ray photoelectron spectroscopy (XPS), and auger electron spectroscopy (AES)] electrolyte decomposition products during battery operation. In the first year, the team addressed the gas composition and kinetics for both hydrocarbon and fluorocarbon as a function of several charge/discharge conditions. In the second year, the project will transition into analysis of the SSE decomposition components of its tested batteries to obtain valuable information about solid electrolyte interphase (SEI) layer formation and how it manifests change in both the anode (graphite) and cathode (LCO and NMC). The third year is focused on measuring changes in the solid-state structure of the cathode following high-voltage operation. The project aims to quantify any dissolved metal ions originating from the cathode and deposited on the anode using inductively coupled plasma – mass spectrometry (ICP-MS). It will also study changes in the cathode structure using powder X-ray diffraction (XRD).

Out-Year Goals. Work will progress toward understanding how electrolyte formulation and cell operation affect stability of TMs in the cathode structure. The project aims to quantify metal ions, if any, dissolved into solution as a function of operating parameters (that is, voltage, time, etc.) and electrolyte formulation. In addition, measurements will be made using powder XRD to detect changes in the crystal structure of the cathode (LCO and NMC). Understanding effects on the solid-state structure in Li-ion batteries will provide valuable information on the required cathode chemistry for increased performance at high voltage.

Collaborations. The project has initiated a collaboration with Dr. J. Chan (University of Texas, or UT, at Dallas) for powder XRD measurements of cathode materials from tested cells.

Milestones

1. Film composition (elemental) versus time/voltage – Milestone 2.2. (Q1, FY 2019; Completed)
2. Battery thickness (non-gas) versus time/voltage – Milestone 2.3. (Q3, FY 2019; Completed)
3. Metal dissolution versus time/voltage – Milestone 3.1. (Q4, FY 2019; Completed)
4. Cathode Structure versus time/voltage – Milestone 3.2. (Q1, FY 2020; In progress)

Progress Report

Last quarter, the team reported thickness measurements in NMC-532 cells correlating to thickness changes to electrolyte formulation and target voltage. Graphite anodes in cells containing only HFE had the largest concentration of dissolved metals originating from the cathode (Q2, FY 2019). These increased concentrations of dissolved metals in the graphite anode correlate to observed thickness changes post-mortem. Dissolved metals content in NMC-622 cathodes as a function of electrolyte and voltage were investigated this quarter. Figure 1 depicts the dissolved metal concentration in 200 mAh NMC-622 cells following 200 symmetric charge/discharge cycles at .7C.

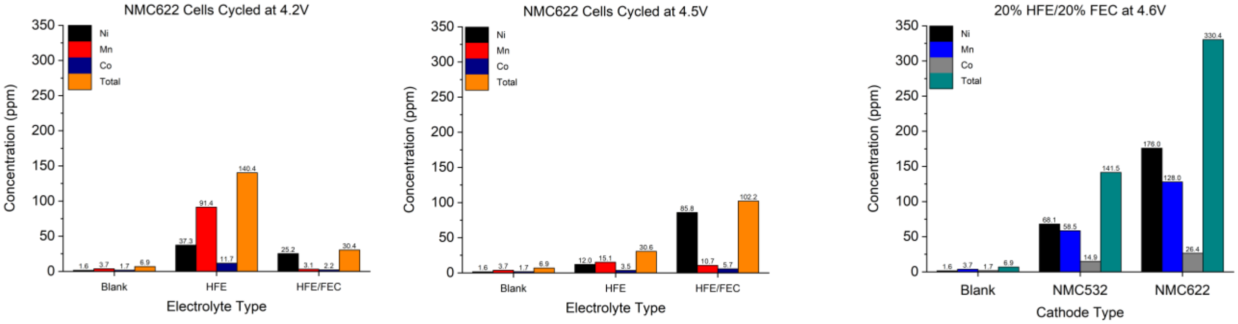

Figure 1. Metals concentration obtained via inductively coupled plasma mass spectrometry analysis following digestion of the graphite anode. Cells cycled at 4.2 V (left) and 4.5 V (middle). Cells cycled at 4.6 V with the HFE/FEC electrolyte in NMC-532 and NMC-622 (right). Total represents the total amount of transition metals (nickel, manganese, cobalt).

To date, the amount of dissolved cobalt shows little variance as a function of cathode/electrolyte/voltage (Figure 1). NMC-622 cycled at 4.2 V with the HFE electrolyte contains more dissolved metals than seen with the HFE/FEC electrolyte (Figure 1, left). This trend is consistent with observations in NMC-532 cells (Q3, FY 2019). NMC-622 cells cycled at 4.5 V with HFE and HFE/FEC electrolytes are also depicted in Figure 1 (middle). The HFE/FEC electrolyte resulted in the highest concentration of nickel, in addition to the largest amount of total dissolved metals. Also seen in Figure 1 are cells cycled at 4.6 V with the HFE/FEC electrolyte and grouped as a function of cell chemistry (right). The NMC-622 cell contained a higher concentration of each individual metal (nickel, manganese, and cobalt), in addition to a higher overall concentration (330.4 versus 141.5 ppm).

Collaborative efforts with Dr. J. Chan at UT-Dallas were initiated this quarter to study solid-state structural changes in high-nickel-containing cathodes as a function of electrolyte and voltage. Baseline diffraction patterns of 200 mAh cells have been established (Figure 2).

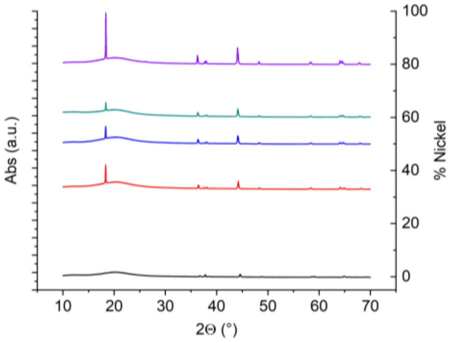

Figure 2. Baseline powder X-ray diffraction patterns for LCO and all NMC cathodes studied to date. Color code: LCO (black), NMC-111 (red), NMC-532 (blue), NMC-622 (teal), and NMC-811 (violet).

Patents/Publications/Presentations

The project has no patents, publications, or presentations to report this quarter.

Task 1.2 – Multi-Functional, Self-Healing Polyelectrolyte Gels for Long-Cycle-Life, High-Capacity Sulfur Cathodes in Lithium-Sulfur Batteries
(Alex Jen and Jihui Yang, University of Washington)

Project Objective. The project objective is to develop self-healing and polysulfide-trapping polyelectrolyte gels containing room-temperature ionic liquid (RTIL) for the Li-S battery system. The battery design will be able to achieve gravimetric and volumetric energy densities of ≥ 800 Wh/kg and ≥ 1000 Wh/L, respectively.

Project Impact. The Li-S battery system is hampered by poor capacity retention, primarily caused by dissolution of polysulfide reaction intermediates in typical organic electrolytes, as well as poor electrical contact between insulating sulfur and the conductive carbon matrix. This project aims to produce a high-capacity, long-cycle-life Li-S battery system by using rational molecular design strategies to address each capacity loss mechanism directly. A long-cycle-life Li-S battery system with the capability of doubling Li-ion energy density would enable production of lighter, longer range EVs at a cost affordable to the average U. S. household.

Approach. The team will develop Li-S coin cells that utilize self-healing, interpenetrated ionomer gel electrolytes in both the cathode and separator. The team will synthesize necessary starting materials and fabricate components of these gels while testing their relevant electrochemical and mechanical properties. All components will be combined into interpenetrating structures, which will be tested both alone and in cell configurations. Device performance data will be collected and used to further optimize designs of both material and cell, culminating in an optimized Li-S battery design capable of doubling the energy density of traditional Li-ion batteries. The team is focusing on (1) design and synthesis of a variety of precursors for gel electrolytes, (2) fabrication and testing of both reference materials and novel materials made from these precursors, and (3) iterative validation and improvement of design principles through both materials and device testing.

Out-Year Goals. Work will progress toward developing structure-property relationships for the self-healing, interpenetrated gel ionomer electrolyte and its individual components, as well as successful incorporation of such an electrolyte into a working Li-S cell. The team plans to demonstrate significant improvements in both capacity and retention when using the project's novel materials, as compared to state-of-the-art reference systems.

Collaborations. This project funds work at UW. Dr. A. Jen, principal investigator (PI), focuses on design, synthesis, and testing of novel materials, as well as device-based verification of design principles. Dr. J. Yang (co-PI) focuses on optimizing device fabrication and testing, as well as investigating failure mechanisms in devices using novel materials. Pacific Northwest National Laboratory (PNNL) facilities are used for detailed material characterization study.

Milestones

1. Provide detailed cell performance data for practical-loading cells containing currently best materials designs, along with conclusions regarding the origin of performance details. (Q2, FY 2019; Completed)
2. Provide detailed cell performance data for concept cells containing currently best materials designs, which should meet, or nearly meet, performance targets. (Q4, FY 2019; Completed)

Progress Report

Multi-functional Ionomer Gels / Gel Cathode. The team has previously demonstrated quasi-solid-state (QSS) Li-S cells, fabricated using the project's novel solvate ionogel (SIG) chemistry, with a number of performance advantages at ~ 1 mg$_S$/cm^2 cathode loading. Higher-loading cathodes (> 3 mg$_S$/cm^2) were fabricated by increasing the coating thickness; however, these cathodes performed poorly due to extreme thickness (approaching 1 mm). To reduce the thickness of such cathodes without compromising their sulfur content, the team has revised its SIG sulfur/carbon (S/C) slurry composition (see Table 1 below) to increase the overall solids content prior to curing-in-place. To compensate for this, they also increased the amount of anisole diluent relative to Li(G4)TFSI solvate ionic liquid to reduce slurry viscosity and promote better mixing. Much of the diluent was evaporated during the casting process and therefore acts merely as a processing solvent. The remaining anisole was meant to promote faster ion transport in the final cathode as a solvent diluent in the SIG electrolyte.

Table 1. Breakdown of solvate ionogel (SIG)/sulfur/carbon slurry (and subsequent cathode) composition by weight. The demonstration cell formula was used for quasi-solid-state cells with ~ 1 mgS/cm^2 cathode loading, while the updated formula is intended for high-loading (4-5 mgS/cm^2) cells.

SIG/S/C Slurry Composition (1g basis)		
	Demonstration Cell Formula	**Updated High-Loading Formula**
Solid Components	**0.1g**	**0.2g**
S_8	117.5mg	133mg
MJ430	117.5mg	57mg
MWCNT	65mg	70mg
Liquid Components	**0.9g**	**0.8g**
PEGDMA (750Da)	153.4mg	143.9mg
Radical Initiator	3.1mg	2.9mg
Li(G4)TFSI	650.9mg	458.8mg
Anisole	92.6mg	195.5mg
(Addt'l Anisole, evap.)	*9.3mg*	*219.6mg*

This updated slurry composition did indeed produce cathodes with 4-5 mg$_S$/cm^2 loading at only ~ 400-500 μm thickness. However, the team found that casted cathode films from the composition were not mechanically robust and did not survive the die-cutting process without significant crumbling and/or delamination from the carbon-coated aluminum substrate. This is almost certainly due to the reduced amount of PEGDMA crosslinker relative to solids content. They are adjusting the ratio of liquid components in the slurry to produce a robust cathode with high loading and reduced thickness, as well as attempting to introduce the project's self-healing polymers into the slurry for additional robustness and electrochemical performance enhancement.

Self-Healing Materials. Previously, the team demonstrated physical integration of S/C cathode with PENDI-350 as binder, blended with PVDF showing improved performance. Although they have fabricated the cathode with sulfur loading of 3.70 mgS/cm^2 by using PENDI-350/PVDF as a composite binder, the CE and discharge capacity of the composite decrease quickly after around 30 cycles. The team thought that PVDF may interfere with interactions between PENDI-350 chains or between PENDI-350 and S/C composite. On the other hand, although the team has demonstrated the effect of PENDI-350 on lithium polysulfides (LiPS) trapping, and possible redox reaction between naphthalenediimide (NDI) units and LiPS, they thought a more detailed investigation of reaction pathways of LiPS in the presence of such binder is necessary. This quarter, the team focused efforts on stabilizing capacity retention of the cathode, through understanding and modulating interactions between LiPS and NDI units of the binder to further improve performance.

First, the team replaced PVDF with PEO to form a polymer blend of PENDI-350 and PEO as a binder for S/C cathode. As shown in Figure 3a, they have fabricated test cells with S/C cathode using PENDI-350/PEO (weight ratio = 3:1) as binder with loading of 3.71 mgS/cm^2. It shows that the cell capacity remains at 718 mAh/g after 100 cycles at 1C. The capacity retention is as high as 91% (based on the 6th cycle with capacity of 789 mAh/g). The team attributes this improved capacity retention to the flexibility of long-chain PEO (Mw = 1000 K) as well as its good compatibility with PENDI-350, resulting in well-dispersed polymer blends. To improve mechanical properties further, the team has added tri-Pyrene crosslinker that can form reversibly crosslinked network structures with PENDI-350 via quadrupolar aromatic pi-pi stacking between NDI and Pyrene units. In the PENDI-350/triPy/PEO (PPP binder), the flexible PEO chains could entangle to form inter-penetrating network structures. As shown in Figure 3b, test cells with S/C cathode with a PPP (PENDI-350 : triPy : PEO = 3 : 2 : 1 by weight) binder were fabricated with sulfur loading of 2.91 mgS/cm^2. The capacity remains around 918 mAh/g after 30 cycles with relative capacity retention of 97% (based on 6th cycle with capacity of 954 mAh/g). The team has also fabricated Li-S cells with the S/C cathode with relatively high loading of 5.04 mgS/cm^2 without cracking (Figure 3c). Cell performance testing is ongoing, and results will be reported in the future.

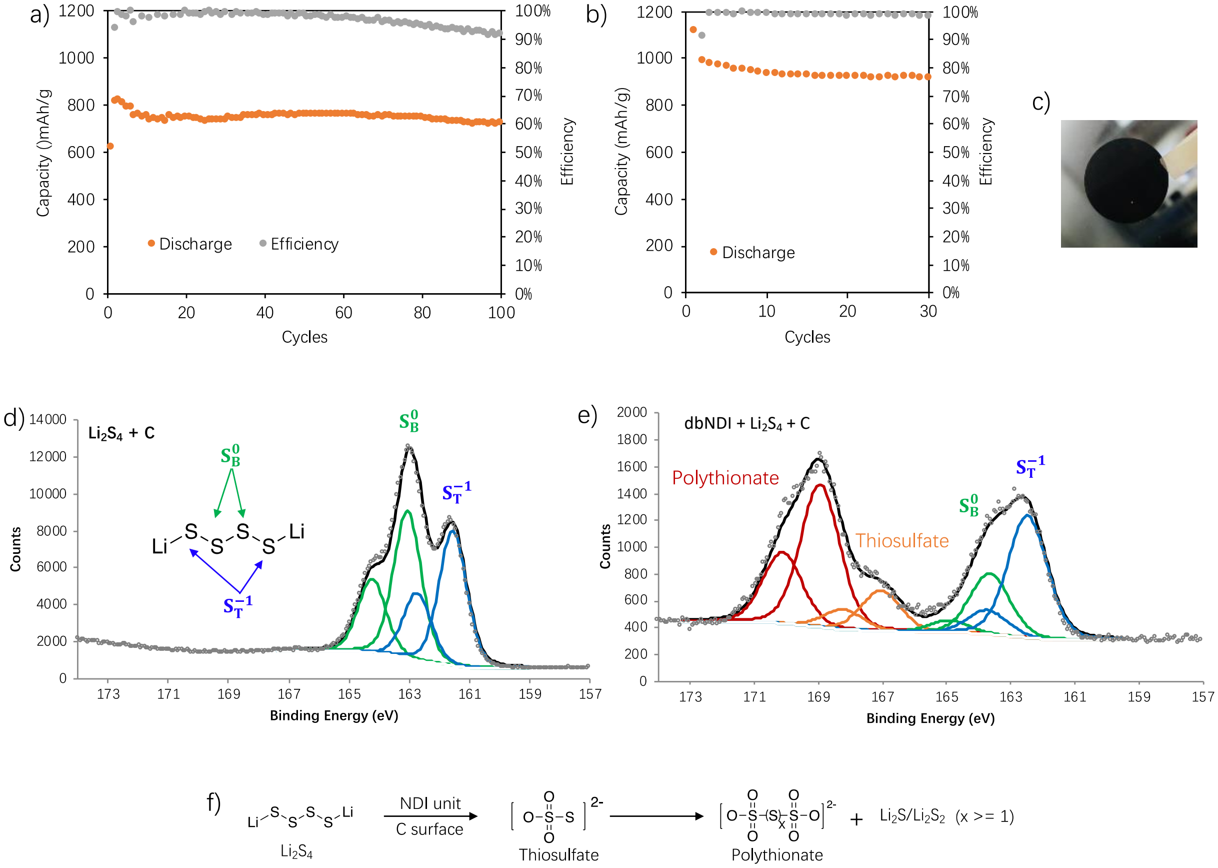

Figure 3. Cycling performances of cells with sulfur cathodes with (a) PENDI-350/PEO as binder (3.71 mgS/cm^2) and (b) PENDI-350/triPy/PEO (PPP) as binder (2.91 mgS/cm^2). All cells were cycled with C rate of C/10 in the first 5 cycles and then 1C in the remaining cycles. (c) Image of sulfur cathode using PPP as binder (5.04 mgS/cm^2); X-ray photoelectron spectrum of (d) Li_2S_4 reacted with mesoporous carbon and (e) Li_2S_4 and dibutyl naphthalenediimide (dbNDI) mixture reacted with mesoporous carbon. (f) Possible reaction route of lithium polysulfides in the presence of NDI.

Meanwhile, the team has performed a series of XPS studies to understand the interaction mechanism between LiPS and NDI units. Li_2S_4 was employed as a representative long-chain LiPS, which was synthesized by stoichiometric mixing of S_8 and Li_2S_2 in DME. Dibutyl-NDI (dbNDI) was used as a NDI model compound to react with Li_2S_4 before XPS test. Mesoporous carbon surface was functionalized with thiophenols using diazonium chemistry to enhance interactions with sulfur species, and the mesoporous carbon was added into Li_2S_4 solution to mimic the cell operation condition. As shown in Figure 3d, the XPS spectrum of Li_2S_4 interacted with the carbon shows two $S2p_{3/2}$ contributions at 161.6 and 130.0 eV, with relative peak ratio of around 1 : 1, referred to as terminal (S_T^{-1}) and bridging (S_B^0) sulfur atoms. A typical XPS spectrum of Li_2S_4 from the test suggests that the existence of mesoporous carbon doesn't change the state of Li_2S_4. However, after adding dbNDI, as shown in Figure 3e, XPS spectra show two more sulfur species. The new S2p3/2 peaks at 166.9 eV and 168.8 eV are in accord with the binding energy of thiosulfate and polythionate complex. As proposed in Figure 3f, Li_2S_4 can be oxidized into polythionates and short chain polysulfides in the presence of NDI units in the binder. The additional electrochemical contribution of NDI can help to explain the exceptional performance enhancement of sulfur cathodes made of NDI containing PPP binder.

Patents/Publications/Presentations

Publication

- Lin, F. "Design and Synthesis of Organic Functional Materials for Energy Conversion and Storage Applications." Ph.D. Thesis, UW, Seattle, Washington (September 2019).

Presentations

- PNNL, Richland, Washington (September 10, 2019): "From Solvate to Cell: A Molecular Engineering Approach to the Li-S Battery"; D. Hubble. Seminar.
- UW, Seattle, Washington (September 27, 2019): "Design and Synthesis of Organic Functional Materials for Energy Conversion and Storage Applications"; F. Lin, Dissertation Defense.

Task 1.3 – Construct and Test Lithium-Metal/Composite Electrolyte/Lithium-Metal Symmetric Cells (Nianqiang (Nick) Wu, West Virginia University; Xiangwu Zhang, North Carolina State University)

Project Objective. The project objective is to develop SSEs based on the highly conductive inorganic nanofibrous network in the polymer matrix for lithium batteries.

Project Impact. The team will conduct research and development (R&D) on solid-state inorganic nanofiber-polymer composite electrolytes that will not only provide higher ionic conductivity, improved mechanical strength, and better stability than the PEO polymer electrolyte, but also exhibit better mechanical integrity, easier incorporation, and better compatibility with the Li-metal anode than the planar ceramic membrane counterparts. The proposed inorganic nanofiber-polymer composite electrolytes will enable practical use of high-energy-density, high-power-density Li-metal batteries, and Li-S batteries.

Approach. Integration of the highly Li^+-conductive inorganic nanofiber network into the polymer matrix not only provides the continuous Li^+ transport channels, but also kinetically inhibits crystallization from the amorphous state of polymer electrolyte. The inorganic nanofibers will be fabricated with an electrospinning technique; the ionic conductivity of inorganic nanofibers will be improved by chemical substitution or doping. Highly ionic-conductive polymers will be developed by cross-linking and/or creation of a block-copolymer structure. The composition and microstructure of the composite electrolyte will be designed to suppress the lithium dendrite formation.

Out-Year Goals. Work will progress toward synthesis of the inorganic nanofibers and polymer matrix. The goal is to find the optimal synthetic route to achieve the desirable conductivity.

Collaborations. This project funds work at WVU and North Carolina State University (NCSU). Dr. N. Wu at WVU serves as PI, and Dr. X. Zhang at NCSU acts as co-PI. P. Zheng and X. Gao (Ph.D. student at WVU), H. Yang (Postdoctoral Fellow at WVU), B. Liu (Ph.D. student at WVU), C. Yan (Ph.D. student at NCSU), and M. Dirican (Postdoctoral Fellow at NCSU) contributed to the project.

Milestones

1. Construct Li-metal / composite electrolyte / Li-metal symmetric cells – Subtask 3.1. (Q4, FY 2019; Completed)
2. Construct Li-metal / composite electrolyte / cathode cells. Test specific energy, energy density, cycle life time, specific discharge pulse power, specific regeneration pulse power, and recharge rate of full cells – Subtask 3.2. (Q4, FY 2019; Completed)
3. Optimize composite electrolytes to achieve best performance of the battery full cells. Overall performance of the full cells will be analyzed – Subtask 3.3. (Q4, FY 2019; Completed)

Progress Report

In the last three years of the project, the team has designed and fabricated six different kinds of solid-state polymer-ceramic composite electrolytes for Li-ion batteries. Here, they summarize the optimized electrochemical performances of all the composite electrolytes, including ionic conductivity, electrochemical window, and full cell performance.

Optimize the Composite Electrolytes

$Li_{0.33}La_{0.557}TiO_3$ (LLTO) Ceramic Nanofiber-Enhanced PEO-Based Composite Polymer Electrolytes for All-Solid-State Lithium Batteries

A PEO-based composite solid polymer electrolyte filled with one-dimensional (1D) ceramic LLTO nanofibers was developed. The ionic conductivity of PEO/LiTFSI solid composite electrolytes reached the maximum value of 2.4×10^{-4} S cm^{-1} at room temperature when 15 wt% LLTO was incorporated; it exhibited a stable voltage window up to 5 V versus Li|Li^+.

Flexible Electrolyte-Cathode Bilayer Framework with Stabilized Interface for Room-Temperature All-Solid-State Li-S Batteries

A bilayer framework, which was integrated with a three-dimensional (3D) carbon nanofiber/sulfur (CNF/S) cathode with 1D LLTO nanofiber PEO solid composite electrolyte, served as both the cathode and the electrolyte for room-temperature all-solid-state Li-S batteries. The PEO/LLTO electrolyte exhibited a high ionic conductivity of 2.3×10^{-4} S cm^{-1} at room temperature, with 13 wt% LLTO nanofibers. The PEO/LLTO solid composite electrolyte exhibited a high decomposition potential of around 4.5 V versus Li|Li^+.

3D Fiber Network Composite Electrolyte Enabled with Li-Ion Conducting Nanofibers and Amorphous PEO-Based Cross-Linked Polymer for Ambient All-Solid-State Li-Metal Batteries

The team has developed a novel PEO-based cross-linked polymer (CLP) as the polymer matrix with naturally amorphous structure. The amount of plasticizer was set as 10, 20, 30, and 40 wt% based on the weight of prepolymer solution; the as-prepared plasticized polymers were denoted as CLP-P1, CLP-P2, CLP-P3, and CLP-P4, respectively. At room temperature, CLP-P4 displayed ionic conductivity of 2.40×10^{-4} S cm^{-1}. Both CLP and CLP-P4 exhibited stable voltage windows between 1 and 5 V versus Li|Li^+. When 30 wt% LLTO nanofibers were incorporated into the CLP matrix, the composite electrolyte CLP-P4-LLTO-3 showed ionic conductivity of 3.3×10^{-4} S cm^{-1}.

Garnet-Rich Composite Solid Electrolytes for Dendrite-Free, High-Rate, Solid-State Li-Metal Batteries

A new type of composite solid electrolyte (CSE) composed of silane-modified $Li_{6.28}La_3Al_{0.24}Zr_2O_{12}$ (s@LLAZO) nanofibers and poly(ethylene glycol) diacrylate (PEGDA) were developed. The ionic conductivity reached 4.9×10^{-4} S cm^{-1} at 60 wt% of s@LLAZO nanofiber content. The oxidized decomposition onset started at 5.3 V for s@LLAZO-60PEGDA composite electrolyte.

Chemical Interaction and Enhanced Interfacial Ion Transport in Ceramic Nanofiber-Polymer Composite Electrolyte for All-Solid-State Li-Metal Battery

A solid-state ceramic/polymer composite electrolyte was developed based on 3D electrospun aluminum-doped LLTO nanofiber network embedded in PVDF-hexafluoropropylene (PVDF-HFP) matrix. In addition, lithium phosphate has been coated on the LLTO nanofiber surface before the nanofibers were embedded into the polymer matrix. The flexible LLTO/Li_3PO_4/polymer composite electrolyte exhibited ionic conductivity of 5.1×10^{-4} S/cm at room temperature and an electrochemical stability window of 5.0 V versus Li|Li+.

Plastic Crystal-Added Solid Polymer – Garnet Composite Electrolytes

The team has developed a plastic crystal-added solid polymer electrolyte based on poly(ethylene glycol) dimethacrylate (PEGDMA) and pentaerythritol tetraacrylate (PETA) cross-linked polymer with addition of puccinonitrile (SN) plasticizer PETA/PEGDMA-SN80, showing ionic conductivity of 8.3×10^{-4} S cm^{-1} at room temperature (Figure 4a), and an electrochemical stability window of 4.7 V versus $Li|Li^{+}$. With 20 wt% LLAZO nanofibers, the PETA/PEGDMA-SN80-LLAZO composite electrolyte demonstrated ionic conductivity of 8.5×10^{-4} S cm^{-1} at room temperature, and an electrochemical stability window of 5.0 V versus $Li|Li^{+}$ (Figure 4b).

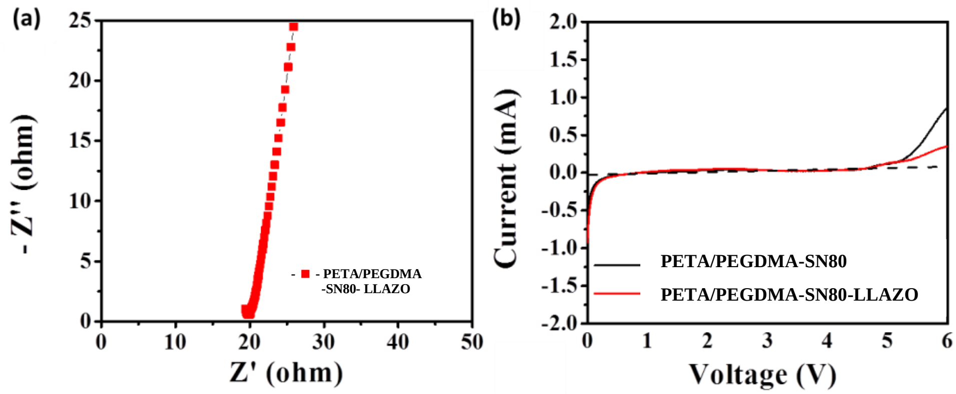

Figure 4. (a) Electrochemical impedance spectroscopy profiles. (b) Linear sweep voltammetry of PETA/PEGDMA-SN80-LLAZO composite electrolyte.

1.3.7 Summary of Ionic Conductivity and Electrochemical Window of Different Composite Electrolytes

Table 2 shows the ionic conductivity and electrochemical window of all the above-mentioned electrolytes developed in this project.

Table 2. Ionic conductivity and electrochemical window of different composite electrolytes.

Electrolytes Developed	Ionic Conductivity ($S\ cm^{-1}$, 25°C)	Electrochemical Window (vs. $Li|Li^{+}$)
PEO/LiTFSI/LLTO	2.4×10^{-4}	5 V
PEO/ LLTO	2.3×10^{-4}	4.5 V
CLP-P4	2.4×10^{-4}	5 V
CLP-P4-LLTO-3	3.3×10^{-4}	-
s@LLAZO-60PEGDMA CSE	4.9×10^{-4}	5.3 V
PVDF-HFP/LiTFSI/LLATO/Li_3PO_4	5.1×10^{-4}	5 V
PETA/PEGDMA-SN80	8.3×10^{-4}	4.7 V
PETA/PEGDMA-SN80-LLAZO	8.5×10^{-4}	5 V

Full Cell Performances with Different Composite Electrolytes

PEO/LiTFSI/LLTO. The electrochemical performance of all-solid-state Li-S batteries was measured using CNF/S-PEO/LLTO as both the cathode and the electrolyte, while a Li-metal foil was used as the anode. The Li-S cell showed a stable cycling performance with the capacity retention of 415 mAh g^{-1} after 50 cycles. The CE remained over 98% after 8 cycles and over 99% after 50 cycles. CNF/S-PEO/LLTO was able to charge/discharge at higher current density up to 0.2 C at room temperature with reversible capacities of 384, 358, and 262 mAh g^{-1} at current densities of 0.05 C, 0.1 C, and 0.2 C, respectively.

CLP-P4-LLTO-3. The assembled $LiFePO_4$ | CLP-P4-LLTO-3 | Li cells were galvanostatically charged and discharged at 25°C between 2.5 and 4.2 V at a current density of 17 mA g^{-1}, that is, 0.1 C rate. The $LiFePO_4$ | CLP-P4-LLTO-3 | Li cell demonstrated high capacity retention of ~ 98% after 100 cycles, indicating that the CLP-P4-LLTO-3 composite solid electrolyte can sustain stable cycling in Li-ion batteries at room temperature. Overall, the CE was 97.8% after 100 cycles. Discharge capacities of 154, 147, 138, 115, and 90 mAh g^{-1} were obtained at varied current densities of 0.05, 0.1, 0.2, 0.5, and 1 C, respectively. After applying cycles at higher current densities, the discharge capacity returned back to as high as 153 mAh g^{-1} when the current density returns back to 0.05 C.

s@LLAZO(6h)-60PEGDA. The $LiFePO_4$|s@LLAZO(6h)-60PEGDA|Li cell retained a capacity of over 115 mAh g^{-1} up to 250 cycles, resulting in 89% of capacity retention at a current density of 1 C. The CE remained at 99%, which indicated good reversibility of redox reactions in the battery. Discharge capacities of 158, 147, 135, 113, and 78 mAh g^{-1} were obtained at varied rates of 0.2, 0.5, 1, 2, and 5 C, respectively. Even at a high current density of 10 C, the cell can still deliver a capacity of 44 mAh g^{-1}. After applying cycles at higher current density, the discharge capacity increased again to as high as 158 mAh g^{-1} when the current density reduced back to 0.2 C.

PVDF-HFP/LiTFSI/LLATO/Li_3PO_4. The $LiFePO_4$ | PVDF-HFP / LiTFSI / LLATO / Li_3PO_4 | Li cell delivered the specific discharge capacity of 130.7 mA h g^{-1} at a current rate of 0.5 C and retained 87.8% (114.7 mA h g^{-1}) of the initial capacity after 160 cycles. The CE remained over 99.4% after 160 cycles. The discharging capacity was measured to be 158, 147, 133, 98, and 76 mAh g^{-1} at rate of 0.1C, 0.2C, 0.5C, 1C, and 2C, respectively. When the current rate was switched back to 0.1 C, the cell exhibited a reversible capacity of 149 mA h g^{-1}.

Patents/Publications/Presentations

Publication

- Yan, C., P. Zhu, H. Jia, J. Zhu, R. K. Selvan, Y. Li, X. Dong, Z. Du, I. Angunawela, N. Q. Wu, M. Dirican, and X. Zhang. “High-Performance 3-D Fiber Network Composite Electrolyte Enabled with Li-Ion Conducting Nanofibers and Amorphous PEO-Based Cross-Linked Polymer for Ambient All-Solid-State Lithium-Metal Batteries.” *Advanced Fiber Materials* 1 (2019): 46–60.

Presentation

- 235th Electrochemical Society (ECS) Meeting, Dallas, Texas (May 27–30, 2019): “Polymer-Ceramic Composite Electrolytes for All-Solid-State Lithium-Ion Batteries.”

Task 1.4 – High Conductivity and Flexible Hybrid Solid-State Electrolyte (Eric Wachsman, Liangbing Hu, and Yifei Mo, University of Maryland)

Project Objective. The project objective is to develop flexible hybrid electrolyte with garnet nanofibers to achieve the following: (1) flexible, with greater mechanical strength (~ 10 MPa) and thermal stability than polymer electrolytes; (2) high room-temperature ionic conductivity, ~ 0.5 mS/cm; (3) stable interface with lithium metal and effective blocking of lithium dendrites at current densities up to 3 mA/cm^2; and (4) battery performance with Li-S chemistry with an energy density of ≥ 450 Wh/kg (and ≥ 1000 Wh/L) and maintaining ≥ 80% of capacity up to 500 cycles.

Project Impact. Instability and/or high resistance at the interface of lithium metal with various solid electrolytes limit(s) the use of the metallic anode for batteries with high energy density, such as Li-air and Li-S batteries. The critical impact of this endeavor will be focused on developing a new type of SSE that is highly conductive, highly flexible, and electrochemically stable. The new SSE will enable Li-metal anodes with excellent interfacial impedance and blocking of lithium dendrite formation.

Approach. The project will synthesize garnet nanofibers, fill the porous region with polymer electrolyte, and characterize the flexible hybrid membrane properties. The flexible hybrid SSE microstructure will be determined using focused ion beam / scanning electron microscopy (FIB/SEM) and integrated with electrochemical methods to investigate the properties and stability with Li-metal anode.

Out-Year Goals. The project will develop a fundamental understanding of the mechanism of Li-ionic diffusion in garnet nanofibers and their mechanical properties, as well as these properties for hybrid garnet-fiber / polymer hybrids. Work will progress toward study of the electrode assembly during electrochemical cycling of the anode.

Collaborations. This project funds work at UMD, College Park. Dr. E. D. Wachsman (PI) will focus on optimizing the garnet network to achieve high ionic conductivity and flexibility using FIB/SEM and electrochemical impedance spectroscopy (EIS) characterization. Dr. L. Hu (co-PI) focuses on synthesis of the hybrid electrolyte and on test for Li-metal anode with the hybrid electrolyte. Dr. Y. Mo (co-PI) will lead efforts on computational modeling of the garnet nanofiber hybrid electrolytes for fundamental mechanistic understanding.

Milestones

1. Modeling of lithium dendrite protection: Understand lithium dendrite growth and protection effect of polymer and interphase layers on garnet nanofiber. (Q1, FY 2019; Completed December 2018)

2. Fabricate porous mixed electron / ion conductor: Fabricate and evaluate porous framework of mixed electron and ion conductor (to fill sulfur cathode). (Q2, FY 2019; Completed)

3. Li-S full cell with hybrid SSE: Fabricate and evaluate Li-SSE-S full cell with a size of 1 cm by 1 cm. (Q3, FY 2019; Completed)

4. Full cell performance: Achieve full cell of 10 mAh and energy density of 450 Wh/kg. (Q4, FY 2019; 50% Completed)

Progress Report

Coin cells were assembled to demonstrate high-capacity Li-S battery. The hybrid solid electrolyte was prepared by infiltrating polymer electrolyte into garnet framework made from cellulose fiber template. Li_2S_8 catholyte was prepared by dissolving lithium metal, sublimed sulfur powder (0.5 mol/L), and LTFSI (1 mol/L) in DOL/DME solvent (50/50 vol) and stirred at 70℃ for 12 h. To prepare the cathode, catholyte was infiltrated in a conductive carbon substrate. For full-cell assembly, a thick Li-metal foil was used as the anode. Electrochemical testing was conducted and analyzed with a battery cycler (Arbin Instruments) in the voltage window of 2.8–1.8 V at current density of 0.1 mA/cm^2. Figure 5 shows the continued (from last quarter) electrochemical performance of a Li-S cell for 300 cycles. The team found that capacity has been continuously increasing for the first 100 cycles, which is distinct from the tendency of battery to lose capacity over time. The capacity almost doubled after 100 cycles, but then started to fade slowly. The battery maintained 95% capacity for 300 cycles. Due to irreversible side reactions, CE over 100% was attained for the initial 40 cycles. Thereafter, the battery shows high reversible cycling capacities with CE above 98%, exhibiting good electrochemical stability over 300 cycles.

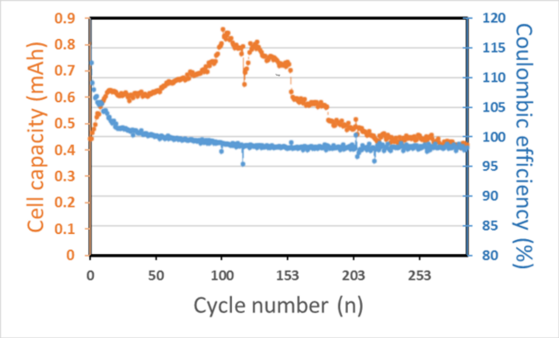

Figure 5. Cycling stability of a low capacity Li-S cell using hybrid electrolyte at 0.1 mA/cm^2. Temperature: 22°C.

The discharge plot of a new higher capacity Li-S cell shows two plateaus at 2.3 V and 2.1 V and a total capacity of 12.5 mAh, which meets the milestone of achieving 10-mAh full cell. Energy densities of the Li-S battery were calculated based on weight and volume of the cell components (spacers, spring, and coin cell case are not considered for energy density calculation). A high volumetric energy density of 776 Wh/L was achieved; note that Li_2S_8 did not add to the volume of cell since it was inside the porous carbon cathode support. Gravimetric energy density was 195 Wh/kg; however, this was significantly impacted by the thick lithium foil anode. If the lithium anode was capacity matched to the cathode, it would have a mass of only 0.004 g, resulting in an energy density of 251 Wh/kg.

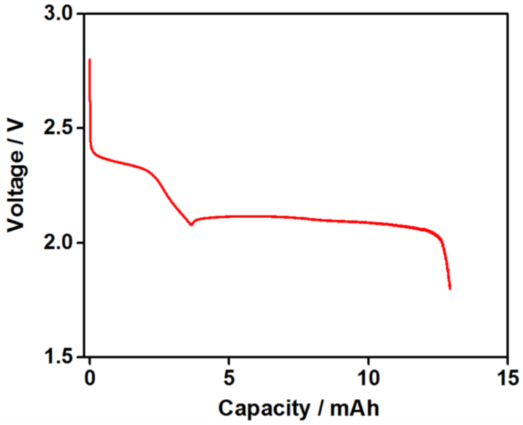

Figure 6. Discharge profile of a high-capacity Li-S cell using hybrid electrolyte at 0.1 mA/cm^2. Temperature: 22°C.

Table 3. Mass and volume energy densities of 12.5 mAh cell.

	Lithium Foil	Hybrid Electrolyte	Carbon Substrate	Li_2S_8 Catholyte	Energy Density
Weight/g	0.0118	0.0093	0.027	0.1105	195 Wh/kg
Volume/cm^3	0.0222	0.004	0.0076	0	776 Wh/L

Notes:

(1) Lithium metal anode: area, 1.27 cm^2; thickness, 175 µm; density, 0.534 g/cm^3.

(2) Hybrid electrolyte: area, 1.98 cm^2; thickness, 20 µm; density of garnet, 5.08 g/cm^3; density of polymer matrix, 1.2 g/cm^3; porosity of garnet framework, 70 V%.

(3) Conductive carbon substrate: area, 1.27 cm^2; thickness, 60 µm; density, 2.1 mg/cm^2.

(4) Catholyte solution: volume: 80 µl; 1 M LiTFSI; 0.5 M Li_2S_8; DOL/DME, 50/50 vol.

Patents/Publications/Presentations

The project has no patents, publications, or presentations to report this quarter.

Task 1.5 – Self-Forming Thin Interphases and Electrodes Enabling 3D Structured High-Energy-Density Batteries
(Glenn Amatucci, Rutgers University)

Project Objective. The project objective is to develop and implement a novel *in situ* formed Li-metal-based metal fluoride battery that will enable packaged 10-mAh batteries of energy densities > 1000 Wh/L and > 400 Wh/kg at 12 V.

Impact. Successful realization of 3D batteries formed *in situ* with a practical approach to large-scale fabrication would address some of the DOE EV performance goals, including: (1) areal capacity increase, (2) improved rates, and (3) designs to enable high-voltage unit cells.

Approach. The project is divided into two main tasks that focus on advance of the self-forming chemistry concurrent to cell design and fabrication. The self-forming chemistry task is comprised of three subtasks encompassing the negative and positive reactive current collectors, and the bi-ion glass conductor. The cell design and fabrication are targeting development and integration of the bipolar configuration to achieve the 12-V single-cell goal.

Out-Year Goals. Work will continue toward improving reactive current collectors and cell design to optimize electrochemical performance of the cell stack in terms of energy density both gravimetric and volumetric, as well as capacity retention on cycling. A secondary focus will be implementation of bipolar design within the cell structure.

Collaborations. All project tasks will be performed at Rutgers University.

Milestones

1. Design and fabricate 10-mAh cell stack that achieves 12 V and delivers energy densities of 1400 Wh/L and 600 Wh/kg per cell stack. (Q1, FY 2019; In progress)
2. Establish negative current collector compositions that enable high efficiency of lithium plating and stripping in excess of 95% during the *in situ* formation step and > 99% during subsequent cycles. (Q2, FY 2019; In progress)
3. Achieve < 30% increase in electrolyte impedance after 50 cycles as characterized by EIS. (Q3, FY 2019; In progress)
4. Establish positive current collector compositions that achieve 90% of the theoretical energy density based on complete utilization of the initial amount of the positive reactive current collector. (Q4, FY 2019; In progress)
5. *Deliverables:* Summary of accomplishments and project work report.

Progress Report

Last quarter, efforts focused on improving transport and diffusion properties within the project's single-cell configuration via two distinct pathways: (1) deposition of excess non-fluorinated lithium salts to offset the localized depletion of Li^+ ions, and (2) incorporation of the previously developed nanolayered multi-component electrode composition into the most optimized cell structure. Each pathway yielded distinct advances. The first approach resulted, through lithium enrichment, in the highest reported first cycle positive electrode utilization of 89%. This gain was attributed to available localized Li^+ ions, free from the effects of F^- ions depletion within the electrolyte. However, while depositions of higher concentrations of solid-state salt enrichment were investigated, these resulted in poor mechanical properties. The team's second approach of combining the nanolayered multi-component electrode composition with the optimized cell structure (60-micron electrode spacing and four times smaller electrode aspect ratio with the new orientation, as described in the second quarter's report) produced a two-fold increase in the positive electrode utilization, leading to 82%. In addition, the irreversible loss between the first and second cycles decreased by approximately 13%. These advances were attributed to an increase in apparent transport by enabling localized access to F^- ions within the bulk of the active positive electrode material. It was concluded that, moving forward, a combination of the methods should allow the team to independently address barriers to maximize cell performance.

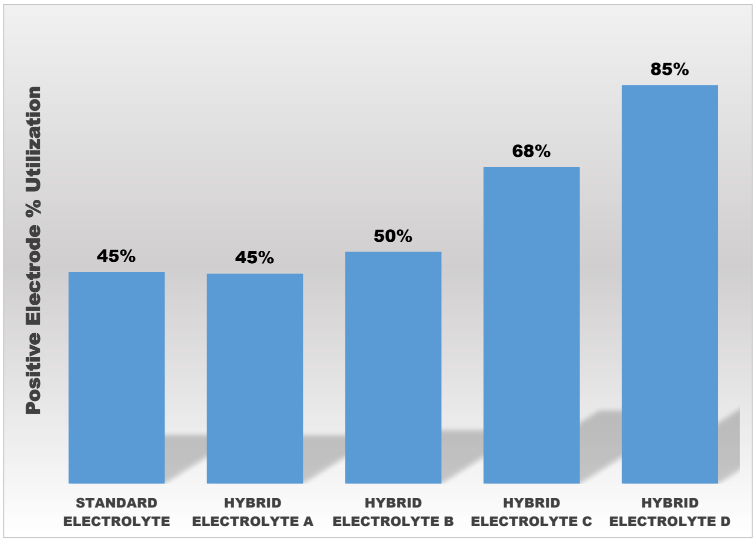

Figure 7. Positive electrode utilization (%) for the first cycle of single-cell configurations with 90-micron spacing and different hybrid electrolyte compositions. The cells were cycled between 1.5 V and 3.5 V.

This quarter, a different concept was investigated in detail to further promote ion transport capabilities. This consisted of inclusion of a hybrid electrolyte in the cell structure. This hybrid electrolyte comprised the project's standard SSE and a small amount of ionic liquid, which was applied to the surface prior to cell formation. Four different hybrid electrolytes were evaluated with the new orientation / cell structure for the single-cell configuration (described in the second quarter's report), but with a 90-micron electrode spacing. Figure 7 compares the positive electrode utilization results obtained with the hybrid electrolytes versus the standard solid electrolyte cell composition. The interactions of hybrid electrolyte A and B had neutral effects without prominent change in electrode utilization in comparison to the standard solid electrolyte. Hybrid electrolyte chemistries C and D both provided significant gains in the positive electrode utilization increasing to 68% and 85%, respectively. It was concluded that these chemistry compositions provided the best interactions to promote F^- and Li^+ ion mobility, leading to higher active material conversion and reaction. The next step in these studies will be to investigate the hybrid electrolyte's interactions applied to the optimized cell structure with 60-micron spacing in addition to the lithium enrichment cell composition and/or the nanolayered multi-component electrode composition described above.

With the end of the project approaching, the various pathways identified as beneficial to transport and subsequently to performance were coalesced to achieve final optimizations. Table 4 is a comprehensive listing of the current studies with data that are still pending. Each of the components, such as hybrid electrolyte chemistry, lithium enrichment via deposited non-fluorinated lithium salts, and nanolayered multi-component electrodes, have been fine-tuned individually. The optimized parameters for each component theoretically should provide beneficial F^- and Li^+ ions mobility to yield better utilization, capacity, and energy density along with cycling retention. These results are pending, but will be available for the final report.

Data Pending Investigations
Hybrid Electrolyte With Optimized Cell Structure
Lithium Enrichment With Nanolayered Multicomponent Electrode
Lithium Enrichment With Hybrid Electrolyte
Nanolayered Multicomponent Electrode With Hybrid Electrolyte

Table 4. Current studies with pending data utilizing the optimized cell structure for the single-cell configuration (60-micron electrode spacing and four times smaller electrode aspect ratio with the new orientation) cycling between 1.5 V and 3.5 V. Each study is combining different optimized parameters that have been investigated individually over the past quarters for improved ion transport and diffusion properties.

In conclusion, during this quarter, one of the final transport and diffusion studies that the project implemented within the single-cell configuration included hybrid electrolytes. The hybrid electrolytes consisted of the standard solid electrolyte in adjunct with a small percentage of ionic liquid. Several chemistries were explored, revealing that electrolyte D yielded the best results for improving electrode utilization from 45% for the standard solid electrolyte to 85%. These advances were attributed to enhanced ionic mobility. Further optimization was performed through the combination of individual optimized components from the project's various transport and diffusion approaches to maximize cell performance. Four studies are still pending, which include combinations of the hybrid electrolyte, lithium enrichment from deposited non-fluorinated Li^+ salts, and the nanolayered multi-component electrode into an optimized cell structure (60-micron electrode spacing with four times smaller electrode aspect ratio and new orientation for the single cell configuration).

Patents/Publications/Presentations

The project has no patents, publications, or presentations to report this quarter.

Task 1.6 – Dual Function Solid-State Battery with Self-Forming, Self-Healing Electrolyte and Separator
(Esther Takeuchi, Stony Brook University)

Project Objective. The project objective is to demonstrate a solid-state rechargeable battery based on a Li-metal anode and iodine cathode with a self-forming, self-healing electrolyte and separator with high gravimetric and volumetric energy density.

Project Impact. This program will enable demonstration of the proposed rechargeable battery with improved power capability, high energy density, and a self-forming, self-healing SSE/separator. Technical insight will be gained regarding improved conductivity of the solid LiI based electrolyte, power capability of the proposed system, the self-healing nature of the LiI layer, the nature of the electrode-electrolyte interfaces, and feasibility of the system to reach the DOE targets.

Approach. The proposed concept is a dual function rechargeable solid-state battery utilizing LiI combined with silver iodide (AgI) as the electrolyte, with lithium metal (and small quantities of silver metal) as the anode and iodine as the cathode and with a self-forming, self-healing separator/electrolyte. The battery will be assembled in the discharged state where the anode and cathode will be created during the first formation (charge) step. Initially, silver ion (Ag^+) will diffuse toward the negative electrode and be reduced to silver metal (Ag^0), and iodine ion (I^-) will be oxidized to elemental iodine (I_2) at the cathode side. As the formation of the battery continues, lithium ion (Li^+) will form a Li-metal layer at the anode, with generation of iodine at the cathode. LiI will remain and serve as both the separator and electrolyte.

Out-Year Goals. This is a multi-year program where the effort is divided into three major tasks.

- Year 1 involves electrolyte preparation and characterization including preparation of SSEs and conductivity measurements.
- Year 2 will focus on cell construction and testing including both *in situ* and *ex situ* analysis.
- Year 3 will focus on cell characterization. Under the program, cycle life, efficiency, energy density, and the functional capacity of cells will be determined.

Collaborations. This project collaborates with A. Marschilok and K. Takeuchi of SBU.

Milestones

1. Destructive analysis of construction A cells. (Q3, FY 2019; Completed)
2. *In situ* analysis of select construction A/B cells. (Q4, FY 2019; Completed)
3. Determine performance at elevated temperature. (Q1, FY 2020; Initiated)

Progress Report

In Situ Analysis of LiI Cells

Energy dispersive X-ray diffraction (EDXRD) utilizes white beam radiation combined with a ‘wiggler’ insertion device to produce high energy radiation capable of penetrating the stainless-steel casing of a conventional coin cell, enabling *in situ* and *operando* data collection. Coin cells, when situated flat on a motorized sample stage, were incrementally moved through the beam, thereby providing a holistic view inside the cell, from the anode to the cathode (Figure 8). A vertical resolution of 20 µm was utilized, ideal for probing small differences in electrode configuration and the study of interfacial properties. This was further supplemented by testing different locations, allowing the team to study the differences in ion diffusion between the edge and the center of an electrode, as diffusion is typically much faster near a boundary. This is of the utmost importance in SSE batteries, which are typically limited by their solid-state diffusion properties. In addition to studying diffusion, EDXRD concurrently can observe side reactions with each scan, creating a full account of the products obtained and their location within the cell during charge or discharge.

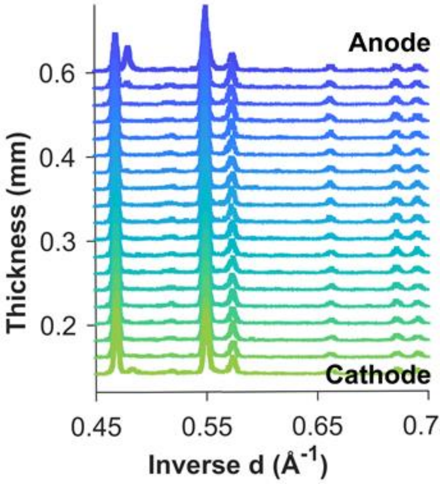

Figure 8. Stacked plot of energy dispersive X-ray diffraction data for a pristine composite LiI solid electrolyte with LiI(3-hydroxypropionitrile)$_2$ additive.

Impact of the New Electrolyte Process on Cell Impedance

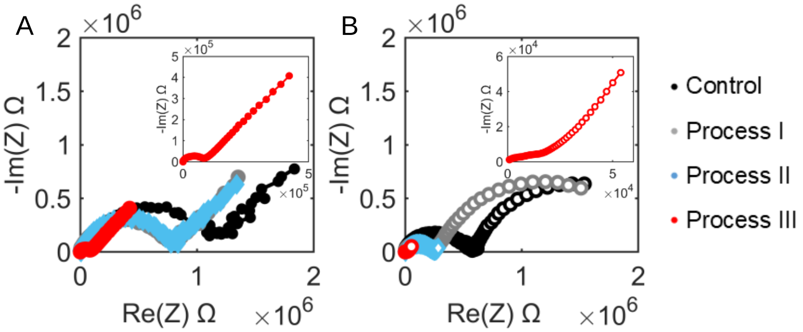

Figure 9. Electrochemical impedance spectroscopy of the Control, Process I, Process II, and Process III composite LiI with LiI(3-hydroxypropionitrile)$_2$ cells in the pristine state before charge (a) and after charging to 0.5% of the theoretical capacity (b). Inset plots are close-ups of the Process III data.

Cell design A included the composite LiI solid electrolyte with LiI(3-hydroxypropionitrile)$_2$ additive, as reported in previous quarters. Efforts were made to decrease the particle size of the LiI electrolyte via a new electrolyte process. Variations in processing progress from the least processed (Process I), to the most processed (Process III). All types were compared to a Control, which received no additional processing. Decreasing particle size typically affects cell resistance; thus, the cells were tested with EIS, which revealed that further processing of the electrolyte indeed induced a decrease in the impedance of the pristine cells (Figure 9). Little difference was seen between Process I and II, but Process III is an order of magnitude lower in impedance than the Control cell. Notably, Process II has approximately 1/8th of the impedance of the project’s previous electrolyte method. On charging to as little as 0.5% of theoretical capacity, all cells show a significant decrease in impedance that is consistent with the formation of a more conductive Li^0 metal layer at the negative electrode interface. Process III again has the lowest impedance of all the cells, and now is 1.5 orders of magnitude less in impedance than Process I. This further exemplifies that the new electrolyte processing method significantly lowers cell resistance in both the pristine and charged states.

Impact of the New Electrolyte Process on the Voltage Profiles

Prior to cycling, all cells were charged to form the battery. Electrochemical cycling measurements were conducted on the Control and Process(es) I, II, and III, with the first discharge profile shown in Figure 10. During discharge, modified processing of the electrolyte material facilitates the formation of a distinct plateau, and increased processing (Process III) allows the cell to deliver the largest capacity and ultimately improve the CE to 100%. Furthermore, as the level of processing is increased, the lithiation potential increases as well, allowing the cell to deliver a significant increase in energy and power density. The processing decreased the particle size, thereby decreasing diffusion path length per particle, improving ionic diffusion.

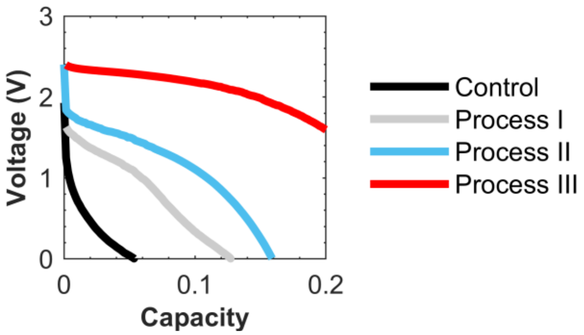

Figure 10. Comparison of the first discharge voltage profiles for the new electrolyte process(es).

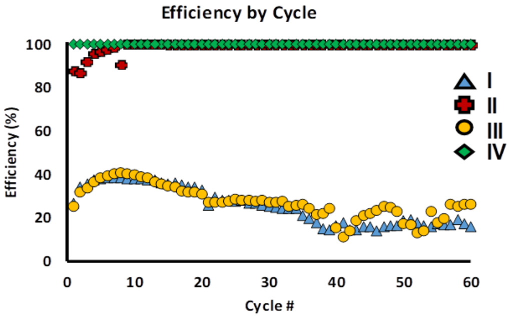

Figure 11. Cell cycling at 40°C for four cell designs.

Impact of Elevated Temperature

To analyze the influence that temperature has on this system, each configuration underwent galvanostatic cycling at an elevated temperature. As shown in Figure 11, extended cycling at elevated temperatures afforded rapid stabilization in efficiency for Li-containing configurations II and IV. Configuration IV provided near 100% CE while cycling at 40°C for 60 cycles.

Patents/Publications/Presentations

The project has no patents, publications, or presentations to report this quarter.

Task 1.7 – High-Conductivity, Low-Temperature Polymer Electrolytes for Lithium-Ion Batteries (Bryan D. McCloskey, University of California at Berkeley)

Project Objective. Design of electrolytes with enhanced transport properties compared to conventional liquid organic electrolytes is key to improving the rate at which a Li-ion battery can be discharged or charged. Ideally, electrolytes would allow high mobility for lithium ions and disallow mobility of inactive ions (for example, the counteranion of the Li^+). However, current liquid electrolyte compositions usually provide higher mobility for the counteranion than Li^+, which results in high concentration polarization that disallows fast charging, particularly in batteries that employ thick porous electrodes, as is necessary for EVs to provide high energy densities. The project objective is to develop a high Li^+ transference number (t_{Li}, the fraction of ionic current carried by Li^+ in an electrolyte of uniform composition) polymer-based electrolyte that, when used in a Li-ion battery, can support current rate capabilities sufficient for EV propulsion at room temperature.

Impact. Development of practical high t_{Li} polymer-based electrolytes for Li-ion batteries would enable safer Li-metal and graphitic anode cycling and thicker porous electrode designs, leading to improved specific and volumetric battery energy densities consistent with the EV Everywhere Grand Challenge. High-energy anode and cathode materials, such as lithium metal, silicon, and high-voltage layered or spinel structures, could be enabled by electrolytes with high t_{Li} and large operating voltage windows, such as those based on sulfones, as proposed here.

Approach. Lowering the operating temperature of polymer electrolytes has been cited as an important challenge to their viability as Li-ion battery electrolytes. The project will address this challenge by using Li^+ neutralized anionically charged polymers as salts in conventional liquid solvents. Using these so-called polyelectrolyte solutions, initial results indicate that the project can access t_{Li} values typical of single-ion conducting polymer electrolytes ($t_{Li} > 0.9$) and conductivity values (> 1 mS/cm at room temperature) that approach those of traditional battery electrolytes.

Out-Year Goals. The optimization of transport and stability properties of these polyelectrolyte systems, through understanding of appropriate polymer and solvent design, is the objective. The goal is to develop new polyelectrolyte compositions that provide superior transport properties (specifically, higher t_{Li} and conductivity) than conventional liquid electrolytes and enable use of high-energy electrode materials, such as lithium metal.

Collaborations. Collaborations on this project include V. Battaglia (porous electrode preparation) and K. Persson (atomistic modeling) at LBNL.

Milestones

1. Complete synthesis and characterization of a new Li^+-neutralized charged polymer (pFTO) with a triflate-like ion ($-CF_2-SO_{3-}$) appended to the polymer backbone to improve ion dissociation. (Q1, FY 2019; Completed October 2018)
2. Complete nuclear magnetic resonance (NMR) transport and viscosity measurements of pFTO dissolved in carbonate-based solvents. Progress measure: Publish an article describing transport properties of polyelectrolyte solutions comprised of sulfonated polysulfone-co-poly(ethylene oxide) in carbonate-based solvents. (Q2, FY 2019; Progress measure completed November 2018)
3. Complete electrochemical transport measurements of pFTO in symmetric cells with Li-metal electrodes and SSEs. (Q3, FY 2019)
4. Complete characterization of rate capabilities of cells comprised of lithium metal, a porous NMC cathode, and pFTO-containing carbonate solutions during electrochemical cycling. (Q4, FY 2019)

Progress Report

Previously, the team showed that Li$^+$-bearing polyelectrolyte solutions can achieve high conductivities and Li$^+$ transference numbers when the Li$^+$ is well-dissociated from the polymer-appended anions. However, they only observed good dissociation in strong Lewis basic nonaqueous solvents that were inadequate for use in batteries (for example, dimethylsulfoxide). When using the sulfonated polymer shown in Figure 12, the team found that the polymer was fully soluble in a 2:1 (vol.) ethylene carbonate:dimethyl carbonate (EC:DMC) solution, but that the sulfonate-Li$^+$ ion pair remained strongly associated in solution, resulting in very poor solution conductivity (~ 0.02 mS/cm, Figure 12, control). The team has pursued two thrusts in an attempt to attain higher conductivity in carbonate-based polyelectrolye solutions to make them useful in batteries: (1) additive engineering, and (2) changing the appended anion. They described the chemistry used for the second thrust in the previous quarterly report and have continued to refine their understanding of ion transport using these new polymers. In this report, they briefly describe the project's results from the first thrust.

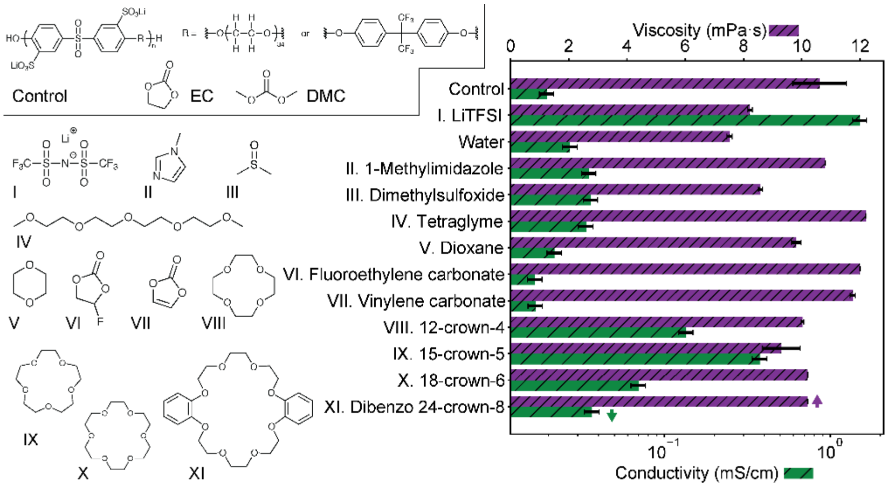

Figure 12. Conductivity and viscosity of a range of potential additives to improve conductivity of the control 0.1 M polymer in 2:1 (vol.) EC:DMC. Each additive is introduced at 0.1 M to match the lithium content of the solution. The structure of the polymer, EC, and DMC in the control solution are also included. See Diederichsen et al. in Publications section.

The team screened a range of potential additives to improve conductivity of a Li$^+$-neutralized, sulfonated polymer studied in the group (shown in the upper left hand corner of Figure 12), finding that 15-crown-5 ether is able to increase polyelectrolyte conductivity by over an order of magnitude (see Figure 12, which presents conductivity and viscosity of polyelectrolyte solutions prepared from the polymer shown in EC:DMC with various additives). The team demonstrated that this is due to increased dissociation of lithium through pulsed field gradient NMR measurements. They further showed that the optimized 15-crown-5 ether-containing solution enables operation of a battery composed of commercial electrodes (see Figure 13, where the cell is comprised of a porous 1.52 mAh/cm^2 lithium iron phosphate cathode and a 2.64 mAh/cm^2 graphite anode, both purchased from MTI).

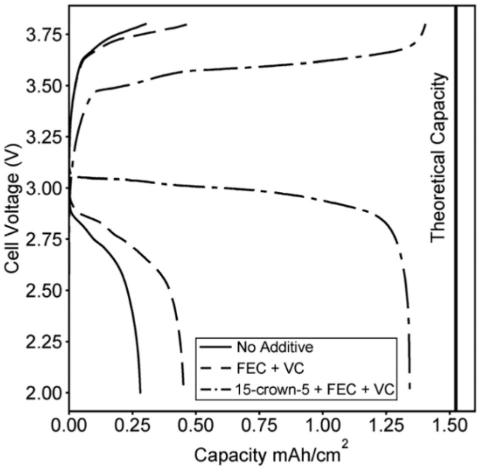

Figure 13. Second charge and discharge curves at C/20 for batteries fabricated with the 0.1 M polymer in 2:1 (vol.) EC:DMC solution containing no additives (control), containing stabilizing additives FEC and VC, and containing 15-crown-5 and the stabilizing additives. The calculated theoretical maximum capacity of the cell is also shown. See Diederichsen et al. in Publications section.

This study is the first report of a polyelectrolyte solution functioning as the electrolyte in a Li-ion battery. A wide array of charged polymers has never been tested as polyelectrolyte solutions within a Li-ion battery; the team will continue to seek optimized versions of these materials as battery electrolytes. This study provided clear proof of concept for the idea of polyelectrolyte solutions as battery electrolytes.

Furthermore, at the end of the last quarter, the team reported on lithium stability issues that hindered ideal transference number

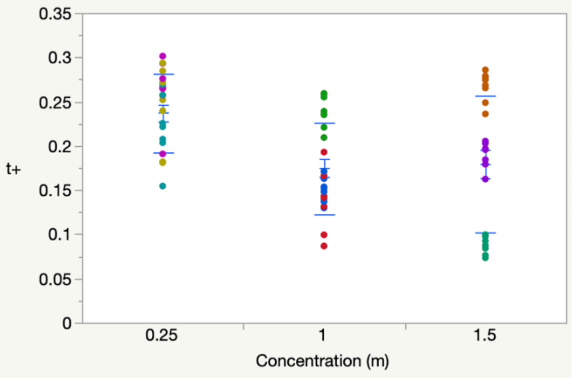

Figure 14. Ideal transference number versus lithium concentration (molal) for LiTFSI in EC:EMC (3:7). Each color represents a separate cell, with each cell polarized subsequently to ±5, ±10, ±15, and ±20 mV.

measurements of liquid electrolytes via the Bruce-Vincent method. This quarter, by using electrolyte-lean systems of lithium bis(trifluoromethyl sulfonamide) (LiTFSI) in ethylene carbonate: ethyl methyl carbonate (EC:EMC, 3:7 w/w), the team was able to attain more stable current responses to applied polarization. All cells were first conditioned for 6 cycles at 20 µA/cm^2, after which the team observed a stable current-voltage response. Bruce-Vincent measurements were then performed on these cells with the interfacial resistance monitored throughout the measurement via impedance spectroscopy. The interfacial resistance appeared stable throughout all measurements. A variability analysis was run using concentrations ranging from 0.25–1.5 molal LITFSI in EC:EMC system with polarization potentials from 5 mV – 20 mV. The team found no clear dependence of the obtained ideal transference number on the applied potential; however, moderate cell-to cell variability is still noted (see Figure14), although values reported are reasonable compared to similar values in the literature. The team found that the current or length of the preconditioning cycle had little effect on the cell-to-cell repeatability. To reduce this variability, the team is exploring the effect of stabilizing coatings on the lithium metal. The project's current strategy includes a copper substrate with a ~ 50 nm amorphous coating as one electrode, which when used in a cell versus lithium metal should help create a stable SEI resembling that of a graphite SEI during the first plating cycle. Subsequent lithium will plate below this SEI, allowing more stable cycle while maintaining the symmetric nature of the cell.

Patents/Publications/Presentations

Publications

- McCloskey, B. D., and K. Xu. "Current Trends in Electrolytes." *ECS Interface* 28, no. 2 (2019): 47.
- Diederichsen, K. M., and B. D. McCloskey. "Additive Engineering to Enable Nonaqueous Polyelectrolyte Solutions for Lithium Ion Batteries." *Molecular Systems Design and Engineering.* Advance article.
- Diederichsen, K. M. "High Transference Number Polymer-Based Electrolytes for Lithium Batteries." University of California at Berkeley. Ph.D. thesis (2019).

Presentation

- American Chemical Society (ACS) Fall National Meeting, San Diego, California (August 25–29, 2019): "Designing Polymer-Based Li$^+$ Electrolytes with High Conductivity and Li$^+$ Transference Number"; B. D. McCloskey. Invited.

Task 1.8 – Advanced Polymer Materials for Batteries
(Zhenan Bao and Yi Cui, Stanford University)

Project Objective. This project will develop new polymer materials for batteries. The team will develop polymer coatings with specific mechanical properties that can accommodate the volume expansion and contraction of the Li-metal anode associated with deposition and stripping (charging and discharging).

Project Impact. The cycling stability and CE of Li-metal electrodes will be increased by implementation of a polymer-based protective layer that functions as an artificial SEI with desired properties. The improved performance will enable further development toward practical utilization of Li-metal anodes with higher cycling efficiency and less susceptibility to dendrite-based failure.

Approach. The project uses soft polymer coatings with dynamic crosslinking to give the resulting polymers liquid-like rheological properties and stretchable and self-healing properties. In previous work, the project has shown that such coatings resulted in uniform deposition/stripping of lithium metal and improved cycling stability of Li-metal electrodes. To understand the design rules for effective polymer coatings, the team chose a few representative polymers to systematically understand structure property relationships. Here, the team investigates the correction between surface energy of the polymer and exchange current for lithium deposition.

Out-Year Goals. Work will progress toward the correlation between dielectric constant and exchange current. These findings will enable further understanding and development of various polymer coatings for protecting Li-metal anodes.

Collaborations. There are no active collaborations this quarter.

Milestones

1. Identify at least two different types of self-healing polymers (SHPs) with promise to suppress dendrites. (Q1, FY 2019; Completed)
2. Characterize the SHPs. (Q2, FY 2019; Completed)
3. Investigate one of the SHP polymers in more detail. (Q3, FY 2019; Completed)

Progress Report

The development of Li-metal batteries is hindered by the high reactivity of lithium metal with the electrolyte. In addition, inhomogenous deposition of lithium leads to high surface area dendritic growth that further exacerbates reaction with the electrolyte. Designing the electrode-electrolyte interface and controlling the lithium deposition morphology is therefore of great importance. The team has focused on the design of polymer coatings that function to limit the electrolyte (polar solvent and salt) accessibility to the electrode surface, thereby limiting undesired reactions. In this report, the team uses a model liquid system to allow them to understand the effect of Li-ion solvation on lithium deposition. The team designs a nonpolar:polar electrolyte mixture where nonpolar alkanes can limit the accessibility of the polar solvent to the electrode surface. They show that hexane and cyclohexane additions to ether solvents (1,3-dioxolane and 1,2-dimethoxyethane) reduce the Li-ion solvation, half the nucleation and growth overpotentials for lithium deposition, increase the cell CE, improve the lithium deposition morphology, increase the electrolyte oxidative stability (> 0.2 V), and double the cycle life, even when compared to a widely used fluorinated ether.

Rationale for Molecule Selection and Study

Lithium metal is stable in the presence of linear alkane media such as mineral oil. Mineral oil is highly viscous; hence, the team focused on shorter chain alkanes such as *n*-hexane with a similar chemical structure to mineral oil, but with low molecular weight and viscosity. Because hexane is nonpolar (and cannot solvate ions), the team needs a polar solvent that is miscible with hexane, but can also dissolve lithium salts. DOL and DME were chosen for this work because they have been heavily explored for Li-metal deposition and stripping, and have been shown to yield higher CE than carbonate-based solvents used in Li-ion batteries. Fluorinated solvent additive (that is, tetrafluoroethyl-2,2,3,3-tetrafluoropropyl ether, or TTE) was chosen to serve as the comparison to the hexane system because TTE has been heavily explored for lithium metal use. Unlike hexane, TTE is expected to react with lithium metal, and should give insight into reactive versus nonreactive additives and their effect on lithium deposition and stripping. Molecular structures of these compounds are shown in Figure 15a.

Influence on Electrochemistry

The influence of the electrolyte mixtures on lithium deposition and stripping was studied. Figure 15b shows that the nucleation overpotential required to deposit lithium is lowest for the DOL:hexane mixture and highest for the TTE mixture. Furthermore, the time (or capacity) required for the nucleation event is lowest for the DOL:hexane mixture and highest for the DOL:TTE mixture. More importantly, the growth overpotential for continued lithium deposition and stripping is lowest in the hexane mixture and is a function of hexane content (Figure 15c). As the cosolvent amount is increased with hexane addition, the nucleation overpotential is decreased compared to DOL and DOL:TTE mixture.

To better understand the effect of the nonpolar alkanes on the electrochemistry, the team fabricated Li/Cu cells and studied the initial lithium deposits using SEM. Figure 16a shows that when 0.1 M DOL is used as the electrolyte, clear dendrites are formed. These dendrites span the entire electrode. However, when a 0.1 M DOL:hexane electrolyte is used (Figure 16a), the density of dendrites present on the electrode surface is much lower. The lack of dominant dendrite formation may help explain the longer cycling lifetime observed in Figure 15b-c. The project's original hypothesis for exploring these nonreactive nonpolar solvents is that they can limit the accessibility of the polar solvent to the electrode surface, hence prolonging cycle life through a mechanism different from reactive additives that instead passivate the surface. However, this hypothesis, termed the surface coverage effect, does not help explain the decrease in nucleation and growth overpotentials.

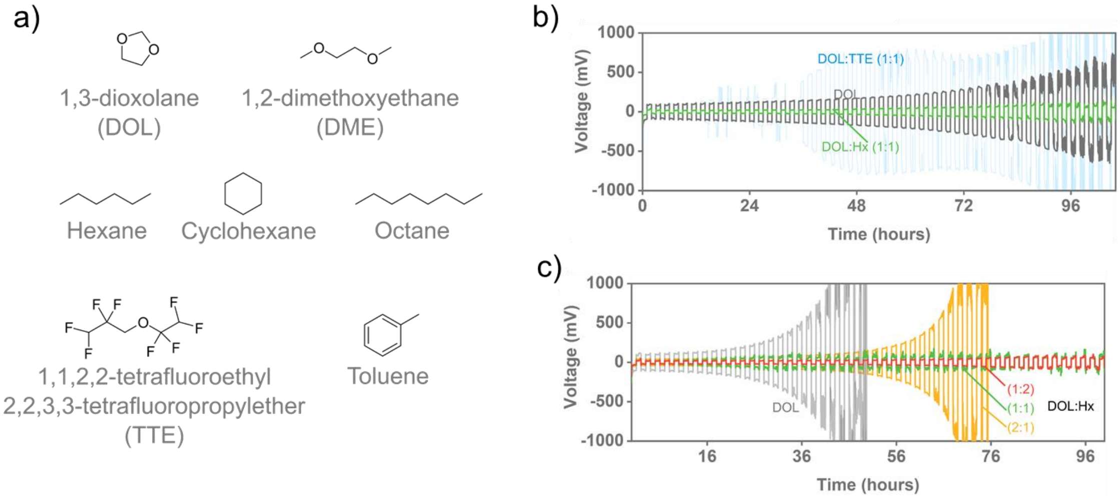

Figure 15. (a) Chemical structures of the compounds studied in this work. (b) Li/Li cycling at 0.5 mA/cm^2 to 0.5 mAh/cm^2 as a function of electrolyte content. (c) Li/Li cycling at 1 mA/cm^2 to 1 mAh/cm^2 as a function of hexane content in the electrolyte. The ratios (for example, 1:1) represent volume ratios. Salt concentration: 0.1 M LiTFSI.

Solvation Effect

To better explain the decrease in nucleation and growth overpotentials, the team probes the Li-ion solvation environment in the different electrolyte mixtures. They used ^{1}H, ^{7}Li, and ^{19}F NMR spectroscopy to study the solvation changes. Figure 16b shows the ^{7}Li NMR spectra of a 0.1 M LiTFSI in DOL solution as the hexane volume content is increased. Despite maintaining the same salt concentration, the lithium peak shifts significantly downfield as a function of hexane content. Downfield shift (shift to higher frequencies) is observed due to deshielding of the electron cloud surrounding the nuclei of interest—a decrease in the electron cloud that opposes the externally applied magnetic field. Therefore, there is less ion pairing and a decrease in Lewis basicity around the lithium ion. In contrast, TTE binds to the Li$^+$ within the Li$^+$–DOL solvation shell and hence increases the electron density around the lithium ion, leading to an upfield shift in the ^{7}Li NMR spectrum.

The solvation free energy of a lithium-ion solvated by different electrolyte mixtures was computed using classical molecular dynamics (MD). Upon hexane and cyclohexane addition to DOL, the magnitude of the lithium solvation free energy continually decreases. For TTE, the magnitude of the solvation free energy increases with higher TTE concentration. These MD simulations corroborate the NMR results in that they show looser Li$^+$ coordination and solvation with hexane or cyclohexane addition, and stronger Li$^+$ solvation with TTE addition. The ionic solvation behavior strongly correlates with the electrochemistry.

Knowledge obtained from this work about the utility of limiting polar electrolyte accessibility to the Li-metal electrode can yield new design approaches regarding polymer selection for Li-metal coatings. The polymer should be designed to frustrate Li-ion solvation within the electrolyte (reduce solvation free energy) and be chemically stable against contact with lithium metal.

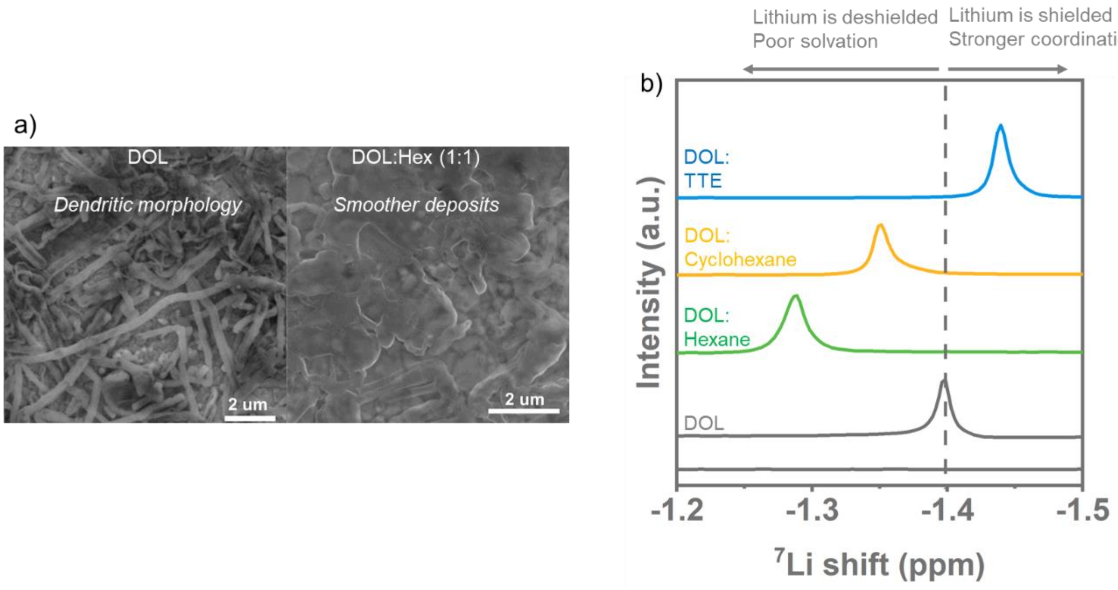

Figure 16. (a) Scanning electron microscopy image of the lithium deposition morphology at a current rate of 1 mA/cm^2 to 0.1 mAh/cm^2 as a function of electrolyte content. (b) ^{7}Li nuclear magnetic resonance chemical shifts of 0.1 M LiTFSI in the respective electrolytes. The dashed line in (b) demarcates the ^{7}Li chemical shift of LiTFSI in DOL; the 'deshielding' and 'shielding' are made with respect to the peak.

Patents/Publications/Presentations

Patent

New PCT Patent Application No.:
PCT/US2019/054298
Based on U. S. Application No.: 62/740,785

Title:	ION-CONDUCTIVE ORGANIC NETWORKS FOR BATTERY APPLICATIONS
Applicant:	The Board of Trustees of the Leland Stanford Junior University
Inventors:	Zhenan Bao, Zhiao Yu, Dawei Feng, Min Ah Lee, Yi Cui, Allen Pei

Publications

- Amanchukwu, C. V., X. Kong, J. Qin, Y. Cui, and Z. Bao. "Nonpolar Alkanes Modify Lithium-Ion Solvation for Improved Lithium Deposition and Stripping." *Advanced Energy Materials* (2019). doi.org/10.1002/aenm.201902116.
- Yu, Z., D. Mackanic, Y. Cui, and Z. Bao. "A Dynamic, Electrolyte-Blocking, and Single-Ion-Conductive Network for Stable Lithium-Metal Anodes." *Joule* (2019). doi.org/10.1016/j.joule.2019.07.025.

Presentation

- 2019 DOE VTO Annual Merit Review (AMR), Arlington, Virginia (June 10–13, 2019): "Stabilizing Lithium-Metal Anode by Interfacial Layer"; Z. Bao.

Task 1.9 – Improving the Stability of Lithium-Metal Anodes and Inorganic-Organic Solid Electrolytes (Nitash Balsara, Lawrence Berkeley National Laboratory)

Project Objective. The project objective is to establish a new hybrid electrolyte that will be stable against cells with a Li-metal anode.

Project Impact. Polymer electrolytes offer increased stability in lithium batteries in comparison to more widely used liquid electrolytes. Nanostructured electrolytes containing both soft, ion-conducting domains and rigid, nonconducting domains offer the opportunity to tune both mechanical and electrical properties separately. Such electrolytes are conveniently made by block copolymer self-assembly. Most of the block copolymer electrolytes studied thus far comprise organic polymer chains for both the conducting and rigid domains. The team hopes to synthesize new electrolytes that simulataneously have high transport properties and have greater stability against lithium in comparison to organic diblock copolymers.

Approach. First, the team synthesizes hybrid diblock copolymers by incorporating monomers that contain an inorganic component. Then, electrolytes are prepared by mixing these diblock copolymers with salt. Electrochemical and mechanical characterization of these materials is performed before carrying out cycling X-ray tomography (XRT) experiments. The combination of these approaches enables rational design of materials that exhibit improved stability against lithium metal.

Out-Year Goals. The project will synthesize a new hybrid electrolyte that is designed to be stable against lithium metal. The material is a block copolymer wherein acryloisobutyl polyhedral oligomeric silsesquioxane (POSS) is covalently bonded to the chain. The second block is a conventional polymer electrolyte, PEO. Electrochemical characterization of this polymer will include measurement of all transport properties including conductivity, diffusion coefficient, and the transference number. The stability against lithium metal will be evaluated by cyclic voltammetry (CV), while its applications as an electrolyte will be evaluated and visualized using cycling XRT experiments on symmetric Li-hybrid-Li cells.

Collaborations. There are no active collaborations this quarter.

Milestones

1. Determine limiting current in solid electrolytes. (Q1, FY 2019; Completed)
2. Determine the nature of lithium/electrolyte interface. (Q2, FY 2019; Completed)
3. Study the effect of lithium metal purity and failure mechanisms. (Q3, FY 2019; Completed)
4. Determine parametric range over which stable lithium electrodeposition is obtained. (Q4, FY 2019; Completed)

Progress Report

The milestone for this quarter, described as follows, has been completed: determine parametric range over which stable lithium electrodeposition is obtained. It is important to determine the conditions under which stable lithium electrodeposition can be obtained for multiple applications.

Stable electrodeposition can also be described as reversible deposition: that is, deposition in which stripping occurs uniformly from a planar lithium surface and plating results in planar lithium. This plated lithium should not be mossy or include lithium protrusions or other features. Perfectly stable deposition during cycling should lead to infinite cycle life.

Stable electrodeposition was observed in an all-organic PEO-based rigid block copolymer electrolyte at a low current density: 0.04 mA cm^{-2} (Figure 17). Although this current density is too low to be used in practical applications, one might imagine leveraging stable deposition at low current density to pre-treat lithium cells to extend cycle life at high current density.

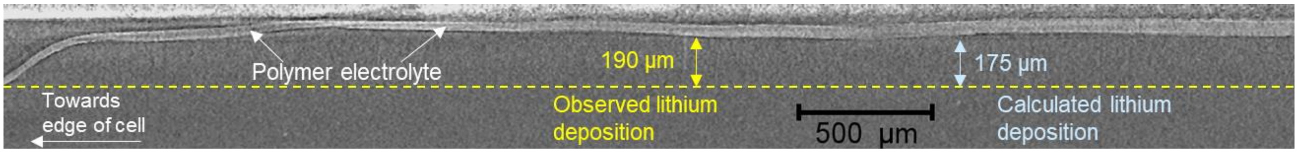

Figure 17. Representative cross section of cell polarized at i = 0.04 mA cm^{-2} for t = 900 h acquired using X-ray tomography. Lithium was deposited downward through the polymer electrolyte, which appears as a light band extending across the cell near the top of the cross-section. No lithium protrusions were observed. This cell did not short circuit. The yellow arrow shows the thickness of the electrochemically deposited lithium, 190 µm, at a representative location based on the analysis of the tomograms, using the electrolyte's original position at the edge of the cell as a reference point. The light blue arrow shows for comparison the estimated thickness of electrochemically deposited lithium, 175 µm, based on the current passed through the cell.

Further, the team has measured higher limiting currents in hybrid-inorganic-organic block copolymer electrolytes than all-organic block copolymer electrolytes (Figure 18).

Stable electrodeposition has been linked to the current density through the electrolyte normalized by the limiting current density of the electrolyte.[1] Thus, the team may achieve stable electrodeposition at higher current density in hybrid inorganic-organic electrolytes: if the limiting current ratio is proportional to the ratio of critical current densities (CCDs) at which stable electrodeposition is achieved, one may expect to see a 9-fold improvement in the critical current density.

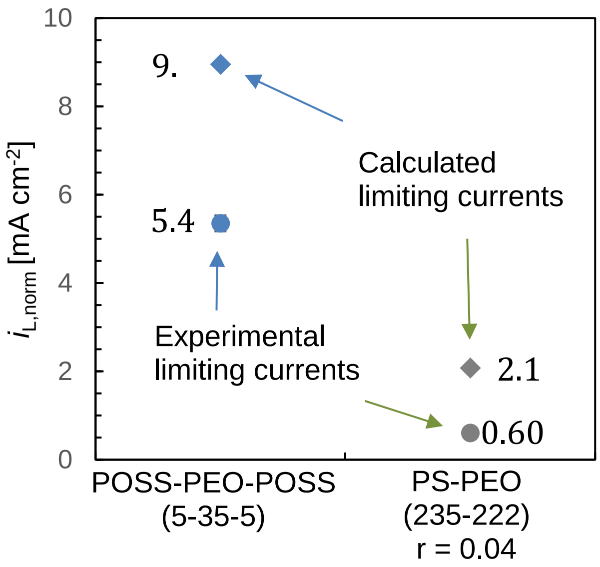

Figure 18. Comparison of the calculated and experimental limiting currents of a POSS-PEO-POSS hybrid inorganic-organic block copolymer electrolyte and a PS-PEO all-organic block copolymer electrolyte. In each case, the calculated limiting current is higher than the experimental limiting current due to considerations for transport in the concentrated solution regime. The limiting current of the POSS-PEO-POSS electrolyte is both higher and proportionally closer to its calculated limiting current than the PS-PEO.

[1] Barai, P., K. Higa, and V. Srinivasan. *Physical Chemistry Chemical Physics* 19 (2017): 20493.

Patents/Publications/Presentations

Publication

- Gribble, D. A., L. Frenk, D. B. Shah, J. A. Maslyn, W. S. Loo, K. I. S. Mongcopa, D. M. Pesko, and N. P. Balsara. "Comparing Experimental Measurements of Limiting Current in Polymer Electrolytes with Theoretical Predications." *Journal of the Electrochemical Society* 166, no. 14 (2019): A3228–A3234.

Presentation

- ACS Fall National Meeting, San Diego, California (August 25–29, 2019): "Self-Assembly Behaviour of Organic-Inorganic Hybrid Triblock Copolymer Solid Electrolytes." S. Chakraborty, G. Sethi, I. Villaluenga, and N. Balsara.

Task 1.10 – Electrolyte/Binder for High Efficiency Lithium-Sulfur Battery: New Materials Design and Computation

(Zhengcheng Zhang, Larry A. Curtiss, and Ahn Ngo, Argonne National Laboratory)

Project Objective. Li-S batteries have received great attention because sulfur exhibits an order of magnitude higher theoretical capacity than that achievable with intercalation-type cathode materials in Li-ion batteries and is considered as a promising battery chemistry to power long-range, low-cost EVs. Sulfur is abundant in nature and nontoxic, which leads to low cost of the cell and environmental benefits. However, low active material utilization and poor cycle life hinder the practical application of Li-S batteries. The project objective is to develop new electrolyte materials to help overcome these challenges and enable high-efficiency Li-S batteries for vehicle application.

Project Impact. Development of novel functional electrolytes tailored for Li-S electrochemistry will enable improved materials utilization and longer cycle life as needed to take advantage of the high potential capacity of Li-S batteries to power long-range, low-cost EVs.

Approach. This project takes a new approach, combining organic synthesis and quantum chemistry computations to obtain an in-depth understanding of the interaction of the discharged lithium polysulfides with the electrolyte solvents and the lithium salt, aiming to develop new electrolyte materials for Li-S batteries. Based on the team's previous study, the fluorinated-ether-based electrolytes have shown very limited Li_2S_x solubility, and at the same time could effectively passivate the lithium anode surface, affording a reversible electrochemistry with high CE. However, the low active material utilization compromises its advantages of high theoretical capacity and energy density. To overcome this, the team will investigate boron-containing fluorinated polyethers as a new class of electrolytes for Li-S batteries. To further improve the cycle life, the project also proposes to design and synthesize new polymer binders bearing a pentafluorophenyl group on the backbone. First principles DFT and wave-function based quantum chemistry methods will be employed to provide accurate atomic/molecular level insight into the experimental studies. The team will also employ *ab initio* molecular dynamics (AIMD) simulations of the solvents for different finite temperatures and concentrations. The AIMD simulations will provide information on the structures of the electrolytes based on the fluorinated ethers synthesized in the experimental part of this project.

Out-Year Goals. The out-year goals are to find electrolytes that promote longer cycle life through electrolytes to reduce material loss.

Collaborations. This project engages in collaboration with Prof. A. Salehi at University of Illinois at Chicago (UIC).

Milestones

1. Design and synthesis of new fluorinated borate electrolytes and baseline studies of sulfur utilization, CE, and cycle life. (Q1, FY 2019; Completed, December 30, 2018)
2. Quantum chemical calculations of the chemical stability and reactivity properties of new borate and fluorinated ethers solvents and with electrode surfaces. (Q2, FY 2019; Completed, March 30, 2019)
3. Electrochemical characterization of performance of various fluorinated ether electrolytes in Li-S cells. (Q3, FY 2019; Completed, June 30, 2019)
4. Correlation of experimental and theoretical results on Li-S cells with ether decomposition during cell operation. (Q4, FY 2019; Initiated).

Progress Report

This quarter, HFB was proposed and systematically studied as a new Li-S battery electrolyte additive by electrochemical testing and DFT calculations. Due to the six electron-withdrawing fluorines, the aromatic ring of HFB is more electron-deficient; this results in strong electrostatic interactions with the electron-rich sulfide species, thus activating the electron-isolating low-order polysulfides (specifically Li_2S and Li_2S_2) and accessing the full spectrum of the capacity for complete redox reaction of sulfur. Both the voltage profiles of the initial electrochemical testing (Figure 19a) and the solubility testing (Figure 19b) confirmed the strong chelating effect of HFB with Li_2S_x (x=2-8) leading to more dissolution into the electrolyte causing a long shuttling plateau.

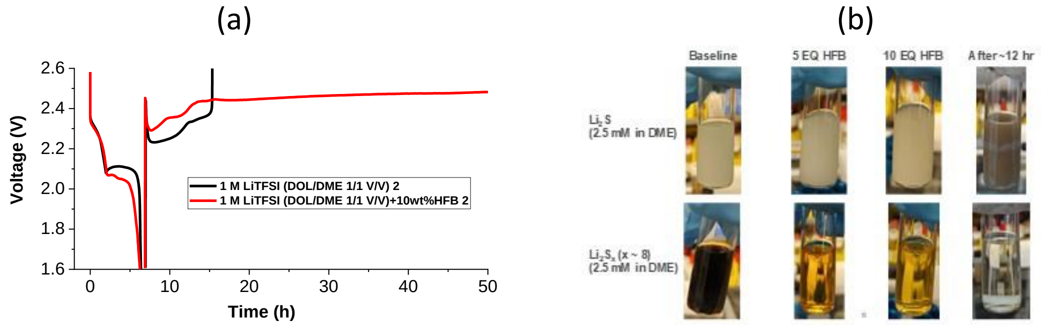

Figure 19. (a) First discharge and charge voltage plots of the Li-S cell with baseline and hexafluorobenzene (HFB) additive electrolyte. (b) Solubility test of Li_2S and Li_2S_8 in DOL/DME/1.0 M LiTFSI + different stoichiometric ratio of HFB.

To eliminate the shuttling and thus enable the normal charging of the Li-S cell, 0.1 M $LiNO_3$ was added to the DOL/DME/1.0 M LiTFSI electrolyte in the presence of various amounts of HFB. Figure 20a shows the first voltage profiles of five Li-S cells. A characteristic "plateau" (circled in red) showed up at the end of the charging process when HFB was present, indicating the oxidation reaction of the HFB-Li_2S_x complex. More surprisingly, the 3% HFB cell showed much improved capacity retention compared with the baseline and the high concentration HFB (20%) one (Figure 20b). The impact of the HFB additive was further investigated in a DOL/TTE/1.0 M LiTFSI cell, and the same effect was observed with high concentration HFB (Figure 20c).

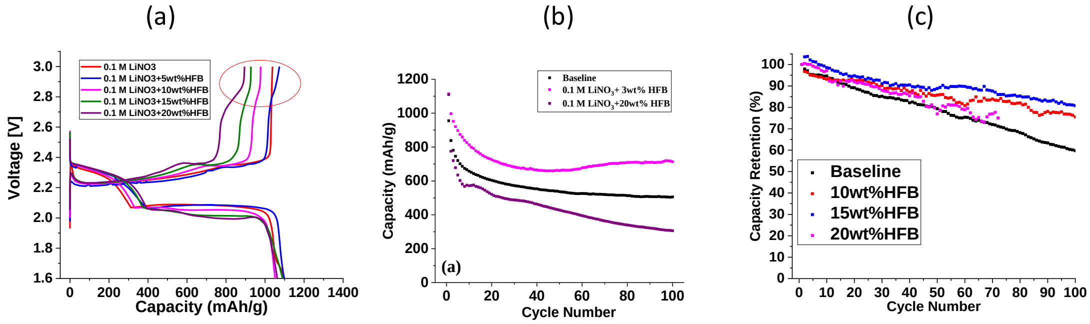

Figure 20. (a) First discharge and charge voltage plots of DOL/DME/1.0 M LiTFSI/0.1 M $LiNO_3$ + hexafluorobenzene (HFB). (b) Capacity retention of the Li-S cells using DOL/DME/1.0 M LiTFSI/0.1 M $LiNO_3$ + 3% and 20% HFB. (c) Capacity retention profile of Li-S cells using DOL/TTE/1.0 M LiTFSI + 10%, 15%, and 20% HFB.

Density functional calculations were then conducted to determine the mechanism by which the HFB might chelate with low-order Li_2S and Li_2S_2 and subsequently react and convert both into active aromatic sulfides, thus facilitating the reutilization of the electronically insulating Li_2S and Li_2S_2. Calculations of the potential energy surfaces were done with the B3LYP/6–311G** method. The PCM continuum solvation method was used for implicit solvation calculations of solvation energies. The nucleophilic aromatic attack of Li_2S with

HFB was found to have a barrier of 0.52 eV for conversion from an encounter complex $C_6F_6...Li_2S$ to a pentafluorophenyl sulfide dilithium fluoride structure $C_6F_6SLi_2F$. This structure is shown in Figure 21. The reaction of HFB with Li_2S_2 was found to have a barrier of 0.75 eV for conversion from an encounter complex $C_6F_6...Li_2S_2$ to a pentafluorophenyl disulfide dilithium fluoride structure $C_6F_6S_2Li_2F$. The higher polysulfides had larger barriers and were less favorable. This confirms the mechanism by which HFB acts as an additive to activate the low order polysulfide and mitigate the loss of the active material as evidenced by the improved cycling performance in two electrolyte cells.

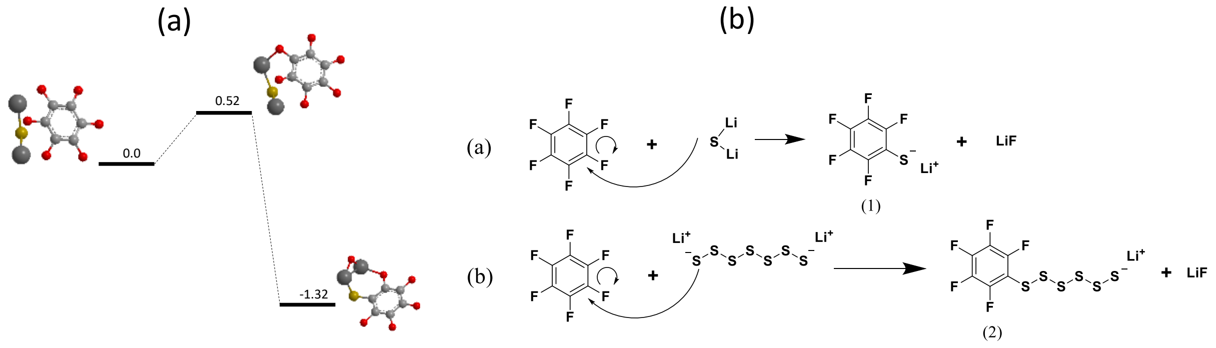

Figure 21. (a) Density functional theory optimized structures of encounter complex, transition state, and product from the reaction of hexafluorobenzene (HFB) and Li_2S showing a small barrier for the reaction (in eVs), and (b) the proposed reactivity of HFB with Li_2S and Li_2S_x.

Patents/Publications/Presentations

Publications

- Meisner, Q. J., T. Rojas, N. L. Dietz Rago, J. Cao, J. Bareño, T. Glossmann, A. Hintennach, P. C. Redfern, D. Pahls, L. Zhang, I. D. Bloom, A. T. Ngo, L. A. Curtiss, and Z. Zhang. "Li-S Battery with Partially Fluorinated Ether Electrolytes: Interplay between Capacity, Coulombic Efficiency, and Li Anode SEI Formation." *Journal of Power Sources* 438 (2019): 226939.
- Cao, J., Q. Meisner, T. Glossmann, A. Hintennach, Y. Wang, P. Redfern, L. A. Curtiss, and Z. Zhang. "Tackling the Issues of Li-S Battery Chemistry by a Functional Additive – Hexafluorobenzene." ACS *Applied Energy Materials* (2019). Pending submission.

TASK 2 – DIAGNOSTICS

Summary and Highlights

To meet the goals of the VTO Multi-Year Program Plan and develop lower-cost, abuse-tolerant batteries with higher energy density, higher power, better low-temperature operation, and longer lifetimes suitable for the next-generation of EVs, hybrid EVs (HEVs), and plug-in hybrid EVs (PHEVs), there is a strong need to identify and understand structure-property-electrochemical performance relationships in materials, life-limiting and performance-limiting processes, and various failure modes to guide battery development activities and scale-up efforts. In pursuit of batteries with high energy density, both high cell operating voltages and demanding cycling requirements lead to unprecedented chemical and mechanical instabilities in cell components. Successful implementation of newer materials such as silicon anode and high-voltage cathodes also requires better understanding of fundamental processes, especially those at the SEI of both anode and cathode.

This Task takes on these challenges by combining model system *ex situ*, *in situ*, and *operando* approaches with an array of state-of-the-art analytical and computational tools. Three subtasks are tackling the chemical processes and reactions at the electrode/electrolyte interface. Researchers at LBNL use *in situ* and *ex situ* vibrational spectroscopy and far- and near-field scanning probe spectroscopy to understand the structure of active materials and the physio-chemical phenomena at electrode/electrolyte interfaces, particularly those of the high-voltage cathodes. GM is developing a number of *in situ* diagnostic techniques, including atomic force microscopy (AFM), nano-indentor, dilatometer, and stress-sensor, to be combined with atomic/continuum modeling schemes to investigate and understand the coupled mechanical/chemical degradation of the SEI layer on Li-metal anode. ANL aims to develop high-conductivity ceramic electrolytes through cation doping and then stabilize the electrode/electrolyte interfaces though co-sintering. Subtasks at Brookhaven National Laboratory (BNL) and PNNL focus on the understanding of fading mechanisms in electrode materials, with the help of synchrotron-based X-ray techniques (diffraction and hard/soft X-ray absorption) at BNL and high-resolution transmission electron microscopy (HRTEM) and spectroscopy techniques at PNNL. UC San Diego (UCSD) is developing advanced diagnostic tools, including scanning transmission electron microscopy / electron energy loss spectroscopy (STEM/EELS), *operando* Bragg coherent diffraction imaging (BCDI), and *ab initio* computation, to probe anion redox and oxygen evolution in Li-excess NMC materials. At LBNL, model systems of electrode materials with well-defined physical attributes are being developed and used for advanced diagnostic and mechanistic studies at both bulk and single-crystal levels. These controlled studies remove the ambiguity in correlating a material's physical properties and reaction mechanisms to its performance and stability, which is critical for further optimization. The final subtask at Stanford University / Stanford Linear Accelerator Center (SLAC) develops and utilizes a correlative X-ray microscopy platform to investigate the lithiation dynamics and understand factors that determine the rate capability and degradation mechanisms in cathode materials. The diagnostics team not only produces a wealth of knowledge that is key to development of next-generation batteries, it also advances analytical techniques and instrumentation that have a far-reaching effect on material and device development in a variety of fields.

Highlights. The highlights for this quarter are as follows:

- LBNL (Chen's group) investigated the effect of surface treatment and found that NH_4F improves discharge capacity, capacity retention, and average voltage retention in cation-disordered rocksalt cathodes. The results suggest that chemical treatment may be an effective mitigation approach to surface-initiated performance degradation in this class of cathode materials.
- UCSD (Meng's group) used cryo transmission electron microscopy (cryo-TEM) to compare the nanostructure of inactive metallic lithium when cycling Li-metal electrode in a high-concentration electrolyte and a commercial carbonate electrolyte. Their results show the formation of different lithium morphologies in the two electrolytes, with significantly less unreacted lithium and higher CE achieved in the high-concentration electrolyte.

- The General Motors team (Xiao, Sheldon, Qi, and Cheng) explored new coating strategies to protect Li-metal electrode, including use of fluorinated polymers through a physical vapor deposition (PVD) process and composite coatings consisting of LiF and a polymer matrix. Their processing effectively suppresses lithium dendrite formation and mossy structure evolution during cycling, largely improving cycle life of Li-metal cells.
- PNNL (Wang's group) used cryo-TEM imaging, energy dispersive spectroscopy (EDS) elemental analysis, and EELS electronic structure analysis to investigate the role of additives and obtain design insights on electrolytes. Their results show that in the presence of vinylene carbonate, electrochemically deposited lithium metal is slightly oxidized, and the SEI adopts a mosaic-like structure, leading to significantly enhanced CE.

Task 2.1 – Model System Diagnostics for High-Energy Cathode Development (Guoying Chen, Lawrence Berkeley National Laboratory)

Project Objective. This project will use a rational, nonempirical approach to design and synthesize next-generation high-energy, high-voltage cathode materials. Combining a suite of advanced diagnostic techniques with model cathode materials and model electrode/electrolyte interfaces, the project will perform systematic studies to achieve the following goals: (1) obtain new insights into solid-state chemistry, particularly cationic and/or anionic redox activities during charge and discharge of high-capacity lithium TM oxides, (2) gain fundamental understanding on cathode/electrolyte interfacial chemistry and charge transfer process as a function of operating voltage, (3) reveal performance- and stability-limiting properties and processes in high-energy, high-voltage cathodes, and (4) develop strategies to mitigate the structural and interfacial instabilities.

Impact. The project will improve the commercial viability of next-generation high-energy cathode materials. The findings will enable more stable high-voltage cycling of existing Li-TM oxides as well as development of novel high-capacity cathode materials for advanced Li-ion batteries.

Approach. The project will prepare crystal samples of Li-stoichiometric and Li-excess TM oxides with well-defined physical attributes. It will perform advanced diagnostic and mechanistic studies at both bulk and single-crystal levels. Global properties and performance of the samples will be established from the bulk analyses, while the single-crystal-based studies will utilize time and spatially resolved analytical techniques to probe the material redox transformation process and failure mechanisms under battery operating conditions.

Out-Year Goals. In the out-years, the project will obtain fundamental knowledge on performance-limiting physical properties, phase transition mechanisms, parasitic reactions, and transport processes that prevent cathode materials from delivering higher capacities and achieving more stable cycling at high voltages. It will develop approaches to mitigate cathode structural and interfacial instabilities during high-voltage operation. Further, it will design and synthesize optimized Li-TM oxide cathodes as well as novel high-energy electrode materials.

Collaborations. This project collaborates with the following: G. Ceder, K. Persson, M. Doeff, B. McCloskey, and P. Ross (LBNL); V. Srinivasan (ANL); D. Nordlund and Y. Liu (Stanford Synchrotron Radiation Lightsource, SSRL); C. Wang (PNNL); C. Grey (University of Cambridge); and A. Huq and J. Nanda (Oak Ridge National Laboratory, ORNL).

`Milestones

1. Understand the interplay between cationic and anionic redox processes in model TM oxides. (Q1, FY 2019; Completed)
2. Characterize interfacial processes and surface changes on anion-active model oxides. (Q2, FY 2019; Completed)
3. Evaluate the effect of particle size/morphology on oxygen redox chemistry and kinetics. (Q3, FY 2019; Completed)
4. Develop design strategies to improve performance of anion-active oxide cathodes. (Q4, September 2019; Completed)

Progress Report

Previous studies performed on a series of model Li-excess TM rocksalt compounds, $Li_{1.4-x}M_{0.4-x}Mn_{0.2+2x}O_2$ (M = d^0 TM), revealed that degradation of cation-disordered cathode originates from surface densification. During charge, the creation of oxygen vacancies on the surface leads to a destabilized rocksalt lattice where the uncoordinated TM cations are reduced and, subsequently, migrate into the neighboring vacancy sites left by the extracted Li^+. This leads to a densified surface layer with fewer lithium vacancies and lower TM oxidation state compared to the bulk. On discharge, lithium cations are reinserted into the oxide, but the surface has lower lithium content due to the densification and loss of lithium sites. This process continues in the following cycles and further degrades the original percolating network for Li^+ transport, accompanied by the progression of reduced TM and increased lithium resistivity from the surface to the bulk (Figure 22). The proposed degradation mechanism suggests that surface is critical in cathode stability and proper surface treatment may alleviate the performance issues in this class of cathode materials.

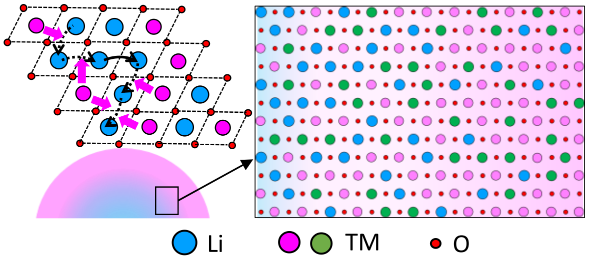

Figure 22. An illustration of the surface-to-bulk densification mechanism. The combination of bulk transition metal reduction and lithium percolation network deterioration renders inaccessible redox couples and performance decay in the rocksalt cathodes.

This quarter, surface modification was explored as a mitigation approach. Two types of coating materials, AlF_3 and NH_4F, were selected to coat the surface of cation-disordered $Li_{1.3}Nb_{0.3}Mn_{0.4}O_2$ (LNMO). AlF_3 was first prepared by solution precipitation from a mixture of $Al(NO_3)_3$ and NH_4F and then annealed in an Ar-purged tube furnace at 400°C for 5 h. The resulting powder was mixed with LNMO (at a 2.5 wt% loading) and ball milled for 12 h. A similar procedure was used to prepare NH_4F-treated LNMO, where 5 wt% of NH_4F was used. Figure 23 compares the electrochemical performance of the pristine and two coated LNMO samples during the first 30 cycles at a current density of 10 mA/g. These samples are labeled as LNMO, LNMO_AlF_3, and LNMO_NH_4F, respectively. Compared to the pristine LNMO cathode material (Figure 23a), AlF_3 coating largely enhances the first-cycle discharge capacity, from ~ 275 to 300 mAh/g (Figure 23b). While the effect on capacity retention is nearly nonexistent (Figure 23e), improvement was seen on retention of average discharge voltage (Figure 23f). For LNMO_NH_4F, ~ 320 mAh was obtained during the first discharge (Figure 23c), more than 16% improvement from the pristine LNMO. Furthermore, significant improvement was observed on both discharge capacity retention as well as average discharge voltage retention.

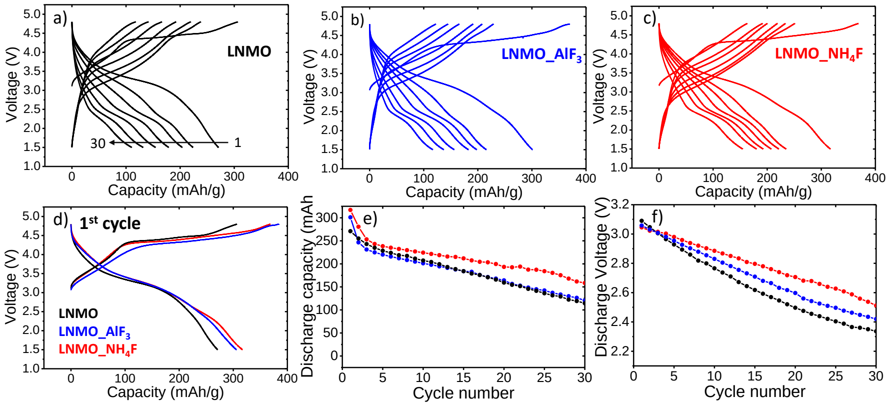

Figure 23. Effect of surface coating on LNMO cathode performance. (a-c) Voltage profiles of LNMO, LNMO_AlF_3, and LNMO_NH_4F during the first 30 cycles (plotted in every 5 cycles), respectively. (d) First-cycle voltage profile comparison of the LNMO cathodes. (e/f) Discharge capacity and average discharge voltage of the LNMO cathodes as a function of cycle number, respectively. Charge and discharge current density is 10 mA/g.

While both AlF_3 and NH_4F coatings lead to a similarly extended first-cycle charging plateau (Figure 23d), which suggests enhanced oxygen contribution in capacity, the latter is shown to be a much more effective treatment in enhancing performance of LNMO. Considering its chemical stability, AlF_3 treatment on LNMO surface largely provides a physical barrier to the electrolyte, although some chemical interactions may also exist. On the other hand, NH_4F is thermally unstable, dissociating to NH_3 and HF during the heating process of sample preparation. Both are gaseous products and capable of chemically modifying LNMO surface. Particularly, HF is known to etch oxide surface and create additional surface area and new pathways for lithium transport and oxygen redox activities. It appears that the chemical modification process is more beneficial than physical, as better performance was achieved on LNMO_NH_4F. Although further understanding in the coating effect is necessary, results show that chemical treatment may be an effective mitigation approach to surface-initiated performance degradation in the rocksalt cathodes.

Patents/Publications/Presentations

Publications

- Chen, D., J. Wu, J. K. Papp, B. D. McCloskey, W. Yang, and G. Chen. "Role of Redox-Inactive Transition-Metals in the Behavior of Cation-Disordered Rocksalt Cathodes." Submitted (2019).
- Shen, H., E. Yi, M. Amores, L. Cheng, N. Tamura, D. Y. Parkinson, G. Chen, K. Chen, and M. M. Doeff. "Oriented Porous LLZO 3D Structures Obtained by Freeze Casting for Battery Applications." *Journal of Materials Chemistry A.* doi: 10.1039/C9TA06520B (2019).

Presentation

- ACS Fall National Meeting, San Diego, California (August 25–29, 2019): "Development of Li-Rich Cation-Disordered Rocksalts as High-Energy Cathodes"; G. Chen. Invited.

Task 2.2 – Interfacial Processes – Diagnostics
(Robert Kostecki, Lawrence Berkeley National Laboratory)

Project Objective. This collaborative project will develop and apply advanced experimental methodologies to study and understand the mechanism of operation and degradation of high-capacity materials for rechargeable cells for PHEV and EV applications. The objective is to develop and apply *in situ* and *ex situ* far- and near-field optical multi-functional probes and synchrotron-based advanced X-ray techniques to obtain detailed insight into the active material structure and physio-chemical phenomena at electrode/electrolyte interfaces at a spatial resolution corresponding to the size of basic chemical or structural building blocks. Through an integrated synthesis, characterization, and electrochemistry effort, the project aims to develop a better understanding of electrode and electrolyte materials so that rational decisions can be made as to their further development into commercially viable cathode materials.

Project Impact. Instability and/or high resistance at the interface of battery electrodes limits electrochemical performance of high-energy density batteries. A better understanding of the underlying principles that govern these phenomena is inextricably linked with successful implementation of high-energy-density materials in Li-based cells for PHEVs and EVs. Pristine and cycled composite and thin-film model electrodes are investigated using state-of-the-art techniques to identify, characterize, and monitor changes in materials structure and composition that take place during battery operation and/or storage. The proposed work constitutes an integral part of the concerted effort within the BMR Program, and it supports development of new electrode materials for high-energy, Li-metal-based rechargeable cells.

Approach. The pristine and cycled composite electrode and model thin-film electrodes will be probed using various surface- and bulk-sensitive techniques, including Fourier transform infrared spectroscopy (FTIR), attenuated total reflectance (ATR)–FTIR, near-field infrared (IR) and Raman spectroscopy and microscopy, and scanning probe microscopy to identify and characterize changes in materials structure and composition. Novel *in situ / ex situ* far- and near-field optical multi-functional probes in combination with standard electrochemical and analytical techniques are developed to unveil the structure and reactivity at interfaces and interphases that determine materials electrochemical performance and failure modes.

Out-Year Goals. In the out-years, the project aims to (1) understand the factors that control charge/discharge rate, cyclability, and degradation processes, (2) design and apply new diagnostic techniques and experimental methodologies capable of unveiling the structure and reactivity at hidden or buried interfaces and interphases that determine material, composite electrode, and full-cell electrochemical performance and failure modes, and (3) propose effective remedies to address inadequate Li-metal-based battery calendar/cycle lifetimes for PHEV and EV applications.

Collaborations. Electrode materials and composite solid electrolytes tested under different cycling regimes by V. Battaglia and M. Doeff (LBNL) will be studied. The diagnostic studies will be carried out in sync with other diagnosticians in this research program.

Milestones

1. Manufacture model thin-film and composite LLZO and lithium thiophosphate (LPS) SSEs by pulsed laser deposition (PLD) as model systems for fundamental electrochemical studies of Li-metal battery systems. (Q1, FY 2019; Completed)
2. Characterize the bulk and surface structure of lithium anode, NMC cathode electrodes, and SSEs and the relationship to electrochemical and interfacial properties. (Q2, FY 2019; Completed)

3. Characterize the chemistry of SSE/Li and electrolyte/cathode interfaces with *ex situ* near-field IR, X-ray absorption spectroscopy (XAS), and XPS. (Q3, FY 2019; Completed)
4. Design and develop new XAS/XPS experimental setup to characterize *in situ* solid/solid (for example, NMC/SSE and Li/SSE) interfaces. *Go/No-Go Decision*: Demonstrate feasibility of *in situ* measurements of solid-solid electrochemical interfaces. (Q4, FY 2019; Completed)

Progress Report

This quarter, the team characterized the surface structure and chemical composition of a carbon-nitrogen modified stainless steel mesh (CNSSM) with Raman and XPS. The morphology of plated lithium on CNSSM was investigated with XRT.

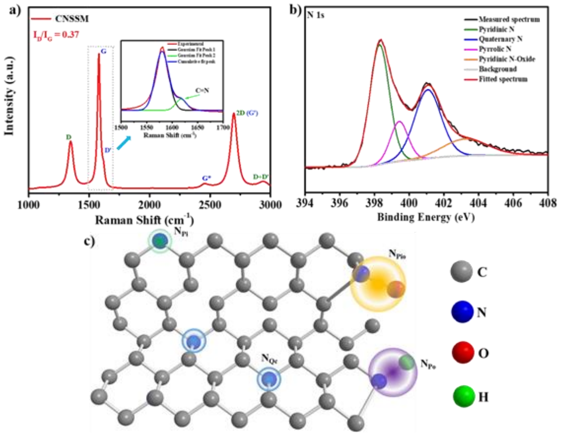

Figure 24. (a) Raman spectrum carbon-nitrogen modified stainless steel mesh (CNSSM); the inset shows the fitted peaks between 1500 cm^{-1} and -1700 cm^{-1}. (b) N1s X-ray photoelectron spectrum and corresponding peak fitting. (c) Schematic representation of the carbon structure with different types of nitrogen atoms doping (NPi: Pyridinic-N; NPo: Pyrrolic-N; NQc: Quaternary-N (center); and NPio: Pyridinic-N oxide).

Figure 24a shows the first-order Raman spectrum of the CNSSM. Two bands, at ~1345 cm^{-1} and ~1570 cm^{-1}, correspond to the D- and G-bands of carbon, respectively. The G-band originates from in-plane vibrations of graphene sheets in graphitic carbons, whereas D-band corresponds to the breathing motion of sp^2-hybridized carbon atoms in rings at edge planes and defects in the graphene sheet in disordered and amorphous carbons. The relatively high I_D/I_G ratio (0.37) in this case implies a relatively large ratio of disordering in the CNSSM outer layer, which may originate from nitrogen doping. The shoulder of the D-band (that is, the D-band at 1638 cm^{-1} in the inset), originates from the intra-valley double-resonance in the presence of nitrogen-induced defects.

Figure 25a-b compares virtual cross-sections reconstructed from the nano-tomographic measurements for both a pristine CNSSM-Li composite and a CNSSM-Li composite after 2 h of lithium electrodeposition at 1 mA cm^{-2}. The bright areas in the lithium metal correspond to internal cracks, likely due to the manufacturing process of the CNSSM-Li composite. The stainless steel rod exhibits coaxial layers, in agreement with the

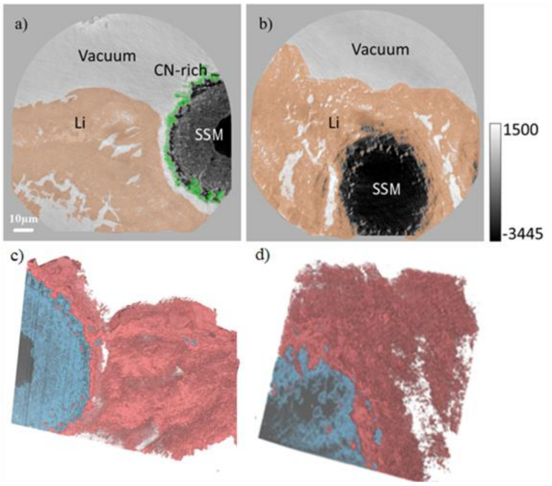

Figure 25. Virtual cross-sections from X-ray holographic nano-tomography on (a) pristine carbon-nitrogen modified stainless steel mesh – lithium (CNSSM-Li) composite. (b) CNSSM-Li composite after 2 h of lithium electrodeposition at 1 mA cm^{-2}. The scale bar of electro density applies to all panels. Rendering of the 3D tomographic reconstructed results from (c) pristine CNSSM-Li composite, and (d) CNSSM-Li composite after 2 h of lithium electrodeposition at 1 mA cm^{-2}. Li: lithium metal (coral); CNSSM: carbon-nitrogen modified stainless steel (pale blue); and SSM: stainless steel (dim gray).

SEM cross-sections. The external carbon-nitrogen coated layer, of ~ 1 µm in thickness can be seen, as can the unmodified residual (black) stainless steel at the core of the wire. Most importantly, it can be seen that a significant amount of lithium has been plated, and the mesh is fully embedded into the deposit.

The team also worked on upgrading the XPS system to prepare it for studies of interfaces in all-solid-state batteries. The sample holder and the manipulator were modified to enable *in operando* characterization. An additional pumping system will be added to the load-lock to accelerate samples turnover and enhance measurements throughput. This report summarizes efforts toward Milestone 4.

Patents/Publications/Presentations

Publications

- Cabo-Fernandez, L., A. Neale, F. Braga, I. Sazanovich, R. Kostecki, and L. Hardwick. "Kerr Gated Raman Spectroscopy of a $LiPF_6$-Based Organic Carbonate Electrolyte for Li-Ion Batteries." *Physical Chemistry Chemical Physics*. doi: 10.1039/C9CP02430A.
- "Uniform Lithium Nucleation and Electrodeposition for Stable 'Dendrite'-Free Lithium-Metal Batteries." *Nano Energy*. Accepted.

Task 2.3 – Advanced *In Situ* Diagnostic Techniques for Battery Materials (Xiao-Qing Yang and Seong-Min Bak, Brookhaven National Laboratory)

Project Objective. The primary objective of this project is to develop new advanced *in situ* material characterization techniques and to apply these techniques to support development of new cathode and anode materials with high energy and power density, low cost, good abuse tolerance, and long calendar and cycle life for beyond Li-ion battery systems to power PHEVs and battery electric vehicles (BEVs). The diagnostic studies will focus on issues relating to capacity retention, thermal stability, cycle life, and rate capability of beyond Li-ion battery systems.

Project Impact. The VTO Multi-Year Program Plan describes the goals for battery: "Specifically, lower-cost, abuse-tolerant batteries with higher energy density, higher power, better low-temperature operation, and longer lifetimes are needed for development of the next-generation of HEVs, PHEVs, and EVs." The knowledge gained from diagnostic studies through this project will help U. S. industries develop new materials and processes for next-generation Li-ion batteries in the effort to reach these VTO goals.

Approach. This project will use the combined synchrotron-based *in situ* X-ray techniques (XRD; and hard and soft XAS) with other imaging and spectroscopic tools such as HRTEM and MS to study the mechanisms governing performance of electrode materials.

Out-Year Goals. In the out years, the project will complete development of diagnostic techniques using X-ray pair distribution function (x-PDF), XRD, and XAS combined with neutron diffraction and neutron PDF (n-PDF), as well as STEM imaging and transmission X-ray microscopy (TXM) for cathode materials studies. It will then apply these techniques to study the structural changes of various new cathode and anode materials.

Collaborations. The BNL team will work closely with material synthesis groups at ANL (Drs. Shin and Amine) for the high-energy composite and at PNNL for the S-based cathode and Li-metal anode materials, and with ORNL on neutron scatterings. This project will also collaborate with industrial partners at GM and Johnson Controls, as well as with international collaborators.

Milestones

1. Complete the *ex situ* soft x-ray absorption (sXAS) studies at oxygen K-edge of novel organic disulfide cathode material (1,2,4,5,6,7,9,10-octathia bis cyclopenta antraquinone-3,8-dithone, or TPQD) for Li-S batteries at different charged and discharged states. (Q1, FY 2019; Completed)
2. Complete the *ex situ* sXAS studies at sulfur K-edge of novel organic disulfide cathode material (TPQD) for Li-S batteries at different charged and discharged states. (Q2, FY 2019; Completed)
3. Complete XAS studies of sulfur electrode harvested from failed high-energy Li/S pouch cells after multiple cyclings. (Q3, FY 2019; Completed)
4. Complete the spatially resolved XAS at sulfur K-edge and imaging of sulfur-based chemical species using X-ray fluorescence microscopy (XRF) on the Li-metal anode in a cycled high-energy Li/S pouch cell. (Q4, FY 2019; Completed)

Progress Report

This quarter, the team completed milestone 4. BNL has been focused on the *ex situ* X-ray microprobe. XRF and sulfur K-edge XAS studies of high energy density Li-S pouch cells. Chemical information of the sulfur species regarding composition and distribution was studied using XRF. Figure 26 depicts XRF and XAS spectra results from R1-R3 regions of the cycled Li-metal anode. Figure 26 also shows the XRF image collected at R1 (7×7 mm) below an energy of 2469 eV, which only detects sulfur species with relatively low absorption energies. Apparently, this area is covered mainly by the low-valence sulfur species (in yellow color), with randomly distributed uncovered spots (in blue color). Further XAS analysis reveals that the low-valence sulfur species (from yellow area) are composed of lithium polysulfides and lithium sulfides; meanwhile, the high valent species (from blue spots) are mainly sulfone and sulfate. When the X-ray beam energy is increased to 2480 eV, more sulfur species with a wider valence range from S^{2-} to S^{4+} can be detected. In contrast to XRF at 2469 eV, more uniform mapping was observed at 2480 eV. It means that the whole R1 area is evenly covered by sulfur species with a wider valance range. Sulfur, poly sulfide, Li_2S, SO_3^{2-}, $COSO_2^-$, and SO_4^{2-} could be observed from the Li-metal anode side. This indicates the shuttling effect of lithium polysulfide as well as SEI formation with sulfur-contained electrolyte (also, heterogeneity of state of charge). Similarly to the cathode results reported last quarter, the middle part of the Li-metal anode side also shows more heterogeneous distribution of sulfur species. Region 3, the region furthest from the tab, shows much more uniform chemical distribution.

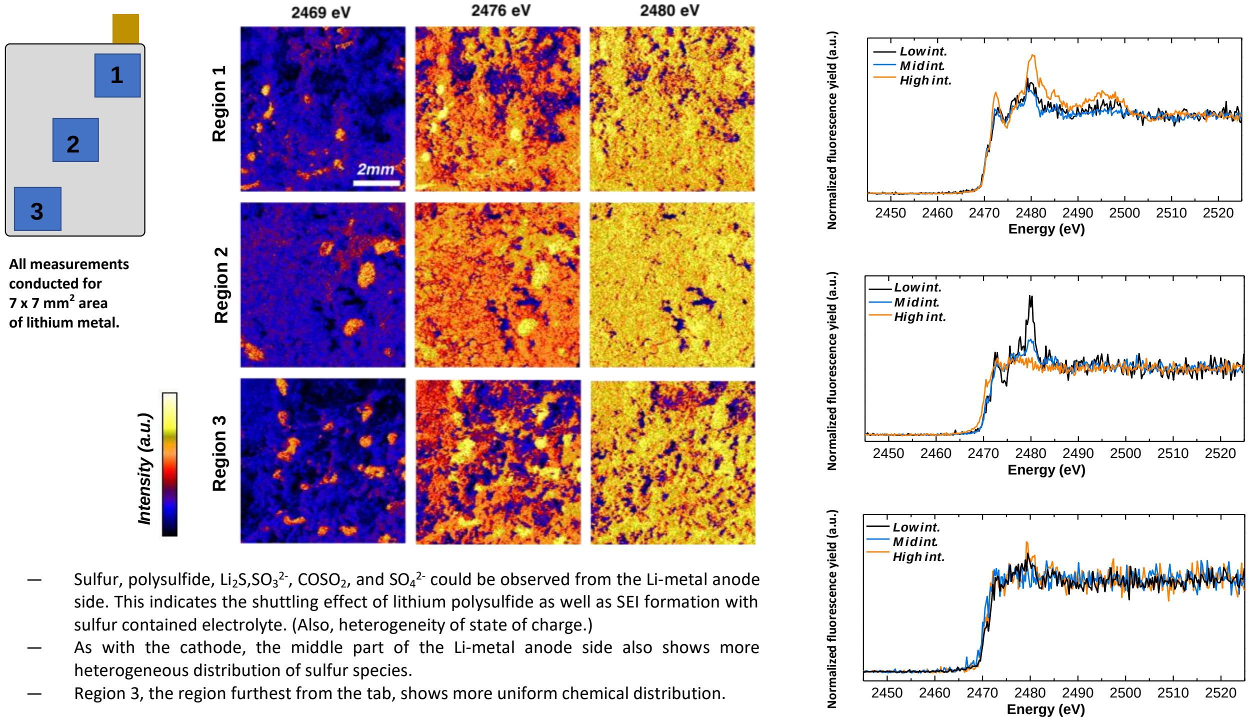

- Sulfur, polysulfide, Li_2S,SO_3^{2-}, $COSO_2$, and SO_4^{2-} could be observed from the Li-metal anode side. This indicates the shuttling effect of lithium polysulfide as well as SEI formation with sulfur contained electrolyte. (Also, heterogeneity of state of charge.)
- As with the cathode, the middle part of the Li-metal anode side also shows more heterogeneous distribution of sulfur species.
- Region 3, the region furthest from the tab, shows more uniform chemical distribution.

Figure 26. Spatially resolved X-ray absorption spectroscopy and X-ray fluorescence microscopy imaging for cycled Li-metal anode (inner side).

Patents/Publications/Presentations

Publications

- Li, S., S-J. Lee, X. Wang, W. Yang, H. Huang, D. S. Swetz, W. B. Doriese, G. C. O'Neil, J. N. Ullom, C. J. Titus, K. D. Irwin, H-K. Lee, D. Nordlund, P. Pianetta, C. Yu, J. Qiu, X. Yu, X-Q. Yang, E. Hu,* J-S. Lee*, and Y. Liu.* "Surface-to-Bulk Redox Coupling through Thermally Driven Li Redistribution in Li- and Mn-Rich Layered Cathode Materials." *Journal of American Chemical Society*. doi: 10.1021/jacs.9b05349, Publication Date (Web): July 9, 2019.
- Liu, S., Z. Liu, X. Shen, X. Wang, S-C. Liao, R. Yu, Z. Wang,* Z. Hu, C-T. Chen, X. Yu, X. Yang, and L. Chen. "Li–Ti Cation Mixing Enhanced Structural and Performance Stability of Li-Rich Layered Oxide." *Advanced Energy Materials*. doi: 10.1002/aenm.201901530, Publication Date (Web): July 15, 2019.
- Zhao, E., M. Zhang, X. Wang, E. Hu, J. Liu,* X. Yu,* M. Olguin, T. A Wynn, Y. S. Meng,* K. Page, F. Wang, H. Li, X-Q. Yang, X. Huang, and L. Chen. "Local Structure Adaptability through Multi Cations for Oxygen Redox Accommodation in Li-Rich Layered Oxides." *Energy Storage Materials*. doi: 10.1016/j.ensm.2019.07.032, Publication Date (Web): July 25, 2019.
- Deng, T., X. Fan,* L. Cao, J. Chen, S. Hou, X. Ji, L. Chen, S. Li, X. Zhou, E. Hu, D. Su, X-Q. Yang, and C. Wang.* "Designing *In-Situ*-Formed Interphases Enables Highly Reversible Cobalt-Free $LiNiO_2$ Cathode for Li-Ion and Li-Metal Batteries." *Joule*. doi: 10.1016/j.joule.2019.08.004, Publication Date (Web): September 4, 2019.

Task 2.4 – Advanced Microscopy and Spectroscopy for Probing and Optimizing Electrode-Electrolyte Interphases in High-Energy Lithium Batteries
(Y. Shirley Meng, University of California at San Diego)

Project Objective. The proposed research aims to develop advanced microscopy and spectroscopy tools to probe, understand, and optimize the anion activities that govern the performance limitations such as capacity and voltage stabilities in high-energy Li-excess TM (such as nickel, cobalt, manganese) oxides cathode materials. The approach uniquely combines atomic resolution STEM, EELS, *operando* BCDI, and first-principles computation to probe anion redox and oxygen evolutions in Li-excess NMC materials. Furthermore, the project will track the lithium and oxygen dynamics under electrochemical testing via *operando* neutron diffraction, which will enhance understanding of the overall structural changes due to anion activities. Ultimately, this will home in on the synthesis efforts to produce the modified materials with optimum bulk compositions and surface characteristics at large scale for consistently good performance. The above-mentioned characterization tools will be extended to diagnose various anode types, such as Li-metal anode.

Project Impact. If successful, this research will enable *operando* imaging at the single-particle level by advanced microscopy imaging and high-energy-resolution oxygen K-edge EELS. This work will provide an in-depth understanding of anion activities in high-voltage electrode materials, which can lead to significant improvement in stabilizing operation voltage and electrode-electrolyte interface for future generation high-energy-density electrodes.

Approach. This unique approach combines STEM/EELS, *operando* BCDI, and *ab initio* computation as diagnostic tools for probing anion redox and oxygen evolutions in Li-excess NMC materials. This allows for pinning down the atomistic/molecular mechanism of anion oxidation and determining the speciation compositions and surface characteristics for enabling high rate and long life in the proposed materials. Neutron enables the characterization of bulk material properties to enhance and further optimize high-energy electrode materials.

Out-Year Goals. The goal is to improve the cycle life and efficiency of Li-excess NMC materials through the modification of both the cathode and the electrolyte. Single particle behavior of the modified Li-excess NMC with new electrolytes will be characterized.

Collaborations. This work funds collaborations on EELS (M. Chi, ORNL), neutron diffraction (K. An, ORNL), and sXAS (M. Doeff, LBNL). It supports collaborative work with Z. Liu and Y. Xia at Ningbo Institute of Materials Technology and Engineering in China. It also supports collaboration with the Battery500 Consortium.

Milestones

1. Benchmarking new electrolyte performance with the optimized Li-excess materials. (Q1, FY 2019; Completed)
2. Conducting XPS characterization of anion evolution on modified Li-excess NMC. (Q2, FY 2019; Completed)
3. Carrying out STEM/EELS characterization on modified Li-excess NMC single particle using optimized electrolyte. (Q3, FY 2019; Completed)
4. Performing EELS and XPS characterization of SEI on electrochemically deposited lithium metal with new electrolyte systems. (Q4, FY 2019; Completed)

Progress Report

Cryo-EM and XPS Comparison of Cycled Li-Rich Layered Oxides in Different Electrolyte

As described in the previous report, a novel electrolyte with LiBOB additive (lithium bis(oxalato) borate) is introduced to further optimize electrochemical performance of modified $Li[Li_{0.144}Ni_{0.136}Co_{0.136}Mn_{0.544}]O_2$ (denoted as LR-NCM). LR-NCM cycled in 2% LiBOB exhibits better cycling stability compared with that of LR-NCM cycled in the baseline electrolyte. To explain the performance improvement, the cathode-electrolyte interphase (CEI) structure and chemistry were characterized with cryo-TEM and XPS. Note that TEM under cryo temperature is necessary to preserve CEI structure/ chemistry and avoid electron beam damage. After the 50th discharge, the CEI structure in the baseline electrolyte, shown in Figure 27a, exhibits significant variations in thickness and uniformity, with open sections of minimal coverage allowing direct exposure of the electrolyte to the cathode particle surface. Conversely, the CEI generated on the LR-NCM particle after 50 cycles with the 2% LiBOB appears much more uniform in thickness and conformal in surface coverage (Figure 27b). XPS was then conducted to the pristine LR-NCM electrode and LR-NCM after different cycles in different electrolyte. Figure 27c shows the XPS C1s spectra where four different carbon types are detected, including C-C peak at 284.8 eV, C-O peak at 286.5 eV, O-C=O peak at 289.0 eV, and C-F (from PVDF) at 291.1 eV. A noticeable feature for the cathode cycled in 2% LiBOB is the appearance of the 289.0 eV peak. This can be attributed to the semicarbonate species produced by the LiBOB decomposition, indicating formation of a stable CEI layer. This is in approximate agreement regarding thickness with another CEI study (*Electrochimica Acta* 104 (2013): 170–177), albeit for a different cathode material and lower voltage cutoff. Due to this stable CEI layer, the cycling performance of LR-NCM is largely improved with the LiBOB additive.

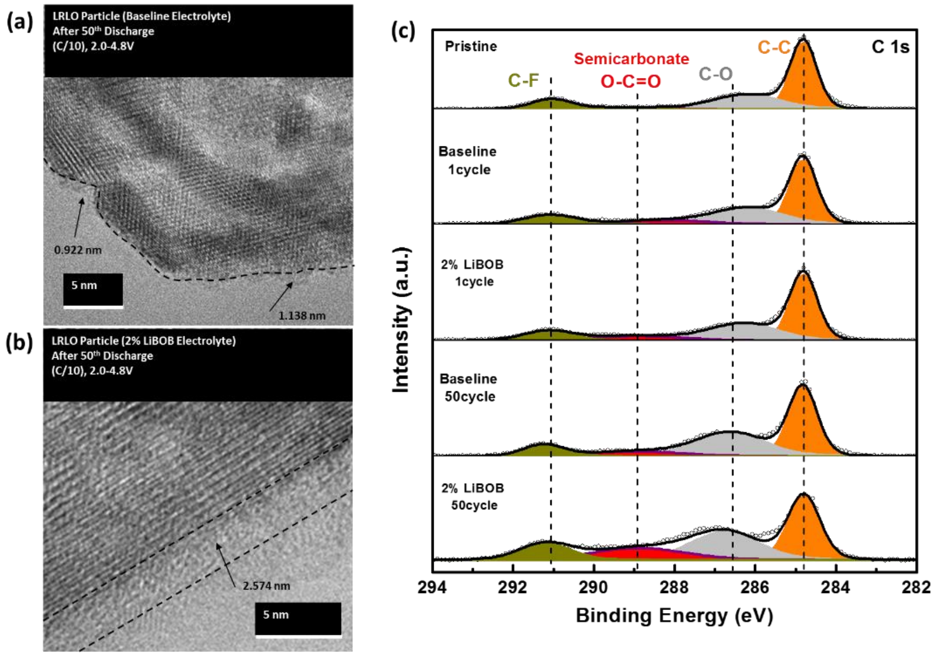

Figure 27. Cryo transmission electron microscopy images of the (a) cycled LR-NCM in the baseline electrolyte and (b) cycled LR-NCM in 2% lithium bis(oxalato) borate (LiBOB) electrolyte. (c) X-ray photoelectron spectra of the pristine and cycled LR-NCM in the baseline electrolyte or in 2% LiBOB electrolyte.

Characterization of SEI on Electrochemically Deposited Lithium Metal with New Electrolyte Systems

As the CE of lithium metal varies greatly with electrolyte properties and current density, the team compared two representative electrolytes, a high-concentration electrolyte (HCE; 4 M lithium bis(fluoro sulfonyl)imide (LiFSI) and 2 M lithium bis(trifluoromethane sulfonyl)imide (LiTFSI) in DME) and a commercial carbonate electrolyte (CCE; 1 M $LiPF_6$ in EC/EMC), at three stripping rates (0.5 mA cm^{-2}, 2.5 mA cm^{-2}, and 5.0 mA cm^{-2}; all plating at 0.5 mA cm^{-2} for 2 h). To elucidate the formation mechanism of inactive lithium, the team uses cryo-TEM to explore the nanostructure of the inactive lithium in HCE and CCE after stripping at 0.5 mA cm^{-2}. Sheet-like inactive lithium appears in the HCE sample (Figure 28a), whereas inactive lithium in the CCE retains a whisker-like morphology (Figure 28e). Based on the (110) lattice plane distance of body-centered cubic lithium, the region that contains crystalline metallic Li^0 is highlighted in green in the HRTEM images for both electrolytes (Figure 28b/f). Compared with the inactive lithium obtained from CCE, a much smaller area of metallic Li^0 component is observed in HCE. This indicates that most of the deposited metallic Li^0 in HCE has been successfully stripped, corresponding to the high CE. Whisker-like unreacted metallic Li^0 up to about 80 nm in length remains in the CCE sample and is well isolated by the surrounding SEI. The SEI components were determined by matching the lattice spacing in HRTEM images with their fast Fourier transform (FFT) patterns (Figure 28c/g). Consistent with the XPS results (Figure 28d/h), Li_2CO_3 and Li_2O constitute the majority of the SEI, which also contains LiF as well as other amorphous organic species for both electrolytes. Further examining the SEI components in HCE and CCE by XPS, the team found that stripping rates have negligible impact on the relative contributions from SEI components. The cryo-TEM analysis and XPS results indicate that the contribution from the SEI Li^+ to the global content of inactive lithium is not as large as commonly believed from previous studies.

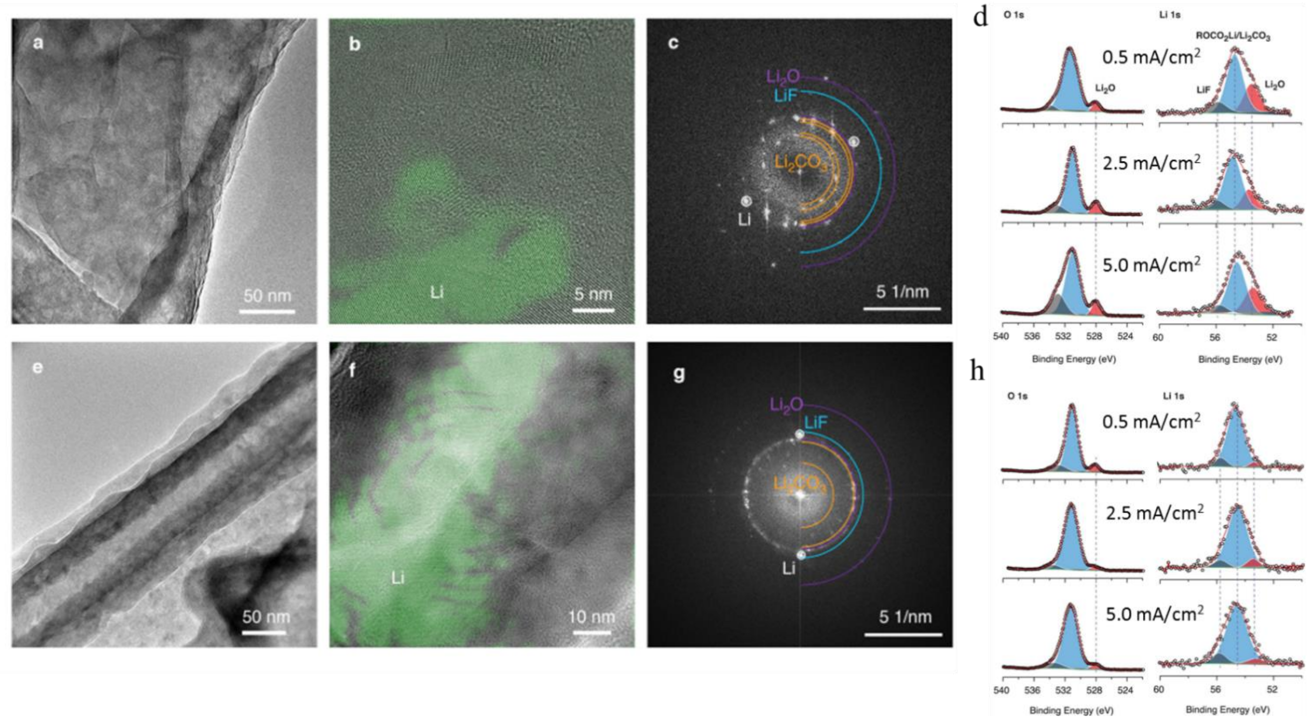

Figure 28. (a-c) Results for high-concentration electrolyte (HCE). (e-g) Results for commercial carbonate electrolyte (CCE). (a/e), Inactive lithium morphology at low magnifications for both electrolytes. (b/f) High-resolution transmission electron microscopy (HRTEM) shows that a different amount of metallic Li^0 is wrapped by SEI in the two types of electrolyte. (c/g) Fast Fourier transform patterns of corresponding HRTEM indicate the SEI component, which contains crystalline Li_2CO_3, Li_2O, and LiF. (d/h) X-ray photoelectron spectroscopy analysis of inactive lithium SEI components formed in HCE (d) and CCE (h) for various stripping rates.

Patents/Publications/Presentations

Publications

- Zhao, E., M. Zhang, Y. S. Meng, et al. "Local Structure Adaptability through Multi Cations for Oxygen Redox Accommodation in Li-Rich Layered Oxides." *Energy Storage Materials* (2019). In print.
- Qiu, B., M. Zhang, Y. S. Meng, et al. "Structural Metastability and Reversibility in Anionic Redox-Based Cathode for Next Generation High Energy Rechargeable Battery." *Cell Reports Physical Science* (2019). Under review.

Presentations

- ACS Fall National Meeting, San Diego, California (August 25–29, 2019): "Oxygen Redox Activities in Li-Rich Layered Oxides: Pushing the Limit of Intercalation"; Y. S. Meng and M. Zhang. Invited.
- Electrochemical Conference on Energy and the Environment (ECEE): Bioelectrochemistry and Energy Storage, Glasgow, Scotland (July 21–26, 2019): "Mitigating Oxygen Release in Anionic-Redox-Active Cathode Materials through Rational Design"; Y. S. Meng. Invited.

Task 2.5 – *In Situ* Diagnostics of Coupled Electrochemical-Mechanical Properties of Solid Electrolyte Interphases on Lithium-Metal Rechargeable Batteries

(Xingcheng Xiao, General Motors; Brian W. Sheldon, Brown University; Yue Qi, Michigan State University; and Y. T. Cheng, University of Kentucky)

Project Objective. The project objective is to develop a comprehensive set of *in situ* diagnostic techniques combined with atomic/continuum modeling schemes to investigate and understand the coupled mechanical/chemical degradation of the SEI layer / lithium system during lithium cycling. The goal of this understanding is to develop a new coating design strategy to achieve dendrite-free, high-cycle efficiency and extend the cycle life of high-energy-density batteries with lithium as the anode for EV application.

Project Impact. The fundamental understanding of the coupled mechanical/chemical degradation of the SEI layer during lithium cycling will enable the project to identify the desirable mechanical properties on SEI/lithium as a system and also the specific transport properties that enable the homogenous lithium stripping/plating while avoiding the mossy structure. Furthermore, it will allow the project to develop a highly impactful strategy to protect lithium metal and achieve dendrite-free high cycle efficiency, which can dramatically increase the energy density of lithium batteries for EV applications.

Approach. Different *in situ* techniques, including AFM, nano-indentor, dilatometer, and stress-sensor, will be developed to investigate the mechanical compatibility between SEI and soft lithium and the relationship between surface morphology and current density distribution that results in an inhomogeneous lithium plating/stripping process. Multiple strategies will be developed to tailor the mechanical and transport properties of SEI and to properly engineer the protective coating / lithium interface.

Out-Year Goals. The out-year goals involve using *in situ* electrochemical tools to reveal failure mechanisms of SEI/lithium as a whole electrode system, including correlating mechanical failure mechanisms of SEI/lithium, morphology evolution, cycle efficiency, and transport properties of SEI. Then, the project will develop continuum framework to establish the failure modes of SEI layer on lithium metal and provide the governing mechanical/material properties of SEI responsible for the critical failure mode based on the experimental results and atomic-scale simulation.

Collaborations. Prof. H. Gao (Brown University) and Dr. Q. Zhang (GM) will be the key researchers involved in continuum simulation and postmortem analysis. Dr. C. Wang (PNNL), Dr. W. Yang (LBNL), and Dr. J. Xiao (PNNL) will be collaborators on advanced *in situ* analysis and electrolyte additives.

Milestones

1. Determine coating design window required to achieve mechanically stable coating on lithium metal. (Q1, FY 2019; Completed)
2. Determine impact of stress on morphological evolution of coated Li-metal surface, and identify failure modes of protective coatings on lithium. (Q2, FY 2019; Completed)
3. Vary coating modulus and investigate its impact on interfacial strength and cycle efficiency, and develop coating with desirable mechanical and transport properties. (Q3, FY 2019; Completed)
4. Establish a design strategy of protective coatings as artificial SEI on Li-metal electrode to achieve high cycle efficiency (> 99.8%). (Q4, FY 2019; Completed)

Progress Report

Established New Coating Strategy to Protect Li-Metal Electrode. Dendrite growth and low cycle efficiency, due to the unstable SEI formed on lithium surface, have been the major bottleneck to practical applications, particularly for EVs. Protective coatings as the artificial SEI layer on lithium metal have been extensively investigated to tackle those two issues. Due to the electrochemical and mechanical incompatibility between soft lithium metal and protective coating, the cycling stability of the coated lithium electrodes with targeted energy density still cannot meet the requirements for EV applications. In this new coating strategy, the team applied a PVD process to coat fluorinated polymers on lithium metal and form an artificial SEI layer by the defluorination reaction between the polymer and lithium. In this process, the ionized C-F fragments from the radio-frequency plasma react with lithium metal spontaneously on reaching lithium surface, resulting in a unique composite coating where nano-sized Li-F crystals are embedded in carbonaceous matrix. The defluorination-derived artificial SEI layer effectively suppresses dendrite formation and mossy structure evolution during cycling. The cycle life is dramatically increased in both carbonate and ether-based electrolytes even under a harsh test condition (1 mA/cm^2 of current density and 4 mAh/cm^2 of capacity equivalent to 20 μm of lithium).

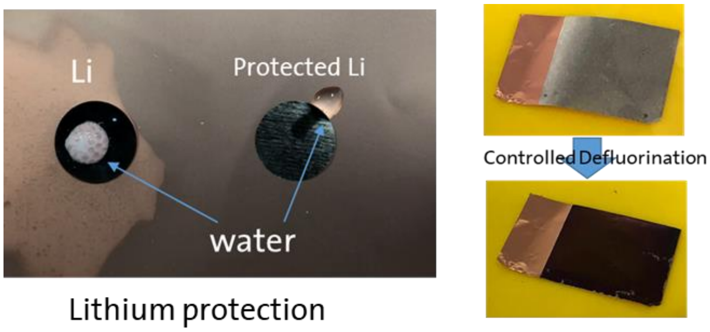

Figure 29. The molecular structure of the polymer coating for protecting lithium. The optical images show that the coating can protect lithium reaction with water.

In addition, the team developed a composite coating that consists of LiF and polymer matrix to protect Li-metal electrode. The coating is derived from the defluorination reaction between lithium metal and fluoropolymer that has $-CF_3$ functional groups such as FEP (fluorinated ethylene propylene) and PFA (perfluoroalkoxy). Employing trifluoro ($-CF_3$) in the molecule structure of SEI can significantly tune the orbital energies and the LUMO gap due to the strong electron-withdrawing property of $-CF_3$ functional groups. The fluorine-based coating is hydrophobic, which effectively protects lithium from water and moisture (Figure 29). It makes lithium handling much easier (no strict requirement such as dry room). The resulted coating can effectively protect Li-metal electrode in both air and electrochemical environment, leading to extended cycle life for high energy density lithium batteries, as shown in full cell test (Figure 30).

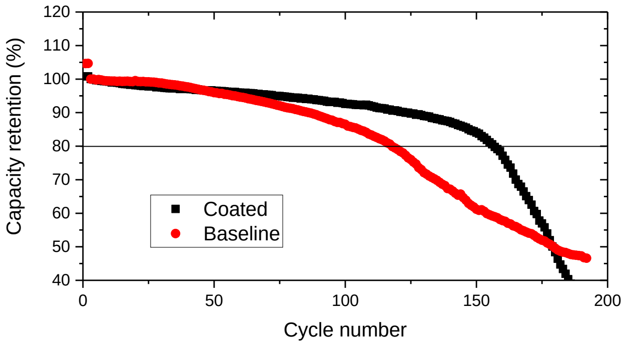

Figure 30. The cycle performance of protected lithium comparing with baseline. Testing condition: 1 M $LiPF_6$ in EMC/FEC (4:1), C/10 charge and C/5 discharge, 20-μm lithium electrode paired with NMC-622 (4.4 mAh/cm^2).

Patents/Publications/Presentations

Publications

- Wang, Y., D. Dang, M. Wang, X. Xiao, and Y-T. Cheng. "Mechanical Behavior of Electroplated Mossy Lithium at Room Temperature Studied by Flat Punch Indentation." *Applied Physics Letters* 115 (2019): 043903. doi.org/10.1063/1.5111150.
- Cho, J. H., X. Xiao, K. Guo, Y. Liu, H. Gao, and B. W. Sheldon. "Stress Evolution in Lithium Metal Electrodes." *Energy Storage Materials* (2019). doi: 10.1016/j.ensm.2019.08.008.

Presentation

- 236th ECS Meeting, Atlanta, Georgia (October 13–17, 2019): "*In Situ* Diagnostics of Coupled Electrochemical-Mechanical Properties of SEIs on Lithium Metal for Rechargeable Batteries"; X. Xiao.

Task 2.6 – Microscopy Investigation on the Fading Mechanism of Electrode Materials (Chongmin Wang, Pacific Northwest National Laboratory)

Project Objective. This work will use a combination of *ex situ*, *in situ*, *operando* and cryo HRTEM and spectroscopy to probe the fading mechanism of both lithium and silicon as high-capacity anode as well as Ni-rich NMC as high-capacity cathode. For high-capacity anode, the research task will focus on revealing how lithium and silicon interact with liquid electrolyte to critically affect their fading process. For the Ni-rich NMC cathode, the project will focus on delineating the structural and chemical evolution of the Ni-rich NMC regarding dependence on operating voltage, charge rate, and chemistry of electrolyte.

Project Impact. The proposed characterization work focuses on atomic-level structural and chemical analysis and direct correlation with battery fading properties. The work can be directly used to guide the designing of electrode materials with tailored microstructure and chemistry for enhanced properties of increasing the energy density of Li-ion batteries and to accelerate market acceptance of EVs, especially for PHEV as required by the EV Everywhere Grand Challenge.

Approach. Aberration-corrected STEM-HAADF and cryo-TEM imaging combined with EELS / energy-dispersive X-ray spectroscopy (EDX) chemical analysis will be used to probe the microstructural and chemical evolution of both cathode and anode. TOF-SIMS, nano-SIMS, and XPS will be used to explore the chemistry and the thickness of SEI layer on cathode and anode material. These characterization results will be used to guide the materials optimization process and establish a solid knowledge base on the correlation between materials selections and structure evolution in the Ni-rich NMC layered cathode materials.

Out-Year-Goals. This project has the following out-year goals:

- Multi-scale *ex situ*/*in situ* and *operando* TEM and cryo-TEM investigation of failure mechanisms for energy-storage materials and devices. Atomic-level *in situ* TEM and STEM imaging to help develop fundamental understanding of electrochemical energy-storage processes and kinetics of electrodes.
- Extension of *in situ* TEM capability for energy storage technology beyond lithium ions, such as Li-S, Li-air, Li-metal, sodium ions, and multi-valence ions.

Collaborations. This project collaborates with G. Chen (LBNL); J. Nanda (ORNL); K. Amine (ANL); D. Wang (Pennsylvania State University); A. Manthiram (University of Texas at Austin, UT Austin); W. Tong (LBNL); G. Liu (LBNL); Y. Cui (Stanford University); J. Zhang (PNNL); J. Liu (PNNL); X. Xiao (GM); S. Meng (UCSD); and S. Whittingham (State University of New York, SUNY, at Binghamton).

Milestones

1. Resolve the true structural nature of the intragranular cracks in Ni-rich NMC and answer questions on the origin of such cracking behavior. (Q1, FY 2019; Completed)
2. Reveal the true structural and chemical information of Si-anode/liquid-SEI layer by integration of cryo-TEM and EELS. (Q2, FY 2019; Completed)
3. Determine the critical factor that controls the correlation between charging rate and fading behavior of Ni-rich NMC. (Q3, FY 2019; Completed)
4. Reveal the true structural and chemical information of Li-metal anode/liquid-SEI layer by cryo-TEM and EELS. (Q4, FY 2019; Completed)

Progress Report

Batteries using lithium metal as anode are considered promising energy storage systems because of their high specific energy densities. The crucial bottlenecks for Li-metal anode are lithium dendrite growth and side reactions with electrolyte inducing low CE and short cycle life. Vinylene carbonate (VC), as an effective electrolyte additive in Li-ion batteries, has been noticed to significantly enhance the CE, while the origin of such an additive remains unclear.

Here, the team uses cryo-TEM imaging combined with EDS elemental and EELS electronic structure analyses to reveal the role of VC additive. They have discovered that the electrochemically deposited lithium metal (EDLi) in VC-containing electrolyte is slightly oxidized, with the SEI being a nanoscale mosaic-like structure comprised of organic species, Li_2O and Li_2CO_3; the EDLi formed in VC-free electrolyte features a combination of fully oxidized lithium with Li_2O SEI layer and pure lithium metal with multi-layer nanostructured SEI. These results highlight the possible tuning of crucial structural and chemical features of EDLi and SEI through additives and, consequently, direct correlation with electrochemical performance, providing valuable guidelines to rational selection, design, and synthesis of additives for new battery chemistries.

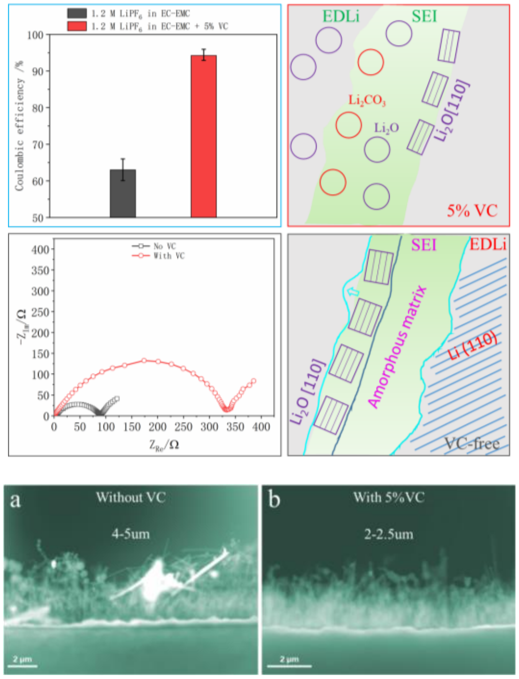

Figure 31. Comparison of Coulombic efficiency (top left), Nyquist plots of impedance spectra (bottom left), schematic drawing of the deposited lithium structure and morphology as well as the corresponding SEI with (top right) and without (bottom right) 5 wt% vinylene carbonate (VC) additive. The base electrolyte is 1.2 M $LiPF_6$ in EC-EMC (3:7 by wt.). The bottom row is the low magnification transmission electron microscopy images of lithium deposits from electrolytes of 1.2 M $LiPF_6$ in EC-EMC (3:7 by wt.) without VC (a) and with 5 wt% VC additive (b).

To understand the contribution of VC additive to the electrochemical performance of Li-metal anode, the electrolytes of 1.2 M $LiPF_6$ in EC-EMC (3:7 by wt.) with and without 5 wt% VC were used to electrochemically deposit lithium metal. The baseline electrolyte (without VC) exhibits a lithium CE of only 63.0%, mainly due to excessive side reactions between the porously deposited lithium metal and the electrolyte components. Adding 5 wt% VC into the baseline electrolyte could significantly improve lithium CE to 94.3%.

The team preserves and images beam-sensitive lithium growth and SEI with atomic resolution, revealing detailed nanostructures and their changes in different electrolyte environments by using cryo-TEM, EDS, and EELS. The electrolyte of $LiPF_6$/EC-EMC without VC additive gives very low lithium CE, but high interfacial ionic conductivity, while the addition of 5 wt% VC additive in the electrolyte could dramatically improve the CE of Li-metal electrode and also increase interfacial impedance. From the microcosmic point of view, the team reveals that the EDLi formed in VC-containing electrolyte has slightly oxidized lithium metal, while some of the EDLi formed in VC-free electrolyte is pure Li_2O, which is the main reason for low lithium CE. In addition, the SEI structures formed in VC-free and VC-containing electrolytes are also different. The SEI formed in VC-containing electrolyte is a mosaic like structure, which is the main reason that the impedance is high in VC-containing electrolyte. On the contrary, the SEI formed in VC-free electrolyte is similar to multi-layer structure containing LiF. The results establish the correlation between the electrochemical performance (CE and interfacial impedance) and the structure of deposited lithium and SEI layer formed in VC-free and VC-containing electrolytes, which will help in designing new electrolytes and additives for emerging battery chemistries that operate at even more extreme conditions.

Patents/Publications/Presentations

Publications

- He, Y., X. Ren, Y. Xu, M. Engelhard, X. Li, J. Xiao, J. Liu, J-G. Zhang, W. Xu, and C. Wang. “Origin of Lithium Whisker Formation and Growth under Stress.” *Nature Nanotechnology* (2019). Accepted for publication.
- Yan, P., J. Zheng, Z-K. Tang, A. Devaraj, G. Chen, K. Amine, J-G. Zhang, L-M. Liu, and C. Wang. “Injection of Oxygen Vacancies in the Bulk Lattice of Layered Cathodes.” *Nature Nanotechnology* 14 (2019): 602–608.
- Zou, L., J. Li, Z. Liu, G. Wang, A. Manthiram, and C. Wang. “Lattice Doping Regulated Interfacial Reactions in Cathode for Enhanced Cycling Stability.” *Nature Communications* 10 (2019): 3447.
- Cao, X., Y. Xu, L. Zhang, M. H. Engelhard, L. Zhong, X. Ren, H. Jia, B. Liu, C. Niu, B. E. Matthews, H. Wu, B. W. Arey, C. Wang, J-G. Zhang, and W. Xu. “Nonflammable Electrolytes for Lithium Ion Batteries Enabled by Ultraconformal Passivation Interphases.” *ACS Energy Letters* 4 (2019): 2529–2534.

Presentations

- 2019 Microscopy and Microanalysis, Portland, Oregon (August 4–9, 2019): “Atomic Structure of Electrochemically Deposited Lithium Metal and Its Solid Electrolyte Interphases Revealed by Cryo-Electron Microscopy”; Y. Xu, Y. He, H. Wu, W. Xu, and C. Wang.
- Lithium Ion Battery Discussions Workshop (LiBD-9), Arcachon, France (September 15–20, 2019): “Insights from High Resolution Transmission Electron Microscopy and Spectroscopy Study of Electrode Materials for Lithium Ion Batteries”; C. Wang. Invited.
- Next Generation TEM Workshop, Portland, Oregon (August 6, 2019): “*In Situ* S/TEM and their Applications for Energy Materials: The Challenge and Opportunities”; C. Wang. Invited.
- Nion Electron Microscopy Company, Kirkland, Washington (October 3, 2019): “S/TEM beyond Aberration Correction: *In Situ* and *Operando* S/TEM: Challenges and Opportunities”; C. Wang. Invited.

Task 2.7 – Correlative Microscopy Characterization of Electrochemical Hotspots in Oxide Electrodes (Yi Cui, William Chueh, and Michael Toney; Stanford University/SLAC)

Project Objective. This project aims to develop and utilize a correlative microscopy platform to investigate the lithiation dynamics of lithium- and manganese-rich (LMR) NMC and NCA, with the specific goal of understanding factors that determine the rate capability and degradation mechanisms at the single primary particle length scale. By developing a nanoscale and single-particle understanding of lithiation, the project addresses specific engineering problems including electrochemical hotspot, electrode utilization, safety, and capacity/voltage fade.

Project Impact. Fundamental insights from this new diagnostic capability are expected to increase the power density and cycle life of oxide electrodes by improving electrode utilization, reducing electrochemical hotspots, decreasing capacity and voltage fade, and enhancing safety, which all improve the viability of Li-ion batteries for vehicle transportation. By understanding lithiation at the single-particle level, this project's success will contribute to improving on-vehicle battery management, such as charging/discharging protocol, and state-of-charge (SOC) and state-of-health monitoring.

Approach. As stated, the project aims to develop a correlative microscopy platform to investigate the lithiation dynamics of LMR-NMC and NCA, with the goal of understanding factors that determine the rate capability and degradation mechanisms at the single primary particle length scale. On recharging time, the specific phenomena to be addressed include nonuniform current distribution and the correlation between surface property and the local lithiation rate. On degradation, phenomena to be addressed include correlating local chemistry and phases to capacity and voltage fading.

Out-Year Goals. Develop X-ray microscopy to investigate NMC and LMR-NMC cathodes at the single primary particle and single secondary particle level.

Collaborations. Commercial battery electrode particles are being supplied by Samsung.

Milestones

1. Quantify the local structure of Li-rich layered oxides using local X-ray probe. (Q1, FY 2019; Completed)
2. Assess the effect of synthesis condition of anion redox. (Q4, FY 2019)
3. Assess the effect of oxygen vacancies on anion redox. (Q4, FY 2019)

Progress Report

This quarter, the team reports on characterization of LMR-NMC as a function of cycle number using scanning transmission X-ray microscopy. To preserve the microstructure of the cathodes, the team employed ultramicrotomy to cross-section secondary particles. Subsequently, nickel L-edge XAS was conducted to assess the local SOC. Because LMR-NMC undergoes anion redox, oxygen K-edge spectroscopy was used additionally to assess the anion redox extent. Because high SOC cathodes are sensitive to air, samples were transferred with minimal exposure to air.

Figure 32 shows that the relative nickel oxidation state varies quite substantially throughout the electrode in the charged state (4.6 V) after 125 cycles. As clearly shown, the entire electrode microstructure is preserved, from primary particles, to secondary particles, to the porous electrode. The spectroscopic signature of oxidized oxygen in the oxygen K-edge remains strong even after 125 cycles. The team notes that there is a clear dependence on primary particle thickness (estimated by the extent of absorption at each pixel), with the thinner particles oxidizing much less. The heterogenous SOC also exists within secondary agglomerates, in addition to primary particles. Because a constant voltage hold was performed, the team does not believe this SOC distribution is due to slow kinetics. Instead, it may be attributed to the presence of point defects of secondary phases near the surface.

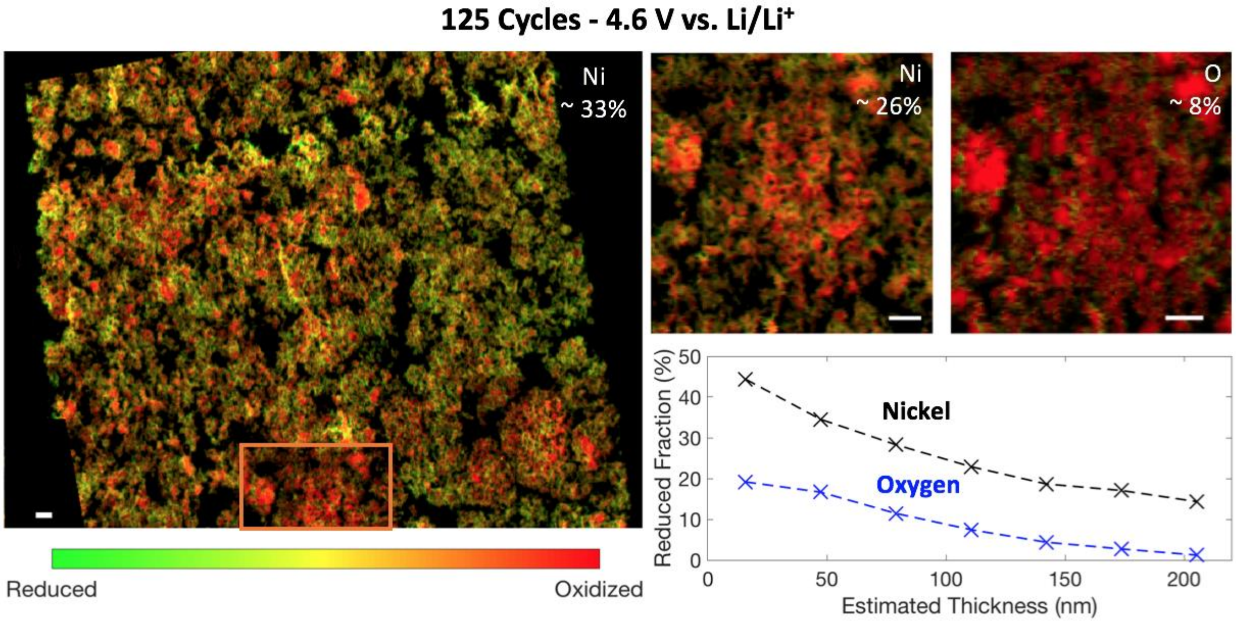

Figure 32. Spatial distribution of the nickel and oxygen oxidation state in the charged state after 125 cycles determined through scanning transmission X-ray microscopy. The far left shows the distribution over an "electrode scale" (~ 30 x 30 μm) determined with only three energies, while the zoomed-in images show distribution within the boxed region determined by fitting of spectra containing > 40 energies. The reduced fraction as a function of thickness is taken using the zoomed in images, although there is no qualitative difference when using the "electrode scale" nickel map instead. The scale bar in each image is 1 μm.

Patents/Publications/Presentations

Publication

- Lim, K. "Structure and Redox of Lithium-Rich Layered Oxides." Materials Science and Engineering, Stanford University (2019). Ph.D. Thesis.

Presentations

- $f^2c\pi^2$: International Conference on Electroceramics, Lausanne, Switzerland (July 18, 2018): W. C. Chueh. Plenary.
- International Conference on Solid State Ionics, PyeongChang, Korea (June 18, 2019): W. C. Chueh. Keynote.

Task 2.8 – Investigate the Impact of Doping on the Structural Stability and Conductivity of Solid Electrolytes
(Zonghai Chen, Argonne National Laboratory)

Project Objective. The project objective is to develop high conductivity ceramic electrolyte through cation doping and to stabilize the structure and cathode/electrolyte interface through cation doping and co-sintering between electrolyte and cathode.

Project Impact. Development of structurally, chemically, and electrochemically stable high conductivity solid electrolytes can significantly improve (1) volumetric energy density and (2) safety characteristics of lithium batteries, and will accelerate the penetration of EVs.

Approach. The project approach is multi-fold: (1) understanding the physics behind the transformation between the low conductivity phase and the high conductivity phase; (2) investigating the bonding strength of the cathode/electrolyte interface using model systems; and (3) developing electrolytes with high ionic conductivity and good bonding to cathodes through cation doping.

Out-Year Goals. The project has the following out-year goals:

- Using $Li_7La_3Zr_2O_{12}$ (LLZO) as a model material to investigate the pathway of path transformation during synthesis of the SSE.
- Investigating impact of cation doping on kinetics of phase transformation.
- Initiating research activity on co-sintering of cathode/electrolyte model system for a chemically/mechanically strong interface.

Collaborations. The project collaborates with Dr. A. Ngo (ANL), Dr. L. Curtiss (ANL), Dr. V. Srinivasan (ANL), Dr. Y. Ren (ANL), Dr. J. Libera (ANL), Dr. T. Li (Northern Illinois University), Dr. F. Wang (BNL), Dr. X. H. Xiao (BNL), and Dr. D. Chen (University of Houston).

Milestones

1. Developing *in situ* high-energy XRD capability to investigate the phase transformation of ceramic electrolytes. (Q1, FY 2019; Completed)
2. Investigating the tetragonal/cubic phase transformation of LLZO. (Q2, FY 2019; Completed)
3. Investigating the impact of bonding between LLZO and cathode materials. (Q3, FY 2019; Completed)
4. Synthesizing W-doped LLZO for investigation on structural stability and mechanical stability. (Q4, FY 2019; Ongoing)

Progress Report

Last quarter, co-sintering between a model cathode material ($LiNi_{0.6}Mn_{0.2}Co_{0.2}O_2$) with the precursor for Al-doped LLZO was conducted without success. A large variation on the lattice parameters of the cathode material was observed, implying a severe exchange of elements between the cathode and the electrolyte, and the SSE exists as a tetragonal phase after co-sintering. The team's investigation on the synthesis of LLZO (reported the second quarter) reveals that the cubic LLZO phase is the overall thermodynamically stable phase for the LLZO family, but with a high activation energy for the formation reaction of cubic LLZO. The presence of tetragonal phase might be related the low kinetics of formation reaction. Therefore, this co-sintering process was revisited by replacing the LLZO precursor with a cubic LLZO powder. The model system investigated is a mixture of $LiNi_{0.6}Mn_{0.2}Co_{0.2}O_2$ (90 wt%) and Ta-doped LLZO (10 wt%, cubic phase.)

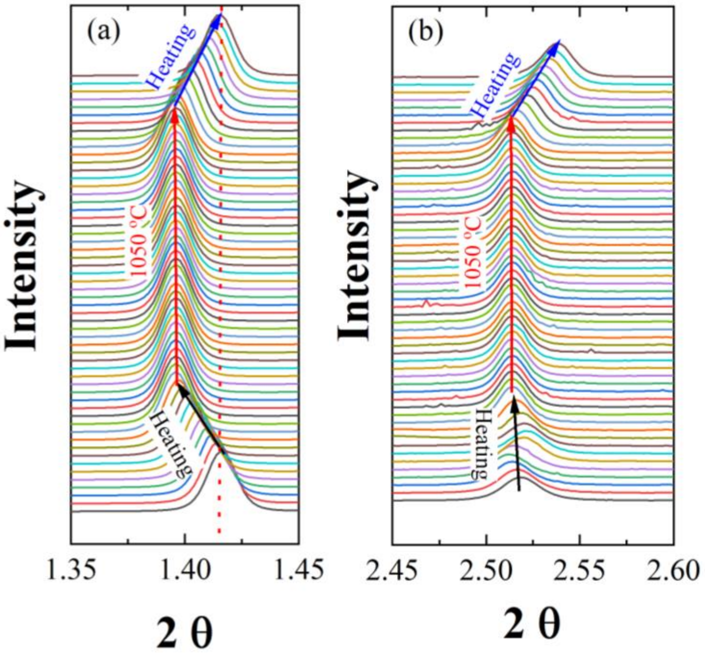

Figure 33. The evolution of (a) (003) peak of $LiNi_{0.6}Mn_{0.2}Co_{0.2}O_2$ and (b) (422) peak of Ta-doped LLZO during the co-sintering process.

Figure 33 shows the evolution of XRD patterns during the co-sintering of the new model system; the sample was heated up to 1050°C with a heating rate of 10°C/min and was then sintered 1050°C for 5 h before being cooled down to room temperature. Figure 33a shows the reversible evolution of (003) peak of $LiNi_{0.6}Mn_{0.2}Co_{0.2}O_2$; the (003) peak has almost identical peak position before and after the co-sintering process, indicating a limited amount of element exchange during the co-sintering. Most importantly, the cubic Ta-doped LLZO maintained a cubic phase after the co-sintering (see Figure 34b for the change on the (442) peak of the cubic phase). Figure 34 implies that the development of a co-sintering process to maintain the layered structure of the cathode and a cubic electrolyte is practical. A good adhesion between the cathode and the electrolyte particles was observed (see Figure 34 for a 3D TXM image). It can also be seen that the LLZO particles are sparsely decorated on the surface of the cathode particles. A higher LLZO content might be needed for better coverage and good Li-ion transport across the interface.

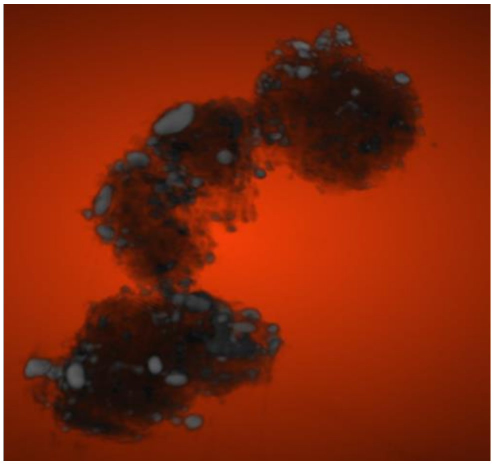

Figure 34. 3D image of the model material after co-sintering. The 3D image (transmission X-ray microscopy) was collected at the absorption edge of lanthanum (6.3 keV). The big particles are $LiNi_{0.6}Mn_{0.2}Co_{0.2}O_2$, and the small ones are LLZO particles.

Patents/Publications/Presentations

Presentation

- ACS Fall National Meeting, San Diego, California (August 25–29, 2019): “Investigating *t*-LLZO/*c*-LLZO Transformation using *In Situ* High-Energy X-Ray Diffraction”; J. Gim, H. Nguyen, T. Li, and Z. Chen. Slide presentation.

TASK 3 – MODELING

Summary and Highlights

Achieving the performance, life, and cost targets outlined by VTO will require moving to next-generation chemistries, such as higher capacity Li-ion intercalation cathodes, silicon and other alloy-based anodes, Li-metal anode, and sulfur cathodes. However, numerous problems plague development of these systems, from material-level challenges in ensuring reversibility to electrode-level issues in accommodating volume changes, to cell-level challenges in preventing cross talk between the electrodes. In this task, a mathematical perspective is applied to these challenges to provide an understanding of the underlying phenomenon and to suggest solutions that can be implemented by the material synthesis and electrode architecture groups.

The effort spans multiple length scales from *ab initio* methods to continuum-scale techniques. Models are combined with experiments, and extensive collaborations are established with experimental groups to ensure that the predictions match reality. Efforts also focus on obtaining parameters needed for the models, either from lower-length scale methods or from experiments. Projects also emphasize pushing the boundaries of the modeling techniques used to ensure that the task stays at the cutting edge.

In the area of intercalation cathodes, effort is focused on understanding working principles of high nickel layered materials with an aim of understanding structural changes and associated changes in transport properties. Coatings, an effective strategy for high-voltage operation, are being explored with the aim of providing a rational design approach for new coating materials. In parallel, design of liquid electrolytes and gaining understanding of their behavior are used to determine their usability at high voltages. In addition, focus is paid to the assembling of porous electrodes with particles to predict the conduction behavior and impact of heterogeneities on electrode behavior.

In the area of Li-metal anodes, the focus is on understanding how materials can be designed to prevent dendrite growth using continuum modeling approaches, combined with calculations on mobility in solid conductors. The results are used to guide materials development by providing the properties needed to prevent dendrites while also achieving the energy and power goals. Models are also starting to examine the role of the SEI on the morphology of the dendrite and to describe the mechanical-electrochemical coupled effects that are critical for dendrite formation. Finally, models are being developed to examine the solid-cathode interface in Li-metal based systems, where interface debonding issues are known to limit cycling.

Models are also being developed for solid electrolytes against intercalation cathodes and for developing methods to predict delamination at the interface during cycling in different cathode materials. These models are being used to understand how to prevent chemo-mechanical failure at the interface.

Highlights. The Balbuena group has been examining various kinds of deposits that occur on lithium metal, including mossy deposition and dendritic growth and is developing models that can help explain why these transitions occurs. These mesoscale models are showing that temperature and charging rates are critically important in determining the nature of the deposit. While higher temperature favors uniform deposition, decreasing temperature could lead to a transition from uniform lithium deposits, to mossy deposits, to lithium dendrite formation. These changes are connected to the temperature dependence of the electrolyte transport and the surface diffusion rates.

Task 3.1 – Design of High-Energy, High-Voltage Lithium Batteries through First-Principles Modeling (Kristin Persson, Lawrence Berkeley National Laboratory)

Project Objective. This project supports VTO programmatic goals by developing next-generation, high-energy cathode materials and enabling stable cathode operation at high voltages through target particle morphology design, functional coatings, and rational design of electrolytes. The end-of-project goals include: (1) understanding of the factors that govern charge transport in nonaqueous, superconcentrated liquid electrolytes (2) new fundamental understanding of the Li-ion dynamics in Si-Sn electrode alloys (and their native oxides), with a design focus on improving stability of the silicon electrode through tin alloying, and finally (3) critical surface and coating design and optimization strategies that will improve cycling of Li-ion battery cathodes by reducing cathode degradation from oxygen loss.

Project Impact. To enhance performance of Li-ion systems, improvements on the cathode and the electrolyte side are needed. This project is aimed to result in an improved understanding of the atomistic mechanisms underlying surface behavior and performance of the Li-ion cathode materials, with the ultimate goal being to suggest strategies, such as coatings, surface protection, and particle morphology design. Furthermore, fundamental studies of electrolyte conductivity and transport mechanisms, as a function of solvent and salt concentrations, and components will be conducted.

Approach. First-principles calculations, both static and dynamic approaches, are used to model solid-state electrode material thermodynamics and kinetics. Liquid electrolytes are modeled through coupled classical MD and first-principles methods to accurately capture solvation structure as well as reactivity of the liquid system.

Out-Year Goals. For the electrolyte development, work will be aimed toward understanding the atomistic interactions underlying the performance of lithium electrolytes specifically elucidating conductivity (as a function of salt concentration) and impact on the charge transport mechanisms at play. Stable interfaces will be determined by focusing initially on degradation mechanisms related to release of surface oxygen at high charge. Tuning particle morphology and coating materials—both of crystalline as well as amorphous structure—will be explored using the Materials Project. Li-ion conduction mechanisms and electrode stability of Si-Sn alloys will be determined, in addition to the reactivity and ionic conduction of the native oxide surface phases.

Collaborations. This project is highly collaborative between BMR PIs G. Chen (LBNL), G. Ceder (LBNL), and V. Srinivasan (ANL). Cathode design and synthesis will be performed by Chen and Ceder, surface design by Persson, and electrolyte design and testing by Persson and Srinivasan.

Milestones

1. Finish benchmarking of algorithms for obtaining reliable solvation structures and ionic conductivity in highly concentrated liquid electrolytes. (Q1, FY 2019; Completed)
2. Identify Li-ion conduction mechanisms in Si-Sn alloy anode, using first-principles modeling. (Q2, January 2019; Completed)
3. Evaluate SiO_2 and SnO_2 as surface phases from the perspective of ionic conduction and reactivity with lithium. (Q3, April–July 2019; Completed)
4. Conduct first evaluation of amorphous oxygen-retention and lithium diffusion enhancing coatings using the Materials Project infrastructure. (Q4, July–November 2019; In progress)

Progress Report

This project is aimed toward amorphous coating design that will improve performance of Li-ion battery cathodes. The team is interested in conformal ultrathin coatings of inactive Al_2O_3 and ZnO realized by atomic layer deposition (ALD), where the defect chemistry and impurity content could lead to off-stoichiometry, trapped charges, and some electronic conductivity. Therefore, the exact composition and model of conformal coating for simulating the electronic and ionic transport through amorphous coating is ambiguous. Here, the team considers three scenarios of lithium diffusion in conformal coatings (see Figure 35), which were initially proposed by Xu et al.[1]:

- **Electron Conducting Model.** Li^+ accompanying electron diffuses through the electronically conductive coating. Al^{3+} is reduced during Li^+ diffusion.
- **Electrolyte Model.** The electronically insulating coating acts as an electrolyte that incorporates Li^+ with compensating negative charge in the coating. Aluminum is not reduced during lithium diffusion.
- **Space Charge Model.** Li^+ tunnels through electronically insulating coating without electron, and a space charge builds up in the coating due to the absence of negative compensating charge.

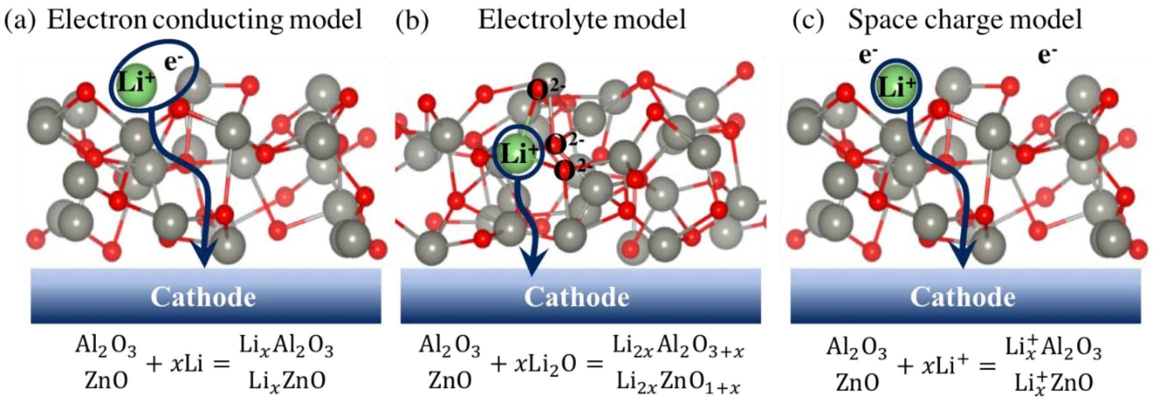

Figure 35. Schematic illustrations of different lithium transport models in amorphous coating.

However, the space charge model was ruled out to be responsible for lithium diffusion in conformal coating, as the build-up overpotential exceeds the dielectric breakdown strength of Al_2O_3. Therefore, the team studied the first two lithium diffusion scenarios in this work, as seen in Figure 35a-b. To simulate an electron-conducting model, the team inserted extra Li^0 into amorphous Al_2O_3 and ZnO to generate $Li_xAl_2O_3$ and Li_xZnO, respectively, with aluminum and zinc being reduced. This model corresponds to previous studies on lithiated amorphous Al_2O_3.[1, 2] To simulate the electrolyte model, the team inserted Li_2O as the coordination shells of Li^+ cations into amorphous Al_2O_3 and ZnO to generate $Li_{2x}Al_2O_{3+x}$ and $Li_{2x}ZnO_{1+x}$, respectively. In this model, there are two transport mechanisms for Li^+ diffusion in amorphous coating, similar to the diffusion of Li^+ cations in electrolyte: (1) vehicular mechanism, where Li^+ diffuses with its coordination shells as lithium complex; and (2) structure-diffusion mechanism, where Li^+ diffuses by exchanging O^{2-} anions in its coordination shell. These diffusion mechanisms can also be applied to O^{2-} anions diffusion, where O^{2-} accompanies Al^{3+} or Zn^{2+} as the coordination shells.

[1]. Xu, S., R. M. Jacobs, H. M. Nguyen, S. Hao, M. Mahanthappa, C. Wolverton, and D. Morgan. “Lithium Transport through Lithium-Ion Battery Cathode Coatings.” *Journal of Materials Chemistry A* 3, no. 33 (2015): 17248–17272.

[2]. Jung, S. C., and Y-K. Han. “How Do Li Atoms Pass through the Al_2O_3 Coating Layer during Lithiation in Li-ion Batteries?” *The Journal of Physical Chemistry Letters* 4, no. 16 (2013): 2681–2685.

Patents/Publications/Presentations

Presentation

- Berkeley Electrochemistry Seminar Series, Berkeley, California (October 7, 2019): "Investigate Li Intercalation Stability of Ni-Rich Cathodes from First-Principles"; J. Cheng.

Task 3.2 – Understanding and Strategies for Controlled Interfacial Phenomena in Lithium-Ion Batteries and Beyond

(Perla Balbuena and Jorge Seminario, Texas A&M University; Partha Mukherjee, Purdue University)

Project Objective. The project objective is to evaluate and characterize interfacial phenomena in lithiated silicon and Li-metal anodes and to develop guidelines for potential solutions leading to controlled reactivity at electrode/electrolyte interfaces of rechargeable batteries using advanced modeling techniques based on first principles.

Project Impact. Understanding SEI growth on constantly evolving silicon surfaces and on highly reactive Li-metal surfaces is expected to allow definition of the electrolyte properties required in high-performance cells. Strategies to control the silicon anode instability and pulverization issues and the well-known safety and short effective lifetimes of Li-metal anodes will be developed by tuning the electrolyte composition, structure, dynamic, and stability, as well as that of the electrode morphology and interactions with the electrolyte, based on multiple characterizations of interfacial phenomena.

Approach. A comprehensive multi-scale modeling approach, including first-principles *ab initio* static and dynamics, classical MD, and coarse-grained mesoscopic models, will focus on the roles of the electrolyte's chemical, structural, and dynamical properties and of the electrode micro- and nano- structure on the formation and evolution of the SEI layer and the associated electrochemical performance on silicon and on Li-metal anodes.

Out-Year Goals. Work will progress toward characterizing lithiation and SEI formation at silicon surfaces as well as the subsequent cracking and reforming events under the most realistic modeling conditions. Similarly, the project will investigate electrolyte effects on reactivity and dendrite formation in Li-metal surfaces. The project aims to capture how the chemistry of the various electrolyte components (mainly liquids, but also solid polymers and gels) affects the main issues that influence the electrode performance.

Collaborations. This project funds work at Texas A&M University (TAMU) and Purdue University. The team has collaborated with Prof. G. Somorjai (UC Berkeley), Prof. S. Yassar (UIC), and Dr. V. Murugesan (PNNL).

Milestones

1. Complete analysis of anode macroscopic effects during cycling. (Q1, FY 2019; Completed)
2. Complete study of improved electrolytes for silicon anodes. (Q2, FY 2019; Completed)
3. Complete study of improved electrolytes for lithium anodes. (Q3, FY 2019; Completed)
4. Complete evaluation of alternative charging strategies for lithium anodes. (Q4, FY 2019; Completed)

Progress Report

Temperature Control and Charging Strategy to Alleviate Dendrite Growth on Li-Metal Anodes. In conjunction with high current rates, low temperatures favor formation of dendritic deposits. The team uses coarse-grained mesoscale models to determine the nature of the deposits as a function of the current density and temperature. As temperature varies, the team examines the results through a continuum scale description of ionic transport in terms of Li^+ concentration behavior in the electrolyte. High local current densities at the metal – electrolyte interface result in electrolyte depletion at the deposition tips and also inhibit surface diffusion rates, resulting in formation of dendrites. Dendrite formation is alleviated at higher temperatures; reduced porosity and rounded tips are observed for film type deposits, and dendrite height is reduced for fractal deposits. For a given local overpotential, lithium is uniformly distributed over the anode surface at high temperature. However, as temperature decreases, the morphology could experience a transition from uniform lithium deposits, to mossy, to lithium dendrite. This is clear from the Arrhenius dependence of the electrolyte diffusivity (k_{ed}) and surface diffusion (k_{sd}) rates as a function of temperature. Moreover, this analysis is also connected to the predictions from DFT, AIMD, and classical MD simulations regarding the nature of the salt anion decomposition and its concentration. These reactions are usually highly exothermic, producing peaks of local high temperature, which favors dendrite formation. For slower anion decomposition kinetics, the system establishes local equilibrium and a preference for mossy formation can be observed. These findings will be reported soon.

The team further investigated combined deposition-stripping behavior mimicking the charge-discharge profiles in an actual battery system. Interestingly, temperature increase is also associated with an increase in the formation of dead lithium during the stripping process. The team found a linear correlation between the number of dead lithium layers and temperature rise. Ionic diffusion barrier of 0.15 eV and surface diffusion barrier of 0.14 eV are used. The amount of dead lithium increases with increasing temperature and with decreasing current density or overpotential. High aspect ratio deposits would disconnect from the substrate on discharging, becoming inert, and this dead material floating in the electrolyte would create obstruction for ionic diffusion during the charging process.

Nucleation Events at the Initial Stages of SEI Formation. Significant efforts were dedicated to understanding nucleation of the SEI products as a function of the electrolyte composition. Classical MD simulations followed nucleation events up to the scale of nanoseconds. Various simulations were conducted to detect formation of Li_2O, Li_2S, and LiF, at interfaces of Li-metal surfaces with an electrolyte containing dissolved O_2, a long chain polysulfide such as Li_2S_8, and an F-rich electrolyte, respectively. In each case, the team found rapid formation of Li_2O, Li_2S, and LiF, respectively; in some cases, additional products were formed. However, the goal was to characterize the initial nucleation of these phases in their natural environments. In addition, they simulated other compositions such as lithium triflate in DME or DOL. The team followed the formation of initial nuclei of Li_xF (with x=1,2,…6), and then evolution of these small nuclei to form larger entities. Figure 36a shows the LiF nuclei formed in DOL solution compared to those

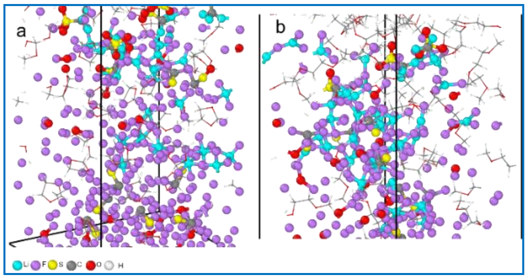

Figure 36. (a) SEI products formed after 530 ps in a solution of lithium triflate in DOL. (b) SEI products formed after 300 ps in a solution of lithium triflate in DME.

formed in DME solution (Figure 36b). Note that the nuclei (Li_xF units: lithium, purple; fluorine, light blue) are disconnected in DOL, indicating slow growth kinetics, whereas they are much more connected in DME solution, revealing the effect of the electrolyte in SEI growth. The results are being written for publication.

Patents/Publications/Presentations

Publications

- Kamphaus, E. P., S. Angarita-Gomez, X. Qin, M. Shao, M. Engelhard, K. Mueller, V. Murugesan, and P. B. Balbuena. "Role of Inorganic Surface Layer on Solid Electrolyte Interphase Evolution at Li-Metal Anodes." ACS *Applied Materials Interfaces* 11 (2019): 31467–31476.
- Hao, F., A. Verma, and P. P. Mukherjee. "Cationic Shield Mediated Electrodeposition Stability in Metal Electrodes." *Journal of Materials Chemistry A* 7 (2019): 18442–18450.

Presentations

- Institute of Physics at Universidad Nacional de Rosario, Rosario, Argentina (July 4, 2019): "Materials for Batteries and Catalysis"; P. B. Balbuena. Invited.
- ACS Fall National Meeting, San Diego, California (August 29, 2019): "Reactivity and Solvation at Solid/Liquid Interfaces of Li-Metal Based Batteries"; P. B. Balbuena. Invited.
- Texas Advanced Computing Center Symposium for Texas Researchers, University of Texas, Austin, Texas (September 26, 2019): "Elucidating the Dynamic Behavior of Complex Solid-Liquid and Solid-Solid Interfaces: Using the Power of Supercomputers"; P. B. Balbuena. Invited.
- ECEE Meeting, Glasgow, Scotland (July 23, 2019): "Classical and Quantum Analysis of Lithium Anodes in Nanobattery Models" (Abstracts 201-201); J. M. Seminario, D. E. Galvez-Aranda, V. H. Ponce, and L. A. Selis.
- ACS Fall National Meeting, San Diego, California (August 28, 2019): "Dendrite Formation in Li−Metal Anodes: Atomistic Machine Learned Molecular Dynamics Study" (Abstract 524); J. M. Seminario, L. A. Selis, and D. E. Galvez-Aranda.
- ACS Fall National Meeting, San Diego, California (August 28, 2019): "Solid-State Electrolytes: Li-Metal Interfaces" (Abstract 446); J. M. Seminario and D. E. Galvez-Aranda.

Task 3.3 – Electrode Materials Design and Failure Prediction
(Venkat Srinivasan, Argonne National Laboratory)

Project Objective. The main project objective is to develop computational models for understanding the various degradation mechanisms for next-generation Li-ion batteries. This year's goal is to use the continuum-based mathematical model to (1) investigate interfacial stability between electrodes and ceramic-based SSEs, and (2) experimentally measure and understand the impedance observed at the cathode/SSE interface. Ceramic-based SSEs are expected to enable high energy density and liquid-free, safe, next-generation Li-ion batteries. Li-metal anodes should be incorporated due to their substantially larger specific capacity, as compared to present day graphite-based anodes. During deposition, lithium dendrite growth through the SSEs and subsequent short circuit has been a major issue, limiting successful implementation of SSEs. Similarly, on the cathode side, diffusion of TMs into the SSEs along with delamination between cathode and SSE lead to increased interfacial resistance. The developed computational model will be used to investigate the impact of microstructural (grain size), physical (mechanical stiffness), and transport (conductivity) properties of the SSE on the overall interfacial degradation observed at both the cathode and anode sides. Due to the SOC-dependent electrochemical and mechanical properties of the cathode, an attempt will be made to experimentally measure the SOC-dependent impedance at the cathode/SSE interface. The main focus will be to elucidate interfacial issues, observed at both anode and cathode sides, and to devise strategies to enable successful implementation of SSE in next-generation Li-ion batteries.

Project Impact. Findings from this research will give a better understanding of the factors, at the cathode/SSE interface, limiting the cycle life of solid-electrolyte-based Li-ion batteries. These results will help to enable incorporation of cathode particles within SSEs.

Project Approach. The approach used here is to develop mesoscale models, based on continuum modeling, to describe the critical processes in the materials, and combining them with electrochemical, microscopic, and spectroscopic data to ensure parameter estimation and model validation. The model is then used to provide insights on impact of material properties on performance and life and as guidance for design of new materials.

Out-Year Goals. At the end of this project, a computational framework will be presented that is capable of estimating delamination and impedance at cathode/SSE interface.

Collaborations. This project collaborates with L. A. Curtiss, A. T. Ngo, and C. M. Phatak at ANL.

Milestones

1. Investigate impact of grain-interior (GI) / grain-boundary (GB) microstructure on overall dendrite growth observed at SSE/lithium interface. (Q1, FY 2019; Completed)
2. Analyze effect of delamination at the cathode/SSE interface as a mode of degradation. (Q2, FY 2019; Completed)
3. Investigate impact of grain size of the electrolyte on the mechanical degradation occurring at the cathode/SSE interface. (Q3, FY 2019; Completed)
4. *Go/No-Go Decision*: Estimate SOC-dependent impedance at cathode/SSE interface. If not possible, proceed with impedance measured at fixed SOC. (Q4, FY 2019; Completed)

Progress Report

Estimate SOC-Dependent Impedance at Cathode/SSE Interface. If Not Possible, Proceed with Impedance Measured at Fixed SOC. The earlier mesoscale computational model used a planar NMC cathode, and a LLZO electrolyte with different grain sizes. Volume change during the lithiation and delithiation of NMC cathodes leads to delamination at the CEI, which can effectively increase the charge transfer resistance. In the present analysis, once the cathode delaminates from the electrolyte, it is assumed to be an irreversible process. In the impedance model, the ionic and electronic conductivities of LLZO electrolyte and NMC cathode are assumed to be infinitely large, which makes their contribution to the overall impedance curve negligible. The semicircle from charge transfer resistance, and the low frequency tail due to diffusion within the cathode, has been modeled here. Figure 37a demonstrates a potential versus SOC curve, as obtained during charge. Impedance plots have been generated at three SOC values of 0.9, 0.7, and 0.5, which are also denoted as A, B, and C, respectively. The corresponding impedance diagrams are shown in Figure 37b, where it is evident that the diffusion process within the cathode is extremely fast, and does not contribute at all to the overall impedance. This fast diffusion of lithium atoms is attributed to the extremely small length of the cathode domain, only 100 nm. However, the charge transfer resistance decreases with increasing SOC. This is due to the dependence of exchange current density on the concentration of lithium at the cathode surface. The charge transfer resistance is also inverse to the exchange current density. Impact of delamination on the charge transfer resistance did not become obvious even at 50% SOC.

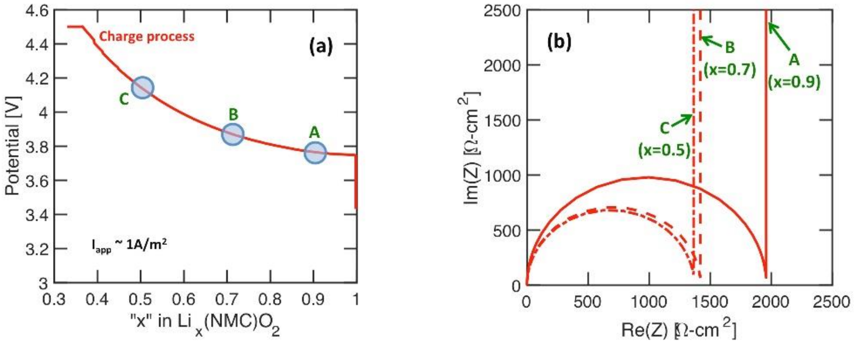

Figure 37. (a) Demonstration of change in potential with stoichiometry of lithium in NMC cathodes during the charge process. Impedance analysis was conducted at three state-of-charge values. (b) Impedance curves at three points denoted by A, B and C.

Voltage profile during the charge (red) and discharge (black) process, with respect to SOC, have been demonstrated in Figure 38a. The corresponding charge transfer resistance (R_{ct}) has been plotted in Figure 38b. The red solid line denotes R_{ct} during charge process, which initially decreases and later increases because of interfacial delamination. The increase in R_{ct} due to delamination becomes obvious only at SOC values lower than 0.5. The black line indicates R_{ct} during discharge process, which changes mostly due to variation in lithium concentration at the cathode surface. These theoretical predictions correlate qualitatively with experimental observations shown in Figure 38b by the red and black symbols. Estimation of SOC-dependent impedance curve successfully completes the milestone for this quarter. Since the charge transfer resistance changes substantially with SOC, SOC-dependent impedance must be used in the future.

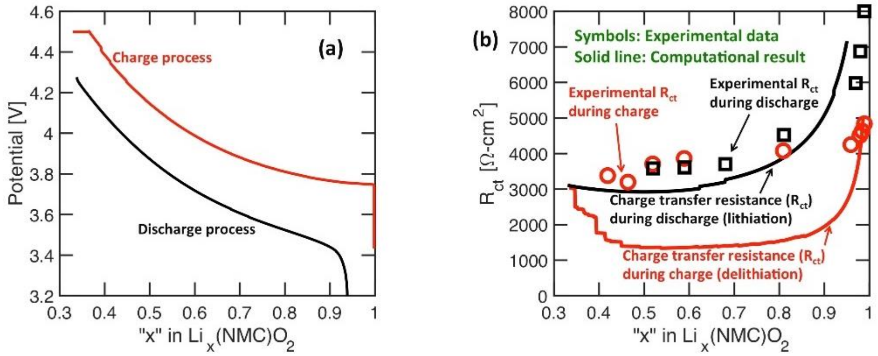

Figure 38. (a) Potential versus lithium stoichiometry curves as obtained during the charge and discharge processes. (b) Variation in charge transfer resistance with lithium stoichiometry during charge (red) and discharge (black) process. The experimental results are denoted by symbols.

Patents/Publications/Presentations

The project has no patents, publications, or presentations to report this quarter.

Task 3.4 – First-Principles Calculations of Existing and Novel Electrode Materials (Gerbrand Ceder, Lawrence Berkeley National Laboratory)

Project Objective. Solid-state batteries are promising to achieve high energy density. The project objective is to determine the design principles needed to create SSEs with high Li-ion conductivity while also achieving stability against common Li-ion cathodes and Li-metal anodes.

Project Impact. The project will lead to understanding the factors that control Li-ion motion in crystalline and amorphous solids and will develop strategies to create stable interfaces against lithium metal and high-voltage cathode materials. The understanding of such processes is necessary to determine design principles to develop reliable all solid-state batteries.

Approach. High-throughput computation method is used to screen suitable solid electrolyte with high electrochemical stability and high ionic conductivity, by incorporating Nudged Elastic Band (NEB) and an AIMD method. Meanwhile, DFT is used to calculate bulk elastic constants of materials, surface energies, and interface decohesion energies of GBs. Thermodynamic interface stability is assessed from *ab initio* computed grand potential phase diagrams in which the lithium voltage can be controlled. Kinetic limits for solid electrolyte decomposition are assessed by topotactic lithium insertion and removal from the solid electrolyte.

Out-Year Goals. Future goals include the following: (1) gain insight into what creates high Li-ion conduction in sulfide and oxide solids, and (2) develop stable, processable solid-state conductors that can be applied in all solid-state batteries.

Collaborations. There are no current collaborations.

Milestones

1. Modeling of the Li_2S-P_2S_5 phase diagram for SSEs: solid phases correctly modeled. (Q1, FY 2019; Completed)
2. Modeling of the Li_2S-P_2S_5 phase diagram for SSEs: include correct modeling of amorphous phase. (Q2, FY 2019; Completed)
3. Model Li-ion conductivity in amorphous LPS (Li-P-S) systems and glass ceramics. (Q3, FY 2019; Completed)
4. Develop understanding on which structural and compositional features make LPS an excellent ionic conductor. (Q4, FY 2019; Completed)

Progress Report

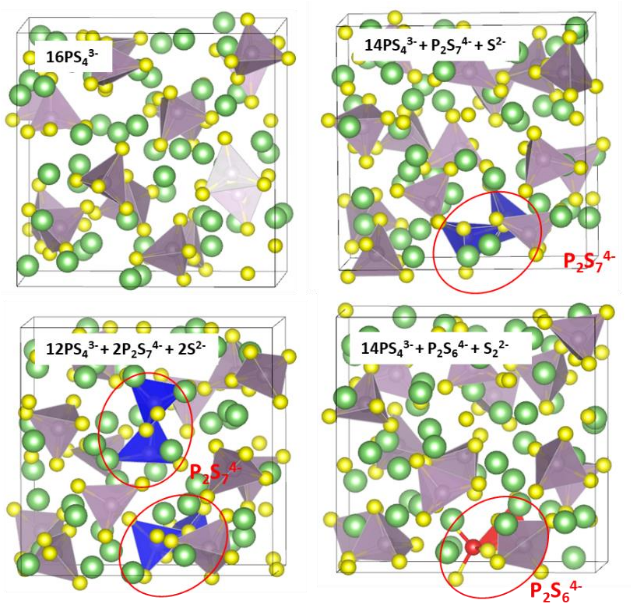

Figure 39. Generated structures of the amorphous Li-P-S systems including different types of anion building blocks at same composition. Green, purple, and yellow balls denote lithium, phosphorus, and sulfur.

Amorphous LPS has been studied as a promising solid-electrolyte material because of its high conductivity and facile synthesis process.[1] Interestingly, the amorphous LPS phase generally shows higher intrinsic ionic conductivity than the corresponding crystalline phase with the same composition.[2] Recent experimental work shows that amorphous LPS consists of anion blocks such as PS_4^{3-}, $P_2S_6^{4-}$, and $P_2S_7^{4-}$.[3] However, the relationship between the structural property and the conductivity in this system is not clearly elucidated. To verify the exact role of each anion building block, amorphous simulation structures consisting of different types of building blocks have been prepared by a high-temperature anneal and quench MD technique. To separate the effect of the Li-ion concentration from that of the structure, the atomic composition of the structures is fixed to Li:P:S = 3:1:4. The density is kept constant at 2 g cm-^{3} for all samples. The reference structure, which only contains PS_4^{3-} anions, is generated by annealing the β-Li_3PS_4 phase at 1000K. This leads to amorphization without breaking of P-S bonds during the annealing timescale (10 ps). The structures with $P_2S_6^{4-}$ and $P_2S_7^{4-}$ building blocks are created through a stoichiometric substitution from the reference structure (1) $2x{\cdot}PS_4^{3-} \rightarrow x{\cdot}P_2S_7^{4-} + x{\cdot}S^{2-}$ and (2) $2y{\cdot}PS_4^{3-} \rightarrow y{\cdot}P_2S_6^{4-} + y{\cdot}S_2^{2-}$. Figure 39 visualizes the structures of the reference, x=1, x=2 and y=1 substitution. Diffusion constants of lithium ions are obtained from AIMD simulations (> 250 ps) on these materials. As shown in Figure 40, the activation barriers of diffusion are determined to be 485, 347, 282, and 289 meV for the reference, x=1, x=2, and y=1 substitution, respectively. These results clearly indicate that modification of PS_4^{3-} into $P_2S_6^{4-}$ or $P_2S_7^{4-}$ reduces the activation barrier for lithium diffusion. The difference between the top right and bottom left plot also indicates that an increasing concentration of substitution (x=1 to x=2) further reduces the activation barrier. These preliminary observations indicate that the structure and composition of the anion building blocks affect the diffusion of lithium ions in LPS in a substantial way, even though there is no long-range order in the structures and no chemical composition change.

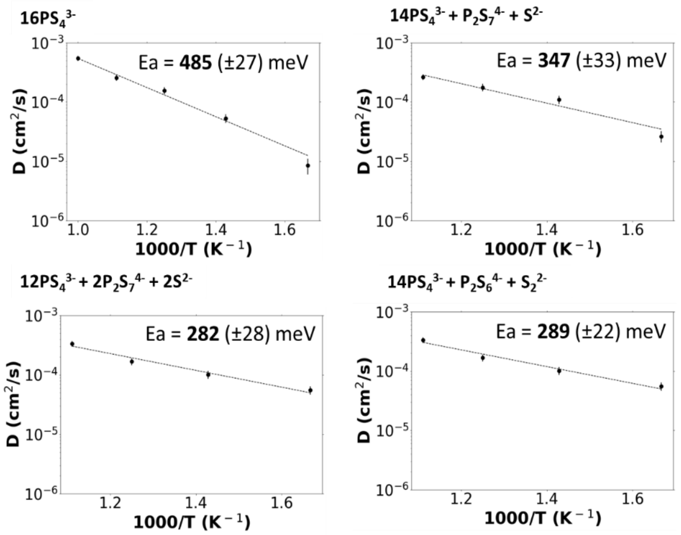

Figure 40. Arrhenius plots of *ab initio* molecular dynamic simulation on the Li-P-S systems with different concentrations of anion building blocks, PS_4^{3-}, $P_2S_6^{4-}$, and $P_2S_7^{4-}$.

[1] Hayashi, A., et al. *Journal of the American Ceramic Society* 84 (2004): 477–479.

[2] Zheng, F., et al. *Journal of Power Sources* 389 (2018): 198–213.

[3] Dietrich, C. *Journal of Materials Chemistry A* 5 (2017): 18111–18119.

Patents/Publications/Presentations

Publications

- Lun, Z., et al. “Design Principles for High-Capacity Mn-Based Cation-Disordered Rocksalt Cathodes.” *Chem*. In press.
- Xiao, Y., et al. “Understanding Interface Stability in Solid-State Batteries.” *Nature Reviews Materials*. In press.

Task 3.5 – Dendrite Growth Morphology Modeling in Liquid and Solid Electrolytes (Yue Qi, Michigan State University)

Project Objective. The project goal is to develop a validated model to predict lithium dendrite morphology evolution in both liquid and solid electrolytes during electrodeposition and stripping to accelerate the adoption of Li-metal electrodes in current and emerging battery technologies. To achieve this goal, the project has four objectives: (1) formulate a general framework that captures the electrochemical-mechanical driving forces for lithium morphology evolution; (2) consider the role of the nm-thin SEI in liquid electrolytes as well as the microstructures of µm-thick solid electrolytes for lithium morphology evolution; (3) connect micron-scale phase-field models and atomic-scale DFT-based simulations via parameter- and relationship-passing to predict lithium dendrite nucleation and growth kinetics and morphology; and (4) validate the key input parameters and main conclusions of the multi-scale model as new capabilities are being developed step-by-step.

Project Impact. This atomically informed, fully coupled, electrochemical-mechanical dendrite morphology evolution model will allow the project to design the desired properties of artificial SEI coatings, the microstructure of solid electrolyte materials, and the corresponding battery operating conditions, so as to avoid dendrite growth during cycling. It will accelerate design of durable and safe lithium anodes for Li-S, Li-air, and all-solid Li-ion batteries. Thus, it directly impacts such emerging technologies that aim to meet the DOE target of the high-energy-density battery cells (> 350 Wh/kg) for EV applications and to push the cost below $\$100/\text{kWh}_{\text{use}}$.

Approach. A multi-scale model approach is taken to connect micron-scale phase-field models and atomic-scale DFT-based simulations via parameter- and relationship-passing.

Out-Year Goals. The second-year goal is to establish the model to simulate metallic lithium precipitation in solid electrolytes while further developing understanding of lithium dendrite growth in liquid electrolytes. To reach this goal, mechanical and electrochemical driving forces for lithium dendrite growth in solid electrolytes will be coupled in phase-field model, while DFT is used to address the lithium plating tendency in various solid electrolyte and coating materials. Validation of the model will come from experiments to correlate the distinctive transport properties of artificial SEI layers with their impact on lithium dendrite morphology.

Collaborations. This project collaborates with UMD, Sandia National Laboratories (SNL), PNNL, University of Arkansas, and University of Houston.

Milestones

1. Identify an ideal microstructure of LLZO to avoid lithium dendrite growth. (Q1, FY 2019. It was predicted a coating layer, such as LiPON, between the Li/LLZO, would be more efficient in resisting lithium dendrite. A *Go* decision was made to experimentally vary this prediction.)
2. Develop a fully coupled Li/SEI/liquid electrolyte dendrite morphology model. (Q2, FY 2019; Completed)
3. Illustrate the relationship between Li/SEI interface roughness, adhesion, and dendrite morphology in a liquid electrolyte. (Q3, FY 2019; Completed)
4. Determine the effect of multi-component SEI layer on dendrite morphology in a liquid electrolyte. (Q4, FY 2019; In progress)

Progress Report

To further figure out the SEI and lithium evolution, an isotope exchange experiment was designed. The process is to first deposit a ~ 5-µm ^{7}Li layer in an ether electrolyte (4 M ^{7}LiFSI DME) then deposit another ~ 5-µm ^{6}Li layer in carbonate electrolyte (1 M $^6LiPF_6$ EC/DEC) under a range of current densities from 0.2 to 3 mA cm^{-2}. While the second lithium layer morphology and CE changed monotonically with the current density (higher current density led to rougher morphology and lower CE), the ^{6}Li/^{7}Li ratio in the top ~ 100 nm did not change monotonically with the current density. As shown in Figure 41, the ^{6}Li/^{7}Li ratio ratios were very close to each other for current densities 1, 2, 3 mA cm^{-2} and became the highest at the current density of 0.5 mA cm^{-2}. It was speculated that the SEI formation rate and the current rate jointly determined the composition of the newly deposited SEI-covered lithium metal. The top SEI layer had mixed compositions from the pre-formed SEI (^{7}Li) and the newly formed SEI (^{6}Li). This indicates that electrolyte decomposition reactions continue to occur inside, instead of on top, of the pre-formed SEI layer, requiring detailed modeling of the inhomogeneity in SEI.

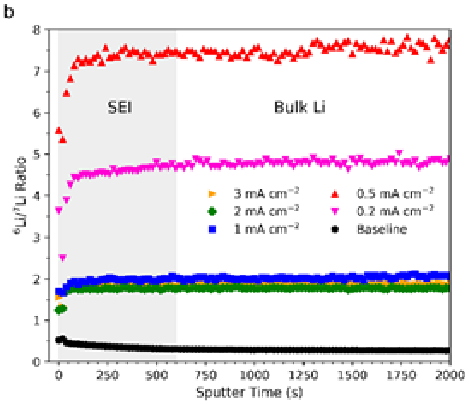

Figure 41. Time-of-flight secondary ion mass spectrometry depth profile of lithium surface under different deposition rate.

One key inhomogeneity in the SEI is the GBs. A systematic study of the electronic properties of GBs was conducted via DFT calculations. All the GBs reduced the bandgaps; the tilt GBs reduced the bandgaps to a larger extent than the twist GBs. Aligning the band structure with the lithium metal suggested that all the conduction bands of these GBs were still above the Li-metal reduction potential and thus would not be occupied. However, electron tunneling would be more likely to occur through the GBs with reduced tunneling barriers.

Table 5. Density functional theory calculated grain boundary energy and bandgaps.

Materials	Structure	GBE (mJ/m^2)	Bandgap (eV)
LiF	Bulk	-	8.83
	GB Twist ∑3 (111)	442.98	8.19
	GB Tilt ∑3 $(\bar{1}2\bar{1})$	701.79	7.26
	GB Twist ∑5 (001)	577.20	7.52
	GB Tilt ∑5 (310)	440.77	7.19
Li_2O	Bulk	-	5.23
	GB Twist ∑3 (111)	662.26	4.79
	GB Tilt ∑3 $(\bar{1}2\bar{1})$	1191.86	3.36

The local charge inhomogeneity (or space charge layer) at GBs or heterogeneous interfaces in the SEI plays an important role in the electrodeposition/intercalation process, particular for the initial stage of dendrite nucleation at Li-metal anode. The actual length scale of space charge distribution can be strongly associated with the grain size and defect density in the SEI or artificial coating layer. In this study, the impact of space charge length scale on lithium electrodeposition morphologies was investigated via the implicit SEI phase-field model. In the simulations, initial setup of different space charge length scales, ranging from 0.1 µm to ∞ (no space charge), was mimicked by point charges (square grids of 20 nm) with a charge density of 8.85 x 10^{-10} C · m^{-3} in SEI layer (the diffuse anode/electrolyte interface). All simulations of lithium electrodeposition were performed in 10 x 10 µm^2 half-cells with applied constant overpotential of –0.1 V. The Li-ion diffusion coefficient in SEI layer was set to be 10^{-11} m^2/s, which is one order of magnitude smaller than that in liquid electrolyte. The anode surface roughness was described by half-spherical protuberances with different sizes ranging from 0 to 1 µm. Based on the phase-field simulation results, conclusions can be drawn that (1) lithium dendrite growth during plating can be suppressed by decreased space charge length scale at anode surface, and that (2) when the space charge length scale is reduced to around the same order of anode surface protuberance size (initial roughness), smooth electrodeposition morphology can be achieved.

Patents/Publications/Presentations

Publications

- Tian, H-K., Z. Liu, Y. Ji, L-Q. Chen, and Y. Qi. "Interfacial Electronic Properties Dictate Li Dendrite Growth in Solid Electrolytes." *Chemistry of Materials* 31 (2019): 7351–7259.
- Xu, J., H-K. Tian, J. Qi, Q. Zhang, Y. Qi, and X. X. Xiao. "Mechanical and Electronic Stabilization of Solid Electrolyte Interphase with Sulfite Additive for Lithium Metal Batteries." *Journal of the Electrochemical Society* 166, no. 14 (2019): A3201–A3206.
- Xu, B., Z. Liu, J. Li, X. Huang, B. Qie, T. Gong, L. Tan, X. Yang, D. Paley, X. Liao, Q. Cheng, H. Zhai, X. Chen, L-Q. Chen, C-W. Nan, Y-H. Lin, and Y. Yang. "Engineering Interfacial Adhesion for High-Performance Lithium Metal Anode." Submitted (2019).
- Liu, Z., Y. Li, Y. Ji, Q. Zhang, X. Xiao, Y. Yao, L-Q. Chen, and Y. Qi. "Dendrite Free Li – Lesson Learned from the Li and Mg Electrodeposition Morphology Simulations." Pending submission (2019).

Presentations

- ECEE Meeting, Glasgow, Scotland (July 21–26, 2019): "Static and Dynamics View of the Solid Electrolyte Interphase during Charge Transfer Reactions—Modeling and Experiments." Invited.
- ACS Fall National Meeting, San Diego, California (August 25–29, 2019): "Atomically-Informed Phase-Field Modeling of Li and Mg Electrodeposition Morphologies." Invited.
- ACS Fall National Meeting, San Diego, California (August 25–29, 2019): "Atomic Prediction of the Energy Landscape of the Charge Transfer Reaction at the Complex Li/SEI/Electrolyte Interface." Invited.

Task 3.6 – First-Principles Modeling and Design of Solid-State Interfaces for the Protection and Use of Lithium-Metal Anodes
(Gerbrand Ceder, University of California at Berkeley)

Project Objective. The project objective is to determine the design principles that control the solid electrolyte / lithium electrode interfaces by determining the reaction products stemming from pairing solid electrolytes (SEs) and lithium metal. The project will conduct rigorous analysis based on computing electrolyte phase-diagrams closed and open to lithium. Li-ion transport properties in bulk electrolytes and interfacial products will be assessed through AIMD and NEB calculations. Simultaneously, a robust framework will be developed to identify factors controlling lithium dendrite propagation within SEs and interfacial products by accounting for irregularities, defects, and GBs, through a model that includes elements of fracture mechanics, thermodynamics, and electrochemistry.

Project Impact. The project will lead to understanding of the complex evolution of lithium metal/SEI during electrochemical cycling. The understanding of this process is necessary to determine design principles to develop reliable all solid-state batteries.

Approach. By incorporating NEB and AIMD methods, high-throughput computation is used to screen candidate solid electrolyte with high electrochemical stability and high ionic conductivity. DFT is used to calculate bulk elastic constants of materials, surface energies, and interface decohesion energies of GBs; continuum theory (elastic-plastic-fracture mechanics) is used to assess the resilience of solid electrolytes and grain/particle boundaries toward lithium dendrite growth and propagation. The finite element method is used to couple several physical processes, including electrochemical deposition, ionic diffusion, thermal expansion, and mechanical contacting.

Out-Year Goals. The out-year goals include the following: (1) obtain design criteria for solid electrolytes that can resist unstable lithium propagation by computing elastic properties, surface energies, and decohesion energies, and (2) adapt fracture mechanics models describing crack propagation to lithium dendrite propagation in different scenarios.

Collaborations. There are no collaborative activities this quarter.

Milestones

1. Development of high-throughput framework to screen SSE materials based on phase stabilities. (Q1, FY 2019; Completed)
2. Adapt fracture models that describe crack propagation in materials to lithium dendrite propagation in perfect crystal with cracks. (Q2, FY 2019; Completed)
3. Adapt fracture models that describe crack propagation in materials to lithium dendrite propagation in perfect crystal with GBs. (Q3, FY 2019; Completed)
4. Adapt fracture models that describe crack propagation in materials to lithium dendrite propagation in pressed/porous electrolyte. (Q4, FY 2019; Completed)

Progress Report

Effect of Defect Geometry and SE Material Property on the Interfacial Deposition Stability. The team has been investigating the combined mechano-transport issues resulting from the deposition of lithium from a solid-state conductor with flaws and irregular surface contact by integrating the transport equations with mechanical models for the materials that incorporate elasticity, plasticity, and fracture. Figure 42 shows the lithium deposition stability, which measures inhomogeneity of current as contour plot against the length of a defect emanating from the lithium anode and the damping length of the SE. The damping length is a materials property of the SE, related to ionic conductivity and exchange current density of the SE with lithium metal, that quantifies the ability of the SE to dampen deposition instability caused by surface irregularities. The lithium deposition is more stable when the defect length decreases and the damping length increases. SE with large damping length (such as LPS) creates more stable deposition than SE with small damping length (such as LLZO) when the surface roughness is similar. That is, SE with larger damping length can tolerate worse surface quality.

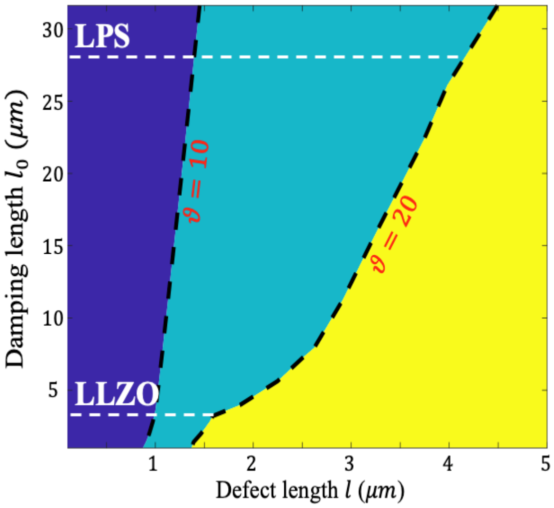

Figure 42. The deposition stability ϑ as a function of defect length l and damping length l_0 of different SE material.

Effect of Stack Pressure on Mechanical Stability of the SE. Most solid-state batteries use an applied stack pressure to retain good interfacial contact on cycling. Internal stress from the stack pressure can provide a driving force for lithium deformation and help to retain contact when an uneven lithium surface forms due to uneven deposition. Low stack pressure may result in insufficient lithium deformation and cause interfacial contact loss, while large stack pressure leads to severe stress concentration and causes lithium infiltration into pores/GBs of the SE, where it may cause fracture if the stress intensity factor is above the limit of the fracture toughness of the SE. Therefore, a "mechanical stability window" of the stack pressure (shown in Figure 43) is available to prevent both contact loss and SE fracture. For solid-state battery system with different combinations of metal electrodes and SEs, the required mechanical stability window for stack pressure can be very different. In general, smaller stack pressure is needed in a Na-metal system than in Li-metal system to maintain intimate contact because of the lower yield strength of Na-metal compared to Li-metal. Oxide-SE systems can withstand much larger stack pressure than sulfide-SE systems because of their much larger moduli and fracture toughness.

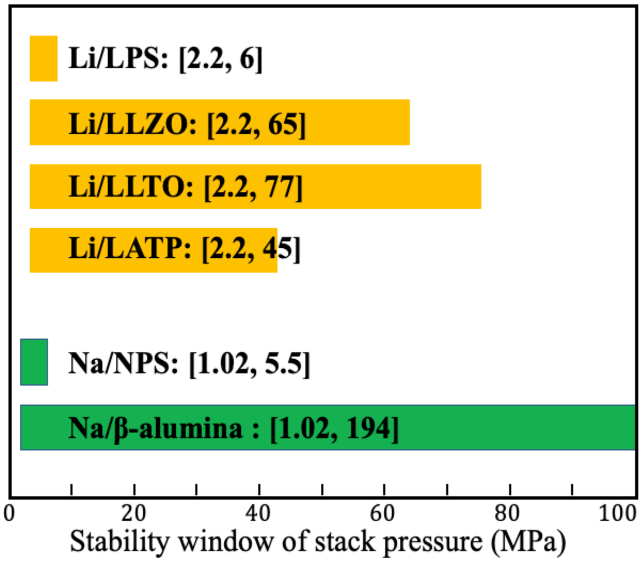

Figure 43. The mechanical stability window of the stack pressure for different solid-state battery systems.

Patents/Publications/Presentations

Publications

- Tu, Q., et al. "Modeling of Electro-Deposition and Mechanical Stability at Li Metal/Solid Electrolyte Interface during Plating in Solid-State Batteries." Submitted to *Joule*.
- Barroso-Luque, L., et al. "An Analysis of Solid-State Electrodeposition-Induced Metal Plastic Flow & Predictions of Stress States in Solid Ionic Conductor Defects." Submitted to *Journal of the Electrochemical Society*.

Task 3.7 – Large-Scale *Ab Initio* Molecular Dynamics Simulations of Liquid and Solid Electrolytes (Lin-Wang Wang, Lawrence Berkeley National Laboratory)

Project Objective. The project objective is to use AIMD simulations and other computational approaches to study the discharging mechanism in Li-S battery, especially for polysulfide interaction with liquid electrolyte solvent molecules, and cathode materials, as well as lithium diffusion mechanisms in various systems. The long-term goal is to use such theoretical understanding to provide guidance to develop better electrolyte and cathode systems to overcome the bottlenecks that prevent commercialization of the Li-S battery.

Project Impact. Making the Li-S battery a commercial reality will have a major impact on society and also help to realize the VTO goal of 500 km per charge for EV. However, the nature of chemical reaction makes it different from the traditional intercalation-based Li-ion battery. The molecular nature of Li_2S_n also allows solvation in the electrolyte. To address these problems, it is essential to have fundamental studies and understandings of the underlying mechanisms. The theoretical simulation can also play an important role in discovering and designing new cathode materials.

Approach. One major issue is solvation of Li_2S_n molecules in the electrolyte. The project seeks to solve this problem by both understanding the Li_2S_n-electrolyte interaction and discovering better cathode materials for optimal Li_2S_n-cathode binding. More specifically, it aims to develop reliable methods that combine classical force field (CFF) simulations with *ab initio* calculations to study thermal dynamic properties of Li_2S_n in different electrolytes, as well as interactions with different species within the electrolytes. It will also study Li_2S_n interaction with different cathode materials, especially for 2D cathode materials comprised with light elements in the right-upper corner of the periodic table. The goal is to have sufficient binding energy between the Li_2S_n molecules and the cathode material, so that, thermodynamically, the Li_2S_n will not be dissolved in the electrolyte. To study Li_2S_n-electrolyte interaction, the project must accurately calculate molecule entropy inside the solvent, which is a rather challenging task. It plans to use the bicanonical method to carry out the calculation. To design new cathodes, the project plans to focus on lightweight 2D materials. Genetic algorithm combined with DFT will be used to explore the structure and morphology of the Li_2S_n cluster on top of the 2D material. The stability of the solid electrolyte will be investigated by studying the surface reaction of such electrolytes.

Out-Year Goals. In outgoing years, the project will further develop the computational methods for more accurate entropy and interaction energy calculations for the electrolyte. This is a critical capability for studying the battery system. The project will also explore different cathode materials and morphologies. In particular, there is a vast space to explore using 2D materials as Li-S battery cathodes. Stability of the solid electrolyte is another topic to be investigated.

Collaborations. The project will collaborate with G. Liu and Y. Cui for cathode design. It has also collaborated with Prof. F. Pan of Beijing University for lithium battery research in general.

Milestones

1. Develop reliable ways to calculate the diffusion barrier of lithium in either crystal or amorphous structure. (Q1, FY 2019; Completed)
2. Continue calculation of Li_2Sn/cathode binding energies, and phase diagrams, discovering new adequate cathode materials and morphologies. (Q2, FY 2019; Initiated)
3. Investigate the solid electrolyte, its pathways and surface stabilities, and electrolyte/anode interface. (Q3, FY 2019)
4. Develop method to calculate Li-ion chemical energy in liquid electrolyte with *ab initio* calculations. (Q4, FY 2019)

Progress Report

Sulfur vulcanization is a well-known process that converts natural rubber or related polymers into materials of a variety of hardness, elasticity, and mechanical durability by heating them with sulfur. One possibility is to take advantage of this process, using the sulfur in such materials for Li-S battery application. Polymers with properly designed structure and specific properties can be used to hold the sulfur chains for applications in Li-S batteries. For this purpose, the team tried to theoretically design proper polymers for easy vulcanization with maximum amount of sulfur to gain better energy capacity. This can be done by adjusting the functional groups in the polymer. As shown in Figure 44, the team tried to find different factors that favor vulcanization. They have compared the vulcanization energy of 5-Decene in two methods (cycloaddition and crosslinking) with different sulfur chains. By calculating the vulcanization energies, the team finds that crosslinking is thermodynamically favorable for vulcanization, and the length of sulfur chains is 6. Meanwhile, the edge C=C is better than in the middle of the polymer chains.

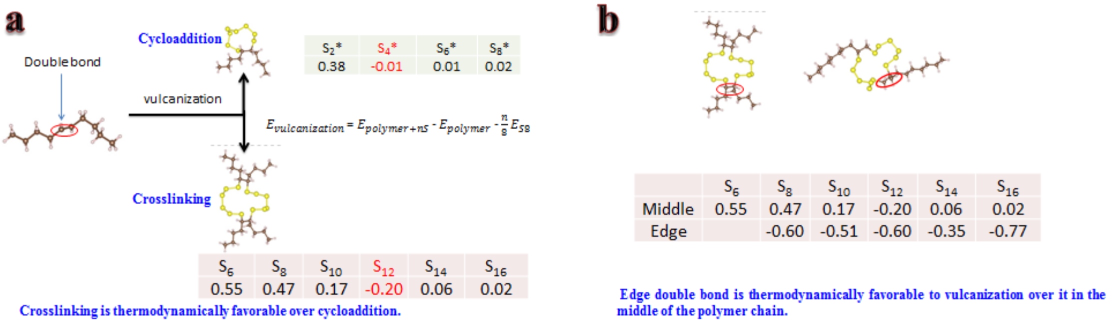

Figure 44. (a) Vulcanization of 5-Decene in two methods (cycloaddition and crosslinking). (b) Two different positions of C=C in Decene are considered as vulcanization sites.

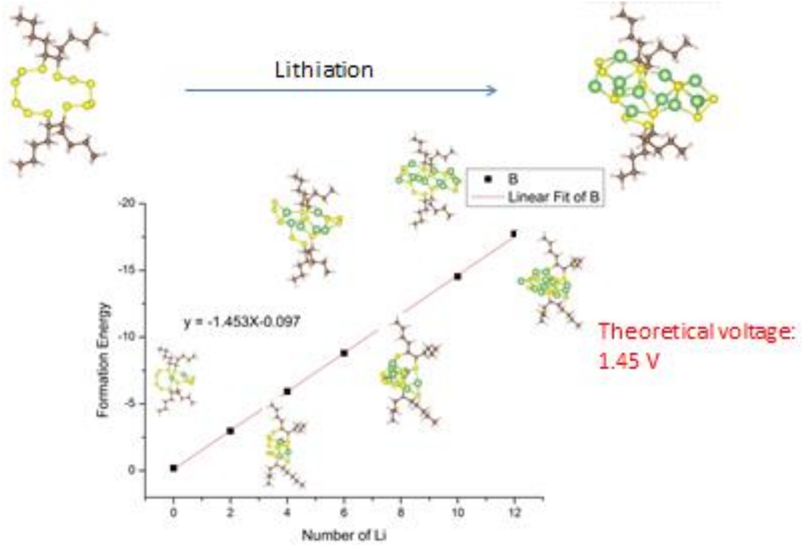

Figure 45. The lithiation process of sulfur vulcanized 5-Decene.

Figure 45 plots the lithiation process of sulfur vulcanized 5-Decene. During the lithiation process, the lithium atoms break long sulfur chains into isolated sulfur, gradually. Meanwhile the structure of 5-Decene is well-preserved. The formation energy is linearly, with the number of lithium added into the complex with a slope of -1.45, indicating a stable energy provided with a voltage of 1.45 V during the discharge process. The voltage is lower than the theoretical voltage of pure lithium polysulfide (2.1 ~ 2.4 V). The gravimetric capacity is 530.35 Wh/Kg. In the following, the team tries to increase gravimetric capacity, enhance conductivity, and obtain higher discharge voltage.

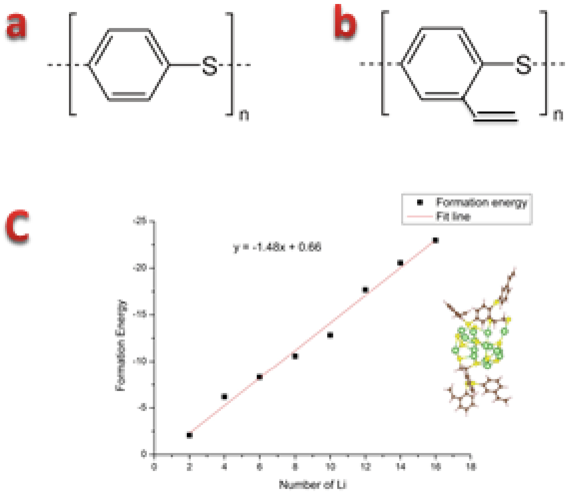

Figure 46. (a) Polyphenylene sulfide. (b) 2-vinyl polyphenylene. (c) The lithiation process of sulfur vulcanized 2-vinyl polyphenylene.

Here, the conductive polymer, polyphenylene sulfide (see Figure 46a) is chosen as the conductive backbone chain. Then, the team induces vinyl group onto the backbone chain (see Figure 46b). Consistent with previous polymer, the edge C=C in the vinyl group is thermodynamically favorable for vulcanization. The vinyl group is able to attract sulfur by vulcanization. During the lithiation process, the lithium only react with the sulfur chain, while the backbone chain is not damage. The formation energy is linearly, with the number of lithium added into the complex with a slope of -1.48, indicating a stable energy provided with a voltage of 1.48 V during the discharge process (see Figure 46c).

The team plans to investigate other structures, especially to increase the voltage, perhaps through use of bigger sulfur clusters. They also need to study bigger systems to investigate the structure of the overall polymer system, especially to understand whether the polyphenylene will still be electrically conductive in such an environment.

Patents/Publications/Presentations

Publications

- Chen, D., J. Jie, M. Weng, S. Li, D. Chen, F. Pan, and L. W. Wang. “High Throughput Identification of Li Ion Diffusion Pathways in Typical Solid State Electrolytes and Electrode Materials by BV-Ewald Method.” *Journal of Materials Chemistry A* 7 (2019): 1300.
- Tsao, Y., M. Lee, E. C. Miller, G. Gao, J. Park, S. Chen, T. Katsumata, H. Tran, L. W. Wang, M. F. Toney, Y. Cui, and Z. Bao. “Designing a Quinone-Based Redox Mediator to Facilitate Li_2S Oxidation in Li-S Batteries.” *Joule* 3 (2019): 872.
- Banerjee, S., X. Zhang, and L. W. Wang. “Motif Based Design of a Mixed Oxygen-Sulfur Framework Towards Improved Stability and Record High Li-ion Conductivity.” *Chemistry of Materials* 31 (2019): 7265.

Task 3.8 – *In Operando* Thermal Diagnostics of Electrochemical Cells (Ravi Prasher, Lawrence Berkeley National Laboratory)

Project Objective. Effective heat dissipation in batteries is important for multiple reasons including performance, reliability, and safety. Currently, the thermal management of battery cells is provided at the system level by either forced air or liquid cooling, leading to reduced system-level energy densities and more failure-prone complex system designs. Furthermore, even given theoretically infinite system-level cooling applied to the external battery surface, peak temperature rise within a cell would still easily exceed acceptable threshold values due to poor thermal transport properties within the cell itself. It has not yet been possible to thermally profile a real cell during operation to provide a spatially resolved map of heat transfer properties throughout the cell. The objective of this research is to create a metrology capable of spatially resolved *in operando* thermal property profiling, and then use this tool to reveal the largest thermal bottlenecks within a functioning Li-ion cell and create a complete materials-level cell thermal model.

Project Impact. The intrinsic thermal resistance of Li-ion cells is currently far higher than the theoretical value predicted by simply combining the known thermal properties of each macro component into an appropriate thermal model. The spatially resolved thermal transport property measurements from this project will reveal what key piece of information is missing. Preliminary data suggest that more than 75% of the total battery thermal resistance may be due to a single interface between the cathode and separator, previously unknown. An accurate understanding of the cell internal thermal transport is necessary to successfully optimize cell thermal performance to meet the challenges of extremely fast charging, mitigating thermal runaway, and improving battery performance, reliability, and safety.

Approach. To accomplish the project goals, the team will utilize two state-of-the-art thermal metrology techniques. They will build an in-house adapted 3-omega technique to measure thermal transport properties throughout the bulk of a Li-ion cell while it is in operation, without affecting the operation of the cell. The 3-omega system will work by using mm-scale sensors on the electrode current collectors to send variable-frequency thermal waves into the operational battery to quantitatively measure heat transport through different layers and interfaces. The team will also use the ultrafast optical time domain thermoreflectance (TDTR) technique to measure nanoscale thermal transport properties of constituent components of the cathode composite. They will then combine these results to create an “all-scale” accurate thermal model of the cell that—unlike existing models—agrees with the empirical measurements of cell thermal performance.

Out-Year Goals. In outgoing years, the project will design, build, and implement the adapted 3-omega metrology. This will involve developing and testing the metrology itself along with accompanying theory, designing compatible battery samples, and applying the technique to live cells. The team will use the TDTR system at LBNL to measure epitaxially grown cathode materials provided by collaborators. Combined, this will provide enough data to construct and validate a realistic all-scale thermal model of the battery.

Collaborations. This project collaborates with two LBNL groups: V. Battaglia’s for cell assembly for 3-omega studies, and R. Kostecki’s for pristine battery active material growths for TDTR studies.

Milestones

1. *Ex situ* high-accuracy measurements of thermal conductivity of individual battery components. (Q1, FY 2019; Completed)
2. Robust thermal model development. (Q2, FY 2019; Completed)
3. *In situ* battery 3-omega thermal measurements from anode and cathode side. (Q3, FY 2019; Completed)
4. Detailed *in operando* thermal measurements performed. (Q4, FY 2019; Completed)

Progress Report

The team has successfully completed detailed *operando* thermal measurements. They have upgraded the system from the last report to be compatible with a battery cycler. This has enabled them to measure the thermal contact resistance (TCR) between the separator and the electrodes ($TCR_{s\text{-}e}$) while cycling the battery. The results of these measurements are shown in Figure 47.

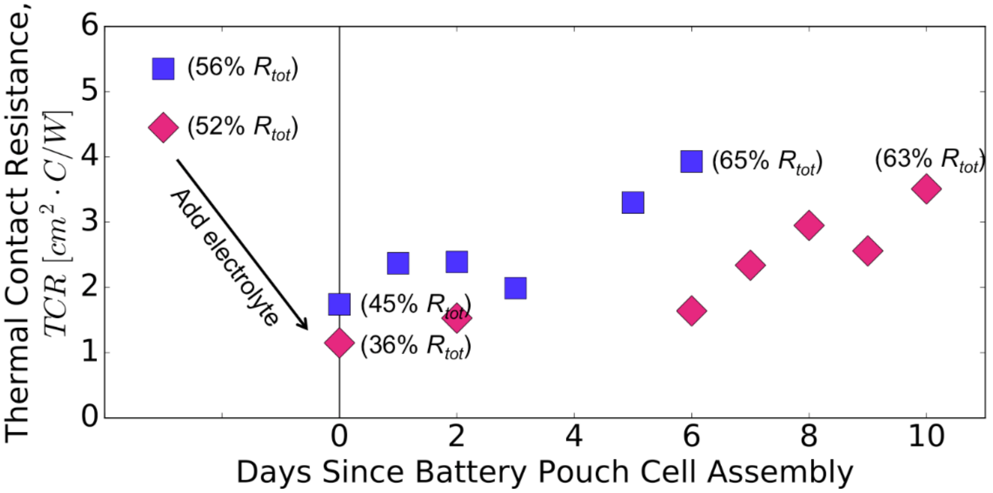

Figure 47. *Operando* cycling of two battery pouch cells with concurrent separator-electrode thermal contact resistance (TCR) measurements. The two different point sets correspond to two separate battery pouch samples, each cycled for 2 to 5 formation cycles at rates of C/20 to C/10. The far left points are before adding electrolyte (that is, for the dry cell). The numbers in parentheses indicate the percent of the battery's total internal thermal resistance resulting from the $TCR_{s\text{-}e}$ alone.

The $TCR_{s\text{-}e}$ measurements were made both during charging and discharging, and during holds in between charging and discharging cycles. The thermal resistance drops considerably between the dry and electrolyte-wetted states. This is consistent with the higher thermal conductivity electrolyte ($k_{electrolyte}$ = 0.2 W/m-K) filling in the voids that had previously been occupied by lower thermal conductivity air (k_{air} = 0.025 W/m-K).

The team observes a significant increase in the $TCR_{s\text{-}e}$ with formation cycling. Possible reasons could be the formation of SEI layers that increase thermal resistance, or possibly micro-bubbles trapped right at the separator-electrode interface resulting from battery outgassing. Note that the batteries were held under a constant pressure of 5 PSI during cycling. Future work should further investigate the possible reasons for the increased thermal resistance with cycling, as well as try to improve sensors so that they can last for more cycles to see at what point the $TCR_{s\text{-}e}$ levels off. Future work should also seek to formulate a physics model of the TCR between the separator and the electrodes, compare it with the data, and seek to explain the high $TCR_{s\text{-}e}$ and why it increases over time.

Patents/Publications/Presentations

Presentation

- American Society of Mechanical Engineering (ASME) International Technical Conference and Exhibition on Packaging and Integration of Electronic and Photonic Microsystems (InterPACK), Anaheim, California (October 7–9, 2019). The work presented received much interest and positive reception from both academics and industry.

Task 3.9 – Multi-Scale Modeling of Solid-State Electrolytes for Next-Generation Lithium Batteries (Anh Ngo, Larry A. Curtiss, and Venkat Srinivasan, Argonne National Laboratory)

Project Objective. This project is part of a multi-scale modeling effort to obtain an in-depth understanding of the interaction of the electrode and the solid electrolyte aimed at developing highly efficient SSE batteries for vehicle applications. Input parameters needed for mesoscale (continuum) level calculations are being obtained from atomistic calculations including DFT and classical MD simulations. This atomistic input will enable a multi-scale computational procedure for SSEs that is capable of successfully capturing the physicochemical aspects during charge and discharge process including lithium transport mechanisms, interfacial phenomena during the insertion and extraction of lithium ions, and mechanical deformation of SSE.

Project Impact. A major safety concern experienced with commercially available Li-ion batteries under some scenarios is leakage of the liquid electrolyte, which can potentially catch fire. Replacement of the liquid electrolyte is necessary to decrease the fire hazard and improve safety associated with present-day Li-ion batteries. In addition, use of solid electrolytes provides a path to prevent dendrites in Li-metal anodes, thereby leading to batteries with significantly higher energy density. The impact of this project will be to help in development of good SSEs as a replacement for the commercially used organic liquid electrolytes to improve safety and energy density in Li-ion batteries.

Approach. Parameters needed for mesoscale modeling of GI, GB, and electrode-electrolyte interface will be calculated by DFT-based calculations along with Monte Carlo (MC) and MD simulations. The calculations will be used to determine properties of the electrode with the solid electrolyte as well as in GB regions of the solid electrolyte. This will include calculations of structure, stability, ionic conductivity, Young's modulus, fracture toughness, exchange current density, and other properties.

Out-Year Goals. The out-year goals of this work are to calculate other properties such as fracture toughness and include other SSEs and coatings in the multi-scale modeling.

Collaborations. This project collaborates with Y. Cui at Stanford.

Milestones

1. Computation of elastic. Conductivity properties of interfaces between LLZO with lithium as function of applied electric field for input into multi-scale modeling. (Q1, FY 2019; Completed)
2. AIMD and interfacial binding energies calculations of the interface structure of the LLZO solid electrolyte and NMC-622 cathode material. (Q2, FY 2019; Completed)
3. Calculations of lithium migration barriers at interface LLZO/NMC cathode material for estimation of exchange current density NMC/LLZO interfaces. (Q3, FY 2019; Completed)
4. Continuum-level mesoscale calculations for LLZO/NMC cathode materials. (Q4, FY 2019; Completed)

Progress Report

Continuum-Level Mesoscale Calculations for LLZO/NMC Cathode Materials. The activation energy barrier, jumping frequency, and reaction rate pre-factor are needed to successfully estimate the magnitude of the exchange current density. All these parameters for NMC/LLZO interface were predicted using DFT-based atomistic calculations last quarter. This quarter, these numbers from the lower length scale were incorporated into the mesoscale model, and the lithium exchange current density between NMC and LLZO is calculated and plotted in Figure 48a. Due to dependence on surface concentration, the magnitude of exchange current density varies with SOC. The red "x" symbol indicates experimental data where the exchange current density between LCO and LLZO was measured. Since the computational value and experimental observation both lie within the same order of magnitude, the team accepted the calculated exchange current density, and used it in the mesoscale simulations. Along with interfacial reaction rate constants, the continuum-level mesoscale simulation of NMC/LLZO interface requires information regarding the partial molar volume of lithium within NMC and open circuit potential of the cathode material, which have been extracted from experiments and also demonstrated in Figure 48b-c. The experimental data are denoted by black circles, and the red solid line indicates mathematical fit. These best-fit equations were used in the mesoscale model. The adhesion energy between NMC and LLZO has been predicted using atomistic calculations, as reported in the second quarter.

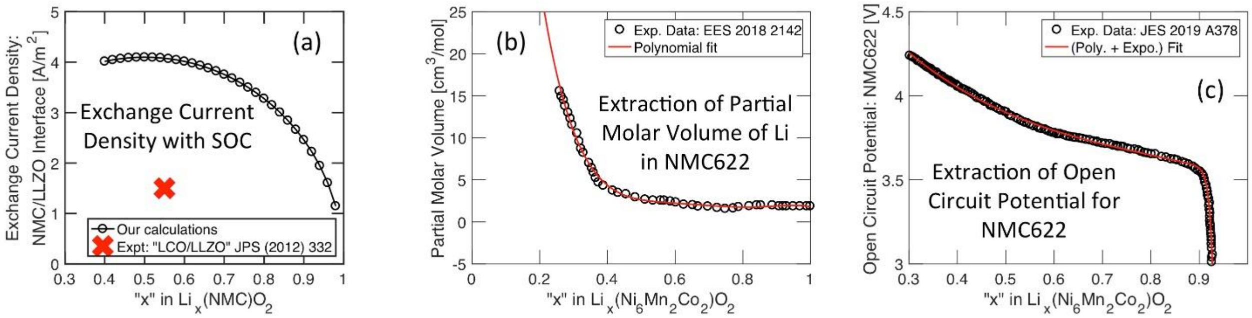

Figure 48. (a) Comparison of the lithium exchange current density between LLZO and NMC as obtained from density functional theory calculations (denoted by black circles) and experiments (red "x" symbol). (b) Extraction of partial molar volume data for NMC-622 from experiments. (c) Extraction of open circuit potential (OCP) data for NMC-622 from experiments.

The NMC/LLZO microstructure shown in Figure 49a was used to conduct mesoscale simulations. Here, the LLZO grains (red) are around 40 nm in size, and the thickness of the GB domain (yellow) is around 10 nm. The black dots indicate broken bonds, and the existence of a large number of broken elements at the NMC/LLZO interface indicates delamination. Extremely small sized LLZO grains have been used here, because LLZO microstructures with larger grains experienced full delamination even before the completion of the first charge process. Figure 48b demonstrates the charge-discharge curves without (red) and with (black) delamination. Increased interfacial resistance due to delamination leads to performance decay. Successful simulation of NMC/LLZO interface at the mesoscale level completes this quarter's milestone.

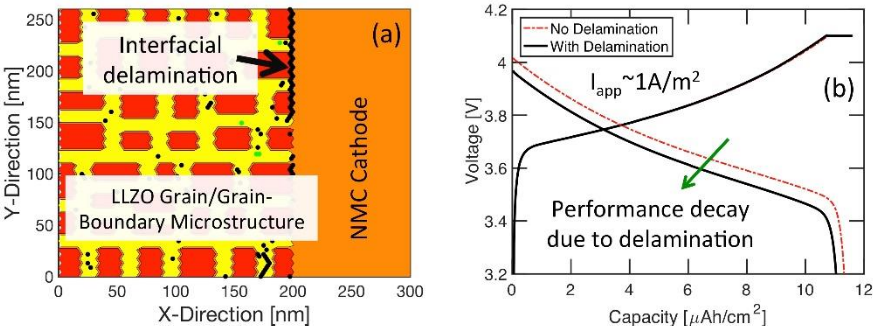

Figure 49. (a) Simulation domain containing LLZO grain/grain-boundary microstructure (denoted by red and yellow) and NMC cathode (shown in orange). Fracture is denoted by the black dots, which indicate interfacial delamination. (b) Charge-discharge curves as predicted without (red) and with (black) delamination.

Patents/Publications/Presentations

Publication

- Barai, P., A. T. Ngo, B. Narayanan, K. Higa, L. A. Curtiss, and V. Srinivasan. "Multiscale Modeling of Current Focusing and Dendrite Growth at Lithium/LLZO Interface." In preparation.

Task 3.10 – Integrated Multi-Scale Modeling for Design of Robust 3D Solid-State Lithium Batteries (Brandon Wood, Lawence Livermore National Laboratory)

Project Objective. This project will develop a multi-scale, multi-physics modeling framework for probing the effects of materials microstructure and device architecture on ion transport within 3D solid-state battery materials, with the goal of enhancing performance and reliability. The project has three primary objectives: (1) integrate multi-physics and multi-scale model components; (2) understand interface- and microstructure-derived limitations; and (3) derive structure-performance relations for optimization.

Project Impact. This project will lead to understanding of interfacial losses and instabilities that impede performance and promote failure of solid-state batteries. The multi-scale and multi-physics modeling framework developed in this work will address shortcomings of existing modeling strategies that either lack coupling of the multi-physics nature of various processes active in 3D batteries or fail to incorporate processes at different length scales to understand function. Ultimately, the tools and understanding generated by this project can be utilized to realize optimization of interface-dominated 3D batteries.

Approach. The project approach integrates simulations at three scales. First-principles and classical MD simulations are used to compute fundamental Li-ion diffusion within bulk solid electrolyte and cathode materials; along/across GBs of the electrolyte; and along/across electrolyte/cathode interfaces. Phase-field simulations are used to generate digital representation of realistic microstructures of the materials, which are combined with the atomistic simulation results to parameterize mesoscale effective property calculations and to establish microstructure-property relationships for ion transport. Finally, these relationships inform a cell-level macroscopic electro-chemo-mechanical modeling framework, which can be used to optimize the performance of 3D solid-state lithium batteries.

Out-Year Goals. Future activities will focus on refining the project's atomistic interface models for improved fidelity of ion transport simulations through crystalline and amorphous LLZO and across interfaces. The team will also work with collaboration partners to reconstruct microstructures of 3D-printed materials and apply them to determine effective stresses and ion transport through the polycrystalline materials.

Collaborations. This project collaborates with Dr. N. Adelstein from San Francisco State University (SFSU, atomistic diffusion modeling) and Dr. Ye from LLNL (3D printing of solid-state battery materials). They also partner with Dr. E. Ivers-Tiffee from Karlsruhe Institute of Technology (KIT, impedance spectroscopy of SSEs), Dr. P. Zapol from Argonne (modeling of solute segregation in LLZO), and Prof. D. Fattakhova-Rohlfing from Forschungszentrum Jülich (FZJ, controlled synthesis of LLZO with varying densities and microstructures) as part of the U. S.–Germany partnership on solid-state battery research.

Milestones

1. Compute mechanical properties of LLZO. (Q1, FY 2019; Completed)
2. Compute barriers for ion transport in LCO and LLZO. (Q2, FY 2019; Completed)
3. Demonstrate multi-scale simulation framework for effective ion transport. (Q3, FY 2019; Completed)
4. Demonstrate agreement between predicted and measured ionic conductivity. (Q4, FY 2019; Completed)

Progress Report

Atomistic Simulation of Mechanical Properties and Activation Energies for Li-ion Diffusion. This quarter's atomistic simulation efforts focused on establishing baseline elastic and mass transport properties of $LiCoO_2$ electrodes and LLZO solid electrolytes, as well as their interdependence. These baseline calculations are essential inputs for the microstructure-level mesoscale modeling. First, the elastic constants were calculated using DFT, with results summarized in Table 6 for cubic LLZO, lithium metal, and hexagonal $LiCoO_2$. The elastic properties will inform the strains that can be induced at the electrode-electrolyte interface in response to cycling or differences in lithium chemical potential across the components.

Table 6. Elastic constants for LLZO, LCO, and lithium metal.

Material	Bulk modulus (GPa)	C_{11} (GPa)	C_{12} (GPa)	C_{44} (GPa)
Li metal (bcc)	13.7	14.2	13.5	11.5
LLZO (sc)	110	180	75	73

Material	Bulk modulus (GPa)	C_{11} (GPa)	C_{12} (GPa)	C_{13} (GPa)	C_{33} (GPa)	C_{44} (GPa)
$LiCoO_2$ (hex)	154	380	119	110	279	125

Second, the activation energy for Li-ion hopping in $LiCoO_2$ as a function of strain was calculated using DFT, combined with the NEB method. It has been proposed that Li-ion can diffuse in $LiCoO_2$ through either single vacancy or di-vacancy mechanism; accordingly, the team evaluated strain-dependent activation energies for Li-ion hopping in $LiCoO_2$ based on these two mechanisms. As shown in Table 7, applying compressive strain along the c-axis will substantially increase the activation energy for lithium diffusion.

Table 7. Strain-dependent activation energies for lithium diffusion in $LiCoO_2$.

Mechanisms	Uniaxial strain, a	Uniaxial strain, b	Uniaxial strain, c
Single vacancy	25 meV/%	17 meV/%	64 meV/%
Di-vacancy	9.4 meV/%	9.4 meV/%	53 meV/%

Third, Li-ion transport in the solid-electrolyte LLZO was evaluated by the NEB method at 0K and classical MD at finite temperatures. Using the NEB method, the team calculated the activation energy for lithium diffusion within LLZO based on three diffusion mechanisms: single-ion hopping, dimer, and trimer concerted motion. Table 8 shows that the activation energy for Li-ion diffusion in LLZO highly depends on the local lithium concentration near the diffusion pathways. In bulk LLZO, all of these mechanisms can contribute to Li-ion diffusion, establishing the importance of a fully dynamical approach that can evaluate the effects of composition on the overall Li-ion mobility. In collaboration with Dr. Adelstein at SFSU, the team used classical MD to examine composition-dependent Li-ion diffusivity in LLZO. They found that the lowest activation energy for Li-ion diffusion, ~ 0.22 eV, is for composition $Li_{6.5}La_3Zr_2O_{12}$.

In addition to composition, structural disorder at interfaces and GBs can play a significant role in determining ion transport kinetics. Accordingly, the team is working with its collaborators to derive ionic diffusivities of generic high-angle grain boundaries of LLZO based on MD simulations of lithium migration in atomistically disordered LLZO. Preliminary values were used to parameterize the project's mesoscale model to compute the effective lithium diffusivity of polycrystalline LLZO.

Table 8. Effects of vacancy on Li-ion transport in LLZO.

Compositions	Single-ion	Dimer	Trimer
Full Li+ occupation	0.15 eV	0.10-0.15 eV	0.16 eV
Single-vacancy near diffusion pathway	0.34 eV	0.38-0.54 eV	0.31-0.49 eV

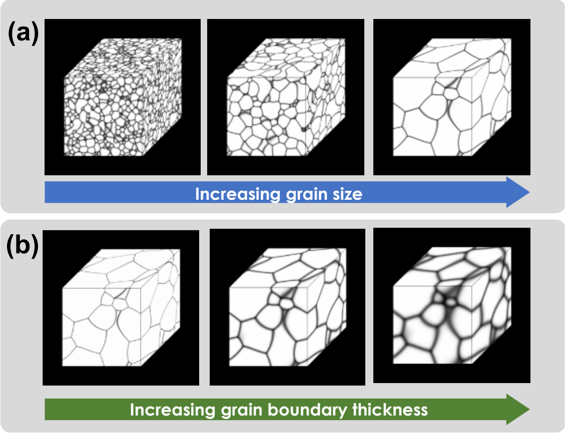

Figure 50. Examples of generated digital microstructures of polycrystalline LLZO with (a) different grain sizes; and (b) different grain boundary thicknesses.

Mesoscale Modeling of Lithium Transport through Complex Microstructures. This quarter's mesoscale modeling efforts focused on parameterizing the mesoscale model of effective ion transport in LLZO as a function of microstructure, as well as systematically investigating the impacts of specific microstructural features. The team first generated 3D digital microstructures of polycrystalline LLZO in a controlled fashion using phase-field simulations. Figure 50 shows examples of generated microstructures with different grain sizes and GB thicknesses. These simulated complex microstructures were used as inputs for mesoscopic effective diffusivity/conductivity calculations. Corresponding position-dependent lithium diffusivity models for the microstructures were parameterized by bulk and GB diffusivities derived from the team's classical MD simulations. Based on these inputs, they have begun performing computations of effective lithium ionic conductivities of a series of systematically generated microstructures as a function of temperature.

Below, the team introduces one example of how microstructure is predicted to affect ionic conductivity (Figure 51a). Using preliminary values from atomistic simulations, the computed effective conductivity of polycrystalline LLZO is predicted to undergo a transition from bulk-dominant to the GB-dominant behaviors. To characterize this transition for the given microstructure, the team defines the "*kink temperature* (T_{kink})" where this transition occurs, which is a function of temperature, grain size, and GB thickness, among other factors (see inset, Figure 51a). Figure 51a-b shows the characterized kink temperatures as functions of grain size and GB thickness, respectively. The extracted kink temperatures exhibit nonlinear and nontrivial behaviors with varying grain size and GB thickness, with implications for performance. In addition, the team notes that kink temperature is highly sensitive to those two microstructural features, indicating the possible tunability of lithium conductivity characteristics/behaviors by controlling LLZO microstructures. In future, parameters will be refined and validated by partnering with microstructural and impedance data from the project's experimental collaborators to connect processing routes to performance.

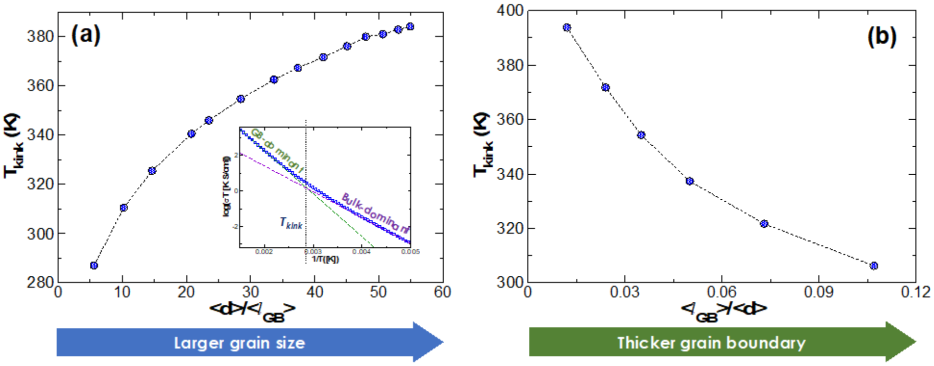

Figure 51. Characterized kink temperatures of computed temperature-dependent ionic conductivities of polycrystals with (a) increasing grain size; and (b) increasing grain boundary thickness.

Patents/Publications/Presentations

Presentations

- Korea Institute of Science and Technology (KIST) – LLNL Workshop, Livermore, California (September 23–26, 2019): “Atomistic Modeling of Interfaces in Solid-State Batteries”; L. Wan.
- Korea Institute of Science and Technology (KIST) – LLNL Workshop, Livermore, California (September 23–26, 2019): “Mesoscale Approach for Modeling Solid-State Electrodes and Electrolytes”; T. W. Heo.
- Korea Institute of Science and Technology (KIST) – LLNL Workshop, Livermore, California (September 23–26, 2019): “Electrochemomechanics of Lithium Dendrite Growth”; A. Jana.

TASK 4 – METALLIC LITHIUM

Summary and Highlights

The use of a metallic lithium anode is required for advanced battery chemistries like Li-ion, Li-air, and Li-S to realize dramatic improvements in energy density, vehicle range, cost requirements, and safety. However, use of metallic lithium with liquid and polymer electrolytes has so far been limited due to parasitic SEI reactions and dendrite formation. Adding excess lithium to compensate for such losses effectively negates the high energy density for lithium in the first place. For a long lifetime and safe anode, it is essential that no lithium capacity is lost either (1) to physical isolation from roughening, dendrites, or delamination processes, or (2) to chemical isolation from side reactions. The key risk, and current limitation, for this technology is the gradual loss of lithium over the cycle life of the battery.

BMR, Battery500, and other DOE programs are addressing this challenge with many innovative and diverse approaches. Key to all is the need for a much deeper analysis of the degradation processes and new strategies to maintain a dense, fully connected lithium and a dendrite-free electrolyte so that materials can be engineered to fulfill the target performance metrics for EV application, namely 1000 cycles and a 15-year lifetime, with adequate pulse power. Projecting the performance required in terms of just the lithium anode, this requires a high rate of lithium deposition and stripping reactions, specifically about 30 µm of lithium per cycle, with pulse rates up to 10 and 20 nm/s (15 mA/cm^2) charge and discharge, respectively, with little or no excess lithium inventory. This is daunting in the total mass and rate of material transport that must be achieved without failures.

The efficient and safe use of metallic lithium for rechargeable batteries is then a great challenge, and one that has eluded R&D efforts for years. This project takes a broad look at this challenge for both solid-state batteries and batteries continuing to use liquid electrolytes. For the liquid electrolyte batteries, Massachusetts Institute of Technology (MIT), with Carnegie Mellon, is investigating fluoridated components and other additives to form self-healing SEI coatings at the lithium surface. At University of Pittsburgh, alternatives to a standard Li-metal anode are being explored, including metal alloys and templated structures. Researchers at PNNL are pivoting from liquid electrolytes to hybrid electrolytes, with addition of a polymer component to a concentrated solvent-in-salt electrolyte. For solid-state batteries, programs are addressing both the electrolytes and the lithium interface. The stability of the garnet ceramic electrolyte with lithium is being investigated at ANL with materials from University of Michigan; this is now expanding to other solid electrolytes. The different mechanical and electrochemical mechanisms leading to the formation of shorting lithium features through the solid electrolytes is under study at ORNL, University of Michigan, and Michigan Technological University. New ceramic-polymer composite electrolytes formed with scalable processing are being investigated to reveal the properties of both the ceramic electrolyte / polymer electrolyte interface and contacts of the solid electrolyte with the solid composite cathode and thin lithium anode.

Highlights. The highlights for this quarter are as follows:

Work led by Chen and Dudney at ORNL is producing a 20-µm-thick sintered ceramic membrane with low area specific resistance (ASR) of ~ 50 ohm. The ~ 30% porosity is filled with a crosslinked PEO-based polymer electrolyte that supports both the ion transport and mechanical strength. The thin spray-coated membrane is not freestanding, but thicker samples are being evaluated for stable cycling. (Task 4.4)

A new project from LLNL, led by J. Ye, is working toward 3D printing of LLZTO. Earlier progress identified the effect of ball milling to achieve a good particle size distribution for sintering and investigated various ink formulations for direct write and projection microstereolithography printing. In this report, progress is reported for sintering of direct write extruded filaments of LLZTO using an infrared halogen lamp. A short exposure of just one minute is sufficient to shrink and densify the sample; however, cracks need to be reduced before conductivity tests can be completed. (Task 4.8)

At ANL, work led by Curtiss and Markovic continued to probe the lithium interfaces with LLTO and LLZO. New AIMD results show the relative lithium exchange differs for various surfaces of the LLTO electrolyte. Within the simulation timescale, there was significant lithium exchange with the (100) surface, but no lithium exchange with either (001) or the amorphous LLTO surface. These simulations support earlier (Quarter 2) experimental findings for the lithium reactivity with different surface and indicate the importance of crystallographic structure for stabilizing the Li-metal interface. (Task 4.6)

Xu and Zhang at PNNL continue to demonstrate performance of a "polymer in quasi-ionic liquid" electrolytes. They show > 150 cycles for several different NMC cathodes as functions of the maximum cut off voltage and the amount of excess lithium provided by the anode. (Task 4.1)

Xu and Zhang have also improved the lithium cycling morphology and reduced the SEI thickness in traditional liquid electrolyte cells. This was accomplished by pretreating the Li-metal anode in a solution of AgTFSI dissolved in DME-FEC. The improvement is quite dramatic and attributed to the silver yielding a reduced lithium nucleation potential. (Task 4.1)

Chiang (MIT) and Viswanathan (Carnegie Mellon University) present the result of a dozen baseline Li-Li cells fabricated using a liquid $LiPF_6$+carbonate electrolyte containing their new DTD additive. Cells were cycled at three stack pressures with most of the improved CE realized at 30 psi. Cycle lives of the best cells approached 1000 hours and over 200 cycles. (Task 4.2)

Other tasks provided interesting insights, but are not directly related to stabilization of the li-metal anode during this quarter. These include work from University of Pittsburgh, where Kumta's group is showing best cycling with nanostructured carbon anodes, rather than lithium (Task 4.3). Prof. Cui's team at Stanford University demonstrated that prelithiated silicon anodes, produced by room-temperature dry pressing, provide higher cycling capacity than what is achievable with unreacted pristine silicon (Task 4.7). Finally, at ORNL, Nanda's team reports the capacity and structure for newly synthesized cathodes of $LiPS_3 \bullet S$. Their future work will investigate the electrochemical performance of this cathode in a lithium solid-state battery with a Li_3PS_4 solid electrolyte.

Task 4.1 – Lithium Dendrite Prevention for Lithium Batteries (Wu Xu and Ji-Guang Zhang, Pacific Northwest National Laboratory)

Project Objective. The project objective is to enable lithium metal to be used as an effective anode in rechargeable Li-metal batteries for long cycle life. The investigation in FY 2019 will focus on effects of various organic solvents, inorganic solid electrolytes, and polymers on ionic conductivity, lithium CE, lithium anode morphology, and battery performances in terms of long-term cycling stability and rate capability at room temperature and elevated temperatures. The compatibility of such electrolytes with 4-V, high-Ni NMC cathode will also be investigated.

Project Impact. Lithium metal is an ideal anode material for rechargeable batteries. Unfortunately, uncontrollable dendritic lithium growth and limited CE during repeated lithium stripping/deposition processes have prevented practical application. This work will explore the new hybrid composite electrolytes that can lead to dendrite-free lithium deposition with high CE. The success of this work will increase energy density of Li-metal and Li-ion batteries and accelerate market acceptance of EVs, especially of PHEVs as required by the EV Everywhere Grand Challenge.

Approach. The approach will encompass several areas. (1) Develop appropriate high-concentration electrolytes (HCEs) that have high lithium CE over 99% and are stable with high-Ni NMC (for example, NMC-532) cathodes. (2) Add a small amount of inorganic solid electrolytes and proper polymers into the HCEs to form uniform mixtures, which will be cast into thin films. (3) Solid-state polymer-in-salt electrolyte will be prepared through the hot-pressing method. The effects of the type and content of inorganic fillers and polymers on the ionic conductivity, the electrochemical window, the lithium CE, and the morphology will also be tested.

Out-Year Goals. The long-term goal of the proposed work is to enable lithium and Li-ion batteries with > 120 Wh/kg (for PHEVs), 1000 deep-discharge cycles, 10-year calendar life, improved abuse tolerance, and less than 20% capacity fade over a 10-year period.

Collaborations. This project collaborates with C. Wang of PNNL on characterization by TEM/SEM; Drs. K. Xu and M. Ding of U. S. Army Research Laboratory (ARL) on solvent purification and differential scanning calorimetry (DSC) measurements; and Dr. B. Polzin at ANL on coated electrode sampling.

Milestones

1. Achieve over 300 cycles for 4-V Li||NMC batteries with ~ 2 mAh/cm^2 cathode loading. (Q4, September 30, 2018; Completed)
2. Investigate effects of HCEs on lithium CE and deposited lithium morphology. (Q1, January 15, 2019; Completed)
3. Investigate effects of polymers in hybrid electrolytes on lithium CE and deposited lithium morphology. (Q2, March 31, 2019; Completed)
4. Develop HCE with lithium CE > 98% and oxidation potential up to 4.4 V. (Q3, June 30, 2019; Completed)
5. Achieve over 100 cycles for Li||NMC-532 batteries with medium cathode loading. (Q4, September 30, 2019; Completed)

Progress Report

This quarter, research in two major areas was conducted. One was continuous testing of polymer-in-“quasi-ionic liquid” electrolytes (PQILEs); the other was to make an *ex situ* protective coating on Li-metal anodes.

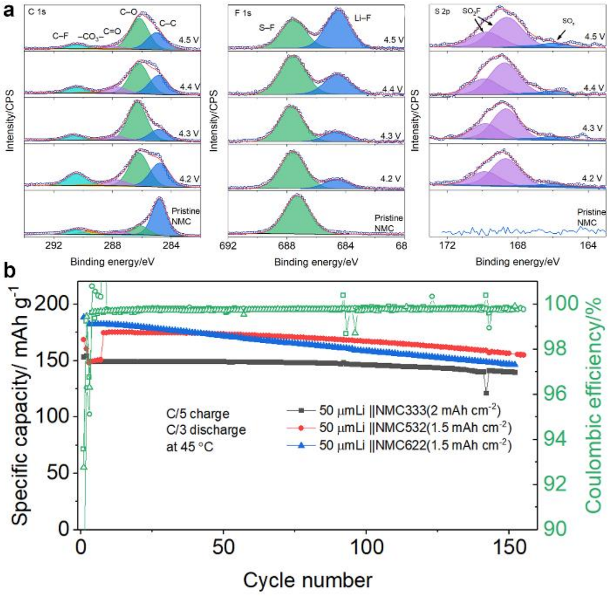

Figure 52. (a) X-ray photoelectron spectroscopy profiles of the pristine NMC-333 cathode and NMC-333 cathodes after 300 cycles with different charge cut-off voltages of 4.2, 4.3, 4.4, and 4.5 V. (b) Cycling performance of Li||NMC cells with different cathode materials and the optimal polymer-in-“quasi-ionic liquid” electrolytes (PQILE) cycled in the voltage range of 3.0-4.3 V.

For high-voltage stability of PQILEs, the cycled lithium anodes and NMC-333 cathodes were fully analyzed. The main difference is that the contents of LiF and oxidized sulfur species in the CEI increased largely when the charge cutoff voltage was increased from 4.4 V to 4.5 V. For example, when the charge cutoff voltage increased from 4.2 V to 4.3 V, 4.4 V, and 4.5 V, the LiF content in CEI increased from 20.4% to 21.8%, 33.8%, and 56.8%, respectively (Figure 52a); the oxidized sulfur species changed from 9.4% to 10.3%, 10%, and 13.1%, respectively. Such changes suggest that when the charge cutoff voltage reached 4.5 V, more PEO, DME, and FSI^- decomposed, leading to more oligomers, LiF, and oxidized sulfur species on NMC surface, which caused faster capacity decay. The charge cutoff voltage of 4.4 V did not cause serious decomposition of the PQILE, so the CEI was still stable enough to maintain good cycling stability.

The cycling stabilities of Li||NMC batteries using the optimal PQILE $Li(DME)_{0.7}FSI\text{-}PEO_{0.6}$ with two Li-metal anodes and three cathode materials were investigated. Under the C/5 charge and C/3 discharge in the voltage range of 3.0 ~ 4.3 V, the Li||NMC cells with 50 µm of lithium after 150 cycles showed capacity retention of 93.5% for NMC-333, 88.6% for NMC-532, and 80.2% for NMC-622 (Figure 52b), indicating decreased cycling stability of the NMC cathode material with increased nickel content. When increasing lithium thickness, cycle life can be largely extended; for instance, the Li||NMC-532 cell with 600 µm of lithium showed 80.5% capacity retention after 300 cycles. Both phenomena are in accordance with the literature reports.

Last quarter, an *ex situ* protective coating on Li-metal anodes was also developed. The lithium metal was treated with a silver-ion (Ag^+) precursor solution consisting of AgTFSI in DME and FEC mixture. Silver nanoparticles were embedded in the crosslinked LiF-rich surface layer on lithium anodes, which enabled a highly stable SEI layer and induced uniform lithium plating/stripping morphologies with reduced overpotential (Figure 53a). The Li||NMC-333 cells with the Ag-LiF decorated lithium anode retained > 80% capacity over 500 cycles (Figure 53b) with a very smooth surface and a thin passivation layer of ~ 76.7 µm (Figure 53c-h).

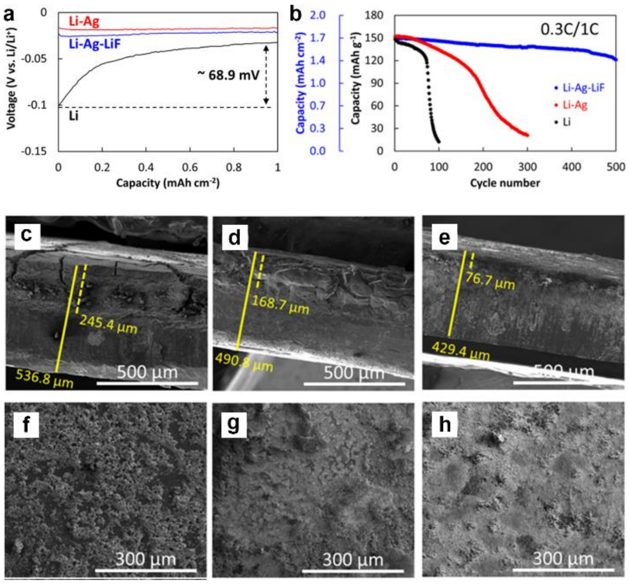

Figure 53. (a) Nucleation overpotentials of lithium plating on Li, Li-Ag, and Li-Ag-LiF surfaces in carbonate electrolyte of 1 M $LiPF_6$ in EC-DMC (1:2 by vol.). (b) Cycling performance of Li||NMC-333 full cells. Scanning electron microscopy images of cycled (c, f) lithium, (d, g) Li-Ag/Li, and (e, h) Li-Ag-LiF/Li anodes disassembled from Li||NMC-333 full cells after 100 cycles at 1C/1C rates.

Patents/Publications/Presentations

Publications

- Wu, H., Y. Xu, X. Ren, B. Liu, M. H. Engelhard, M. S. Ding, P. Z. El-Khoury, L. Zhang, Q. Li, K. Xu, C. Wang, J-G. Zhang,* and W. Xu.* “Polymer-in-“Quasi-Ionic Liquid” Electrolytes for High-Voltage Lithium Metal Batteries.” *Advanced Energy Materials* 9 (2019): 1902108. doi:10.1002/aenm.201902108.
- Peng, Z., J. Song, L. Huai, H. Jia, B. Xiao, L. Zou, G. Zhu, A. Martinez, S. Roy, V. Murugesan, H. Lee, X. Ren, Q. Li, B. Liu, X. Li, D. Wang,* W. Xu,* and J-G. Zhang.* “Enhanced Stability of Li Metal Anodes by Synergetic Control of Nucleation and the Solid Electrolyte Interphase.” *Advanced Energy Materials* 9 (2019): 1901764. doi:10.1002/aenm.201901764.

Task 4.2 – Self-Assembling and Self-Healing Rechargeable Lithium Batteries (Yet-Ming Chiang, Massachusetts Institute of Technology; Venkat Viswanathan, Carnegie Mellon University)

Project Objective. The project objectives are as follows: (1) investigate formation of lithium halide containing SEI, (2) characterize the structure and composition of the SEI surface film and morphology of the electrochemically deposited lithium, and (3) develop combinations of electrolytes (solvents + salts) and electrolyte additives that produce a highly Li-ion conducting, mechanically robust, and self-healing SEI to suppress lithium dendrite formation and improve CE.

Project Impact. Efforts to achieve practical use of the Li-metal anode in rechargeable lithium batteries have long been plagued by lithium dendrite formation and low CE. Lithium dendrites cause battery short-circuits, leading to serious safety hazards. The low CE of Li-metal anodes demands use of excess lithium to offset lithium loss during cycling, which lowers the overall energy density of the battery. If successful, this project will enable self-forming and self-healing SEI containing alkali and/or alkaline earth halides that can suppress dendrite formation and improve CE. This will eventually enable high-energy-density (> 400 Wh/kg) and long-cycle-life (> 500 cycles, 80% capacity retention) Li-metal batteries.

Approach. The project approach involves the following: (1) identifying suitable combinations of solvents, Li-electrolyte salts, and halide and other additives that can produce highly Li-ion conducting, mechanically robust, and self-healing SEI, (2) using integrated theory and experiment, and (3) assembling and testing symmetric and asymmetric cells and Li-metal batteries comprising a high areal-capacity cathode (> 3 mAh/cm^2) and a capacity-limited Li-metal anode (< 130% lithium excess).

Out-Year Goals. The project will down-select electrolyte compositions, develop designs for prototype full cells of > 10 mAh capacity, and fabricate/deliver cells to DOE-specified laboratories for testing and evaluation.

Collaborations. This project collaborates with 24M Technologies Inc. on 18 cm^2/80 cm^2 pouch cell fabrication and tests.

Milestones

1. *Go/No-Go Decision*: Demonstrate Li-Li symmetric cells that meet established criteria cycling at ≥ 3 mAh/cm^2 at C/5 rate over 30 cycles. (Q1, FY 2019; Completed ahead of schedule)
2. Demonstrate at least one Li-Li symmetric cell that cycles ≥ 3 mAh/cm^2 at C/5 rate over 50 cycles without short-circuit. (Q2, FY 2019; Completed)
3. Build 12 baseline cells of > 10 mAh capacity for testing under different stack pressures. (Q3, FY 2019; Completed)
4. Establish quantitative criteria for solid-electrolyte/liquid electrolyte combinations that exhibit self-healing functionality. (Q4, FY 2019; Completed)

Progress Report

All milestones for the project have been met. The third quarter milestone was to build 12 baseline cells of > 10 mAh capacity for testing under different stack pressures. The configuration of these cells is a Li-Li asymmetric cell of 18 cm^2 area, fabricated using lithium foil thicknesses of 30 μm and 1.5 mm, respectively, as shown in Figure 54. Cell capacity is nominally 111 mAh, being limited by the thinner Li-metal electrode. Cells were cycled to plate and deplate 3 mAh/cm^2, meaning that the operating cell capacity is 54 mAh. 500 μL of an electrolyte FEC-DMC (1:1 v) + 1M $LiPF_6$ + 3 wt% DTD was used, which previously demonstrated the highest CE in smaller cells. Of the 12 cells, three each were tested under applied pressure of 5, 30, 60, and 100 psi.

Results for the three cells at each applied pressure are shown in Figure 54, along with the individual and average CE values. At 5 psi pressure, the average CE from three cells is 98.1%. An increase in CE to 98.6% is seen at 30 psi, which seems to be clearly beyond measurement error. At higher pressure, the CE increases slightly further to ~ 98.8%. The highest single value is 99.1%, measured in a cell that cycled 224 cycles. These values are similar to the best values seen in coin cells, also 98.8%. The team concludes that, in the current cell design, a pressure of ~ 30 psi is sufficient to achieve most benefits of applied pressure.

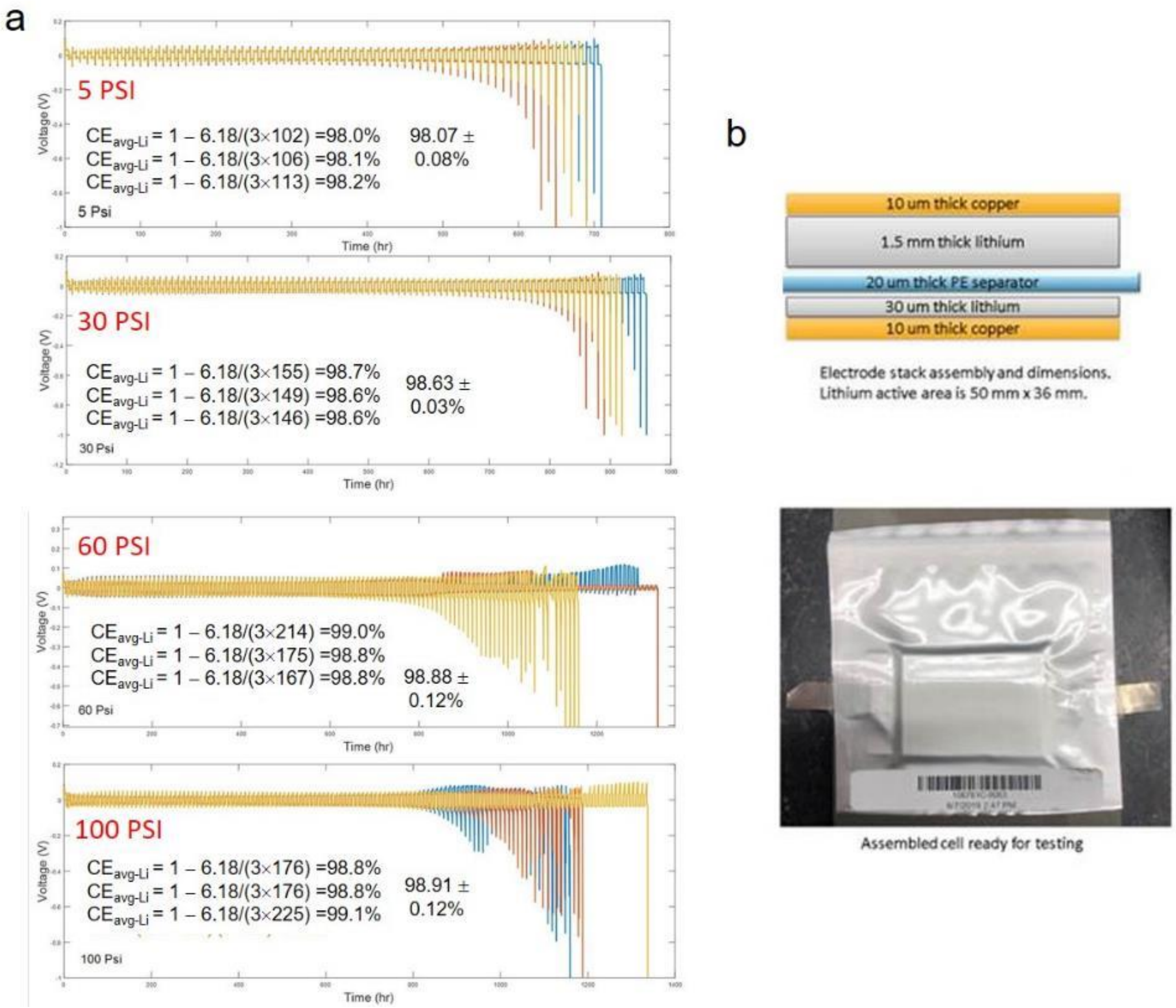

Figure 54. (a) Results for the three cells at each applied pressure, along with individual and average Coulombic efficiency values. (b) Electrode stack assembly and dimensions (upper) and assembled cell ready for testing (lower).

Patents/Publications/Presentations

Patent

- Pande, V., V. Viswanathan, and Y-M. Chiang. "Computational Screening of Current Collectors for Enabling Anode-Free Lithium Metal Batteries." Provisional Application #: 62/922,648.

Publication

- Zhu, Y., V. Pande, L. Li, B. Wen, S. Pan, D. Wang, Z-F. Ma, V. Viswanathan, and Y-M. Chiang. "Design Principles for Self-Forming Interfaces Enabling Stable Lithium Metal Anodes." Under revision.

Presentations

- MIT Club of Northern California, Palo Alto, California (October 10, 2019): "The Future of Energy Storage"; Y-M. Chiang.
- Fall Meeting of the Aeronautics and Space Engineering Board – Panel on Innovations in Electric Aircraft Propulsion, Irvine, California (September 26, 2019): "Pathways to Batteries with High Energy Density and High Power for Electric Aviation"; Y-M. Chiang.

Task 4.3 – Engineering Approaches to Dendrite-Free Lithium Anodes (Prashant Kumta, University of Pittsburgh)

Project Objective. This project will yield Li-metal anodes with specific capacity ≥ 2000 mAh/g (≥ 4 mAh/cm^2), ~ 1000 cycles, and CE ≥ 99.99% with superior rate capability. The goal is to (1) systematically characterize different approaches for generation of dendrite-free Li-metal anodes while also providing understanding of the scientific underpinnings, and (2) evaluate the microstructure and electrochemical performance of dendrite-free Li-metal anodes. Generation of high-performance, dendrite-free Li-metal anodes will successfully demonstrate generation of novel sulfur cathodes, affording fabrication of Li-S batteries meeting the targeted gravimetric energy densities ≥ 350 Wh/kg and ≥ 750Wh/l with a cost target $125/kWh and cycle life of at least 1000 cycles for meeting the EV Everywhere Grand Challenge blueprint.

Project Impact. Dendrite formation in electrochemical systems occurs due to inhomogeneous current densities coupled with local diffusion gradients, surface roughness, and kinetic roughening. Lithium dendrite formation and growth are, however, not well understood; adding to the complexity is SEI formation. Control and elimination of lithium metal dendrite formation are challenging. If overcome, this would render universal adoption of Li-anode batteries for stationary and mobile applications. This project is a scientific study of novel approaches to address dendrite formation in Li-anode batteries, electrolyte decomposition, and associated cell failure. Development of dendrite-free, high-performance lithium anodes will enable use of Li-free cathodes, opening a myriad of possibilities to push the envelope in terms of cathode capacity and battery energy density.

Approach. This project will explore several approaches focused on engineering new structurally isomorphous metallic alloys (SIAs) combined with engineering the surface of metallic lithium as well as the current collectors, including development of novel high Li-conducting conjugated polymers and composite structures. The unifying theme is to initiate a uniform nucleation with homogenous growth, eliminating preferential reversible plating and de-plating and thus resulting in dendrite-free, high-energy-density Li-metal anodes for Li-metal batteries.

Out-Year Goals. This project comprises three major phases to be successfully completed in three years:

- Year 1 – Synthesis, characterization, and scale up of suitable porous foams (PF) for use as current collectors for lithium anodes and Li-ion conductor (LIC) materials to prepare multi-layer porous foams (MPF).
- Year 2 – Development of Li-rich SIA anodes. Generation of composite multi-layer anodes (CMAs).
- Year 3 – Advanced high-energy-density, high-rate, extremely cyclable cell development.

Collaborations. The project works with Dr. M. K. Datta and Dr. O. I. Velikokhatnyi at University of Pittsburgh as co-PIs. It also collaborates with Dr. A. Manivannan at Global Pragmatic Materials on XPS analysis, Dr. D. Krishnan Achary at University of Pittsburgh on solid-state magic angle spinning NMR (MAS-NMR) characterization, and Dr. J. R. Gaines and Dr. J. Hrebik at the Kurt J. Lesker Company on thin-film system fabrication/characterization.

Milestones

1. Integrated electrode (IE) generation to encompass the three paths of development, that is, coating development/PF development of CMA, and SIA exploration including optimizing the maximize lithium content in SIA with no dendrite formation over extended cycling, especially at high rates to demonstrate high capacity. (October 2019; Completed)
2. Fabrication/characterization of 10-mAh cell configurations. (October 2019; Completed)

Progress Report

Carbon-based nano-architectures show a CE of ~ 95-97% during initial cycles, reaching ~ 99.71-99.87% for over 200 cycles for a plating charge of 4 mAh/cm^2 and current densities of 1 mA/cm^2 and 4 mA/cm^2 (see the second quarter report). A study of the voltage profile for this cell (Figure 55) between the 40th and 50th cycles indicates a distinct region where the system transitions from nucleation and growth to plating regime without nucleation. Following this, the plating phenomenon utilizes pre-existing nucleation sites without creating new plating regions.

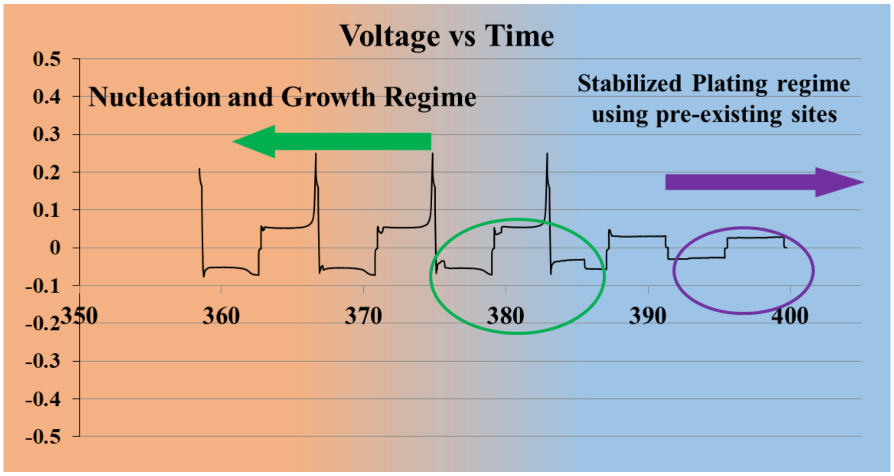

Figure 55. Voltage (V) versus time (hour) profile of carbon-based electrodes showing the transition region in a traditional coin cell test.

In normal coin cell testing (the lithium foil area is smaller than the working copper electrode area), the lithium plating spreads with each cycle due to the resistance to plating created by the formation of the SEI layer. Hence, the system shows false results of stable lithium plating for 30 to 80 cycles depending on the current/charge density. A new insulated coin cell design was introduced confining the lithium plating only on the copper working electrode and, correspondingly, recording the actual performance of the electrodes by insulating the stainless steel in the coin cell from the electrolyte contact while preserving the electrical continuity with the copper working electrode (Figure 56). The CE of the copper foil decreases to ~ 75-80% within the first five cycles in this new insulated coin cell design, with continued decline over the 50 cycles compared to the traditional testing set up where the copper foil shows stable plating for 50 cycles.

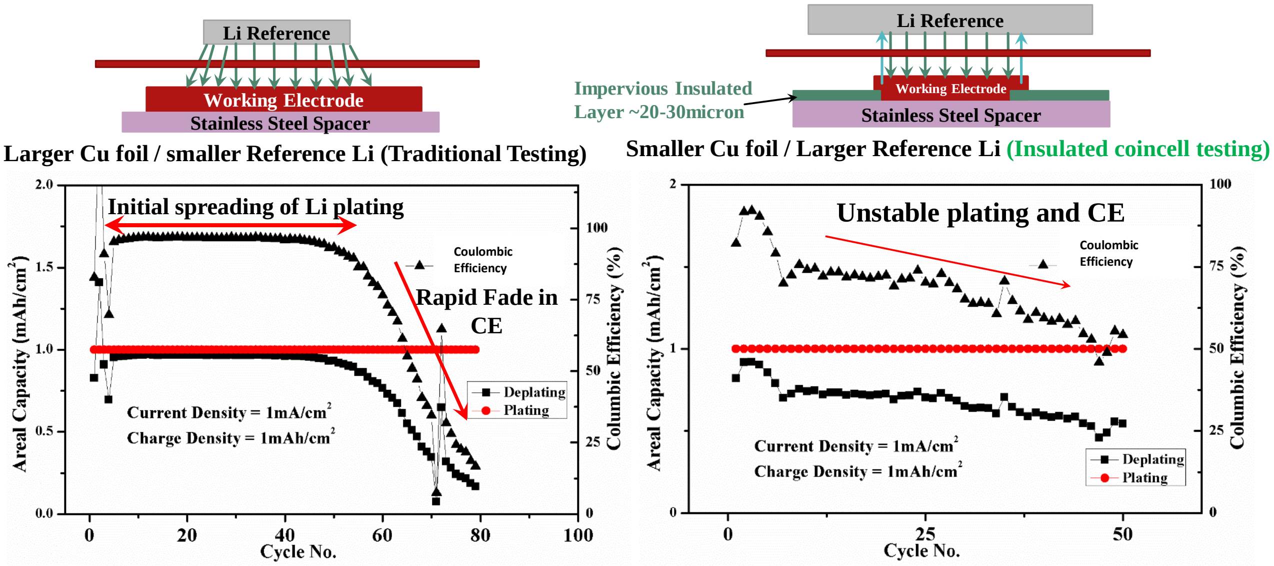

Figure 56. Schematic of the traditional and new insulated coin cell testing along with the recorded performance for the copper foils.

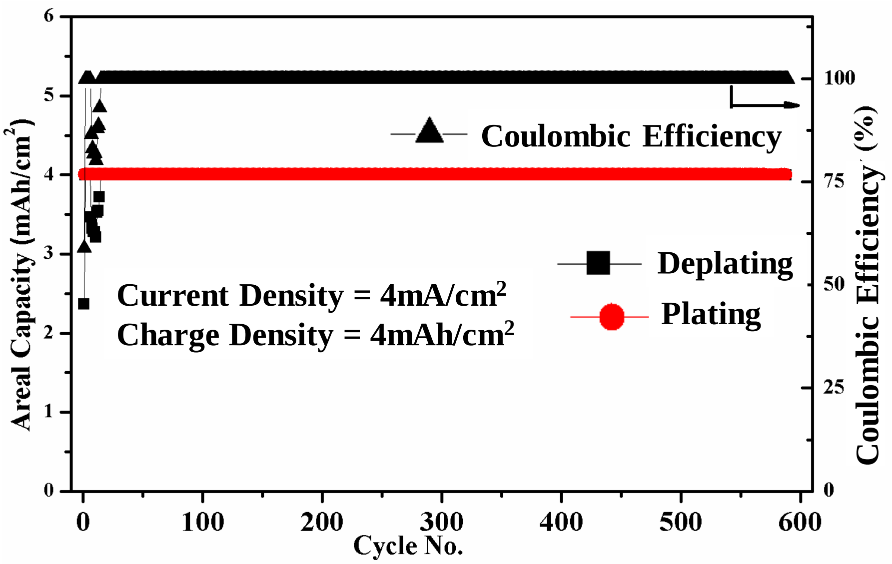

Figure 57. Coulombic efficiency of lithium plating and deplating @ 4 mA/cm^2 and 4mAh/cm^2 in Li/Li$^+$ cell (insulated coin cell).

Similarly, novel engineered carbon-based architectures in traditional coin cell testing show an initial low CE of plating (~ 95-97%) due to spreading of the lithium plating marked by distinct nucleation and growth regimes during each cycle, after which the spread of lithium plating reaches saturation. Subsequently, the system shows a CE of ~ 99.71-99.87%, representing the actual performance of the carbon nano-architectures. Novel engineered carbon nano-architectured electrodes thus tested in an insulated coin cell (Figure 57) show a high CE of > 99.85% in the first 10 cycles of lithium plating and deplating @ 4 mA/cm^2 and 4 mAh/cm^2, and a high CE of > 99.9% for over 500 cycles on long-term cycling. The CE fluctuations observed in the initial 10 cycles are, however, due to activation of new regions in the nanostructures. Rate and charge capability testing as well as STEM studies of the post-cycled electrodes are in progress, and the results will be detailed in the final report.

Patents/Publications/Presentations

Publication

- Datta, M. K., B. Gattu, R. Kuruba, P. Shanthi, and P. N. Kumta. “Constitutional Under-Potential Plating (CUP) – New Insights for Predicting the Morphological Stability of Deposited Lithium Anodes in Lithium Metal Batteries.” *Journal of Power Sources* (2019). Under review.

Presentation

- GGB Bearings (September 9, 2019): “Engineering Approaches to Dendrite Free Li-Metal Anodes”; P. N. Kumta.

Task 4.4 – Composite Electrolytes to Stabilize Metallic Lithium Anodes (Nancy Dudney and X. Chelsea Chen, Oak Ridge National Laboratory)

Project Objective. The project has several objectives: (1) prepare composites of representative polymer and ceramic electrolyte materials to achieve thin membranes that have the unique combination of electrochemical and mechanical properties required to stabilize the metallic-lithium anode while providing for good power performance and long cycle life, (2) understand the Li-ion transport at the interface between polymer and ceramic solid electrolytes, which is critical to effective conductivity of the composite membrane, (3) identify key features of composite composition, architecture, and fabrication that optimize performance, and (4) using practical and scalable processing, fabricate thin electrolyte membranes to use with a thin metallic lithium anode to provide good power performance and long cycle life.

Project Impact. A stable lithium anode is critical to achieve high energy density with excellent safety, lifetime, and cycling efficiency. This study will identify key design strategies that should be used to prepare composite electrolytes to meet the challenging combination of physical, chemical, and manufacturing requirements to protect and stabilize the Li-metal anode for advanced batteries. By utilizing well characterized and controlled component phases, design rules developed for composite structures will be generally applicable toward substitution of alternative and improved solid electrolyte component phases as they become available. Success will enable DOE technical targets: 500-700 Wh/kg, 3000-5000 deep discharge cycles, and robust operation.

Approach. This project seeks to develop practical solid electrolytes to provide stable, long-lived protection for the Li-metal anode. Current electrolytes have serious challenges when used alone; oxide ceramics are brittle, sulfide ceramics are air sensitive, polymers are too resistive and soft, and many electrolytes react with lithium. Composites provide a clear route to address these issues. While work continues to emphasize study of ceramic electrolyte/polymer electrolyte interfaces, this effort has expanded to address (1) practical processing routes to fabricate full batteries using better composite electrolytes with a composite cathode and thin Li-metal anode, and (2) introduction of alternative polymer and ceramic phases to replace well-known model materials and develop improved composite electrolytes. In addition to solid-state devices, hybrid batteries are investigated using a fluid or gel catholyte within the porous cathode. Coatings have also been employed to stabilize electrode interfaces. These directions increase complexity of the studies, but are needed to improve cycling stability and rate performance and to advance practical implementation of the solid electrolyte and Li-anode technology.

Out-Year Goal. The goal is to use advanced manufacturing processes where the architecture of the composite membrane can be developed and tailored to maximize performance and cost-effective manufacturing.

Collaborations. Work is conducted by Dr. Y. Zhang and Dr. X. Chen. Ceramic electrolyte powders (LICGC^{TM}) are obtained from Ohara Corporation. Polymer electrolytes are provided by Prof. Z. Bao (Stanford University) and T. Saito (ORNL) and in collaboration with Prof. J. Schaefer (University of Notre Dame). The team will work with partners from the U. S.–German Cooperation on Energy Storage.

Milestones

1. Fabricate full cell using thin evaporated lithium anodes. Compare full-cell performance using thick and thin evaporated lithium anodes. (Q1, FY 2019; Completed)
2. Fabricate gel composite electrolytes with a target room-temperature conductivity of 1×10^{-4} S/cm. Evaluate ion transport, and thermal and structural properties. (Q2, FY 2019; Completed, achieved target)
3. Expand composite materials to include non-PEO type of polymer electrolytes. Identify promising polymer ceramic systems with interfacial ASR < 10 ohm. (Q3, FY 2019; Completed, ASR ~ 50 ohm)
4. Work with partners from the U. S.–German Cooperation on Energy Storage. (Q4, FY 2019; Initiated)

Progress Report

This quarter, the team mapped the performance of all types of cells shown in Figure 58 based on the percentage of theoretical capacity versus capacity fade rate. The cells can be grouped by different lithium sources (thick lithium, 6-µm lithium on either copper or polymer electrolyte, and lithium-free). Cells with thick lithium showed much lower capacity fade rate. Cells with only polymer electrolyte (PE) had more overcharge capacity than those with composite polymer electrolyte (CPE). For cells not showing overcharge, the capacity loss is a way to measure the lithium loss in a lithium limited test (both 6-µm lithium and lithium-free cells). Overall, the performance of thick lithium >> thin lithium >> lithium free in both charge and discharge. Notably, cells with LiPON electrolyte performed the best in both PE and CPE cases.

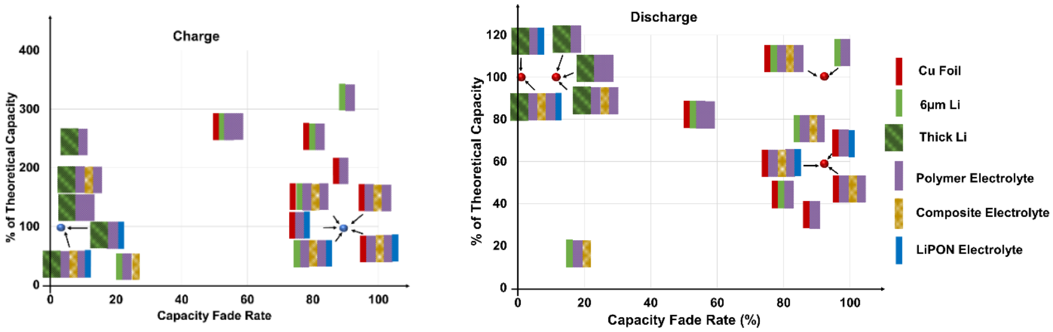

Figure 58. Map of charge (left) and discharge (right) performance of all cells. Note: LFP cathode is on the right side of each cell. Some cells have very similar capacity fade rate and % of theoretical capacity, represented by dots and arrows.

Following up on last quarter, the oxidation state of titanium from CPE is examined after cell cycling using an XAS technique. (Data were collected at 9-BM of the Advanced Photon Source.) In Figure 59, both pristine and reduced LICGC^{TM} ceramic are shown for comparison. As with the team's last results, Ti^{4+} does not change in cells of Cu PE CPE PE LFP and 6-µm Li PE CPE PE LFP, indicating that CPE did not consume lithium in both cases. However, the Ti^{4+} gets reduced in Cu PE CP EPE LiPON LFP, indicated by the left shift of titanium edge (red line). The results indicate that the charge mechanism may be different in cells with LiPON and without LiPON. Further examinations are needed.

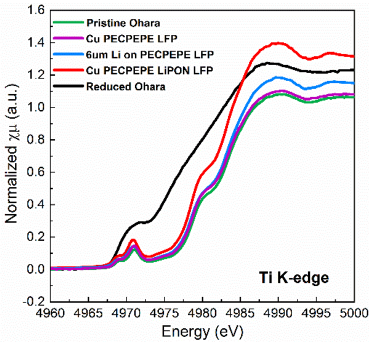

Figure 59. Titanium K-edge of pristine composite polymer electrolyte (CPE) and CPE after cycling from the cell Cu PE CPE PE LFP, 6 µm Li on PECPE PE LFP and Cu PE CPE PE LiPON LFP.

Following the second quarter, the team thoroughly analyzed the ionic conductivity of composite electrolytes with a 3D interconnected ceramic network. An ASR of 50 Ω·cm^2 was achieved for the thin-film composite layer; this is close to the milestone 3 target. This was determined by comparing the impedance spectra of 1-mm thick composite pellet with the spray-coated 25-µm thin film. A surface polymer-rich overlayer (Figure 60) increased the total resistance of each sample by about 300-500 Ω·cm^2. This interfacial resistance can be minimized by finding a

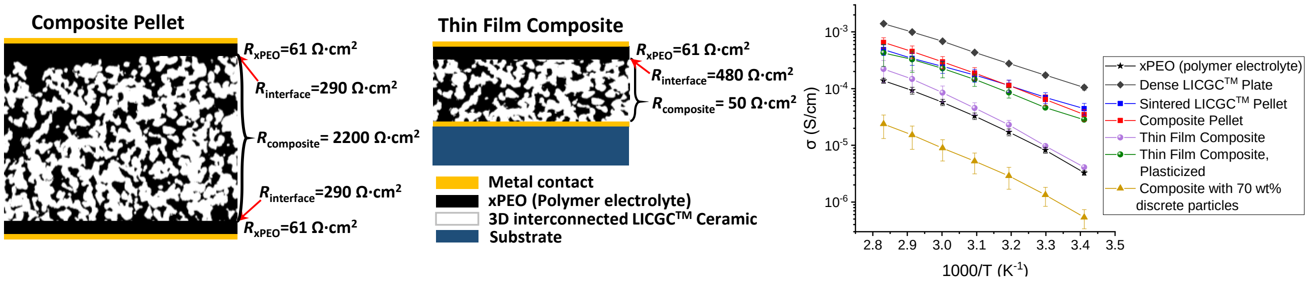

Figure 60. (left and middle) Area specific resistance of each layer in the composite thick pellet and the thin film. (right) Conductivity of composite pellet and thin film compared to neat polymer, pristine ceramic, and a composite with dispersed ceramic particles.

way to remove the excess xPEO layer or by the addition of tetraethylene glycol dimethyl ether (TEGDME) plasticizer. The plasticized composite thin film had an exceptionally high ceramic loading of ~ 77 wt% and gives an ionic conductivity of 3.5 x 10^{-5} S/cm at 20°C, an order of magnitude larger than the neat polymer electrolyte and about two orders of magnitude larger than randomly dispersed ceramic particles in polymer with a similar loading.

Patents/Publications/Presentations

Publications

- Palmer, M., S. Kalnaus, M. Dixit, A. Westover, K. Hatzell, N. Dudney, and X. C. Chen. “A Three-Dimensional Interconnected Polymer/Ceramic Composite as a Thin Film Solid Electrolyte.” Submitted.
- Merrill, L. C., X. C. Chen, Y. Zhang, H. O. Ford, J. L. Schaefer, and N. Dudney. “The Effect of Ceramic Particle Addition on Ion Association in Single Ion Conducting Polymer Electrolytes.” In preparation.

Presentations

- 236th ECS Meeting, Atlanta, Georgia (October 13–17, 2019): “A Three-Dimensional Interconnected Composite of Ceramic/Polymer as a Thin Film Solid Electrolyte”; M. Palmer, S. Kalnaus, M. Dixit, A. Westover, K. Hatzell, N. Dudney, and X. C. Chen.
- Solid State Electrolytes Workshop, PNNL, Richland, Washington (October 24, 2019): “Composite Electrolytes to Stabilize Li Metal Anodes”; N. Dudney
- ECS Fall National Meeting, Symposium in Honor of Bob Huggins: Fast Ionic Conduction – Principles and Applications, Atlanta, Georgia (October 13–17, 2019): “Thin Film Batteries have Interesting Lessons for Lithium Batteries”; N. Dudney.

Task 4.5 – Lithium Batteries with Higher Capacity and Voltage (John B. Goodenough, University of Texas at Austin)

Project Objective. The project objective is to develop an electrochemically stable alkali-metal anode that can avoid SEI layer formation and alkali-metal dendrites during charge/discharge. To achieve the goal, a thin and elastic solid electrolyte membrane with a Fermi energy above that of metallic lithium and an ionic conductivity $\sigma > 10^{-4}$ S cm^{-1} will be tested in contact with alkali-metal surface. The interface between the alkali-metal and the electrolyte membrane should be free from liquid electrolyte, have a low impedance for alkali-metal transport and plating, and keep good mechanical contact during electrochemical reactions.

Project Impact. A safe alkali-metal anode that can be plated/stripped reversibly at low resistance and high rates over many thousands of charge/discharge cycles would maximize the volumetric energy density for a given cathode of a rechargeable battery for powering an all-electric road vehicle. Such a battery could also be used for stationary back-up storage of electric power from energy sources other than fossil fuels.

Approach. The project will design, make, and test cells. The approach is to introduce a solid-electrolyte interfacing the anode and a coating on the anode current collector that is wet by a lithium anode. The solid electrolyte should also be wet by the anode to create a bond that is strong enough to constrain the anode volume changes to be perpendicular to the anode/electrolyte interface.

Out-Year Goals. The out-year goal is to develop coin cells that are safe and low-cost with a long cycle life at a voltage $V > 3.0$ V that can compete with the internal combustion engine for powering a road vehicle.

Collaborations. This project collaborates with A. Manthiram at UT Austin and K. Zaghib at HQ.

Milestones

1. Test a new, low-cost ceramic separator concept with a liquid electrolyte and an alkali metal anode. (Q1, FY 2019; Completed)
2. Test redox energies and cyclabilities of novel NASICON-structured cathode materials in a Na-ion battery. (Q2, FY 2019)
3. Synthesize and evaluate solid sulfide electrolytes. (Q3, FY 2019)
4. Investigate oxygen redox chemistry for reversible high-voltage Na^+ intercalation. (Q4, FY 2019)

Progress Report

Progress for work conducted by this Task in the fourth quarter was not available at publication. Accordingly, the milestone status reported herein reflects third-quarter progress.

Task 4.6 – Advancing Solid-State Interfaces in Lithium-Ion Batteries
(Nenad M. Markovic and Larry A. Curtiss, Argonne National Laboratory)

Project Objective. The project objectives are multi-faceted, including development of a new mechanically and chemically stable and Li-ion conductive ($\geq 2 \times 10^{-4}$ S/cm at 298 K) solid electrolyte for a solid-state battery encompassing a Li-metal anode, Li-oxide-based cathode, and nonflammable crystalline and amorphous solid electrolytes that can operate at cathode potentials > 5 V (denoted as a S_{Li}-S_{EL}-S_C system).

Project Impact. Protective organic and inorganic compounds can enhance stability of the interface, improve Li-ion interfacial transport, minimize dendrite formation, and increase safety in Li-ion batteries.

Approach. The project proposes to develop and use interdisciplinary, atomic-/molecular-level insight obtained from integrating both experimental- and computational- based methodologies to define the landscape of parameters that control interfacial properties for a new generation of the Li-ion solid-solid battery systems. The strategy will involve transferring knowledge gained from well-characterized thin-film materials to real-world materials. This strategy forms a closed loop wherein the knowledge gained from model systems is used to design more complex, real-world materials, and vice versa. The work will focus on utilizing existing in-house synthesis and characterization methods to enable rapid transition from fundamental science to realistic cells.

Out-Year Goals. The out-year goals are to use and develop the physical and chemical synthesis methods for design of solid-solid interfaces with unique chemical/mechanical/conductivity properties. The proposed work will develop and exploit a variety of *ex situ* and *in situ* experimental optical and surface sensitive techniques and electrochemical methods to explore and explain bulk and interfacial properties of the selected materials. The results will serve to unravel many puzzling bulk and interfacial properties of S_{Li}-S_{EL}-S_C systems, including various types of ceramic and glass materials.

Collaborations. This project funds work at ANL and collaboration with J. Sakamoto at University of Michigan.

Milestones

1. Understand the impact of different dopants in LLZO (niobium versus tantalum versus aluminum) on reactivity by surface and bulk sensitive techniques and spectroscopic methods. (Q1, FY 2019; Completed)
2. Determine the impact of solid electrolyte crystallinity (single crystal versus polycrystalline versus amorphous) on electrolyte reactivity by surface- and bulk-sensitive techniques and spectroscopic methods. (Q2, FY 2019; Completed)
3. Distinguish chemical versus electrochemical reactivity at the interface and bulk of model solid-state electrochemical systems with Li-metal anodes and $LiCoO_2$ cathodes by electrochemical testing and characterization. (Q3, FY 2019; Completed)
4. Determine dopant-dependent impact on chemical reactivity of different interfaces of SSEs with lithium metal by computational characterization. (Q4, FY 2019; Completed)

Progress Report

Li-LLZO AIMD. The team has been investigating Li-metal interfaces with Nb- or Ta-doped cubic garnet LLZO and $La_{0.66-x}Li_{3x}TiO_3$ (LLTO) to understand chemical reactivity at solid electrolyte/anode interfaces. They have carried out AIMD simulations of Li/LLZO interfaces with different dopants and Li/LLTO to compare interfacial and dopant-dependent changes with the chemical reactivity observed from ultra-high vacuum (UHV) lithium deposition studies. AIMD simulations for the lithium interfacial structures with Ta- and Nb-doped LLZO at 300K at the scale of several ps were performed using 1.3-nm thick lithium film on (001) LLZO surfaces. The results show no change in coordination numbers of lanthanum, zirconium, or dopants in LLZO, but considerable exchange of positions of lithium ions in the metal region. Thus, these results do not change the previous conclusions based on DFT calculations that found Li/Ta-doped LLZO interfaces to be more stable than Li/Nb doped-LLZO interfaces.

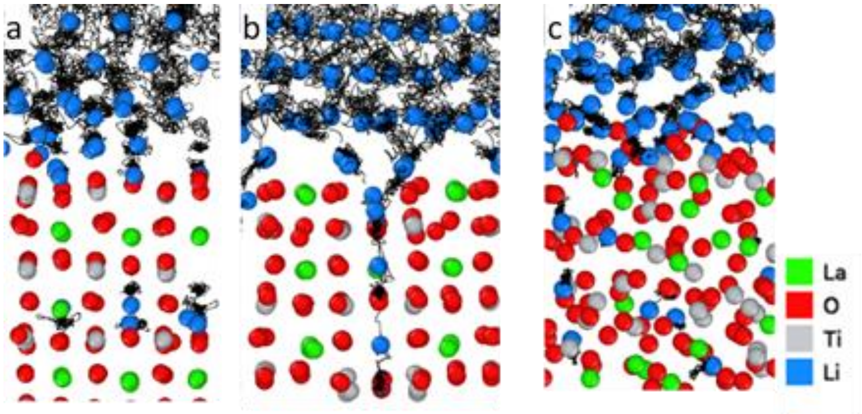

Figure 61. *Ab initio* molecular dynamics trajectories for (a) Li/LLTO (001) interface; (b) Li/LLTO (100) interface, and (c) Li/amorphous LLTO interface. Initial atomic positions are shown with balls, and Li-ion trajectories are shown with black lines.

Li-LLTO AIMD. The team's calculations for $Li/La_{0.55}Li_{0.33}TiO_3$ interfaces were performed using different terminations for three different interfaces—Li/(001) LLTO, Li/(100) LLTO, and Li/amorphous LLTO. The (001) and (100) orientations are distinguished by preferential layering of lithium and lanthanum in LLTO parallel and perpendicular to the surface, respectively. The amorphous structure was prepared by equilibrating molten LLTO for 10 ps, then quenching it to melting temperature for 20 ps and quenching it further to 300K for 20 ps, all using NPT ensemble, and equilibrating for 10 ps using NVT ensemble. Atomic density distribution for all species with distance from the interface remained relatively unchanged during the simulations. For the Li/(100) LLTO interface, considerable lithium exchange between the metallic lithium and lithium in LLTO was observed, with lithium ions hopping across the interface and along Li-rich planes of LLTO. For the Li/(001) LLTO interface, there was no lithium exchange between lithium metal and LLTO at the simulation timescale. For the Li/amorphous LLTO interface, lithium motion was localized within LLTO, despite higher volume per formula unit compared to the ordered LLTO.

The project's experimental results in the second quarter report indicated that the crystalline LLTO orientation with lanthanum layers parallel to the interface with lithium metal shows much less reactivity than the interface with lanthanum layers oriented normal to the interface. The AIMD simulations provide support for these observations by evidence of considerably faster Li-ion diffusion along the Li-rich layers parallel to lanthanum layers in crystalline LLTO. The AIMD results on amorphous LLTO indicate no redistribution of atomic species or lithium exchange in LLTO, which is in agreement with the experimental results in the report, indicating that amorphous LLTO thin films show no evidence of surface reactivity upon Li-metal deposition. Overall, AIMD simulations suggest that reactivity of LLTO films toward lithium metal correlates with feasibility of Li-ion exchange in LLTO.

Patents/Publications/Presentations

Publication

- Zhu, Y., J. G. Connell, S. Tepavcevic, P. Zapol, J. W. Freeland, D. D. Fong, L. A. Curtiss, and N. M. Markovic. "Comparison of Chemical Reactivity of Amorphous LLTO to Epitaxial Films of Different Orientation towards Metallic Li Anode." In preparation (2019).

Presentations

- ACS Fall National Meeting, San Diego, California (August 25–29, 2019): "Solid-Solid Interfaces in Li-Ion Batteries"; S. Tepavcevic, Y. Zhu, P. Zapol, D. D. Fong, V. Stamenkovic, and N. M. Markovic. Invited.
- ACS Fall National Meeting, San Diego, California (August 25–29, 2019): "First-Principles Studies of Electrochemical Reactions at Interfaces"; P. Zapol. Invited.

Task 4.7 – Prelithiation of Silicon Anode for High-Energy Lithium-Ion Batteries
(Yi Cui, Stanford University)

Project Objective. Prelithiation of high-capacity electrode materials is an important means to enable those materials in high-energy batteries. This study pursues three main directions: (1) developing facile and practical methods to increase first-cycle CE of anodes, (2) synthesizing fully lithiated anode to pair with high-capacity Li-free cathode materials, and (3) prelithiation from the cathode side.

Project Impact. Prelithiation of high-capacity electrode materials will enable those materials in next-generation high-energy-density Li-ion batteries. This project's success will make high-energy-density Li-ion batteries for EVs.

Approach. Silicon electrode film will be prepared by coating the slurry of silicon nanoparticles, carbon black, and binder mixture on copper foil through a doctor-blading method. The silicon electrode film will be prelithiated by pressing a Li-metal foil on top of it and heating it in an argon glovebox for a certain time. Then, Li_xSi electrode film can be obtained by removing the redundant lithium foil through a peeling-off approach. The redundant lithium foil is reusable for the next prelithiation. The structure, morphology, and other properties can be analyzed by SEM, TEM, XPS, Raman spectroscopy, XRD, etc. In the first year, the team aims to fabricate Li_xSi freestanding electrode film and improve its air stability. In the second year, the team aims to improve the electrochemical stability in full cells.

Out-Year Goals. Materials containing a large quantity of lithium will be synthesized for pre-storing lithium ions inside batteries. Materials and process will be developed to be compatible with battery electrode and cell fabrication. First-cycle CE of anodes will be improved and optimized by prelithiation materials. Develop materials for prelithiation from the cathode side.

Collaborations. This project engages in collaboration with the following: BMR PIs; SLAC National Accelerator Laboratory: Dr. M. Toney *(In situ* X-ray); and Stanford: Prof. Nix (mechanics) and Prof. Bao (materials).

Milestones

1. Demonstrate anode prelithiation reagent with specific capacity > 900 mAh/g with stability in ambient air. (Q1, FY 2019; Completed)
2. Demonstrate heat-free and solution-free anode prelithiation method with optimized initial CE. (Q2, FY 2019; Completed)
3. Demonstrate morphology and structure evolution of silicon anode after heat-free and solution-free prelithiation treatment. (Q3, FY 2019; Completed)
4. Demonstrate prelithiated anodes with high initial CE and excellent cycling stability for Li-LFP full cells. (Q4, FY 2019; Completed)

Progress Report

Substantial improvements on energy density of Li-ion batteries require development of high-capacity electrodes. Alloy anodes with much higher capacity have been recognized as promising alternatives to graphites. Without pre-stored lithium in anodes, the energy density is limited by the low capacity of Li-metal oxide cathodes. Recently, lithium metal has been revived as a high-capacity anode; however, many challenges result from its high reactivity and uncontrolled dendrite growth.

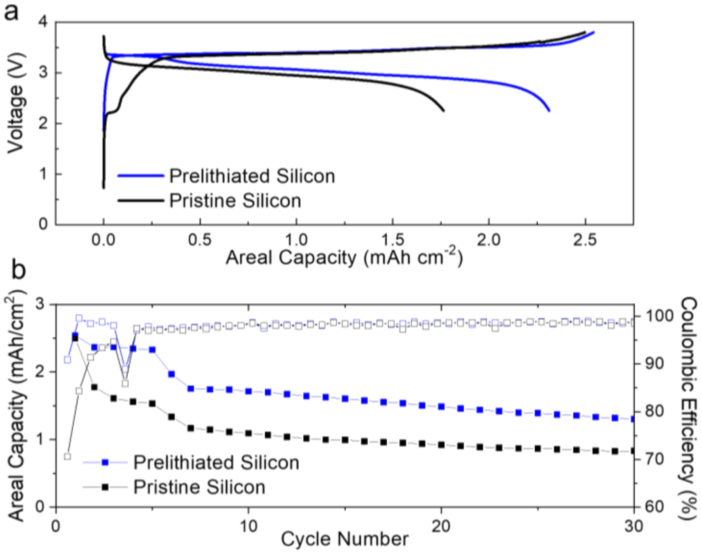

Figure 62. (a) First-cycle voltage curves and (b) cycling stability of Si-LiFePO$_4$ and Li$_x$Si-LiFePO$_4$ full cells operated between 2.5 and 3.8 V.

In previous reports, the team shows that prelithiation can be achieved at the electrode level through a heat-free and solution-free pressing method, which is more facile and compatible for industry application than the previously reported method. The initial Coulombic efficiency (ICE) of the Li$_x$Si-Li half cell increases as the prelithiation pressure increases and/or the prelithiation time increases, which is due to the better lithium metal – silicon contact under a higher pressure and more adequate prelithiation reaction at a longer time.

The excellent performance of prelithiated Li$_x$Si electrode film in half cells makes it possible to be used in full cells. The team paired its prelithiated Li$_x$Si electrode film with a traditional LiFePO$_4$ cathode. Figure 62a shows voltage curves of the prelithiated LixSi-LiFePO$_4$ and pristine Si-LiFePO$_4$ full cells operated between 2.5 and 3.8 V at 1C. These two full cells show similar first-cycle charge capacity of ~ 2.5 mAh/cm^2. However, the prelithiated Li$_x$Si-LiFePO$_4$ delivers a much higher reversible discharge capacity of 2.3 mAh/cm^2, corresponding to a high ICE of 91%, while the pristine Si-LiFePO$_4$ obtains a much lower reversible discharge capacity of 1.76 mAh/cm^2, corresponding to a low ICE of 70%. Figure 62b shows the CE and capacity of the following cycles. Obviously, the prelithiated Li$_x$Si-LiFePO$_4$ achieves much higher CE than that of the pristine Si-LiFePO$_4$ cell for the initial several cycles, indicating a severe irreversible lithium loss of the unprelithiated Si-LiFePO$_4$ cell. As a result, the later-cycle capacity of the prelithiated Li$_x$Si-LiFePO$_4$ cell is much higher than that of the pristine Si-LiFePO$_4$ cell. Future efforts will be devoted to demonstrating the CE, rate capability, and cycling stability of the prelithiated electrode film for Li-S full cells.

Patents/Publications/Presentations

Publications

- Zhao, J.,* G. Zhou,* K. Yan, J. Xie, Y. Li, L. Liao, Y. Jin, K. Liu, P-C. Hsu, J. Wang, H-M. Cheng, and Y. Cui. “Air-Stable and Freestanding Lithium Alloy/Graphene Foil as an Alternative to Lithium Metal Anodes.” *Nature Nanotechnology* 12 (2017): 993.
- Zhao, J.,* J. Sun,* A. Pei, G. Zhou, K. Yan, Y. Liu, D. Lin, and Y. Cui. “A General Prelithiation Approach for Group IV Elements and Corresponding Oxides.” *Energy Storage Materials* 10 (2018): 275.

Task 4.8 – 3D Printing of All Solid-State Lithium Batteries
(Jianchao Ye, Lawrence Livermore National Laboratory)

Project Objective. This project has three objectives: (1) tuning microstructures of 3D-printed SSE separators; (2) determine material and processing compatibilities with cathode printing; and (3) 3D printing of sintering-free SSE separators.

Project Impact. All solid-state lithium batteries are difficult to process due to the brittleness of ceramic materials, poor solid-solid contact, and the electrolyte-electrode stability issues. As a result, the energy and power density and also cycling stability are far from satisfying. This project will address fabrication difficulties by using the state-of-the-art 3D-printing techniques, which can introduce 3D interfaces and architectures to enhance the solid-solid contact and reduce charge transfer resistance. Success of the project will benefit the DOE by establishing the best manufacturing methods for all solid-state batteries to achieve VTO goals on the performance of beyond Li-ion batteries.

Approach. The project employs 3D-printing techniques to manufacture SSEs and related components for all solid-state batteries. The team starts with direct ink writing (DIW) to develop ink recipes with desired rheological properties and explore post-sintering approaches to achieve high densification. In parallel with DIW 3D printing, the team also explores other 3D printing options, such as projection microstereolithography (PuSL), electrophoretic deposition (EPD), and projection-based two-photon polymerization. Both sintering and sintering-free approaches can gain benefit from 3D printing and therefore will be investigated in this project.

Out-Year Goals. The team will identify any trade-offs between printability and properties and performance. Furthermore, they will determine particle sizes and morphologies as well as post-processing conditions that deliver good ionic conductivity and mechanical properties.

Collaborations. Microstructures, ionic conductivities, and mechanical properties will be provided to the LLNL simulation team, led by PI B. Wood, for establishing and validating phase-field modeling methods.

Milestones

1. Obtain different particle size distributions of SSE powders. (Q1, FY 2019; Completed)
2. Down select SSEs, binders, and solvents for the 3D printing. (Q2, FY 2019; Completed)
3. Determine post-processing conditions for good ionic conductivity and mechanics. (Q3, FY 2019; Completed)
4. Achieve capability to 3D print SSE separators with varied feature sizes and microstructures. Achieve < 100 μm feature size and > 10^{-5} S/cm ionic conductivity. (Q4, FY 2019; In progress)

Progress Report

150°C Lower Sintering Temperature Achieved Using High Energy Ball Milled Powders with Reduced Particle Size with No Lithium Loss

Ionic conductivity of 8 x 10^{-4} S/cm was obtained. Two ball milling conditions were chosen to for comparison: one ball milled in ethanol (200 proof), and the other one ball milled in acetonitrile with Triton X-100 surfactant.

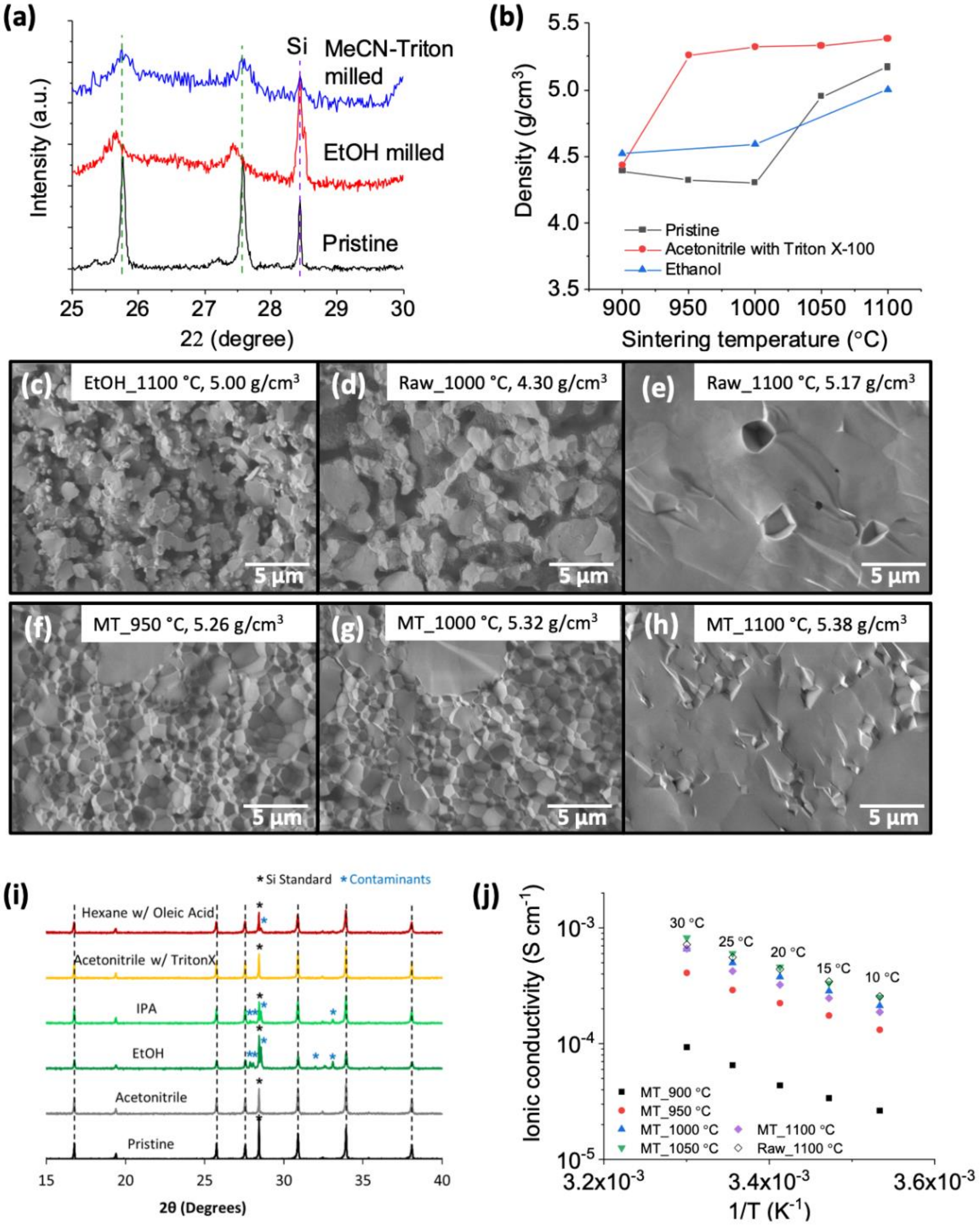

Figure 63. Particle size effects on sintering temperature, density, and ionic conductivity. (a) X-ray diffraction (XRD) results of pristine, ethanol milled, and MeCN-Triton milled LLZTO powders. (b) Density of LLZTO pellets sintered at different temperatures. (c-h) Scanning electron microscopy images of the fracture surface of sintered pellets. (i) XRD results of sintered pellets from different milling conditions. (j) Temperature-dependent ionic conductivity of LLZTO pellets.

Both ball milling conditions dramatically reduce particle size from 5 μm down to ~ 200 nm within 1 hour. However, the team found that ethanol milling leads to lithium loss due to the reactivity of ethanol with LLZTO in high-energy ball milling condition, which is evidenced by lattice expansion from XRD (Figure 63a) and compositional analysis from XPS. As a result, ethanol milled powders cannot be densified well (Figure 63b-c) and a large amount of impurity phases including $La_2Zr_2O_7$ was found in the XRD analysis (Figure 63i). This is also true for other alcohols like IPA. In contrast, the acetonitrile plus Triton (MT) ball milled powders show no or little peak shifting in XRD and only slight lithium loss (ICP). Those MT-milled powders with reduced particle sizes can be sintered at temperatures as low as 950°C, which is 150°C lower than raw powder samples. Relative density of 96-98% was achieved in the sintering temperature range from 950°C to 1100°C. The ionic conductivity of the sintered pellets made of ball MT-milled powders is comparable to that of well sintered raw powder pellets, reaching ~ 8 x 10^{-4} S/cm at 30°C.

Based on MT-Milled Powders, Developed Various Ink Recipes for 3D Printing

Table 9 lists several ink recipes developed under this project. They are divided by three ink categories: solvent based, solvent/binder based, and liquid binder based. Pure solvent-based (that is, NMP) inks can be densified after sintering. However, extreme care is needed to avoid drying-induced cracking. The addition of polymer binders removes cracks. A PEGDA recipe with simple chemistry allows flexible mechanical properties of green film and ultraviolet (UV)/thermal curing for fast shape forming. It can be printed using two printing techniques: DIW and paste PuSL). Therefore, significant efforts were put into this versatile recipe.

Table 9. Development of ink recipes for 3D printing.

Types of Inks	Compositions	Notes
Solvent based	NMP/LLZTO	High solid content. Slippery ink. Easy cracking after drying. Can be densified.
	Ethylene glycol/LLZTO	< 60 wt% solid content. Viscous but homogeneous ink. Easy cracking after drying. No success yet in densification.
Solvent based with binders	Cyclohexanone/cellulose /LLZTO	Slippery ink. No success yet in 3D printing.
	Ethylene glycol/cellulose /LLZTO	Uniform ink; slow drying. No success yet in densification.
	Acetonitrile/PEO /LLZTO	Direct Ink Writing (DIW) printable. Fast drying.
	NMP/Acetonitrile/PEGDA/LLZTO	DIW printable. Can be densified.
Liquid binder based	PEGDA/LLZTO	Ultraviolet/thermal curable; DIW printable. Can be densified.

To produce thin and uniform SSE separator films with high efficiency, PuSL is much faster than DIW. PEGDA/LLZTO inks with solid content from 50 wt% to 85 wt% were developed and printed using a house-made Paste PuSL system. The PEGDA is crosslinked by shining a UV light for several to tens of seconds. For thin film fabrication, an area projection is utilized. Selective polymerization can also be developed using computer designed light patterns and optimizing initiator/absorbent/inhibitor contents, which will be explored in the project's next plan. For now, the team has employed DIW to write simple structures on top of PuSL printed films (Figure 64a-d) and determine proper sintering conditions for densification. The initial solid content of the PEGDA/LLZTO ink used for printing and sintering as shown in Figure 64 is 60 wt%. Even with such low LLZTO content, the film can still be densified at proper sintering conditions (Figure 64e-f) without commonly used pre-pressing for improving packing density.

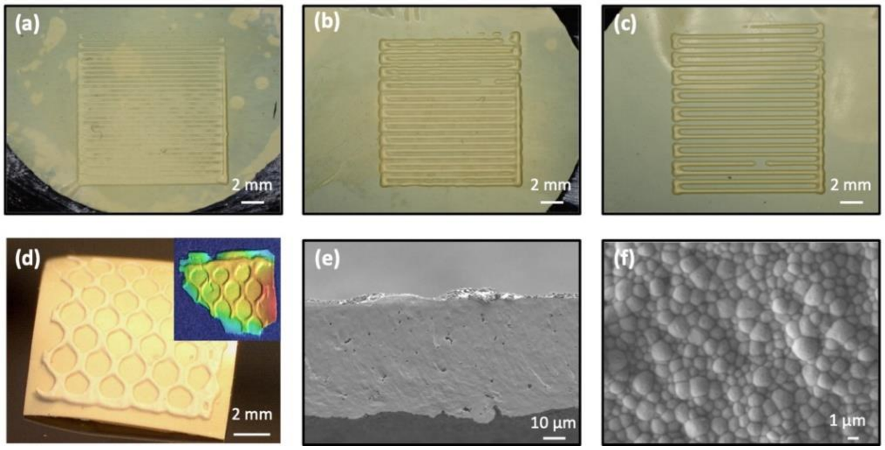

Figure 64. PEGDA-recipe 3D printing and post-sintering. PEGDA/LLZTO ink was first printed as a thin film using a paste PuSL system and then direct ink writing (DIW) printed zig-zag structures with varying spacings (a-c). (d) A honeycomb structure on film substrate. Inset is a piece after 1100°C sintering. (e) The cross-section scanning electron microscopy (SEM) image of the printed film after sintering, showing high densification with thickness of ~ 50 µm. (f) The surface SEM view of sintered film revealing grain size of a few µm.

Post Sintering for Densification

The densification is benefited from the use of MT-milled powders. Raw powders with particle size of ~ 5 µm cannot be densified well in tube furnace even with 83 wt% solid content in NMP/LLZTO recipe, as shown in Figure 65a. By replacing raw powders with ~ 200 nm MT-milled powders, even with lower solid content (that is, 73 wt% for this case), LLZTO film can be densified in tube furnace at 1100°C for 6 h (Figure 65b).

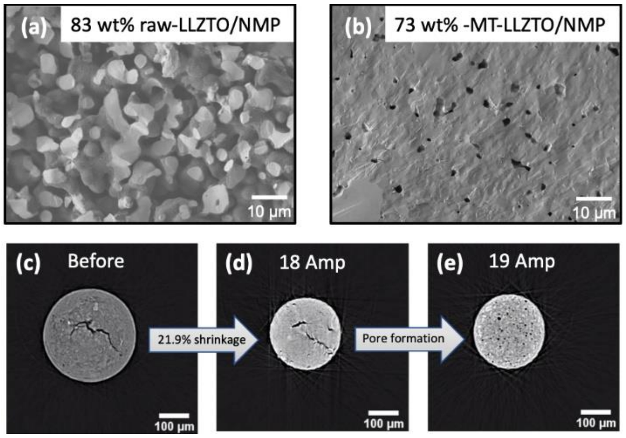

Figure 65. Sintering of direct ink writing (DIW)-extruded LLZTO filaments. (a) 1100°C-furnace sintered filament from 5-µm-LLZTO/NMP (83 wt%) ink. (b) 1100°C-furnace sintered filament from ball milled LLZTO/NMP (73 wt%) ink. (c-e) *In situ* tomography results on halogen-lamp sintered of ball milled LLZTO filament. Sintering temperature is proportional to the applied current of the lamp heating source.

In situ synchrotron radiography/tomography was conducted to reveal sintering kinetics. DIW-extruded filament is the ideal sample for this purpose. As shown in Figure 65c-e, the diameter of the filament shrinks 21.9% within one minute of infrared light irradiation. Further increasing of temperature leads to the evolution of pores, which indicates occurrence of decomposition and needs further investigation.

Although the densification of printed parts is demonstrated, problems remain in post sintering such as cracking and warpage especially for thin film, that hinder measurements of ionic conductivity and integration with other battery components. The team is tackling these issues through various stress/strain management methods; progress will be reported later.

Patents/Publications/Presentations

The project has no patents, publications, or presentations to report this quarter.

Task 4.9 – Lithium-Thiophosphate-Based Super-Ionic Conductors and Cathodes (Jagjit Nanda, Oak Ridge National Laboratory)

Project Objective. Thiophosphate-based solid electrolytes such as Li_3PS_4 (LPS), $LiGe_{10}P_2S_7$ (LGPS), and $Li_7P_3S_{11}$have high Li-ion conductivity (for example, 10^{-3}-10^{-4} S/cm at room temperature), but they suffer from poor electrochemical stability with respect to both Li-metal and cathode materials (>3 V versus Li/Li^+). Typically, sulfide solid electrolytes based on thiophosphates are reduced around 1.6 V and oxidized between 2.5-3 V (with regard to Li^+/Li^0). The thermodynamic instability at the anode and cathode interfaces leads to resistive reaction layers that impede Li-ion transport and limit cell cycling stability. This project specifically aims to measure interfacial resistance between sulfide-based solid electrolytes (SE) with sulfide or metal-sulfide based cathodes. Engineering approaches to kinetically stabilize the electrolyte/electrolyte interfaces (for example, using buffer layers or chemically bridging a sulfur cathode with ionic conductor) will be pursued. One of the project's critical goals is to obtain an ASR < 50 ohm*cm^2 between the solid electrolyte and cathode. If successful, in follow-on years the project will extend these studies to solid-state interfaces with non-sulfur-based cathodes. The team will collaborate with modeling groups at Virginia Commonwealth University (Prof. P. Jena) and LBNL (Prof. G. Ceder) to obtain guidance on synthesis**.**

Project Impact. Solid-state batteries are poised to be the next-generation battery technology for meeting EV goals in terms of energy density, cycle life, and safety. Among other technical barriers, the success of this technology relies on design of stable electrode/electrolyte interfaces. Sulfide-based solid electrolytes have high ionic conductivity (> 10^{-4} S/cm) and are mechanically soft, which simplifies processing compared to their oxide counterparts. Furthermore, sulfide SEs are comprised of earth abundant materials (for example, sulfur and phosphorus) and can be easily synthesized using scalable, low-temperature solution-based routes.

Approach. Low-temperature (< 350°C) solution-based synthesis methods are used to synthesize LPS solid electrolytes. The structure of these materials is characterized using XRD, Raman spectroscopy, and neutron scattering. Standard AC/DC electrochemical methods are used to characterize ionic conductivity, electrochemical stability, and critical current density.

Out-Year Goals. Develop low ASR thiophosphate SE-sulfide cathode interfaces for all-solid-state batteries.

Collaborations. This project will collaborate with Profs. G. Ceder (LBNL) and P. Jena (Virginia Commonwealth University) on modeling and synthesis guideline, as well as with Prof. S. Greenbaum on solid-state NMR to measure ion-diffusivity and local bonding.

Milestones

1. Undertake synthesis and structural characterization of lithium thiophosphate superionic conductors. The team will begin with synthesis of Li_3PS_4 and extend to other phases such as $Li_7P_3S_{11}$ based on the Li-P-S phase diagram. (Q1, FY 2019; Completed December 31, 2018)
2. Attain Li-ion conductivity in the range of 10^{-3} - 10^{-4} S/cm at room temperature by optimizing the synthesis method, dopant concentration, and surface properties. (Q2, FY 2019; Completed March 31, 2019)
3. Complete spectroscopic characterization and evaluate passivation layers at SE/cathode interface using AC impedance and DC polarization tests. (Q3, FY 2019; Completed June 30, 2019)
4. Develop interfacial coatings and tailor the sulfur cathode chemistry to reduce the ASR to 50 ohm*cm^2. (Q4, FY 2019; Completed September 30, 2019)

Progress Report

During the second and third quarters, the team synthesized Li_3PS_4 using a solution-based method and reported the material's ionic conductivity and electrochemical stability. This quarter, work focused on developing a synthesis route for catenated thiophosphate-based cathodes for solid-state batteries. Figure 66a shows a Li-P-S ternary phase diagram that highlights several compounds of interest. The present work investigated catenation of 1 S onto $LiPS_3$ to produce $LiPS_3{\bullet}S$. Unlike sulfur cathodes, which often exhibit poor reversibility (for example, due to formation of an insulating Li_2S phase), $LiPS_3{\bullet}S$ is expected to form the superionic conductor Li_3PS_4 during discharge (see Equation 1 and the green line in Figure 66a). This favorable charge/discharge mechanism is anticipated to produce a cathode with good rate capabilities and cyclability.

$$LiPS_3{\bullet}S + 2\ Li^+ + 2\ e^- \leftrightarrow Li_3PS_4\ (Q_{theoretical} = 323\ mAh/g_{LiPS3{\bullet}S}) \qquad (1)$$

The $LiPS_3$ moiety was first synthesized using a solution-based method in which Li_2S and P_2S_5 were mixed in either tetrahydrofuran (THF) or acetonitrile (AN) followed by thermal annealing at 140-270°C. As shown by the XRD patterns in Figure 66b, either crystalline or amorphous $LiPS_3$ was produced, depending on synthesis conditions. Sulfur catenation was then performed by reacting the $LiPS_3$ with elemental sulfur in THF followed by thermal annealing. Interestingly, the catenated $LiPS_3{\bullet}S$ compounds were completely amorphous regardless of whether a crystalline or amorphous $LiPS_3$ precursor was utilized. The catenated compounds remained amorphous after heating to 260°C and thermally decomposed at 320°C. Vibrational spectroscopic studies are under way to resolve the local bonding and structure of these amorphous materials.

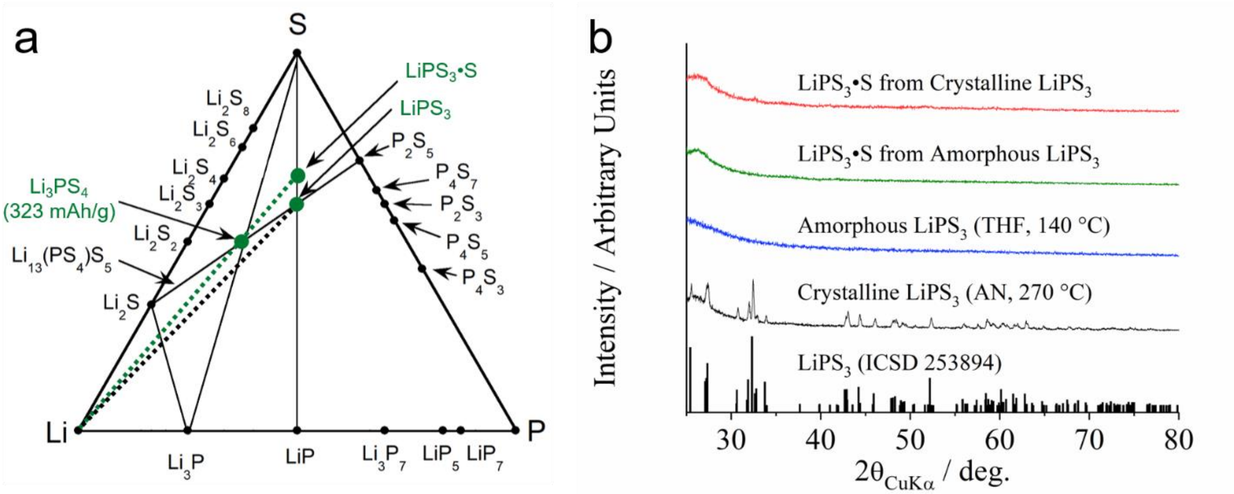

Figure 66. (a) Li-P-S ternary phase diagram. Due to limited available thermodynamic quantities (for example, free energies of formation), not all tie lines are known for this system. (b) X-ray diffraction (XRD) patterns of $LiPS_3$ and catenated $LiPS_3{\bullet}S$ cathode powders. The sloping profiles at 2theta < 30° are due to the Kapton film that was used to prevent air exposure during XRD measurements.

The lithium storage properties of several $LiPS_3$ and $LiPS_3{\bullet}S$ compounds were screened using chemically mediated reactions. In this setup, the cathode powders were chemically reduced using a titrant solution containing lithium biphenyl anion radical ($Li^+\text{ß}^{\bullet -}$) dissolved in diglyme. As titrant was added dropwise to the cathode powders, the solution changed from dark blue (indicating the presence of $Li^+\text{ß}^{\bullet -}$) to translucent yellow (indicating the absence of $Li^+\text{ß}^{\bullet -}$). The total titrated capacities for $LiPS_3$ and $LiPS_3{\bullet}S$ are listed in Table 10. While the amorphous $LiPS_3$ had a relatively low lithium capacity (206 mAh/g), the crystalline $LiPS_3$ exhibited an 8-fold higher capacity (1,683 mAh/g), which indicates this material was fully reduced to form Li_2S + Li_3P

(see Equation 2). The discrepancy between the measured and theoretical capacities is within the measurement error. Overall, these results illustrate that the cathode's structure has a dramatic impact on its electrochemical properties.

$$LiPS_3 + 8\,Li^+ + 8\,e^- \leftrightarrow 3Li_2S + Li_3P\ (Q_{theoretical} = 1{,}600\ mAh/g_{LiPS3}) \qquad (2)$$

Compared to $LiPS_3$, the catenated cathodes exhibited modest capacities ranging from 340-400 mAh/g, which indicates these materials were not fully reduced to form $Li_2S + Li_3P$. The measured capacities are reasonably close to that expected for $LiPS_3•S$ reduction to Li_3PS_4 (323 mAh/g, see Equation 1), although more work is needed to determine the reduction mechanism. Future work will investigate the electrochemical properties of these materials in all-solid-state batteries containing a Li-metal anode and Li_3PS_4 solid electrolyte.

Table 10. Chemically titrated capacities of $LiPS_3$ and $LiPS_3•S$ cathode powders. Titrations were performed by reducing the active material powder using a lithium biphenyl anion radical species (Li+ß•-) dissolved in diglyme. The electrochemical potential of the titrant solution was approximately 0.2 V versus Li/Li^+.

Cathode	Chemically Titrated Lithium Capacity (mAh/g)
$LiPS_3$ (amorphous)	206
$LiPS_3$ (crystalline)	1,680
$LiPS_3•S$ (from amorphous $LiPS_3$)	401
$LiPS_3•S$ (from crystalline $LiPS_3$)	339

Patents/Publications/Presentations

Patent

- Delnick, F. M., J. Nanda, and E. C. Self. "High Capacity Catenated Polysulfidophosphate Cathodes for Lithium Batteries." ORNL Internal Invention Disclosure No. 201904369.

TASK 5 – SULFUR ELECTRODES

Summary

The collected work in this Task involves six projects that have focused on the following areas:

- Conducting focused fundamental research on the mechanism of "shuttle effect" inhibition for rechargeable Li-S batteries.
- Developing electrode and electrolyte systems that can mitigate the "shuttle effect" so the low self-discharge and long cycle life can be achieved.
- Synthesizing sulfur composite materials with an emphasis on polymer sulfur composite materials.
- Developing creative electrode-making processes to improve processability and aerial capacity; for example, polymeric sulfur composites may not be suitable for the traditional slurry casting process.
- Developing a novel S_xSe_y cathode material for rechargeable lithium batteries with high energy density and long life, as well as low cost and high safety.
- Delivering an electrochemically responsive self-formed hybrid LIC as a protective layer for Li-metal anodes, enabling Li-metal anodes to cycle with a high efficiency.
- Developing high-energy, low-cost Li-S batteries with long lifespan.

Highlights. The highlights for this quarter are as follows:

- Stanford University (Cui's group) investigated sulfur morphology change on nickel, carbon, and aluminum substrates during charging and discharging. The researchers found that the presence of a thin and dense oxidation layer (Al_2O_3) on aluminum surface weakens the adsorption of sulfur species on the interface, rendering the surface inert to sulfur conversion, and the thin layer of insulating sulfur/Li_2S on the inactive interface passivates the electrode. This terminates further accumulation of sulfur species and leads to the negligible capacity in charging/discharging processes. On the other hand, nickel substrates favor reversible polysulfide conversion yielding high area capacity. The finding provides important understanding of the various substrates in Li-S batteries.
- Pennsylvania State University (Wang's Group) developed a functional porous sponge sulfur (FSS) electrode using cross-linked polymers with Li-ion-affinity to eliminate the self-discharge and enable high performance of Li-S battery. At an E/S ratio of 5 µl/mg, the FSS electrode with a sulfur mass loading of ~ 11.7 mg cm^{-2} exhibits a high energy density of 412 Wh/kg and good cycling stability for 100 cycles. When the E/S ratio is further reduced to 3.5 µl/mg, the FSS electrode shows an initial energy density of 432 Wh/kg, with highest energy density reaching 460 Wh/kg. The results show an important influence of the cross-linked polymers on sulfur loading, cycling response, and energy density in Li-S system.
- ANL (Amine's group) has examined Li-metal plating/stripping in fluorinated ether and DME based electrolytes. The results showed that the fluorinated ether-based electrolytes demonstrate much better lithium plating/stripping reversibility and CE as well as long-term cycle stability than DME-based electrolytes. This finding provides a route for future efforts to optimize electrolytes for the safe and highly efficient utilization of Li-metal electrodes for high-energy Li/S_xSe_y battery.
- University of Wisconsin at Madison (Qu's group) and BNL (Yang's group) studied prelithiated phosphorus/carbon (P/C) anode in half cell and full cell configurations. The P/C anode shows good rate capability and cycling stability despite being limited lithium source. At 1 A/g, it delivered an initial capacity of 460 $mAh/g_{(S/C)}$ and retains a reversible capacity of 312 $mAh/g_{(S/C)}$ after 300 cycles, with a capacity fade of 0.10% per cycle and an average CE over 99%. The newly configured S/P cell could provide a theoretical

maximum energy density of 967 Wh/kg and an energy density of 358 Wh kg^{-1} was realized in a non-optimized coin cell, based on the total mass of active materials (P/C and S/C). This chemical prelithiation could be extended to development of high-capacity Li-S batteries as well as Li-ion batteries using other anode materials showing the importance of the P/C system.

- LBNL (Liu's group) focused on developing new electrolytes and additives for Li-S rechargeable batteries. The newly developed electrolyte system successfully prevents lithium polysulfide dissolution into the electrolyte, demonstrating a cyclable gravimetric capacity of ~ 800 mAh/g-S material along with very high CE. The result shows an important influence of the new electrolytes and additives for preventing polysulfide dissolution in Li-S batteries.
- PNNL (Liu and Lu's group) prepared three categories of liquid electrolytes [conventional liquid electrolyte (E-121), solvated ionic-liquid like electrolyte (E-SIL), and room-temperature ionic liquid electrolyte (E-IL)] and studied compatibility toward $Li_7P_2S_8Br_{0.5}I_{0.5}$ SSE; they also built a procedure for SSE and LE compatibility assessment in a relevant battery configuration. Their designed ionic liquid shows well balanced permeability and interfacial stability with both the lithium anode and the SSE. This type of ionic liquid electrolyte was used for a hybrid Li-S battery concept demonstration, by coupling with the sulfur cathodes that had optimized composition and architectures showing the importance of this new hybrid system for Li-S batteries.

Task 5.1 – Novel Chemistry: Lithium Selenium and Selenium Sulfur Couple (Khalil Amine, Argonne National Laboratory)

Project Objective. The project objective is to develop a novel S_xSe_y cathode material for rechargeable lithium batteries with high energy density and long life, as well as low cost and high safety.

Project Impact. Development of a new battery chemistry is promising to support the goal of PHEV and EV applications.

Approach. The dissolution of lithium polysulfides in nonaqueous electrolytes has been the major contribution to the low energy efficiency and short life of Li-S batteries. In addition, the insulating characteristics of both end members during charge/discharge (sulfur and Li_2S) limit their rate capacity. To overcome this problem, sulfur or Li_2S is generally impregnated in a carbon-conducting matrix for better electronic conductivity. However, this makes it difficult to increase the loading density of practical electrodes. It is proposed to solve these barriers using the following approaches: (1) partially replace sulfur with selenium, (2) nano-confine the S_xSe_y in a nanoporous conductive matrix, and (3) explore advanced electrolytes with suppressed shuttle effect.

Out-Year Goals. This new cathode will be optimized with the following goals:

- A cell with nominal voltage of 2 V and energy density of 600 Wh/kg.
- A battery capable of operating for 500 cycles with low capacity fade.

Collaborations. This project engages in collaboration with the following: Professor C. Wang of UMD, Dr. Y. Ren and Dr. C. Sun of Advanced Photon Source (APS) at ANL, Dr. L. A. Curtiss at ANL, and Prof. A. X. Sun (Western University, Canada).

Milestones

1. Parasitic reactions study of Li/Se and Se-S systems in different electrolytes. (Q1, FY 2019; Completed)
2. Characterization on the solvation chemistry of concentrated siloxane based electrolytes. (Q2, FY 2019; Completed)
3. Modify the electrode/electrolytes interface using ALD and molecular layer deposition (MLD). (Q3, FY 2019; In progress)
4. Electrochemical test of lithium stripping/plating efficiency and reversibility in Li-Cu and Li-Li cells using different electrolytes. (Q4, FY 2019; Completed)
5. Interface characterization of cycled lithium metal in different electrolytes. (Q1, FY 2020; In progress)

Progress Report

In addition to the shuttle effect, reversible lithium plating/stripping is another challenge for long-life Li/S and Li/S_xSe_y battery. In their previous study, the team found both concentrated siloxane based electrolytes and fluorinated ether based electrolytes can suppress the shuttle effect. However, their effectiveness in suppressing lithium dendrite is not yet investigated. Despite the ability of concentrated siloxane based electrolytes to enable a robust SEI the S_xSe_y cathode, the relatively higher viscosity would raise a concern on the cost and wetting ability of electrolytes especially for high-loading electrodes and fast charging. Hence, the team has mainly focused on study of lithium stripping/plating in the fluorinated ether based electrolytes compared to the common ether based electrolytes this quarter.

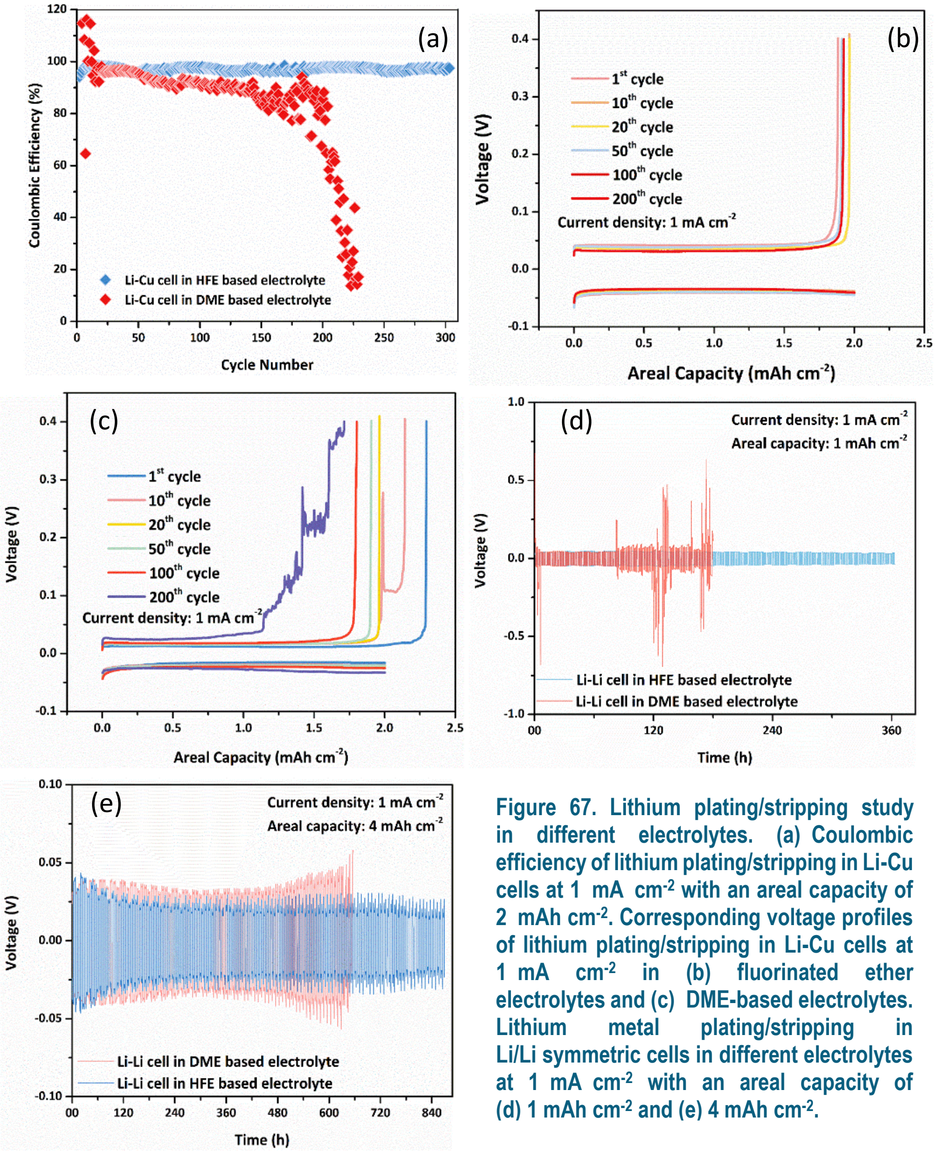

Figure 67. Lithium plating/stripping study in different electrolytes. (a) Coulombic efficiency of lithium plating/stripping in Li-Cu cells at 1 mA cm^{-2} with an areal capacity of 2 mAh cm^{-2}. Corresponding voltage profiles of lithium plating/stripping in Li-Cu cells at 1 mA cm^{-2} in (b) fluorinated ether electrolytes and (c) DME-based electrolytes. Lithium metal plating/stripping in Li/Li symmetric cells in different electrolytes at 1 mA cm^{-2} with an areal capacity of (d) 1 mAh cm^{-2} and (e) 4 mAh cm^{-2}.

Figure 67a compares the CE of Li-metal plating/stripping in Li-Cu cells at a current density of 1 mA cm^{-2} using HFE (fluorinated ether) based and DME based electrolytes, in which a high CE close to 100% can be achieved up to 300 cycles in HFE-based electrolytes, while the CE in the DME-based electrolytes was continuously decreased after 50 cycles and dramatically decreased to below 10% after 225 cycles. Figure 67b-c compares the corresponding voltage profiles of Li/Cu cells at different cycles using HFE and DME electrolytes, respectively. As shown, the voltage profiles of Li/Cu cell in HFE-based electrolytes is highly reversible for the first 200 cycles during both charge and discharge process, corresponding to a highly reversible lithium plating/stripping process. In contrast, the voltage polarization was significantly increased after 200 cycles. Moreover, less and less lithium could be stripped from the copper electrode during cycling, indicating a significant amount of lithium deposited on the copper substrate reacts with the electrolyte and could not be recovered during the stripping process.

The team further compares Li-metal plating/stripping behavior in different electrolytes using Li/Li symmetric cells. Figure 67d shows the lithium plating/stripping voltage profiles in the Li/Li symmetric cells in different electrolytes at 1 mA cm^{-2} with an areal capacity of 1 mAh cm^{-2}. The interfacial resistance of the Li/Li cell in the HFE-based electrolytes remains constant even after 360 h. However, the identical Li/Li cell in the DME-based electrolytes cycled at the same current density demonstrated significant impedance after only 80 h. After 180 h, the over potential of the cell was even ten times higher than the one in HFE-based electrolytes. To satisfy the need for high-loading S_xSe_y electrodes (> 4 mAh cm^{-2}), the team further increases the areal capacity loading of Li/Li symmetric cells to 4 mAh cm^{-2}. As shown in Figure 67e, the over potential of the Li/Li symmetric cell can be stabilized over 840 h, even with such a high areal capacity loading, compared to less than 600 h in the DME-based electrolytes (over potential started to increase).

In conclusion, both fluorinated ether and DME based electrolytes have been examined in the study of Li-metal plating/stripping. The results showed that the fluorinated ether based electrolytes demonstrate much better lithium plating/stripping reversibility and CE as well as long-term cycle stability than DME-based electrolytes. This finding provides a route for future efforts to optimize electrolytes for the safe and highly efficient utilization of Li-metal electrodes for high-energy Li/S_xSe_y battery. The team will conduct interface characterization to elucidate the underlying mechanism behind the performance next quarter.

Patents/Publications/Presentations

Patent

- Xu, G., and K. Amine. “Rechargeable Lithium Batteries.” ANL-IN-19-034.

Task 5.2 – Development of High-Energy Lithium-Sulfur Batteries (Dongping Lu and Jun Liu, Pacific Northwest National Laboratory)

Project Objective. The project objective is to develop high-energy, low-cost Li-S batteries with long lifespan. All proposed work will employ thick sulfur cathode (≥ 2 mAh/cm^2 of sulfur) at a relevant scale for practical applications. The diffusion process of soluble polysulfide out of thick cathode will be revisited to investigate cell failure mechanism at different cycling. The fundamental reaction mechanism of polysulfide under the electrical field will be explored by applying advanced characterization techniques to accelerate development of Li-S battery technology.

Project Impact. The theoretical specific energy of Li-S batteries is ~ 2300 Wh/kg, which is almost three times higher than that of state-of-the-art Li-ion batteries. The proposed work will design novel approaches to enable Li-S battery technology and accelerate market acceptance of long-range EVs required by the EV Everywhere Grand Challenge.

Approach. The project proposes to (1) identify and address key issues of applying high-energy sulfur cathodes including materials, binders, electrode architectures, and functional electrode additives, (2) advance mechanism study of sulfur cathode and electrolyte by using *in situ*/*ex situ* techniques and custom-designed hybrid cell setup, and (3) verify effectiveness of the new approaches with coin/pouch cells by using high-loading electrodes (> 4 mg/cm^2), limited lithium ($< 200\%$ lithium excess), and lean electrolyte (E/S < 4 μL/mg).

Out-Year Goals. This project has the following out-year goals:

- Fabricate Li-S pouch cells with thick electrodes to understand sulfur chemistry/electrochemistry in environments similar to real application.
- Leverage the Li-metal protection project funded by the DOE and PNNL advanced characterization facilities to accelerate development of Li-S battery technology.
- Develop Li-S batteries with a specific energy of 400 Wh/kg at cell level, 1000 deep-discharge cycles, improved abuse tolerance, and less than 20% capacity fade over a 10-year period to accelerate commercialization of EVs.

Collaborations. This project engages in collaboration with the following: Dr. X-Q. Yang (BNL), Dr. D. Qu (University of Wisconsin at Madison), Dr. G. Zhang (University of Alabama), and Dr. J. Tao (PNNL).

Milestones

1. Synthesize high Li$^+$ conductivity sulfide-based Li$^+$ conductors with room-temperature conductivity > 1 mS/cm for sulfur cathodes. (Q1, FY 2019; Completed)
2. Develop electrode preparation method for sulfur/Li$^+$-conductor cathodes with sulfur mass loading > 4 mg/cm^2 and sulfur > 75 wt% in whole electrode. (Q2, FY 2019; Completed)
3. Complete electrode composition and architecture optimization for low porosity sulfur electrodes (electrode density >1 g/cm^3). (Q3, FY 2019; Completed)
4. Complete electrochemical evaluation of high-loading sulfur electrodes (> 4 mg/cm^2) at E/S < 3 μL/mg, and identify compatible liquid electrolytes with the cathodes. (Q4, FY 2019; Completed)

Progress Report

A solvent-free fabrication method was demonstrated last quarter for the preparation of free-standing sulfur electrodes with SSEs ($Li_7P_2S_8Br_{0.5}I_{0.5}$) by using a very lean amount of binder (< 5 wt%). This provides a critical basis for the design of the hybrid Li-S battery (HLSB), where the SSE facilitates Li^+ transport within the individual particles while the additional liquid phase electrolyte enables the ionic conduction between the particles. A prerequisite to the realization of the HLSB is to identify appropriate liquid electrolytes that are chemically stable or self-passivated toward both the lithium anode and the SSE. On contact with certain liquid electrolytes/additives, a lithium anode can be eventually stabilized by forming an effective SEI. However, it is challenging to maintain stability of a sulfide-based SSE in the presence of liquid electrolytes for long-term operation. This is due to the highly reactive nature of the sulfide-based SSE toward the polar organic solvents used in conventional electrolytes. Selection of compatible liquid electrolytes can be rationalized by tuning the solvent solubility to sulfide and nucleophilic reactivity with the SSE.

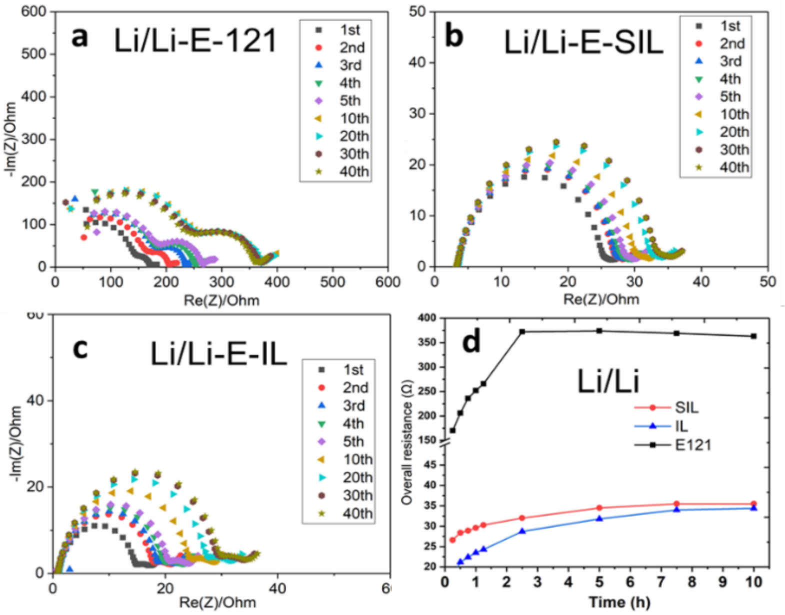

Figure 68. Interfacial stability of lithium anode in contact with different electrolytes: Nyquist plots of Li/Li symmetric cells with (a) 1 M LiTFSI/DOL/DME + 0.3 M $LiNO_3$ (E-121), (b) solvated ionic liquid electrolyte (E-SIL), (c) room temperature ionic liquid electrolyte (E-IL), and (d) corresponding overall resistance evolution with a test duration of 10 hours.

This quarter, the key achievements are as follows: (1) prepared three categories of liquid electrolytes [conventional liquid electrolyte (E-121), solvated ionic-liquid like electrolyte (E-SIL), and room-temperature ionic liquid electrolyte (E-IL)] and studied their compatibility toward $Li_7P_2S_8Br_{0.5}I_{0.5}$ SSE; and (2) built procedure for SSE and liquid electrolyte compatibility assessment in a relevant battery configuration. To study the interactions of SSE with liquid electrolyte in a practical electrode scenario, the high-loading sulfur cathodes (S > 6 mg/cm^2) with a S/C: SSE: binder ratio at 84:15:1 were prepared using the solvent-free processing method and used as model electrodes. The electrolyte amount was controlled at E/S=2 mL/g for each Li-S cell. The stability of the liquid electrolytes with the lithium anode was studied first. Figure 68a-c compares the EIS evolution of the lithium anode in contact with different electrolytes during the 10-h rest (acquired 40 EIS spectra with a 15-min interval). Results obtained with the same cell configuration indicate that IL and SIL are prone to forming lower resistance interface on the lithium anode, compared to the E-121. This corroborates excellent stability of the IL-based electrolytes toward lithium metal and suggests that less free-solvent would be desired for the electrolyte design in pursuit of a low resistance and stable lithium anode interface, which is consistent with recent discoveries of concentrated electrolytes for lithium batteries. However, the SSE containing sulfur electrodes exhibits different responses when exposed to those electrolytes. The cell using conventional E-121 electrolyte quickly reaches a stable interface within 1 h (Figure 69a); the cell with E-SIL needs > 5 h to establish a stable interface with very high resistance (Figure 69b). Those observations can be explained by both the permeability and reactivity of the liquid electrolyte. During the EIS measurement period, the liquid electrolyte involves simultaneous processes of cathode infiltration and side reactions with SSE and lithium anode. The former process improves electrode wetting, thus lowering cell impedance, while the side reactions contribute to overall cell resistance. For E-121, viscosity is much lower than for the other two, thus requiring a shorter time to complete electrolyte infiltration in the low-porosity sulfur electrode and establish stable interfaces on both electrodes through passivation reactions. In the case of the SIL electrolyte with high viscosity, the electrolyte infiltration process and associated side reactions are both slowed down. It was noticed that the residual free solvent in the SIL is very reactive with SSE, generating high interfacial resistance and even blocking the electrode after 5 h. The project's designed IL shows well balanced permeability and interfacial stability with both the lithium anode (blue in Figure 68d) and the SSE (blue in Figure 69d). This kind of IL electrolyte was used for HLSB concept demonstration, by coupling with sulfur cathodes that had optimized composition and architectures.

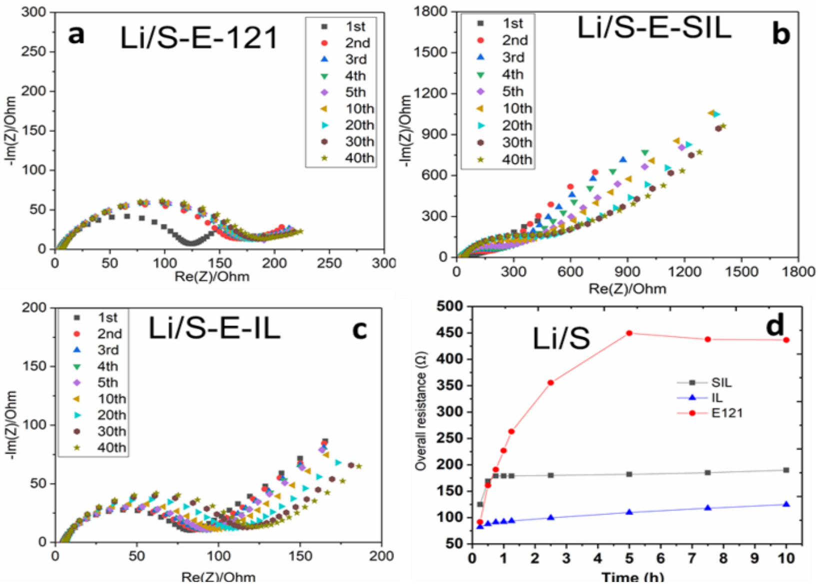

Figure 69. Interfacial stability of solid-state electrolyte contained sulfur cathode in contact with different electrolytes: Nyquist plots of Li-S cells with (a) E-121, (b) E-SIL, (c) E-IL, and (d) corresponding overall resistance evolution with 10-h test duration.

Patents/Publications/Presentations

The project has no patents, publications, or presentations to report this quarter.

Task 5.3 – Nanostructured Design of Sulfur Cathodes for High-Energy Lithium-Sulfur Batteries (Yi Cui, Stanford University)

Project Objective. The charge capacity limitations of conventional TM oxide cathodes are overcome by designing optimized nano-architectured sulfur cathodes. This study aims to enable sulfur cathodes with high capacity and long cycle life by developing sulfur cathodes from the perspective of nanostructured materials design, which will be used to combine with Li-metal anodes to generate high-energy Li-S batteries. Novel sulfur nanostructures as well as multi-functional coatings will be designed and fabricated to overcome issues related to volume expansion, polysulfide dissolution, and the insulating nature of sulfur.

Project Impact. The capacity and the cycling stability of sulfur cathode will be dramatically increased. This project's success will make Li-S batteries to power EVs and decrease the high cost of batteries.

Approach. The approach comprises the three main parts shown below, with primary activities listed.

- ***Advanced Nanostructured Sulfur Cathodes Design and Synthesis.*** (1) Engineer empty space into sulfur cathode to solve the problem of electrode volume expansion. (2) Develop novel sulfur nanostructures with multi-functional coatings for confinement of S/Li polysulfides to address issues of active materials loss and low conductivity. (3) Develop/discover optimal nanostructured materials that can capture the polysulfide dissolved in the electrolyte. (4) Develop space efficiently packed nanostructured sulfur cathode to increase volumetric energy density and rate capability. (5) Identify the interaction mechanism between sulfur species and different types of oxides/sulfides, and find optimal material to improve capacity and cycling of sulfur cathode.
- ***Structure and Property Characterization.*** (1) *Ex situ* SEM. (2) XPS analysis. (3) *In operando* XRD and optical microscopy.
- ***Electrochemical Testing.*** (1) Coin cells and pouch cells. (2) A set of electrochemical techniques.

Out-Year Goals. The cycle life, capacity retention, and capacity loading of sulfur cathodes will be greatly improved (200 cycles with 80% capacity retention, > 0.3 mAh/cm^2 capacity loading) by optimizing material design, synthesis, and electrode assembly.

Collaborations. This project collaborates with the following: BMR PIs; SLAC National Accelerator Laboratory: Dr. M. Toney *(In situ* X-ray); and Stanford: Prof. Nix (mechanics) and Prof. Bao (materials).

Milestones

1. Build *in situ* characterization platform to monitor nucleation/dissolution of sulfur/Li_2S_n. (Q1, FY 2019; October 2018, Completed)

2. Develop a noninvasive imaging method with sub-micron, sub-second resolution for Li-S battery in label-free, native organic liquid electrolyte. (Q2, FY 2019; January 2019, Completed)

3. Demonstrate the substrate-dependent electrochemical formation of super-cooled liquid sulfur and crystals, as well as rapid solidification of a super-cooled sulfur droplet. (Q3, FY 2019; April 2019, Completed)

4. Provide direct evidence about a long-debated reaction pathway of surface mechanism versus solution mechanism for sulfur and the current collector effect on sulfur evolution. (Q3, FY 2019; Completed)

5. Investigate the sulfur growth behaviors on different current collectors and correlate the results with their electrochemical performance. (Q4, FY 2019, October 2019; Completed)

6. Direct real-time observation of sulfur species evolution at the microscale, and investigation of the reaction kinetics. (Q1, FY 2020, January 2020; In progress)

Progress Report

Last quarter, the team systematically investigated sulfur growth behaviors on different current collectors and correlated the results with electrochemical performance. This quarter, the team investigated the morphology change for the sulfur species on different substrates during charging and discharging.

The cells based on the nickel, carbon, and aluminum electrodes were disassembled in the glovebox at charged state (3.0 V) or discharged state (1.0 V), washed using DOL, and examined by SEM. The morphologies of the sulfur species are displayed in Figure 70. The aluminum surface is relatively inert with an ultra-low capacity, and with only a thin layer of sulfur/Li_2S coating the surface during charging and discharging (Figure 70a/d). This is confirmed by EDS elemental analysis, which shows a very weak sulfur signal coexisting with peaks from aluminum and oxygen. In contrast, large amounts of flower-shaped Li_2S particles composed of small sheets with sizes of about ~ 2-3 μm were observed under SEM that randomly deposited on the surface of the carbon electrode during discharging (Figure 70b). After charging to 3.0 V, in addition to sulfur crystals produced by oxidation of Li_2S, some insoluble, flower-like Li_2S deposits remained on the carbon surface (inset, Figure 70e). This insoluble Li_2S causes capacity decay due to irreversible sulfur conversion reactions, which is consistent with cycling results. More interestingly, high density of vertically grown Li_2S nanosheets was observed for the nickel electrode during the discharging process (Figure 70c), and the SEM image (Figure 70f) combined with EDS spectrum indicate complete conversion from Li_2S nanosheets to sulfur on the nickel surface after charging to 3.0 V. This reversible deposition/dissolution of the sulfur species on the nickel surface is critical to maintain efficient charge transfer kinetics and achieve long-term cycling stability for Li-S batteries.

To obtain a more detailed understanding of the Li_2S oxidation process, XPS was used to analyze the products on nickel and carbon substrates at the charged states. In the high-resolution Li 1s spectrum, it is worth noting that no obvious features can be observed in the lithium signal from the nickel sample, indicative of the absence / little amount of lithium polysulfide intermediates or Li_2S after the charging process (Figure 70g). However, the distinct lithium signal at around 55.3 eV can be clearly seen from the carbon sample (Figure 70g), implying existence of lithium sulfides that match well with SEM results (Figure 70e). As for the sulfur 2p spectrum of the charged carbon electrode shown in Figure 70h, other than the peaks that correspond to elemental sulfur (162.7 and 163.9 eV), the appearance of S^{2-} peaks (160.6 and 161.8 eV) in the XPS spectra, corresponding to Li_2S, indicating existence of remaining Li_2S covering the surface of the carbon current collector. As for the nickel current collector, all peaks can be ascribed to S^0, confirming complete conversion of polysulfides to sulfur (Figure 70h). Therefore, the nickel layer speeds up not only the electron transfer but also the redox reaction of polysulfide conversion on the electrode surface, which is expected to promote reversibility of sulfur chemistry and enable high power capability for Li-S batteries.

Based on the above discussion, Figure 71a-c presents schematics of sulfur species evolution on nickel, carbon, and aluminum substrates during the charging and discharging processes. During the charging process, some sulfur droplets start to nucleate on the surface of the nickel electrode. These liquid droplets are generated at small sizes, then grow up and merge into larger sizes after touching each other. The liquid sulfur droplets leave plenty of unoccupied current collector surface as electrochemically active sites for polysulfide conversion, which enables the high area capacity on the nickel surface. On discharging, the liquid sulfur droplets reversibly reduce into soluble polysulfides and finally form sheet-like Li_2S depositing on the nickel surface (Figure 71a). In contrast, on the carbon substrate, the accumulation of insulating Li_2S and disconnected sulfur crystals during repeated cycling will block charge transport across the electrode/electrolyte interface and cause active material loss, resulting in poor reaction kinetics and fast capacity decay (Figure 71b). For aluminum substrates, there is generally a thin and dense oxidation layer (Al_2O_3) on the surface, which weakens adsorption of sulfur species on the interface, rendering the surface inert to sulfur conversion. Therefore, the thin layer of insulating sulfur/Li_2S on inactive interface passivates the electrode, terminating further accumulation of sulfur species and leading to the negligible capacity in charging/discharging processes (Figure 71c).

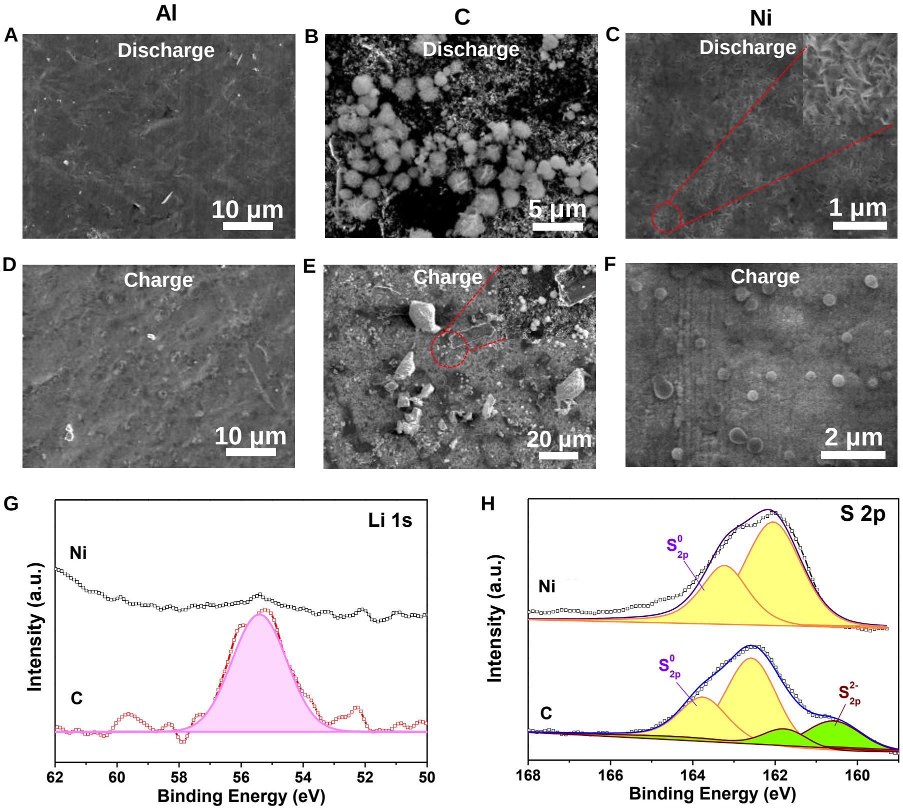

Figure 70. Scanning electron microscopy (SEM) images of the discharging products formed on the (a) aluminum, (b) carbon, and (c) nickel substrates. Inset in (c) is the magnified area, indicated by the red circle. SEM images of the charging products formed on the (d) aluminum, (e) carbon, and (f) nickel substrates. Inset in (e) is the magnified area indicated by the red circle. (g) Lithium 1s X-ray photoelectron spectroscopy (XPS) spectra of the nickel and carbon substrates. (h) Sulfur 2p XPS spectra of the nickel and carbon substrates.

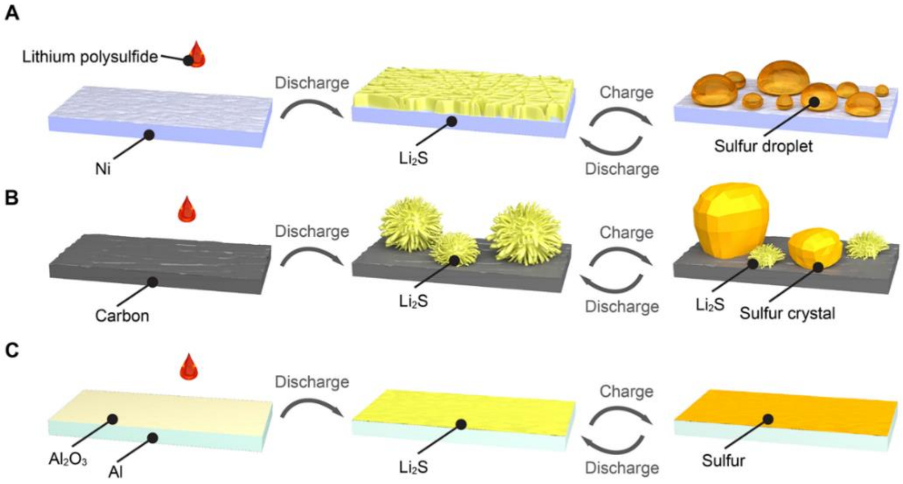

Figure 71. Schematic illustration of sulfur species evolution on (a) nickel, (b) carbon, and (c) aluminum substrates during charging and discharging processes.

Patents/Publications/Presentations

The project has no patents, publications, or presentations to report this quarter.

Task 5.4 –Investigation of Sulfur Reaction Mechanisms (Deyang Qu, University of Wisconsin at Milwaukee; Xiao-Qing Yang, Brookhaven National Laboratory)

Project Objective. The primary objectives are:

- To continue conducting focused fundamental research on the mechanism of “shuttle effect” inhibition for rechargeable Li-S batteries;
- To continue developing electrode and electrolyte systems that can mitigate the “shuttle effect” so low self-discharge and long cycle life can be achieved.
- To synthesize sulfur composite material with an emphasis on polymer sulfur composite materials.
- To develop creative electrode making processes to improve processability and aerial capacity; for example, polymeric sulfur composite may be unsuitable for the traditional slurry casting process.

The ultimate goal is to develop a practical rechargeable Li-S battery that meets the challenges of powering the next generation of EVs beyond Li-ion technologies.

Project Impact. With development of unique *in situ* electrochemical high-performance liquid chromatography (HPLC)/MS and *in situ* electrochemical microscopic techniques, the mechanisms of all reactions in a Li-S cell can be further understood. Better understanding the sulfur redox reaction will lead to mitigation of the “shuttle effect.” The project results will thus guide development of polymer sulfur cathode and Li-S designs for EVs.

Approach. This project will use *in situ* electrochemical HPLC/MS, XPS, SEM, and XRD to study electrochemical reactions associated with sulfur electrodes. Electrochemical techniques such as AC impedance, rotation ring disk electrode, and galvanostat will be used to study the electrode process kinetics. The project will use an *in situ* electrochemical optical method to investigate the surface of lithium anode during cycling of Li-S cell. It will develop thicker sulfur electrode with high areal capacity using dry process.

One-Year Goals. The one-year goals include the following areas: (1) complete investigations of new electrolytes for mitigating the “shuttle effect” and improving Li-anode performance, and (2) complete preliminary design of new electrode processes and tests of polymeric sulfur composite electrodes.

Collaborations. The PI, D. Qu, is the Johnson Controls Endowed Chair Professor; thus, the team from University of Wisconsin at Madison and BNL has close collaboration with Johnson Controls’ scientists and engineers. This collaboration enables the team to validate outcomes of fundamental research in pilot-scale cells. This team has been closely working with top scientists on new material synthesis at ANL, LBNL, and PNNL, with U. S. industrial collaborators at GM, Duracell, and Johnson Controls, as well as with international collaborators in China, Japan, and South Korea. These collaborations will be strengthened and expanded to give this project a vision on both today’s state-of-the-art technology and tomorrow’s technology in development, with feedback from the material designer and synthesizers upstream and from industrial end users downstream.

Milestones

1. Literature review and molecular design of polymeric sulfur compounds. (Q1, FY 2019; Completed)
2. Complete screening electrolyte and additives for the Li-S batteries. Start synthesis of polymeric sulfur compounds. (Q2, FY 2019; Completed)
3. Complete preliminary designs of electrode manufacture process and start to explore feasibility for the synthesized polymeric sulfur composite. (Q3, FY 2019; Completed)
4. Complete initial design of electrode manufacture processes and tests of synthesized polymeric sulfur materials. (Q4, FY 2019; Completed)

Progress Report

This quarter, while continuing to explore conditions for chemical synthesis of sulfur-containing copolymer materials; the team investigated alternative anode materials aiming to alleviate polysulfide "shuttle" effect by limiting the chemical reactions between dissolved polysulfides and lithium-containing anodes. They also started to explore how to process polymeric sulfur cathode materials.

The prelithiated phosphorus/carbon (P/C) anode, which had been reported second quarter, was further studied both in half-cell and full-cell configurations. Good cycling performance and rate capability were demonstrated. The team expects that this chemical prelithiation could be extended to development of high-capacity Li-S batteries as well as Li-ion batteries using other anode materials.

Prelithiated P/C Anode and Sulfur Batteries. A prelithiated P/C electrode was obtained by immersing the pristine P/C electrode into 1 M Li-Bp/THF. Apart from compensating the initial capacity loss due to consumption of active lithium ions during formation of the SEI layer, the anode prelithiation also enabled P/C electrode to pair with Li-free sulfur cathode given that reversible lithium can also be pre-loaded into P/C matrix. Due to less negative potential of prelithiated P/C electrode against lithium, when a fully-prelithiated P/C electrode is used to replace the Li-metal anode, the "shuttle" effect may be limited due to less reactive anode with dissolved polysulfides. In Figure 72, a full cell made with fully-prelithiated P/C anode and S/C cathode is schematically illustrated. Good rate and cycling performance of a prelithiated P/C electrode is also demonstrated in Figure 72. In a full S/P cell, a good rate capability and cycling stability are shown in the Figure in spite of a limited lithium source. At 1 A/g, it delivered an initial capacity of 460 mAh $g^{-1}{}_{S/C}$ and retains a reversible capacity of 312 mAh $g^{-1}{}_{S/C}$ after 300 cycles, with a capacity decrease of 0.10% per cycle and an average CE over 99%. The S/P cell exhibited a voltage profile similar to that of S/Li cell, except at different

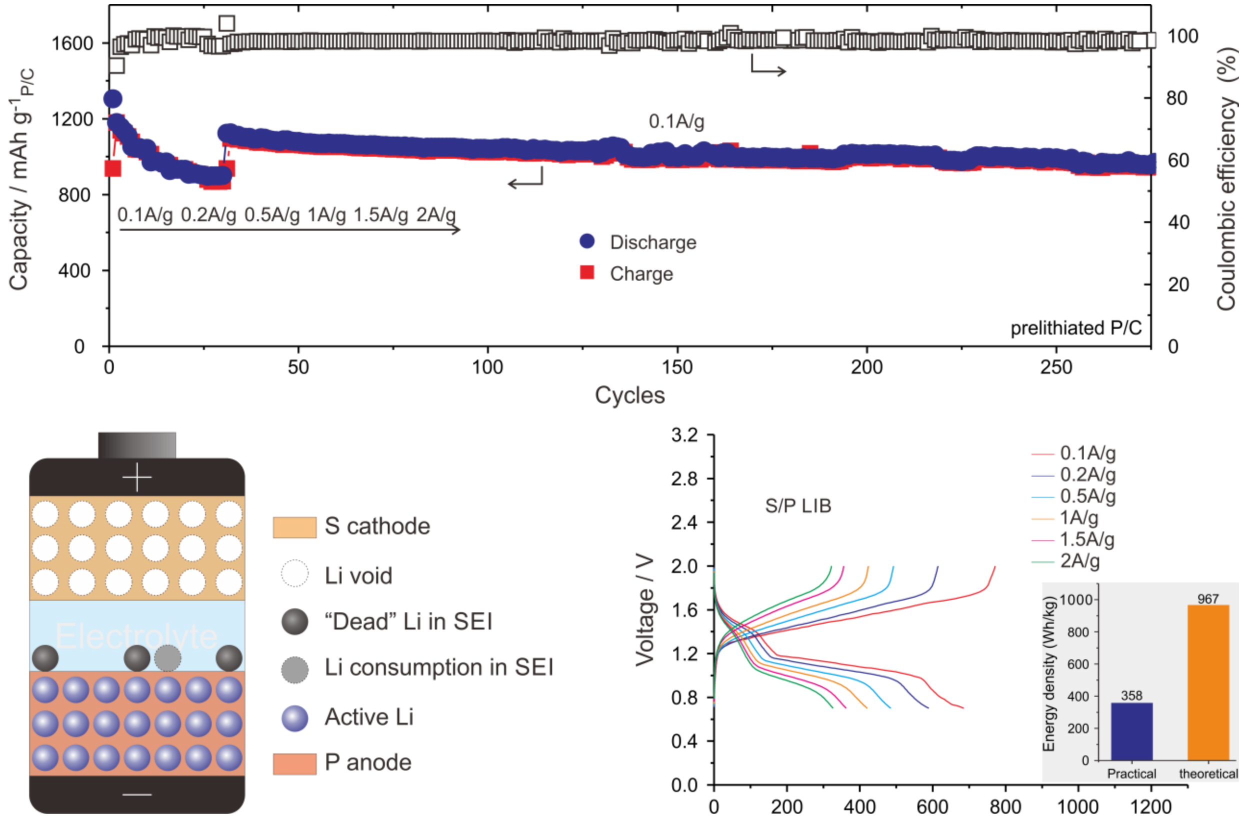

Figure 72. Schematic illustration of the S/P batteries (bottom left); rate and cycling performance of a fully pre-lithiated P/C anode prepared through patented chemical method (top); and typical voltage profiles at different current densities (bottom right). Inset shows the theoretical and practical energy densities of the S/P Li-ion battery (bottom right).

voltages, displaying two discharge plateaus at 1.4 V and 1.1 V. Despite the output voltage being a little low, the newly configured S/P cell could provide a theoretical maximum energy density of 967 Wh kg^{-1}. An energy density of 358 Wh kg^{-1} has been realized in an unoptimized coin cell, based on total mass of active materials (P/C and S/C). In addition, both sulfur and phosphorus are cheap and environmentally abundant.

Patents/Publications/Presentations

Publication

- Wang, G., F. Li, D. Liu, D. Zheng, C. J Abeggien, Y. Luo, X-Q. Yang, T. Ding, and D. Qu. “High Performance Lithium-Ion and Lithium–Sulfur Batteries Using Prelithiated Phosphorus/Carbon Composite Anode.” *Energy Storage Materials*. doi.org/10.1016/j.ensm.2019.08.025.

Task 5.5 – Electrochemically Responsive, Self-Formed, Lithium-Ion Conductors for High-Performance Lithium-Metal Anodes
(Donghai Wang, Pennsylvania State University)

Project Objective. The project objective is to develop and deliver an electrochemically responsive self-formed hybrid LIC as a protective layer for Li-metal anodes, enabling Li-metal anodes to cycle with a high efficiency of ~ 99.7% at high electrode capacity (> 6 mAh/cm^2) and high current density (> 2 mA/cm^2) for over 500 cycles. The project will also demonstrate prototype ~ 300 mAh Li-S battery cells with energy densities of ~ 200 Wh/kg and ~ 80% capacity retention for ~ 300 cycles at ~ 80% depth of discharge using Li-metal anodes with this protective layer.

Project Impact. This project aims to develop a new hybrid LIC that enables safe and high-performance Li-metal anodes. Use of these anodes in turn enables Li-S batteries with high energy density and long cycling life. Such anodes can also lead to a 50% increase in the energy density of conventional Li-ion batteries with Li-metal oxide cathodes. Meeting the technical targets will potentially develop a new high-energy-density lithium battery, promote increased adoption of EVs and PHEVs, and reduce petroleum consumption in the transportation sector by helping battery-powered vehicles become accepted by consumers as a reliable source of transportation.

Approach. The novel multi-phase organo-Li_xS_y or organo-$Li_xP_yS_z$ hybrid ion conductors with tunable multi-functional organic components and controlled Li_xS_y and $Li_xP_yS_z$ inorganic components will be designed and prepared, and thus enable safe use of lithium metal with high CE. In the third year, the team will develop the organo-Li_xS_y/organo-$Li_xP_yS_z$ composite lithium protection layers with tuned functionality: (1) finding appropriate composition, (2) developing appropriate synthesis and fabrication methods, and (3) optimizing organo-Li_xS_y/organo-$Li_xP_yS_z$ components in a protection layer to improve CE and Li-S battery performance.

Out-Year Goals. The project is working toward developing the organo-Li_xS_y/organo-$Li_xP_yS_z$ composite lithium protection layers with tuned functionality. Characterization, performance, and compatibility tests on materials and systems will be conducted. Uniform, dendrite-free lithium deposition under protection of organo-Li_xS_y/organo-$Li_xP_yS_z$ composite lithium protection layers will be demonstrated; CE will be improved.

Collaborations. There are no active collaborations.

Milestones

1. Develop the organo-Li_xS_y/organo-$Li_xP_yS_z$ composite lithium protection layers with tuned functionality. Conduct characterization and performance tests on the materials. (Q1, FY 2019; Completed)
2. Demonstrate uniform and dendrite-free lithium deposition under protection of the organo-Li_xS_y/organo-$Li_xP_yS_z$ composite lithium protection layers. (Q2, FY 2019; Completed)
3. Optimize the organo-Li_xS_y/organo-$Li_xP_yS_z$ composite lithium protection layers and demonstrate lithium anodes cycling with ~ 99.4% CE for ~ 200 cycles. (Q3, FY 2019; Completed)
4. Demonstrate lithium anodes with optimized organo-Li_xS_y/organo-$Li_xP_yS_z$ composite lithium protection layers and ~ 99.7% CE for ~ 300 cycles. (Q4, FY 2019; Completed)

Progress Report

The team has developed a functional porous sponge sulfur (FSS) electrode to eliminate self-discharge and enable high performance of Li-S battery.

The FSS electrode is fabricated by an ice-templating method through cross-linking reaction between Li-ion-affinity polymers. Figure 73a shows pictures of as-prepared FSS electrodes, which can be peeled off and cut into different sizes. The FSS electrodes contain many functional groups (C-N, C-O), evidenced by FTIR spectra. These functional groups have strong Li-ion affinity and endow the electrodes with strong LiPS chemisorption. Figure 74 shows the ability of FSS electrodes to adsorb the LiPS.

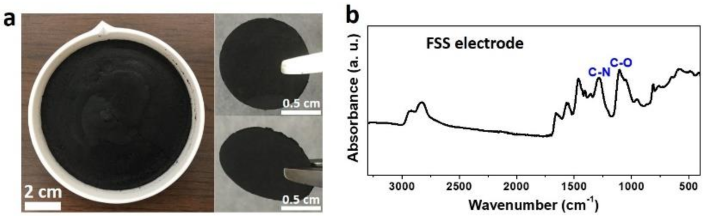

Figure 73. (a) The photos of prepared functional porous sponge sulfur (FSS) electrodes. (b) Fourier transform infrared spectra of FSS electrode.

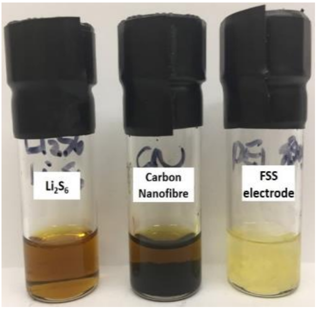

Figure 74. Li_2S_6 adsorption of functional porous sponge sulfur electrodes.

The strong LiPS chemisorption and the unique structure can enable the FSS electrode with excellent performance. As shown in Figure 75a, at an E/S ratio of 10 µl mg^{-1}, the FSS electrodes with various sulfur mass loading of 6.0, 8.78, and 10 mg cm^{-2} deliver high initial capacities of 1180.2, 1149.9, and 1132.9 mA h g^{-1}, respectively, indicating high sulfur utilization even under high sulfur mass loading; they maintain stable cycling over 200 cycles with good capacity retention. At the conditions of high sulfur mass loading (11 mg cm^{-2}) and low E/S ratio (≤5 µl mg^{-1}), the FSS electrode delivers an initial discharge capacity of 973.8 mA h g^{-1}, corresponding to a high areal capacity of 10.63 mA h cm^{-2} and an energy density of ~ 250 W h kg^{-1} (considering total mass of the cathode, anode, and electrolyte). At a much lower E/S ratio of 3 µl mg^{-1} (Figure 75c), the FSS electrode still exhibits initial discharge capacity of 973.8 mA h g^{-1} (areal capacity: 10.45 mA h cm^{-2}), corresponding to a much higher energy density of 308 W h kg^{-1}; it maintains stable cycling over 100 cycles.

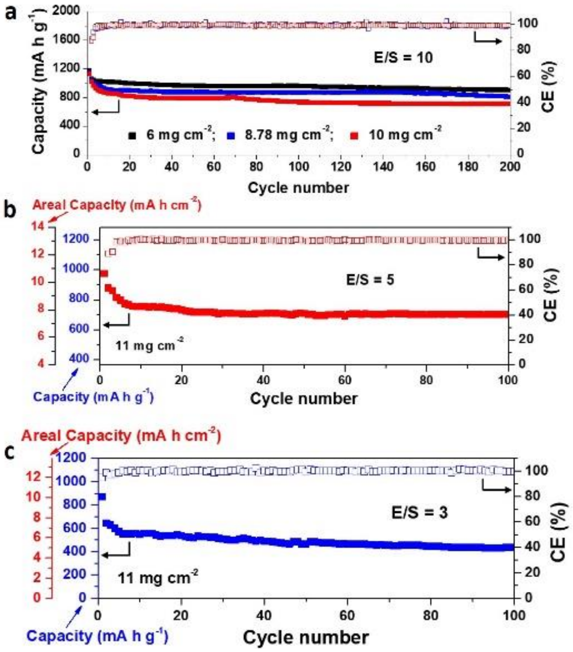

Figure 75. (a) The cycling performance of the functional porous sponge sulfur (FSS) electrode with various sulfur mass loading of 6, 8.78, and 10 mg cm^{-2} at an E/S ratio of 10 µl mg^{-1}. Cycling performance of the FSS electrodes with the sulfur mass loading of 11 mg cm^{-2} at the E/S ratios of 5 µl mg^{-1} (b) and 3 µl mg^{-1} (c). The electrolyte used here is 1 M LiTFSI/DOL + DME + 4 wt% $LiNO_3$.

The team further uses organosulfide as the additive in the electrolyte to push energy density to a much higher level. As shown in Figure 76a, at an E/S ratio of 5 µl mg^{-1}, the FSS electrode with a sulfur mass loading of ~ 11.7 mg cm^{-2} exhibits a high energy density of 412 Wh kg^{-1} and good cycling stability for 100 cycles. When the E/S ratio is further reduced to 3.5 µl mg^{-1} (Figure 76b), the FSS electrode shows an initial energy density of 432 Wh kg^{-1}; the highest energy density can reach 460 Wh kg^{-1}.

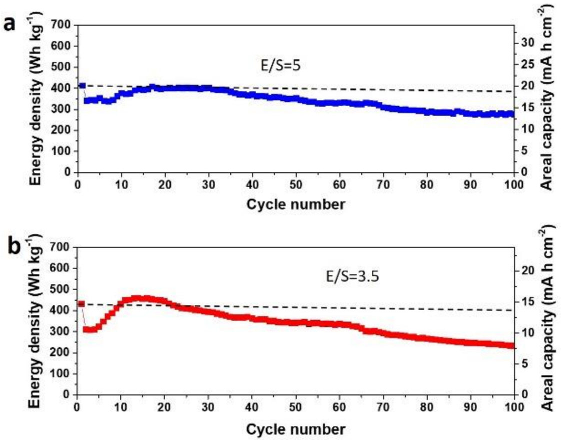

Figure 76. (a) Cycling performance of the functional porous sponge sulfur (FSS) electrodes with the sulfur mass loading of ~ 11.67 mg cm^{-2} at the E/S ratios of 5 µl mg^{-1}. (b) Cycling performance of the FSS electrodes with the sulfur mass loading of ~ 8.3 mg cm^{-2} at the E/S ratios of 3.5 µl mg^{-1}.

Patents/Publications/Presentations

The project has no patents, publications, or presentations to report this quarter.

Task 5.6 – New Electrolytes for Lithium-Sulfur Battery
(Gao Liu, Lawrence Berkeley National Laboratory)

Project Objective. The project objective is to develop new electrolytes, additives, and electrode compositions for Li-S battery with high ion-conductivity, stable toward polysulfide and promoting the polysulfide affiliation with the electrode substrate to prevent polysulfide dissolution.

Project Impact. This work will address the high cost and low energy density of the Li-ion rechargeable batteries. The emerging Li-S batteries could be both high energy density and low cost. This project enables the applications of the low-cost, abundant sulfur element as a major chemical component for electrical energy storage. This project will develop new approaches for electrolytes and electrode compositions of Li-S rechargeable batteries.

Approach. This project aims to develop new electrolytes and additives for Li-S battery. The properties of the ideal electrolyte for sulfur electrode would be high ion conductivity, stable towards polysulfide, and promoting the polysulfide affiliation with the electrode substrate to prevent polysulfide dissolution. The project is designed to first understand the electrode substrate interaction with the polysulfides in different electrolytes. This will lead to better understandings of the polysulfide nucleation and precipitation mechanisms in common electrolytes. The second stage of the project will focus on chemically modifying the structures of the solvent and salt electrolyte molecules to increase electrolyte stability and ionic conductivity and to prevent polysulfide dissolution and promote polysulfides precipitation.

Out-Year Goals. The team will also investigate the contribution of Li-metal electrodes to the overall Li-S battery performance and develop methods to stabilize Li-metal surface.

Collaborations. This project collaborates with Dr. J. Guo and Dr. W. Yang (ALS/LBNL), Prof. A. Minor (National Center for Electron Microscopy at LBNL/UC Berkeley), Dr. L-W. Wang (LBNL), and Prof. P. Balbuena, TAMU.

Milestones

1. Identify the baseline electrolyte compositions and electrode composition and configuration for Li-S study. (Q1, FY 2019; Completed)
2. Develop polymer binders with different affiliation functional groups with polysulfides, and use baseline electrolytes to investigate dissolution and precipitation of polysulfides. (Q2, FY 2019; Completed)
3. Develop *in situ* cells for synchrotron analysis with improved spatial resolution. (Q3, FY 2019; Completed)
4. Formulate one composition of the new electrolyte for Li-S battery and test its performance. (Q4, FY 2019; Completed)

Progress Report

This quarter, research focused on new electrolyte and additive development and testing for Li-S rechargeable battery applications. Li-S batteries face a few challenges common to other lithium batteries, such as lithium dendrite formation and volume expansion; however, the most critical obstacle for Li-S battery application is the unique polysulfide problem that arises from the electrochemistry between lithium and sulfur. The Li-S reaction ($16Li + S8 \leftrightarrow 8Li_2S$) is a rather complicated step-wise process involving various polysulfide intermediates, and the detailed mechanism is subject to investigation. Generally, the solid-phase S8 would first reduce to soluble lithium polysulfides Li_2S_x ($4 \leq x \leq 8$), which would then further reduce to Li_2S_2 and Li_2S. The readily soluble polysulfide intermediates not only cause severe loss of active materials, but also shuttle back and forth between cathode and anode, leading to undesired polysulfide redox reaction cycle, which is responsible for fast self-discharge and low CE. This phenomenon is known as the ‘shuttling effect’ of Li-S batteries.

The new electrolyte system developed in this project can successfully prevent lithium polysulfide dissolution into the electrolyte. The cyclable gravimetric capacity is around 800 mAh/g-S material. The cycling CE is very high, as shown in Figure 77.

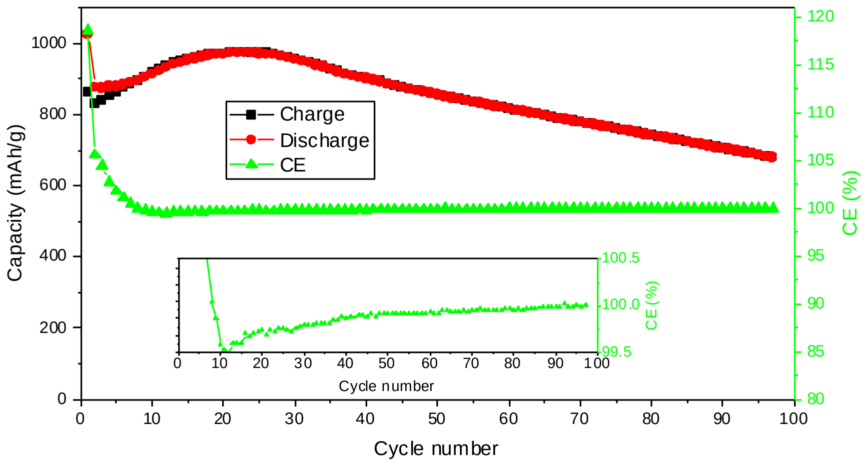

Figure 77. Cycling performance of a sulfur electrode against a Li-metal counter electrode in the new electrode system.

Patents/Publications/Presentations

Patent

- Liu, G. “New Lithium-Sulfur Rechargeable Battery Electrolyte and Additives.” Patent disclosure submitted to LBNL; LBNL Doc# 2019-169, 2019.

TASK 6 – AIR ELECTRODES / ELECTROLYTES

Summary and Highlights

High-density energy storage systems are critical for EVs required by the EV Everywhere Grand Challenge. Conventional Li-ion batteries still cannot fully satisfy the ever-increasing needs because of their limited energy density, high cost, and safety concerns. As an alternative, the rechargeable lithium-oxygen (Li-O_2) battery has potential to be used for long-range EVs. The practical energy density of a Li-O_2 battery is expected to be ~ 800 Wh kg^{-1}. The advantages of Li-O_2 batteries come from their open structure; that is, they can absorb the active cathode material (oxygen) from the surrounding environment instead of carrying it within the batteries. However, the open structure of Li-O_2 batteries also leads to several disadvantages. The energy density of Li-O_2 batteries will be much lower if oxygen must be provided by an onboard container. Although significant progress has been made in recent years on fundamental properties of Li-O_2 batteries, research in this field is still in an early stage, with many barriers to be overcome before practical applications. These barriers include:

- Instability of electrolytes—The superoxide species generated during discharge or O_2 reduction process is highly reactive with electrolyte and other components in the battery. Electrolyte decomposition during charge or O_2 evolution process is also significant due to high over-potentials.
- Instability of air electrode (dominated by carbonaceous materials) and other battery components (such as separators and binders) during charge/discharge processes in an O-rich environment.
- Corrosion of Li-metal anode in an electrolyte saturated with oxygen.
- Low energy efficiency associated with large over-potential and poor cyclability of Li-O_2 batteries.
- Low power rate capability due to electrode blocking by the reaction products.
- Absence of a low-cost, high-efficiency oxygen supply system (such as oxygen selective membrane).

The main goal of this Task is to provide a better understanding on the fundamental reaction mechanisms of Li-O_2 batteries and identify the required components (especially electrolytes and electrodes) for stable operation of Li-O_2 batteries. This task will investigate several new approaches to improve stability of Li-metal anode in Li-O_2 batteries:

- Li-metal anodes will be protected using two approaches: (1) *in situ* formation of a stable SEI layer before Li-O_2 cell operation through various electrolyte formulations and treatment protocols, and (2) *ex situ* formation of stable inorganic/polymeric hybrid electrolyte layers through dip-coating or tape-casting method to coat the inorganic/polymeric hybrid electrolyte layer on Li-metal surface.
- A joint theoretical/experimental approach for design and discovery of new cathode and electrolyte materials will act synergistically to reduce charge overpotentials and increase cycle life. Synthesis methods, in combination with design principles developed from computations, will be used to make new cathode architectures. Computational studies will be used to help understand decomposition mechanisms of electrolytes and how to design electrolytes with improved stability.
- A new cathode will be developed based on high-efficiency catalyst such as two-dimensional TM dichalcogenides. These cathode materials will be combined with new electrolyte blends and additives that work in synergy to reduce charge potentials and increase stability of the Li-air system.

State-of-the-art characterization techniques and computational methodologies will be used to understand charge and discharge chemistries. Success of this Task will establish a solid foundation for further development of Li-O_2 batteries toward practical applications for long-range EVs. The fundamental understanding and breakthrough in Li-O_2 batteries may also provide insight on improving performance of Li-S batteries and other energy storage systems based on chemical conversion process.

Highlights. The Task highlights for this quarter are as follows:

- The ANL group (Amine/Curtiss) found that defect sites on conductive carbon supports can be leveraged as deposition sites for palladium films, serving the dual purpose of mitigating carbon degradation while reducing the oxygen evolution reaction (OER) over-potential to ~ 0.2 V for a Li-O_2 battery. Compared with pristine carbon electrodes, the palladium-deposited carbon also exhibited higher cycle stability.
- The ANL / University of Illinois at Chicago group (Curtiss/Ngo/Salehi-Khojin) shows that use of InI_3 as an additive to the appropriate electrolyte can provide both an excellent Li-anode protection coating as well as a redox mediator to reduce the charge over-potential that enables long cycle life of over 200 cycles for a Li-air battery.
- The PNNL group (Zhang/Wu) demonstrated that the combination of the optimized pre-treat process and a lithium anode protected by Nafion-Al_2O_3 composite layer (NCL) can further enhance cycle life and reduce over-voltage of Li-O_2 batteries.

Task 6.1 – Rechargeable Lithium-Air Batteries
(Ji-Guang Zhang and Wu Xu, Pacific Northwest National Laboratory)

Project Objective. The objective of this project is to develop rechargeable lithium-oxygen (Li-O_2) batteries with long-term cycling stability. In FY 2019, the team will pay more attention to lithium anode stabilization and building a more stable Li-O_2 battery based on the protected lithium anode and optimized air electrodes to develop practical Li-O_2 batteries with stable, long-term cycling capability.

Project Impact. Li-air batteries have a theoretical specific energy more than five times that of state-of-the-art Li-ion batteries and are potential candidates for use in next-generation, long-range EVs. Unfortunately, the poor cycling stability and low CE of Li-air batteries have prevented their practical application. This work will explore well-protected Li-metal anodes, new electrolytes, and high-loading air electrodes that could lead to long cyclability and high CE in high-energy Li-air batteries that can be used in the next-generation EVs required by the EV Everywhere Grand Challenge.

Approach. Li-metal anodes will be protected using highly elastic and stable protective composite layers and gel-polymer crosslinked electrolytes. These membranes will be prepared through dip-coating or tape-casting method to coat the inorganic/polymeric hybrid electrolyte layers. Stable host structures for lithium metal will also be investigated to stabilize Li-metal anode in oxygen atmosphere. The electrochemical performances of Li-O_2 batteries using the protected Li-metal anodes and the previously developed carbon/catalyst composite air electrodes based on carbon nanotubes (CNTs) and TM oxides such as RuO_2 will be evaluated. The lithium anodes, air electrodes, and Li-O_2 cells at different stages of cycling (including as-prepared, after discharge, after recharge, and after cycling) will be analyzed by microscopy and spectroscopy techniques such as SEM, EDX, TEM, XRD, and XPS.

Out-Year-Goals. The long-term goal is to enable rechargeable Li-air batteries with a specific energy of 800 Wh/kg at cell level, 1000 deep-discharge cycles, improved abuse tolerance, and less than 20% capacity fade over a 10-year period to accelerate commercialization of long-range EVs.

Collaborations. This project collaborates with C. Wang of PNNL on characterization of cycled air electrodes by TEM/SEM.

Milestones

1. Develop highly elastic and stable protective composite layers for lithium anode in Li-O_2 batteries. (Q1, FY 2019; Completed)
2. Protect Li-metal anode by using gel-polymer crosslinked electrolytes Li-O_2 batteries. (Q2, FY 2019; Completed)
3. Develop stable host structure to protect lithium anode in oxygen rich environment. (Q3, FY 2019; Completed)
4. Complete evaluation of cycling performance of Li-O_2 batteries with protected Li-metal anodes and optimized air electrodes. (Q4, FY 2019; Completed)

Progress Report

This quarter, the team evaluated cycling performance of Li-O_2 batteries with protected Li-metal anodes and optimized air electrodes. The Nafion-Al_2O_3 composite layer (NCL) was used to coat on Li/C composite anode surface, and the optimization of RuO_2/CNTs air electrodes was conducted by *in situ* electrochemical pre-discharging and pre-charging (D0.8V-C4.3V, see Figure 78a) process of the cells in an argon atmosphere. After pretreatment, large particles of RuO_2, as shown in Figure 78b-c, were clearly redistributed and formed ultrafine RuO_2 catalyst, as shown in Figure 78d-e, which can largely improve efficiency of catalytic effect and leads to reduced over-voltage, as shown in the subsequent evaluation in oxygen environment.

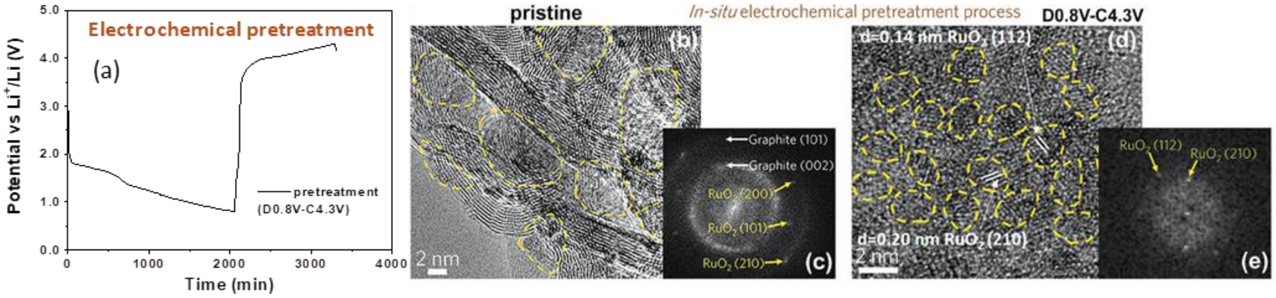

Figure 78. (a) Voltage profiles of cells for electrochemical pretreatment (D0.8–C4.3 V) in argon atmosphere. Transmission electron microscopy image and corresponding fast Fourier transform pattern of pristine RuO_2 / carbon nanotubes electrode (b-c) and pre-treated electrode (d-e).

After the *in situ* electrochemical pretreatment, the cycling performance of Li-O_2 cells was systematically investigated at 0.1 mA cm^{-2} under a capacity-limited protocol of 1000 mAh g^{-1} based on total mass of RuO_2 and CNTs (Figure 79). The untreated RuO_2/CNT air electrode was also evaluated as a comparison. The voltage profiles of the Li-O_2 cells clearly demonstrate that pretreatment enhanced the catalytic effect of RuO_2 on the air electrode, which induced lower charge potential. In addition, more stable cycle performance of Li-O_2 cells can be observed with pretreatment. The team noticed that the cycle life of such Li-O_2 cells was still limited, although the optimized catalytic air electrode and the protected Li/C anode were adapted; this is due to inability to suppress all electrolyte side reactions occurring at the anode and the air electrode interfaces. To further improve performance of Li-O_2 cells, electrolytes with more stable organic solvents against highly reactive reduced oxygen species are needed. In other words, development of stable electrolytes is a key factor for development of Li-O_2 batteries with long cycle life. This will be the focus of the project's new effort to improve performance of Li-O_2 and Li-air batteries.

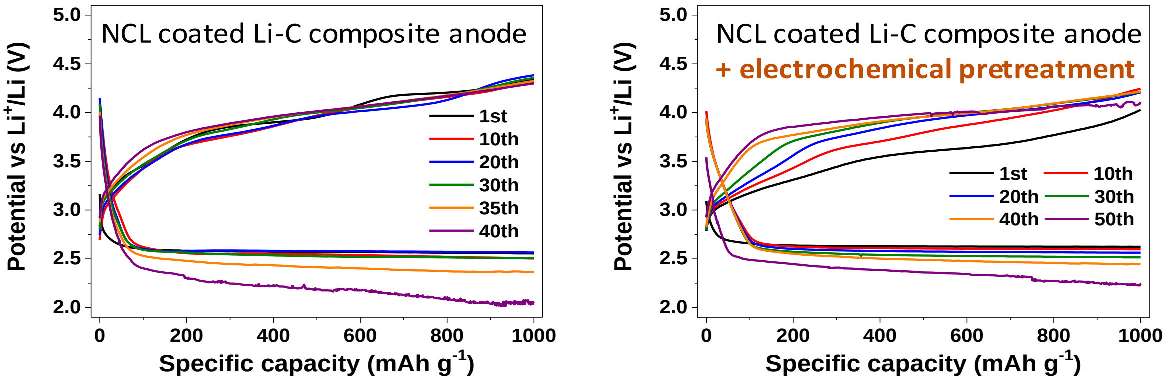

Figure 79. Cyclic stability tests of Li-O_2 cells composed of RuO_2 / carbon nanotubes air-cathodes, 1 M LiTf-TEGDME electrolyte, and protected Li/C composite anode at 25°C at a current density of 0.1 mA cm^{-2} under a capacity limited protocol of 1,000 mAh g^{-1} with or without electrochemical pretreatment.

Patents/Publications/Presentations

The project has no patents, publications, or presentations to report this quarter.

Task 6.2 – Lithium-Air Batteries
(Khalil Amine and Larry A. Curtiss, Argonne National Laboratory)

Project Objective. This project will develop new cathode materials and electrolytes for Li-air batteries for long cycle life, high capacity, and high efficiency. The goal is to obtain critical insight that will provide information on the charge and discharge processes in Li-air batteries to enable new advances to be made in their performance. This will be done using state-of-the-art characterization techniques combined with state-of-the-art computational methodologies to understand and design new materials and electrolytes for Li-air batteries.

Project Impact. The instability of current nonaqueous electrolytes and degradation of cathode materials limits performance of Li-air batteries. The project impact will be to develop new electrolytes and cathode materials that are stable and can increase energy density of electrical energy storage systems based on lithium.

Approach. The project is using a joint theoretical/experimental approach for design and discovery of new cathode and electrolyte materials that act synergistically to reduce charge overpotentials and increase cycle life. Synthesis methods, in combination with design principles developed from computations, are used to make new cathode architectures. Computational studies are used to help understand decomposition mechanisms of electrolytes and how to design electrolytes with improved stability. The new cathodes and electrolytes are tested in Li-O_2 cells. Characterization, along with theory, is used to understand the performance of materials used in the cell and make improved materials.

Out-Year Goals. The out-year goals are to find catalysts that promote discharge product morphologies that reduce charge potentials and find electrolytes for long cycle life through testing and design.

Collaborations. This project engages in collaboration with Prof. K. C. Lau (UC at Norridge), Prof. Y. Wu (Ohio State University), Dr. D. Zhai (China), and R. Shahbazian-Yassar (UIC).

Milestones

1. Synthesis and testing of low-cost TM catalysts that give low charge potentials in Li-O_2 batteries. (Q1, FY 2019; Completed)
2. Investigations of the role of mass and charge transport in discharge and charge reactions in Li-O_2 batteries. (Q2, FY 2019; Completed)
3. Characterization of electronic conductivity in discharge products via electrochemical impedance measurements. (Q3, FY 2019; Completed)
4. Investigation of suppression of electrolyte side reactions using thin-film coatings of carbon cathodes. (Q4, FY 2019, Completed)

Progress Report

High charge overpotential and poor cycle stability are the limiting factors in nonaqueous lithium-oxygen (Li-O_2) batteries, causing poor round-trip efficiency and failure of the cell device. Many types of electrocatalysts have been explored to facilitate the OER. However, even with the application of OER catalysts, it remains difficult to achieve stable operation, as the carbon electrode (especially on the defects) easily undergoes side reactions with the electrolyte and reactive intermediates. To achieve high stability and round-trip efficiency, rational design of OER catalysts is required. The team has employed a wet impregnation chemistry method to form a very thin layer of palladium nanoparticles on the surface of carbon, which largely suppresses the electrolyte side reactions through a selective coating on the carbon defect sites. Simultaneously, the palladium films serve as an electrocatalyst enabling decomposition of lithium peroxide at a very low overpotential. This rational design of the cathode catalyst is found to improve overall cell efficiency and extends the cycle life of the lithium-oxygen battery.

The as-prepared Pd-coated carbon sample was tested in a Li-O_2 cell, together with the pristine carbon as the control, as shown in Figure 80. Figure 80a shows the voltage profiles of a single discharge and charge cycle for the two cathodes with capacity limited to 1000 mAh/g at a current density of 50 μA/cm^2. The charge potential of pristine carbon cathode (4.2 V) was found to be substantially higher than that of the Pd/C sample (3.2 V), indicating that the coated palladium film served as a good OER catalyst to facilitate decomposition of the Li_2O_2. Cycle performance of the pristine carbon cathode is shown in Figure 80b; the first-cycle charge potential is 4.2 V and gradually increases with cycle number. After only 15 cycles, the cell fails, with the charge voltage exceeding the 5.0 V cut off (Figure 80d). The increase in overpotential is likely due to accumulation of products from the side-reaction occurring on the carbon defect sites. In contrast, the Pd/C cathode shows a low first-cycle charge potential of 3.2 V (Figure 80c) with good cyclability. The cell fails at about 50 cycle (Figure 80d). In the case of Pd/C cathode, the discharge product of Li-O_2 batteries is confirmed to be largely Li_2O_2, according to SEM, Raman spectroscopy, and high-energy XRD results, while the discharge product on the pristine carbon contained Li_2CO_3 and LiOH in addition to Li_2O_2.

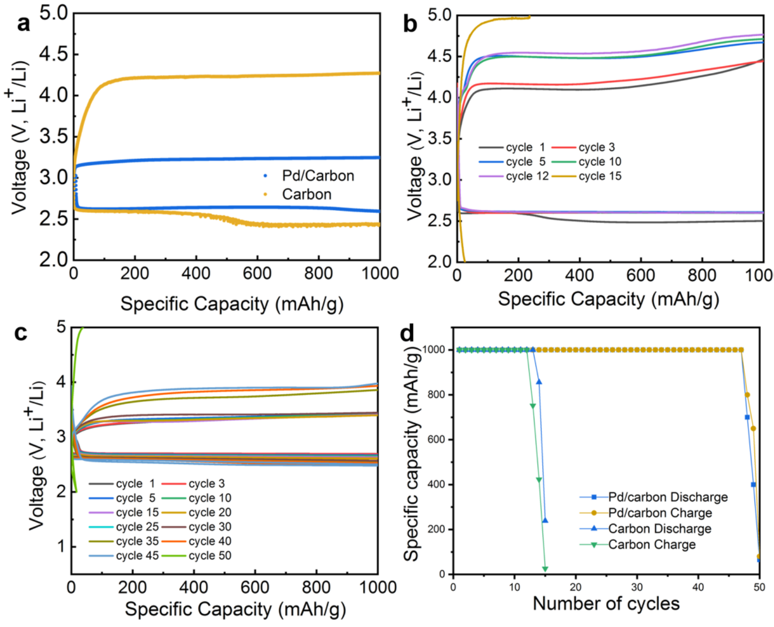

Figure 80. (a) Voltage profiles of the cells (to 1000 mAh/g) based on carbon and Pd/C air electrodes. (b) Voltage profile during discharge-charge of cells (to 1000 mAh/g) based on carbon. (c) Voltage profile during discharge-charge of cells (to 1000 mAh/g) based on Pd/C. (d) Cyclability of cells based on under capacity-controlled mode.

This work demonstrates that the defect sites on conductive carbon supports can be leveraged as deposition sites for palladium films, serving the dual purpose of mitigating carbon degradation while reducing the OER overpotential to ~ 0.2 V. Compared with pristine carbon electrodes, the Pd-deposited carbon exhibited fewer side reactions, lowered overpotentials, and ultimately higher cycle stability. This work provides a new method for achieving high-performance Li-O_2 batteries and will be used with new electrolytes for longer cycle life in these batteries.

Patents/Publications/Presentations

Publication

- Halder, A., A. T. Ngo, X. Luo, H-H. Wang, J. G. Wen, P. Abbasi, M. Asadi, C. Zhang, D. Miller, D. Zhang, J. Lu, P. C. Redfern, K. C. Lau, R. Amine, R. S. Assary, Y. J. Lee, A. Salehi-Khojin, S. Vajda, K. Amine, and L. A. Curtiss. "*In Situ* Formed Ir_3Li Nanoparticles as Active Cathode Material in Li-Oxygen Batteries." Submitted.

Presentation

- ACS Fall National Meeting, Advances in Fundamental Research for Energy Storage Beyond Lithium-Ion Symposium, San Diego, California (August 2019): "Insights into Li-O_2 Electrochemistry for Energy Storage from Computational Studies."

Task 6.3 – Lithium Oxygen Battery Design and Predictions
(Larry A. Curtiss/Anh Ngo, Argonne National Laboratory; Amin Salehi-Khojin, University of Illinois at Chicago)

Project Objective. The objective of this work is to develop new materials for Li-O_2 batteries that give longer cycle life and improved efficiencies in an air environment. New electrolyte blends and additives will be investigated the can reduce clogging and at the same time promote the cathode functionality needed to reduce charge overpotentials. New cathode and anode materials will be investigated that can work in conjunction with the electrolytes to improve cycle life in the presence of air components.

Project Impact. Li-air batteries are considered as a potential alternative to Li-ion batteries for transportation applications due to their high theoretical specific energy. The major issues with the existing Li-O_2 systems include degradation of the anode electrode, reactions with air components, clogging of the cathode, and electrolyte instability. Thus, this project is using a comprehensive approach to improve cycle life and efficiency through development of new materials for electrodes, anodes, and electrolytes that work in synergy.

Approach. The experimental strategy is to use cathode materials based on 2D TM dichalcogenides (TMDCs) that the team has found to be among the best oxygen reduction and evolution catalysts. These cathode materials will be combined with new electrolyte blends and additives that work in synergy to reduce charge potentials and increase stability of the Li-air system. DFT and AIMD simulations are used to gain insight at the electronic structure level of theory of the electrolyte structure and function both in the bulk and at interfaces with the cathode, anode, and discharge product. Classical MD is used to obtain understanding at longer length and time scales of processes occurring in the electrolyte and growth mechanisms of discharge products. The team will also utilize a high-throughput screening strategy based on experiment and theory to develop a large database of properties and outcomes of electrolyte combinations that can be analyzed using machine learning to predict electrolytes and additives that will have the best performance.

Out-Year Goals. The out-year goals are to find electrolytes that give high capacities and long cycle life in an air atmosphere using high throughput screening.

Collaborations. This project engages in collaboration with R. Assary (ANL), B. Narayanan (University of Louisville), J. G. Wen (UIC), and R. Klie (UIC).

Milestones

1. Investigate possible lithium anode protection additives and redox mediators (RMs) for electrolyte blends that can work with MoS_2 cathode to extend cycle life and reduce charge overpotentials of Li-O_2 cells. (Q1, FY 2019; Completed)

2. Assess electrolyte blends and additives that will work in concert with MoS_2 cathode in Li-O_2 cells. (Q2, FY 2019; Completed)

3. Evaluate, using experiment and theory, properties of RMs for electrolyte blends to lower charge potentials for increased efficiency of Li-O_2 cells. (Q3, FY 2019; Completed)

4. Develop first-generation electrolytes that work in concert with MoS_2 cathode for increased CE of Li-O_2 cells running in a realistic air environment. (Q4, FY 2019; Completed)

Progress Report

$Li-O_2$ batteries are considered as an advanced energy storage system that could provide much higher specific energy than Li-ion batteries for electrical transportation. However, there are major issues with existing $Li-O_2$ systems, including degradation of the anode electrode, clogging of the cathode, electrolyte instability, and high charge overpotential. The team has demonstrated a $Li-O_2$ battery that operates up to 700 cycles in an air-like atmosphere [*Nature* 555 (2018): 502], yet it has a high charge potential (> 4.0 V versus Li/Li^+) for decomposition of discharge product (that is, Li_2O_2).

The team has performed extensive study on a wide range of RMs for decomposition of Li_2O_2 products to reduce charge potential. Results indicate that iodide-based RMs are efficient in terms of redox potential and reversibility. However, a problem arises after oxidation of iodide to triiodide on the cathode surface during the charge process where soluble triiodide ions diffuse toward the lithium anode. This results in a shuttle effect. To resolve this issue, this quarter the team used InI_3 as RM, in which iodide decreases charge overpotential to ~ 3.4. Meanwhile, indium reacts with the surface of the Li-metal anode to create a barrier layer that prevents redox shuttling of LiI_3. The team believes that this barrier is a Li-In alloy that is formed by reaction of the InI_3 with the lithium metal on the basis of XPS and computational calculations. This barrier seems to effectively protect the anode surface against both corrosion and redox shuttling.

In this work, the team has explored several electrolyte combinations with use of the InI_3. They found that the best battery performance is obtained using molybdenum disulfide cathode in a hybrid electrolyte of 10% ionic liquid (EMIM BF_4) and 90% DMSO containing 0.025 M of InI_3 and 0.1 M LiTFSI. This optimal composition enabled the team to operate the battery in a dry air environment with a capacity of 1Ah/g at high rate of 1A/g up to 475 cycles. They obtained a polarization gap of less than ~ 0.7 for more than 200 cycles (Figure 81). The average discharge and charge potentials for 200 cycles are 2.75 V and 3.5 V, respectively. Also, capacity loss of the battery is less than 10% after more than 200 cycles. Different characterization techniques have been used to show the discharge product; all of them verify the presence of Li_2O_2 including Raman spectra, XRD, XPS, and high-resolution TEM (HRTEM). Figure 82 shows the Raman and XRD characterizations on the cathode side. Also, XPS characterization shows formation of Li-In alloy on the anode surface.

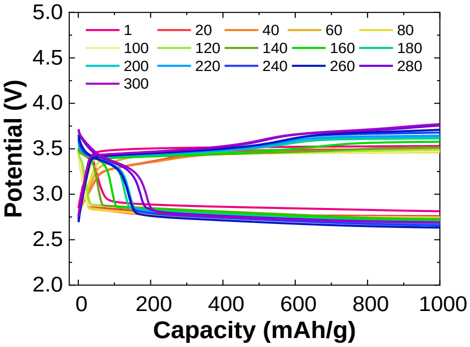

Figure 81. Voltage profiles for Li-air battery.

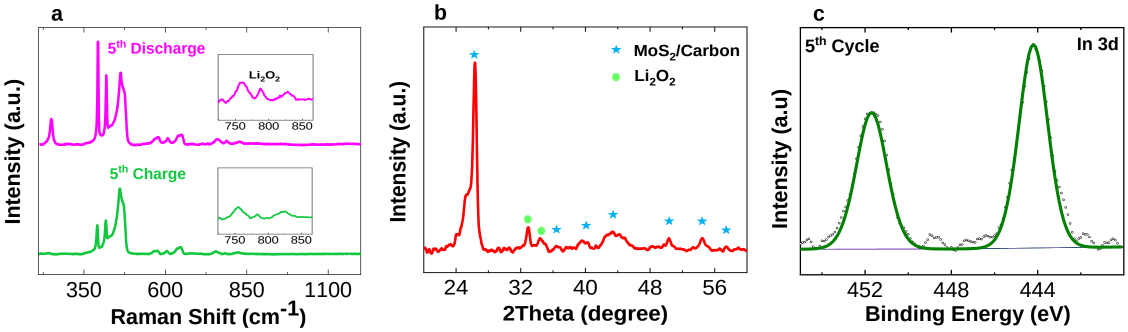

Figure 82. (a) Raman characteristics of the cathode sample and (b) X-ray diffraction pattern of discharged cathode show the presence of Li_2O_2 discharge product after the fifth cycle. (c) X-ray photoelectron spectroscopy of the lithium anode after the fifth cycle that shows the presence of In^0.

Often, when LiI is used as RM, capacity loss occurs due to reduction of triiodide to iodide (I_3^-/I^-) during discharge process, which is unfavorable. This capacity loss is significantly suppressed in this new system because of having indium and the correct amount of salt and solvent. However, this is not the case using LiI RM in LiTFSI and DMSO/IL electrolyte, confirming the importance of the indium presence along with the iodide, that is, InI_3 The exact nature of the protective layer is still being investigated. Thus, these results demonstrate that the use of a redox mediator, the appropriate electrolyte, and an electrolyte component that creates an *in situ* lithium anode protection can enable long cycle life in a Li-air battery with low charge potentials.

Patents/Publications/Presentations

Publication

- A. Ahmadiparidari, M. Asadi, R. E. Warburton, L. Majidi, A. Chammani, J. R. Jokisaari, S. Rastegar, Z. Hemmat, B. Sayahpour, R. S. Assary, B. Narayanan, P. Abbasi, P. C. Redfern, A. Ngo, M. Vörös, J. Greeley, R. Klie, L. A. Curtiss, and A. Salehi-Khojin. "Long Cycle Life Lithium-CO_2 Battery with Carbon Neutrality." *Advanced Materials* (2019):1902518. doi: 10.1002/adma.201902518.

Presentation

- ACS Fall National Meeting, Advances in Fundamental Research for Energy Storage Beyond Li-Ion Symposium, San Diego, California (August 2019): "Insights into Li-O_2 Electrochemistry for Energy Storage from Computational Studies."

TASK 7 –SODIUM-ION BATTERIES

Summary

During FY 2019, the BMR will add five new projects, including several in the area of Na-ion batteries. Progress on four of these new projects is described in this report; the fifth project will begin reporting soon. The Na-ion battery will require investigations to identify optimal electrode materials, electrolytes, separators, and binders to reach its full potential. The BMR program will therefore have a limited effort directed toward identifying Na-ion battery materials that have potential value for vehicle applications. More detailed information on this BMR Task will be provided in upcoming reports.

Highlights. The highlights for this quarter are as follows:

- Synchrotron-based XRD studies of a new P2-type $Na_{0.72}[Li_{0.24}Mn_{0.76}]O_2$ cathode material for Na-ion batteries have been completed. The phase evolution exhibited a reverse manner during charge-discharge process, providing evidence for the reversible structural changes and stability of this cathode material during cycling.
- The binder, electrolyte solvent, and salt have a profound effect on the electrochemical performance for Pb-PbO-C composite anodes for Na-ion cells. TEGDME and NaTFSI turn out to be the best combination for this material, yielding ~ 400 mAh/g capacity at current rates approaching 100 mA/g.
- Dehydrated sodium nonatitanate exhibits structural complexity and some tunnel characteristics.
- Sodium nonatitanate dehydrated at 500°C gave the highest capacity (nearly 200 mAh/g) on the second cycle in sodium half cells.
- An optimized electrolyte has been identified that has enabled hard carbon (HC) anode to have a capacity of 280 mAh g^{-1} (0.5 C) and more than 80% capacity retention after 250 cycles. The initial CE of Na||HC cell is 87.71% and long-term cycling CE is > 99.9.

Task 7.1 – Exploratory Studies of Novel Sodium-Ion Battery Systems (Xiao-Qing Yang and Enyuan Hu, Brookhaven National Laboratory)

Project Objective. The objective of this project is to develop new advanced *in situ* material characterization techniques and apply these techniques to explore the potentials, challenges, and feasibility of new rechargeable battery systems beyond the Li-ion batteries, namely the Na-ion battery systems for EVs, such as PHEV and BEV. To meet the challenges of powering PHEVs and BEVs, new rechargeable battery systems with high energy and power density, low cost, good abuse tolerance, and long calendar and cycle life need to be developed. This project will use the synchrotron based *in situ* X-ray diagnostic tools, combined with TEM and STEM imaging techniques developed at BNL, to evaluate the new materials and redox couples to obtain fundamental understanding of the reaction mechanisms of these materials aiming for improvement of and guidance for new material and new technology development regarding Na-ion battery systems.

Project Impact. In the VTO MYPP, the goals for battery were described: "Specifically, lower-cost, abuse-tolerant batteries with higher energy density, higher power, better low-temperature operation, and longer lifetimes are needed for the development of the next-generation of HEVs, PHEVs, and EVs." The knowledge learned from diagnostic studies and collaborations with U. S. industries through this project will help U. S. research institutions and industries to develop new materials and processes for a new generation of rechargeable battery systems, namely Na-ion battery system, in their efforts to reach these VTO goals.

Approach. This project will use the synchrotron-based *in situ* X-ray diagnostic tools developed at BNL to evaluate the new materials and redox couples to enable a fundamental understanding of the mechanisms governing performance of these materials and provide guidance for new material and new technology development regarding Na-ion battery systems.

Out-Year Goals. Complete the synchrotron based *in situ* XRD and *ex situ* absorption (XAS) studies of low-cost P2-type iron-based cathode materials ($Na_{0.7}[Cu_{0.15}Fe_{0.3}Mn_{0.55}]O_2$) as new cathode materials for Na-ion batteries during charge-discharge cycling.

Collaborations. The BNL team has been closely working with top scientists on new material synthesis at ANL, LBNL, and PNNL and with U. S. industrial collaborators at General Motors and Johnson Controls, as well as with international collaborators.

Milestones

1. Complete *in situ* XRD studies of new low-cost P2-type iron based cathode materials ($Na_{0.7}[Cu_{0.15}Fe_{0.3}Mn_{0.55}]O_2$) for Na-ion batteries during charge-discharge cycling. (Q1, December 2018; Completed)
2. Complete the synchrotron-based XAS studies and XAS analysis of $Na_{0.7}[Cu_{0.15}Fe_{0.3}Mn_{0.55}]O_2$ and $Na_{0.7}[Cu_{0.2}Fe_{0.2}Mn_{0.6}]O_2$ electrodes at different SOCs at iron K-edge, copper K-edge, and manganese K-edge. (Q2, March 2019; Completed)
3. Complete the sXAS studies of $Na_{0.7}[Cu_{0.15}Fe_{0.3}Mn_{0.55}]O_2$ and $Na_{0.7}[Cu_{0.2}Fe_{0.2}Mn_{0.6}]O_2$ electrodes at different SOCs at iron L-edge, copper L-edge, and oxygen K-edge. (Q3, June 2019; Completed)
4. Complete *in situ* XRD studies of new stabilized global P2 phase cathode material ($Na_{0.72}[Li_{0.24}Mn_{0.76}]O_2$) for Na-ion batteries during charge-discharge cycling. (Q4, September 2019; Completed)

Progress Report

This quarter, the fourth FY 2019 milestone was completed. BNL has been focused on synchrotron-based XRD studies of a new P2-type $Na_{0.72}[Li_{0.24}Mn_{0.76}]O_2$ cathode material for Na-ion batteries. This cathode material exhibits exceptionally high initial charge capacity of about 210 mAh/g (0.72 Na) based on a pure anionic redox reaction (ARR). Surprisingly, global P2 structure can be maintained with minimal volume change (1.35%) on complete removal of Na^+ ions. This is due to the reduced Coulombic repulsion associated with ARR and consequent suppression of the phase transition, as observed in other P2 materials. The team revealed for the first time that ARR has the functionality of stabilizing the structure, in addition to its role in increasing its already known capacity. This would pave the way for the further improvement of high-energy-density Na-ion batteries.

To investigate the structural evolution of $Na_{0.72}[Li_{0.24}Mn_{0.76}]O_2$ upon Na^+ deintercalation and intercalation, the team performed *in situ* XRD measurements, the results of which are displayed in Figure 83. It could be observed that on initial sodium deintercalation process, the (002) peak first shifts to a lower angle and then slightly shifts to a higher angle, while (100), (102), and (104) peaks continuously shift to higher angles. No notable sign of the formation of O2 or OP4 phase (or Z phase), as reported in $Na_{0.67}[Ni_{0.33}Mn_{0.67}]O_2$ or $Na_x[Fe_{0.5}Mn_{0.5}]O_2$, can be observed. The phase evolution proceeds in a reverse manner in general over the discharge process, and no new peak can be observed. This result is also confirmed by the *ex situ* XRD analysis.

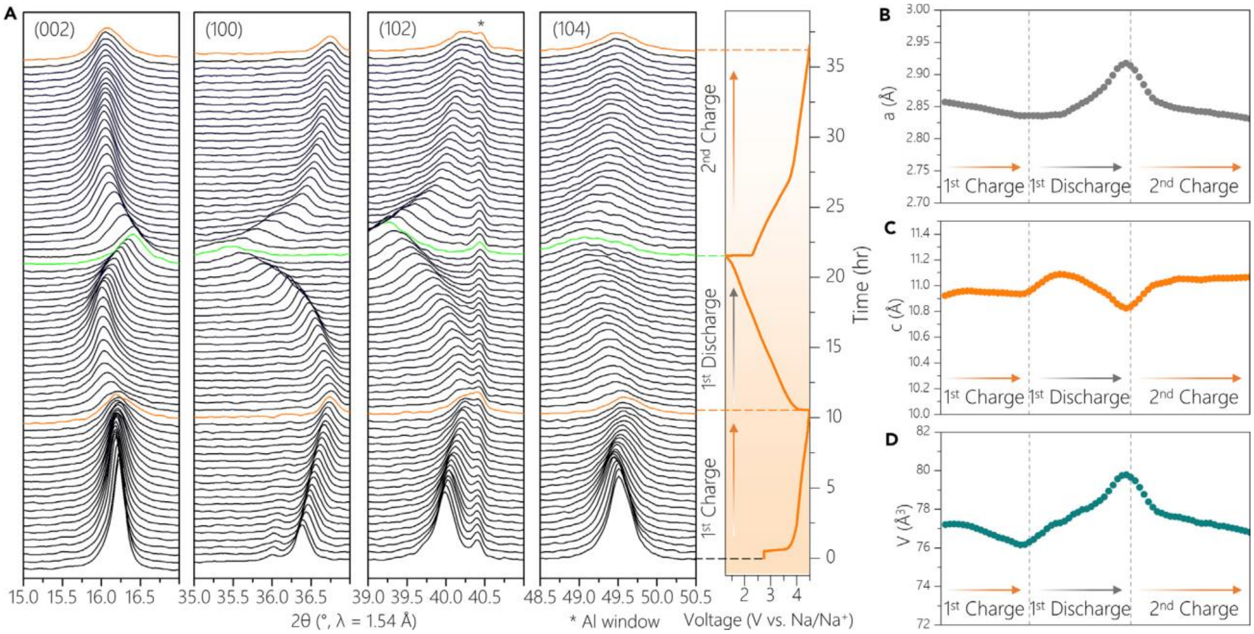

Figure 83. Crystal Structural Evolution of $Na_{0.72}[Li_{0.24}Mn_{0.76}]O_2$ electrodes. (a) *In situ* X-ray diffraction patterns collected during the first charge/discharge and the second charge of the $Na_{0.72}[Li_{0.24}Mn_{0.76}]O_2$. (b-d) Evolution of the lattice parameters during the charge/discharge process: a axis (b); c axis (c); and unit cell volume (d).

Patents/Publications/Presentations

Publication

- Cao, M-H., Z. Shadike, S-M. Bak, T. Wang, E. Hu, S. Ehrlich, Y-N. Zhou,* X-Q. Yang,* and Z-W. Fu.* “Sodium Storage Property and Mechanism of $NaCr_{1/4}Fe_{1/4}Ni_{1/4}Ti_{1/4}O_2$ Cathode at Various Cut-Off Voltages.” *Energy Storage Materials*. doi: 10.1016/j.ensm.2019.07.022, Publication Date (Web): July 22, 2019.

Task 7.2 – Development of a High-Energy Sodium-Ion Battery with Long Life (Chris Johnson and Khalil Amine, Argonne National Laboratory)

Project Objective. The project objective is to develop a high-energy Na-ion battery with long life. Moreover, the battery chemistry should utilize low-cost materials. The energy density target is 200 Wh/kg and/or 500 Wh/L, wherein the anode and cathode capacity targets are 600 $mAhg^{-1}$ and 200 $mAhg^{-1}$, respectively.

Project Impact. A Na-ion battery on par with the energy density of a Li-ion battery can have a high impact in the transportation sector with the assumption that the cost is significantly below $85/kWh and the battery pack provides a 300-mile range. The consumer is not concerned about the battery chemistry employed if these metrics can be met. Development of these battery chemistries will situate the United States in a strong position as relates to new low-cost energy storage systems beyond Li-ion.

Approach. In a team approach, the Na-ion battery group will create a versatile Na-ion battery chemistry with beneficial advantages such as low cost, safety, recycling, and sustainability of materials used. The team will work in a synergistic way so that the final design is the culmination of advances in phosphorus carbon composites mated with optimized lead or other highly dense metalloids, such as tin and/or antimony and derivatives thereof, for the recyclable anode. Synthesis and optimization of such blended composite anodes will be conducted in parallel to diagnostic characterization of structures, phase formation, and cycling stability. Cathode work will begin at the end of the first year and will involve (1) gradient cathodes consisting of Fe-Mn compositions, and (2) intergrowths of layer stacking sequenced oxides. If resources allow, the team also will attempt to stabilize cathode surfaces using ALD methods, particularly for the benefit of staving off dissolution of manganese and iron/electrolyte reactivity. Electrolytes will be partly procured from Dr. H. Li at PNNL.

Out-Year Goals. The state-of-the-art Na-ion battery in the literature has now been surpassed by this team, but performance is still too low for commercialization. Thus, the goal is to move forward and continually invent the most superior Na-ion battery chemistry that can compete worldwide through work output from this project.

Collaborations. Researchers from PNNL who are developing electrolytes for Na-ion batteries will provide this project with formulations to test with the various electrode combinations investigated at ANL. The team also exchanges commercial samples with Dr. J. Barker of Faradion Ltd. in the United Kingdom.

Milestones

1. Report on the BatPaC cell cost and energy density for the proposed Na-ion battery cell couple. (Q1, FY 2019; Completed).
2. Report on the synthesis, characterization, and initial cycling performance data on relevant Na-ion anode battery materials. (Q2, FY 2019; Completed)
3. Optimize anode composites produced in Q2. Continue characterization of materials for understanding. (Q3, FY 2019; Completed)
4. Demonstrate cycle life of optimized anode. (Q4, FY 2019; Completed)

Progress Report

Process Optimization of Pb-PbO-C Composite Anodes

The synthesis and process optimization of Pb-containing anodes for Na-ion batteries have been conducted through varying parameters: (1) starting lead oxide (PbO and Pb_2O_3) materials, (2) lead oxide/carbon ratio, (3) milling time, (4) electrode binder (PVDF), and (5) electrolyte and additives. This optimization is designed to maximize stability and promote higher capacity of Pb-based Na-ion battery anodes.

The relative fractional amounts of Pb and PbO phases and the particle morphologies in the final products are affected by the starting type of lead oxides, lead oxide/carbon ratio, and milling time. Figure 84 shows the effect of milling time as an example. As the milling time increases, the fractional amounts of metallic lead increases (Figure 84a). Longer milling also resulted in kneading of soft lead metal powders together to form a larger aggregate (SEM; Figure 84b). The right choice of binder appears to be critical for stable cycling of the conversion-alloying electrodes like lead oxides. Improved cycle stability is observed when PVDF content is increased. A PAA-based binder, while useful for Si-alloying anodes in Li-ion batteries, in the presence of the Pb-Pb oxide anodes caused slurry gelling. The addition of FEC improved the electrochemical performance (specific capacity and cycle stability) in both sodium and lithium cells.

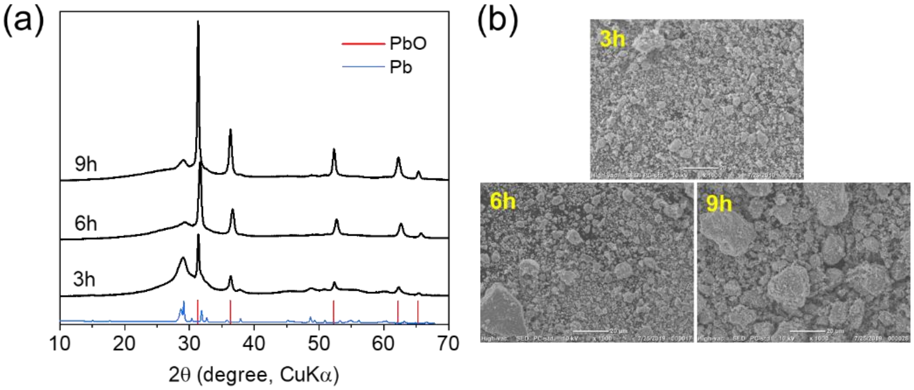

Figure 84. (a) X-ray diffraction patterns and (b) scanning electron microscopy images of the Pb-PbO-C composite samples prepared by SPEX mill with various milling times.

Air Stability

As-synthesized Pb-PbO-C composite powder, which was freshly coming out of the milling jar, contains a high Pb/PbO ratio. However, the sample is gradually oxidized when stored in air. The team suspects that the fresh metallic lead nanoparticles have highly active surfaces that easily oxidize in contact with oxygen in air. The high Pb/PbO ratio could be maintained by fabricating the electrode laminates inside of Ar-filled glove box, as depicted in the stable XRD shown in Figure 85a.

Figure 85b shows the initial voltage profiles of the electrodes prepared in air and in a glove box. It is clear that the electrode preparation atmosphere (that is, difference in the Pb/PbO ratio) has only a marginal effect on electrochemical performance. Slightly increased capacity for the air-prepared electrode corresponds to the higher theoretical capacity of PbO and the conversion of PbO to Li_2O plus lead during the cycling.

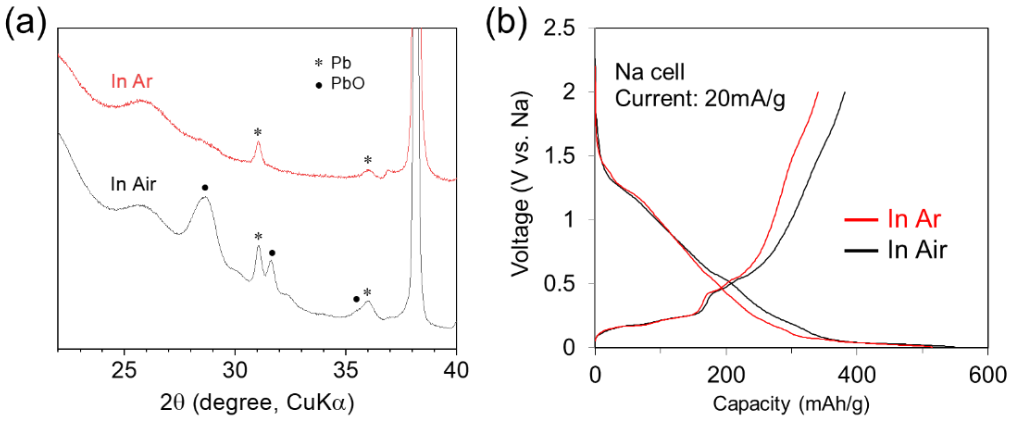

Figure 85. (a) X-ray diffraction and (b) initial voltage profiles of the Pb-O-C electrodes prepared in air and in Ar-filled glove box.

Sodium Insertion/Extraction Kinetics

Figure 86 compares the optimized coin cell performances of Pb-PbO-C in lithium and sodium cells. Conventional electrolytes ($LiPF_6$ or $NaPF_6$ dissolved in carbonate solvent) were used, and a moderate current density (100 mA/g) was applied for the comparison. While both cells show excellent cycle stability, the specific capacity of the same Pb-PbO-C electrode in the sodium cell was lower than that in the lithium cell.

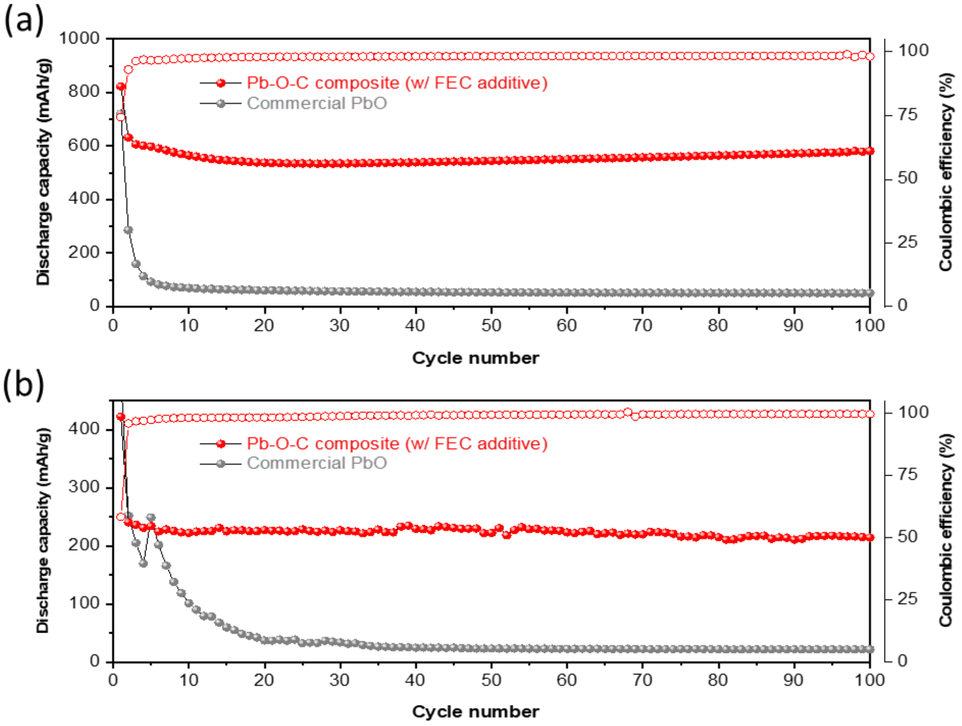

Figure 86. Cycle performance of optimized Pb-PbO-O anode in (a) lithium and (b) sodium half cells. Carbonate electrolytes are used for both cells, and 100 mA/g current density was applied.

The coin cell tests conducted at varying current density revealed that the lower specific capacity for the sodium cell shown in Figure 86b, as compared to the Li-cell, is due to the inability to sodiate down to $Na_{15}Pb_4$ at a low voltage of 0.1 V (versus sodium) from Na_9Pb_4. The high cell impedance seen at high current density of 100 mA/g is the reason for the lower capacity.

Figure 87a-b shows that the sodium cell has higher cell impedance, and slower sodium cycling makes the 0.1-V plateau accessible and increases specific capacity significantly.

In Figure 87c, the sodium coin cell prepared with an ether-based electrolyte (1 M NaTFSI dissolved in TEGDME) has much better cell impedance behavior, thus the high discharge capacity is obtained even at 100 mA/g current density. Ether-based electrolyte is reported to have better cathodic stability and form thinner SEI layer on the anodes.

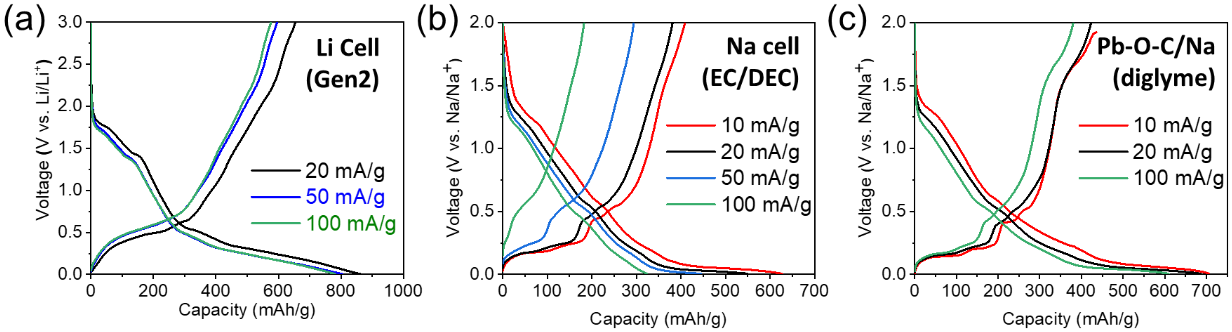

Figure 87. Initial voltage profiles of the Pb-PbO-C nanocomposite anode cycled in different electrolytes: (a) Gen2 electrolyte, (b) 1 M $NaPF_6$ in EC/DEC, and (c) 1 M NaTFSI in TEGDME.

Patents/Publications/Presentations

Presentations

- ACS Fall National Meeting, San Diego, California (August 25–29, 2019): “Where are Sodium-Ion Batteries Headed? An Analysis of Their Future”; C. Johnson.
- 236th ECS Meeting, Atlanta, Georgia (October 12–17, 2019): “An Evaluation of Electrochemical Properties for a Series of Sodium-Ion Battery Anodes”; C. Johnson.
- 236th ECS Meeting, Atlanta, Georgia (October 12–17, 2019): “Pb-Based Nanocomposite Anodes for Li- and Na-Ion Batteries”; J. Han, J. Park, Y. Kim, S. Ahmed, E. Lee, and C. Johnson.

Task 7.3 – High-Capacity, Low-Voltage Titanate Anodes for Sodium-Ion Batteries
(Marca Doeff, Lawrence Berkeley National Laboratory)

Project Objective. The objectives are to understand differences in the sodium intercalation mechanism of various sodium titanate anodes through an array of synthetic, electrochemical, and structural characterization techniques, and to overcome practical impediments to their use, such as the high first-cycle Coulombic inefficiencies that are currently observed. The ultimate goal is to produce a 200-250 mAh/g anode that cycles reversibly.

Project Impact. Although several suitable cathode materials for Na-ion batteries exist, there are few suitable anode materials due to their low potential instabilities. Therefore, sodium titanate variations will be synthesized through different routes to develop materials with various morphologies and dopants. Decreasing the first-cycle inefficiencies and improving cycling performance will allow enabling technology for a practical high-energy Na-ion battery.

Approach. Candidate stepped layered titanates will be synthesized by appropriate routes (hydrothermal, solid state routes, etc.). Materials will then be characterized electrochemically and physically. Structure-function relationships will be built to correlate the effect of changing structure (for example, step size) on electrochemical properties.

Out-Year Goals. A series of synchrotron characterization techniques will be used to further develop sodium titanate anode materials with stable cycling while delivering high capacities.

Collaborations. TXM is done in collaboration with Dr. Y. Liu (SSRL). Synchrotron hard, sXAS, and X-ray Raman efforts are in collaboration with Dr. D. Nordlund and Dr. D. Sokaras (SSRL). Electrolyte design is done in collaboration with Dr. K. Xu (ARL).

Milestones

1. Hydrothermal synthesis of sodium nonatitanate (NNT). (Q1, FY 2019; Completed)
2. Ion exchange sodium NNT with magnesium. (Q2, FY 2019; Completed – *No Go*)
3. Complete synchrotron XRD and XAS analysis on sodium NNT. (Q3, FY 2019; Completed)
4. *Go/No-Go Decision*: Magnesium exchange; stop if electrochemical properties are not improved. (Q4, FY 2019; Completed – *No Go*)

Progress Report

The electrochemical properties of "sodium nonatitanate" (NNT or $NaTi_3O_6(OH)\cdot 2H_2O$) as a function of drying temperature were studied this quarter. The HR-TEM/electron diffraction study (done in collaboration with H. Zheng of LBNL) of this material dehydrated at 600°C was a close match to what is expected for $Na_2Ti_6O_{13}$ (Figure 88), a tunnel compound with a very different voltage profile than dehydrated NNT.

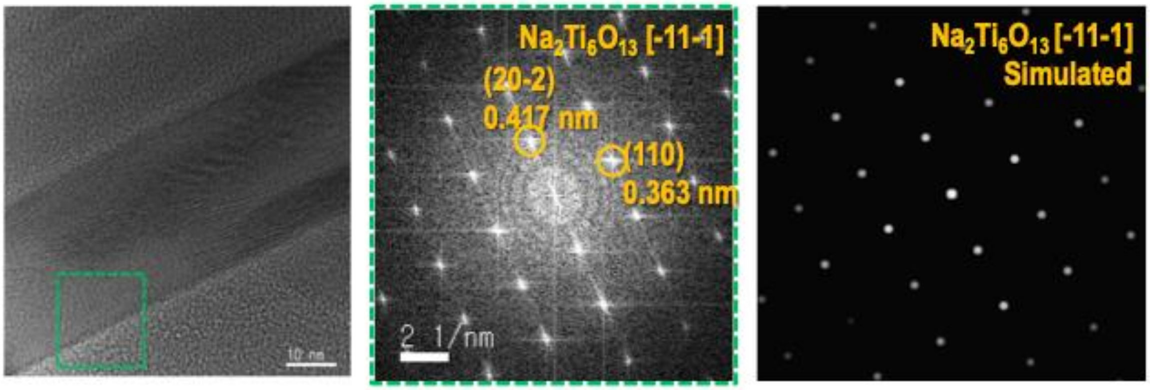

Figure 88. High-resolution transmission electron microscopy image of nonatitanate dehydrated at 600°C (left). The electron diffraction pattern of the area within the green box is shown in the middle image. The simulated pattern of $Na_2Ti_6O_{13}$ is shown at right.

These results might suggest that NNT partially converted to $Na_2Ti_6O_{13}$ at a lower temperature than previous *in situ* thermal XRD studies indicated, or that the structure has some characteristics similar to $Na_2Ti_6O_{13}$ when heated to 600°C (previous Raman studies indicate that dehydration results in some rearrangement of the structure so that "pinch points" form. In other words, the structure, although it retains the corrugated layer structure overall, starts to form some tunnel-like features on heating.) To investigate this further, samples were heated to various temperatures, and the electrochemistry was studied (Figure 89).

The voltage profiles of most of the samples consist of two regions, a sloping section from about 1.5 to 0.3 V with small plateaus near 0.9 V and 0.7 V, and a longer flatter section at about 0.3 V versus Na^+/Na. The exception is the profile of the NNT heated to 800°C, a temperature at which it decomposes to form $Na_2Ti_3O_7$ (another corrugated layer structure) and $Na_2Ti_6O_{13}$. For this sample, the sloping section (corresponding to $Na_2Ti_6O_{13}$) is shorter and lacks the small plateaus, and the flat section is at a somewhat lower potential than for the other samples, similar to what is observed for $Na_2Ti_3O_7$. The sample with the highest capacity (nearly 200 mAh/g) was the one dehydrated at 500°C. All samples showed excellent capacity retention on cycling, with exception of the phase mixture formed at 800°, where rapid fading was observed. The hydrated sample, surprisingly, also showed excellent cycling behavior, a function of carbon coating and the use of a CMC binder; previous electrodes made with PVDF binder and the hydrous NNT cycled poorly, in contrast. These results suggest that dehydrated NNT undergoes complex structural changes on heating, but does not fully undergo phase conversion, even at 600°C; rather it may resemble an intergrowth, with areas that resemble $Na_2Ti_6O_{13}$.

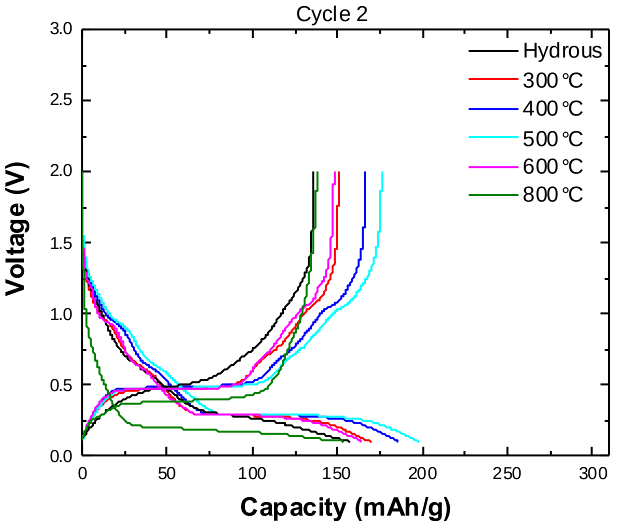

Figure 89. Second discharge profiles of sodium cells containing nonatitanate heated to various temperatures.

Patents/Publications/Presentations

The project has no patents, publications, or presentations to report this quarter.

Task 7.4 – Electrolytes and Interfaces for Stable High-Energy Sodium-Ion Batteries (Ji-Guang Zhang, Pacific Northwest National Laboratory)

Project Objective. This project will develop innovative electrolytes and enable fundamental understanding on the interface between electrode and electrolyte for stable operation of high-energy Na-ion batteries for potential application in EVs. The proposed research will enhance the achievable capacities of both anode and cathode for Na-ion battery and improve the stability of electrodes/electrolyte interface, build correlation (electrolyte design rule) between electrochemical performances of Na-ion batteries and the electrolyte/interface properties, and enable long cycle life and safe operation of high-energy Na-ion batteries.

Project Impact. This project will enable a fundamental understanding on the electrolyte/electrode interface in Na-ion battery systems. Successful project execution will improve their energy density, cycle and calendar life, and safety. The project will provide a solid contribution to development of Na-ion battery technology and promote its practical application as a competitive alternative to the current Li-ion batteries, as well as greatly reduce the cost of energy storage systems for EVs.

Approach. This project will optimize the electrolyte components and concentrations to develop innovative electrolyte and additives with improved physical and (electro) chemical properties. *In situ* and *ex situ* spectroscopy methods will be used to unravel the origin of the SEI at the dynamic interface, providing guidance for the electrolyte and interface design and enabling high achievable capacity and long life of Na-ion batteries.

Out-Year Goals. This project will select the electrolyte compounds and use *in situ* and *ex situ* techniques to identify the formation of interfacial SEI layer and its effect on the electrode materials. It will also provide guidance to electrolyte optimization to improve the hard carbon anode capacity to > 300 mAh g^{-1} and enable its long-term stable operations.

Collaborations. This project will collaborate with ANL and LBNL and other leading scientists in the field of cathode and anode materials for Na-ion batteries. It will collaborate with Dr. C. Wang and Dr. M. Engelhard for TEM and XPS characterization.

Milestones

1. Determine the physical-chemical properties of carbonate-based electrolytes, and identify the key factor affecting the stability of these electrolytes in sodium batteries. (Q1, FY 2019; Completed)
2. Design new phosphate-based electrolyte with improved electrochemical and thermal stability in sodium batteries. (Q2, FY 2019; Completed)
3. Characterize chemical coordination structure of selected carbonate- and phosphate-based electrolytes for sodium batteries. (Q3, FY 2019; Completed)
4. Demonstrate improved capacity, CE, and cyclic stability of electrode materials using the electrolytes developed in this work; achieve hard carbon capacity of > 250 mAh g^{-1}, initial CE > 85%, and cycle life > 200 times. (Q4, FY 2019; Completed)

Progress Report

The fourth quarter milestone has been accomplished. The performance of hard carbon anode in carbonate electrolytes was investigated and improved. To achieve high initial Coulombic efficiency (ICE), the team studied charge and discharge curve of initial cycle for Na||HC cells (HC electrode: HC: PVDF: CB=90:5:5, mass loading: 2-3 mg cm^{-2}) in 1 M $NaPF_6$ electrolyte with different solvents. As demonstrated in Figure 90a, ICE is 78.36% (PC), 34.82% (DMC), 78.25% (EC+PC, 1:1 in mass), 86.40% (EC+DMC, 1:1 in mass) and 80% (PC+DMC, 1:1 in mass) at 0.1 C (1 C=300 mAh g^{-1}). At the 5th cycle at 0.1 C, the reversible capacity is 268.3 mAh g^{-1} (PC), 98.3 mAh g^{-1} (DMC), 261.6 mAh g^{-1} (EC+PC, 1:1 in mass), 291.5 mAh g^{-1} (EC+DMC, 1:1 in mass), and 238.3 mAh g^{-1} (PC+DMC, 1:1 in mass), respectively, as shown in Figure 90b. Among these different electrolytes, 1 M $NaPF_6$ in EC+DMC shows the highest ICE and reversible capacity, and thus is chosen as the optimal electrolyte to study rate and long-term cycling performance.

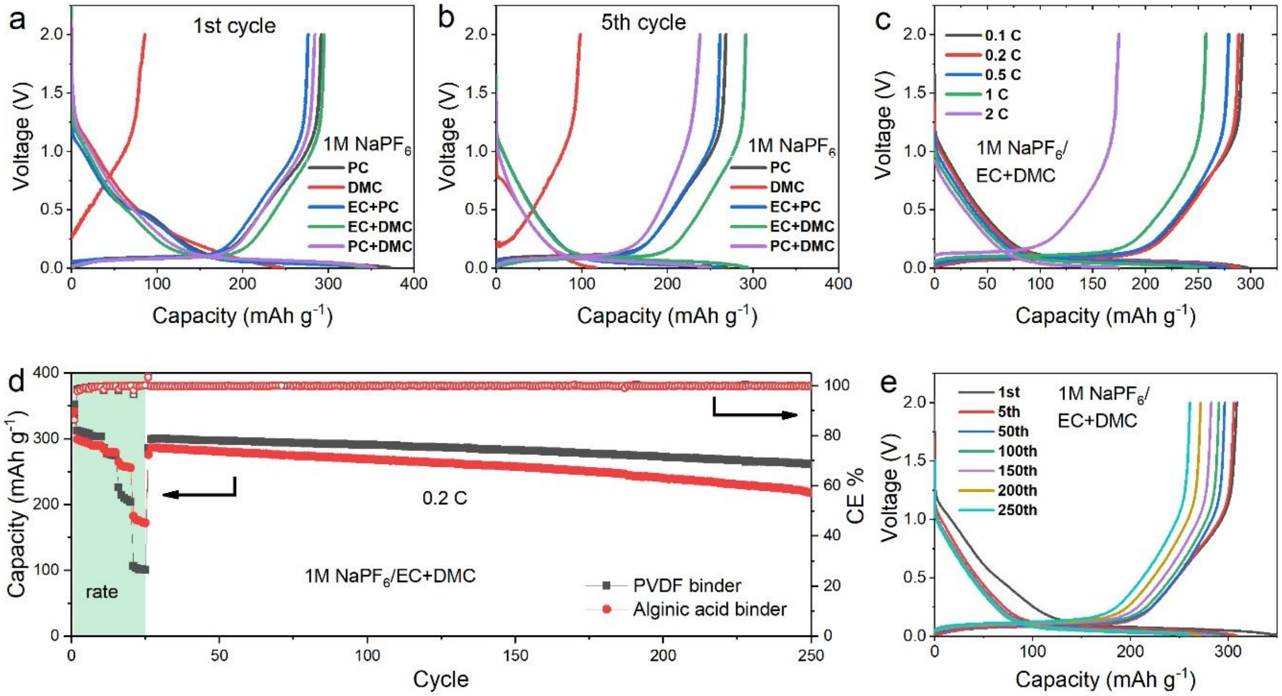

Figure 90. (a-b) Galvanostatic charge–discharge curves of Na||HC cells in 1 M $NaPF_6$ electrolyte with different solvents at the first (a) and fifth (b) cycles. (c) Rate performance of Na||HC cells in 1 M $NaPF_6$/EC+DMC electrolyte. (d) Cycling stability of Na||HC cells in 1 M $NaPF_6$/EC+DMC electrolyte. (e) Charge–discharge profiles of Na||HC cells in 1 M $NaPF_6$/EC+DMC electrolyte at different cycles.

Hard carbon anode shows good rate performance in optimal 1 M $NaPF_6$ in EC+DMC electrolyte. As rate increases from 0.1 C to 2 C, the reversible capacity is 292.2 mAh g^{-1} (0.1 C), 288.8 mAh g^{-1} (0.2 C), 279.4 mAh g^{-1} (0.5 C), 257.8 mAh g^{-1} (1 C), and 174.8 mAh g^{-1} (2 C), as shown in Figure 90c. For long-term cycling test, hard carbon anode with two different binders (HC:binder:CB = 90:5:5, mass loading: 2-3 mg cm^{-2}) was cycled at 0.2 C, as shown in figure 90d. One binder is PVDF, and the other is alginic acid aqueous binder. The reversible capacity of HC electrode with PVDF binder after 200 and 250 cycles (including the initial 25 cycles for rate test) is 240.2 and 218.0 mAh g^{-1}, respectively. Hard carbon anode with alginic acid aqueous binder shows better long-term cycling performance, as shown in Figure 90d. The reversible capacity of HC electrode with alginic acid aqueous binder after 200 and 250 cycles (including the initial 25 cycles for rate test) is 271.1 and 261.2 mAh g^{-1}. The CE is 87.71% for the first cycle and > 99.9 for long-term cycling. The charge–discharge profiles of hard carbon anode with alginic acid aqueous binder at different cycles further demonstrate the stable long-term cycling performance, as shown in Figure 90e.

Patents/Publications/Presentations

Presentation

- DOE Na-Ion Workshop, Richland, Washington (August 27, 2019): “Electrolytes and Interfaces for Stable High-Energy Na-Ion Batteries”; J-G. Zhang,* H. Pan, P. M Le, T. D. Vo, Y. Jin, and N. Sabi.

Innovation Center for Battery500
(Jun Liu, Pacific Northwest National Laboratory; Yi Cui, Stanford University)

Project Objective. The project aims to develop commercially viable lithium battery technologies with a cell-level specific energy of 500 Wh/kg through innovative electrode and cell designs that enable the extraction of the maximum capacity from advanced electrode materials. In addition to achieving high specific energy, the project aims to be able to achieve 1,000 cycles for the developed technologies.

Project Impact. The Battery500 Consortium will develop next-generation lithium battery technologies that will significantly increase energy density, improve cycle life, and reduce cost. This will greatly accelerate deployment of EVs and reduce carbon emission associated with fossil fuel consumption. The consortium will utilize first-class expertise and capabilities in battery research in the United States and develop an integrated and multi-disciplinary approach to accelerate development and deployment of advanced electrode materials in commercially viable high-energy batteries. The advances made in this consortium will also benefit the improvement of current Li-ion battery technologies.

Approach. This project will utilize an assortment of national resources located at the national laboratory level and university level. The lithium anode combined with a compatible electrolyte system and two cathodes—one high-Ni $LiNi_xMn_yCo_zO_2$ and another sulfur—will be studied and developed to reach high-energy density. The project focus is to design novel electrode and cell architectures to meet the 500 Wh/kg goal. The consortium will work closely with R&D companies, battery/materials manufacturers, and end users/OEMs to ensure that the developed technologies are aligned with industry needs and can be transitioned to production.

Out-Year Goals. This project aims for the following out-year goals. (1) Integrate materials and components developed in FY 2018 into 1-Ah pouch cell and demonstrate 400-Wh/kg cell with more than 30 charge discharge cycles, and provide analytical results for materials selection, cell design and fabrication, and further refinement for FY 2019. (2) Evaluate the seedling projects for key findings.

Collaborations. Collaboration among consortium team members will be well coordinated by the leadership team, which includes the keystone project leads and co-leads along with PIs at all member institutions. Collaboration with the community outside of this consortium and with industry will be facilitated by the executive committee, the advisory board, and the industry committee.

Milestones

1. Synthesize high-nickel layered oxide cathodes (nickel content > 90%) with a capacity of > 210 mAh/g and test. (Q1, FY 2019; Completed)
2. Implement lithium protection approaches to demonstrate 20% cycle life improvement. (Q2, FY 2019; Completed)
3. Fabricate and test a pouch cell capable of 350 Wh/kg and 250 cycles. (Q3, FY 2019; Completed)
4. Fabricate and test a pouch cell capable of 400 Wh/kg and 30 cycles. (Q4, FY 2019; Completed)

Progress Report

This quarter, the fourth milestone for FY 2019 was completed. Pouch cells capable of 400 Wh/kg and 30 cycles have been fabricated and tested. One patent application was filed by a consortium member (the PNNL team), 18 invited talks were delivered by PIs of the Battery500 consortium, and 14 papers were published in peer-reviewed journals during the fourth quarter of FY 2019.

Keystone Project 1: Materials and Interfaces

This quarter, a localized high-concentration electrolyte (LHCE) based on a class of fluorinated solvents, hydrofluoroorthoformate, has been developed; this has led to CE of lithium cycling up to 99.5%. In addition, an anomalously large d-spacing peak at 7 Å for $LiNi_{0.6}Mn_{0.2}Co_{0.2}O_2$ (NMC-622) cathode material at highly charged state (> 4.5 V) has been identified, which provides structural insight into potential problems of high-voltage charging.

One example of hydrofluoroorthoformate-based LHCEs is 1 M LiFSI in DME – tris(2,2,2-trifluoroethyl)orthoformate (1:9 by wt. and 1.2:3 by mol., named as 1 M LiFSI/DME-TFEO). TFEO diluent has a much higher boiling point (145°C) than that of bis(2,2,2-trifluoroethyl) ether (BTFE, 63°C) diluent used in previous work and largely improves stability of the electrolyte. The SEI formed during cycling in this electrolyte exhibits a monolithic feature by cryo-TEM images (see Figure 91a-d), which is in sharp contrast to the widely-reported mosaic- or multilayer-type SEIs that are not homogeneous and could lead to uneven lithium stripping/plating and fast lithium and electrolyte depletion over cycling. The highly homogeneous SEI not only prevents dendritic lithium formation, but also minimizes lithium loss and volumetric expansion. Furthermore, this electrolyte strongly suppresses the phase transformation of $LiNi_{0.8}Co_{0.1}Mn_{0.1}O_2$ (NMC-811) from layered structure to rock salt and stabilizes the structure. Tests of high-voltage Li||NMC-811 cells show long-term cycling stability and high rate capability, as well as reduced safety concerns. The dashed lines in Figure 91c show consistent SEI thickness of ~ 10 nm on lithium surface. Interestingly, the dominant components of this SEI layer are amorphous inorganic compounds. This SEI is proved to be not only uniform in horizontal coverage, but also in depth through the SEI from the surface to the bottom (close to lithium metal).

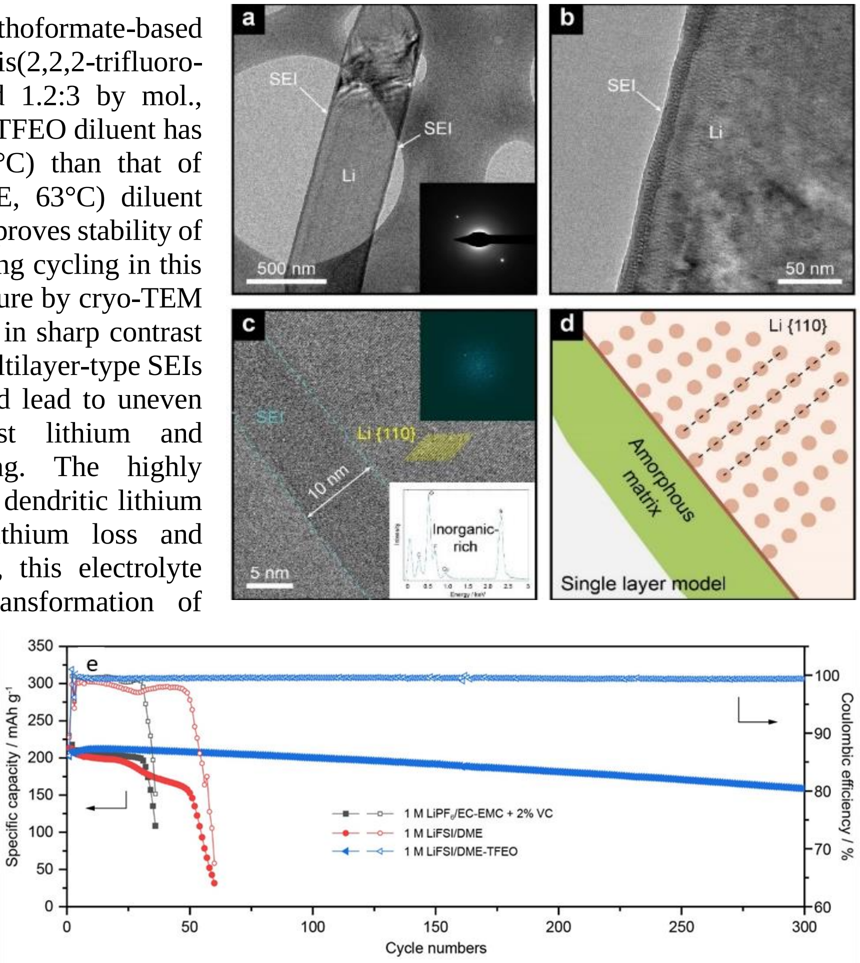

Figure 91. SEI on Li-metal anode. (a-c) Cryo – transmission electron microscopy (TEM) images of lithium deposited on a TEM grid at different scales. Insert in (a) shows corresponding selected area electron diffraction (SAED) pattern. Insert in (c) shows corresponding reduced fast Fourier transform (top) and the energy-dispersive X-ray spectroscopy spectra (bottom) of the SEI layer, where the yellow lines show the lattice space of the crystalline lithium. (d) Schematic of the observed single-layer SEI structure on deposited lithium in the 1 M LiFSI/DME-TFEO electrolyte. (e) Li||NMC-811 cell cycling performances of the investigated electrolytes, where the lines with full and hollow circles represent specific capacity and Coulombic efficiency of the cells, respectively.

This electrolyte leads to a CE of up to 99.5% as measured in Li||Cu cells. This is one of the best values reported for Li-metal anodes. It can also form a stable cathode electrolyte interface (CEI) layer at high-voltage cathodes. Figure 91e shows that the Li||NMC-811 cell using this electrolyte exhibits a capacity retention of 80% after 300 cycles and a high CE of 99.7% over cycling.

In addition, an anomalously large d-spacing peak at 7 Å is observed for NMC-622 cathode material at highly charged state (> 4.5 V) (see Figure 92a). This unique feature has never before been reported. Neutron pair distribution function (nPDF) analysis, combined with Reverse Monte Carlo simulation, reveals that significant structural heterogeneity is induced by deep charging (see Figure 92b-c). This in turn leads to structural modulation in the TM layer, meaning that TM cations deviate from the ideal crystallographic 3b site (0, 0, 0.5) and the extent of deviation varies periodically. Such structural modulation is directly observed in high-resolution TEM study (Figure 92d). It shows that such modulation gives rise to a large spacing at around 7 Å. Such a structural feature is unique to the Ni-rich layered materials and only appears at highly charged state. This study provides structural insight into potential problems of high-voltage charging, which is beneficial for higher energy-density cathode materials.

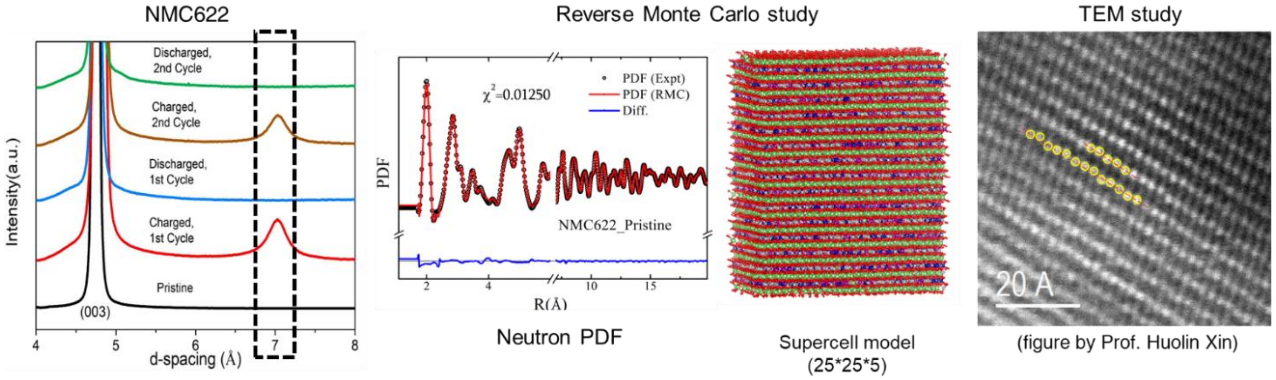

(a) (b) (c) (d)

Figure 92. Abnormal d-spacing observed in NMC-622 cathode material at highly charged state (> 4.5 V). (a) Large d-spacing peak at 7 Å. (b) Neutron pair distribution function (nPDF) analysis with (c) supercell model. (d) Transmission electron microscopy observation of the abnormal structure formed at highly charged state.

Highlights of Keystone Project 1

The highlights for this quarter are as follows:

- Developed an LHCE based on hydrofluoroorthoformate (TFEO) which leads to a monolithic and highly homogenous SEI structure and stable cycling of Li||NMC-811 cells.
- Identified an anomalously large d-spacing peak for NMC-622 cathode material at highly charged state (> 4.5 V), which provides structural insight into potential problems of high-voltage charging.

Keystone Project 2: Electrode Architecture

The goal of the Keystone 2 is to design, model, fabricate, and characterize the effect of electrode architecture on electrode and cell performance in support of reaching the project of 500 Wh/kg cell specific energy. Included in this Keystone are architecture design of thick cathodes (UCSD), Li-metal electrode architectures (PNNL, UCSD, and Stanford), inorganic (UT-Austin) and polymer (Stanford) electrolytes, and electrode performance modeling (UW). Highlighted this quarter are recent advancements at multiple institutions in understanding the importance of Li-metal architecture and developing approaches to address the failure mechanisms.

In this quarter, Meng's group at UCSD utilized cryogenic electron microscopy techniques to study different lithium morphologies under different conditions and their correlations to lithium anode failure. Cryogenic focused ion beam-scanning electron microscopy (Cryo-FIB-SEM) was used to explore the microstructures of inactive lithium. High concentration ether-based electrolyte (HCE) and commercial carbonate electrolyte (CCE) samples under different stripping rates were chosen for the morphological study. The team found that as the stripping rate increases, the morphology of inactive lithium in HCE evolves from uniform sheets to local clusters (Figure 93a-c) with a thickness increased from 500 nm to 2 µm (Figure 93d-f). For the CCE, the

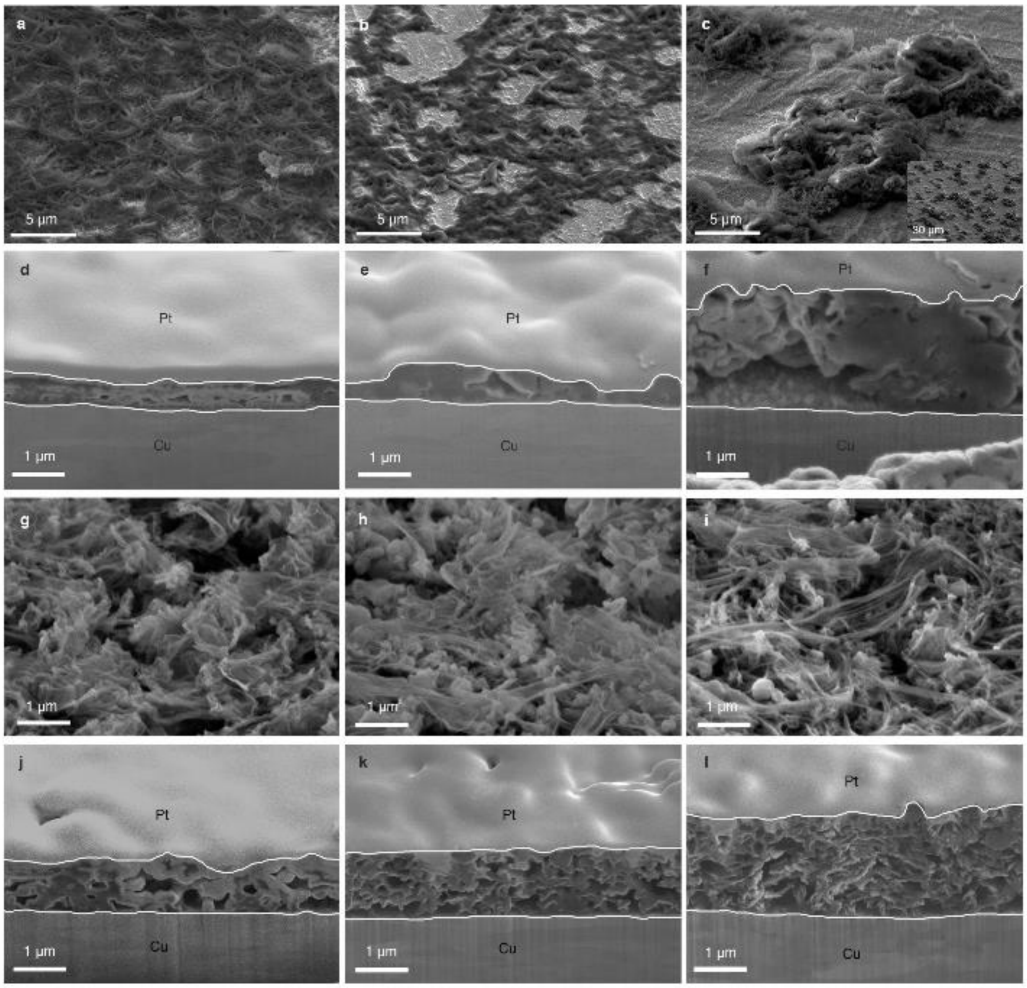

Figure 93. Microstructures of inactive lithium generated in high-concentration ether-based electrolyte (HCE) (a-f) and commercial carbonate electrolyte (CCE) (g-l) imaged by cryo – focused ion beam scanning electron microscopy (FIB-SEM). (a-c) and (g-i) are top views of the inactive lithium at 52° tilted stage. (d-f) and (j-l) are cross-sections obtained by cryo-FIB. Each column represents a stripping rate: (a/d/g/j) are at 0.5 mA cm^{-2}; (b/e/h/k) are at 2.5 mA cm^{-2}; and (c/f/i/l) are at 5.0 mA cm^{-2}.

deposited whisker-like lithium becomes thinner after stripping (Figure 93g-i), and turns thicker in cross-section along with the increased stripping rates (Figure 93j-l), corresponding to the increased loss of CE at high rates. It is worth noting that these residues exhibit poor connection to the current collector, indicating the loss of electronic conductive pathways.

The team further used cryo-TEM to investigate the nanostructure of the inactive lithium in HCE and CCE after stripping at 0.5 mA cm^{-2}. Sheet-like inactive lithium appears in the HCE sample (Figure 94a), while inactive lithium in the CCE remains a whisker-like morphology (Figure 94e). Based on the (110) lattice plane distance of bcc lithium, the region that contains crystalline metallic Li^0 is highlighted in green in the high-resolution TEM (HRTEM) images for both electrolytes (Figure 94b/f). Compared with the inactive lithium obtained from CCE, a much smaller area of metallic Li^0 component is observed in HCE. This indicates that most deposited metallic Li^0 in HCE has been successfully stripped, corresponding to the high CE. Whisker-like unreacted metallic Li^0 as large as ~ 80 nm in length remains in the CCE sample and is well isolated by the surrounding SEI. The SEI components were determined by matching the lattice spacing in HRTEM images with their FFT patterns (Figure 94c/g). Li_2CO_3 and Li_2O constitute the major part of SEI, which also contains LiF as well as other amorphous organic species for both electrolytes. The above observations from cryo-TEM are summarized in the schematic plot (Figure 94d/h), which reveals the form of inactive lithium with two different morphologies at nanoscale.

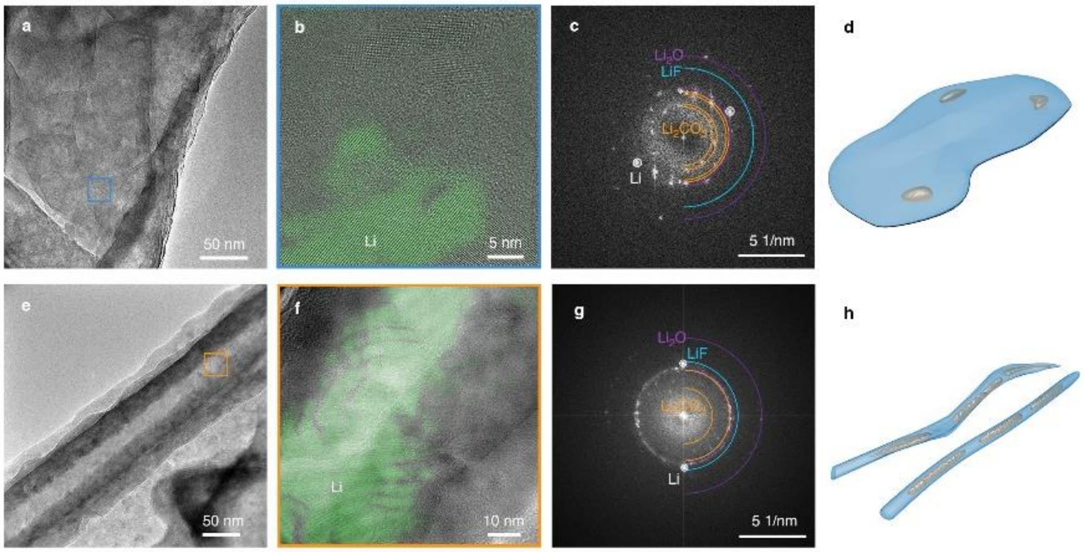

Figure 94. Nanostructures of inactive lithium generated in high-concentration ether-based electrolyte (HCE) (a-d) and commercial carbonate electrolyte (CCE) (e-h) by cryo – transmission electron microscopy (TEM). (a/e) Inactive lithium morphology at low magnifications for both electrolytes. (b/f) High-resolution TEM (HRTEM) shows a different amount of metallic Li^0 is wrapped by SEI in the two types of electrolytes. The highlighted metallic Li^0 region in green is identified through fast Fourier transform (FFT) – mask filtering-inverse FFT-image overlay process. (c/g) FFT patterns of corresponding HRTEM indicate the SEI component that contains crystalline Li_2CO_3, Li_2O, and LiF. (d/h) Schematic of inactive lithium nanostructure in both electrolytes. Small area of metallic Li^0 is embedded in a sheet-like SEI layer for HCE, while a large bulk of metallic Li^0 is isolated in whisker-like SEI layer in CCE.

In a separate effort, a new artificial SEI layer based on a polymeric network with both self-healability and high Li^+ single-ion conductivity has been developed in Bao's group at Stanford (Figure 95). An ideal artificial SEI must have several key properties. First, flowability and self-healability are desirable so that the SEI can adapt to huge volume changes during lithium stripping/deposition and prevent dead lithium from detaching. Second, high Li^+ single-ion conductivity in the artificial SEI is beneficial to reduce 'hot spots,' increase critical lithium deposit size, and stabilize the Li-metal anode. Last, but not least, the SEI needs to be both chemically and electrochemically inert in the presence of liquid electrolyte (insoluble and unreactive) as well as lithium metal to minimize deleterious side reactions. To date, several attempts have been made to design artificial SEIs with desirable properties such as viscoelasticity, self-healability, or high ion conductivity. However, few are able to combine all of these properties. Additionally, the majority of the reported Li-metal artificial SEIs are only compatible with ether-based electrolytes, making them impractical when paired with high-voltage, high-energy-density Ni-rich NMC cathodes that are used in today's commercial Li-ion batteries. In this newly developed polymeric network, tetrahedral $Al(OR)_4^-$ anions are introduced as a novel dynamic motif with freely transporting Li^+ counter ions that are directly introduced during the reaction. With this self-healable single-ion-conductive network (SSN, Figure 95a) as the Li-metal artificial SEI, more than 400 stable plating/stripping cycles have been obtained in Li||Cu cells using a commercial carbonate-based electrolyte. More importantly, > 85% capacity retention for more than 160 cycles in a Li||NMC full battery was achieved. To the team's knowledge, this is the first time that self-healability and single-ion conductivity are incorporated into one chemical structure to create an effective artificial SEI for Li-metal batteries.

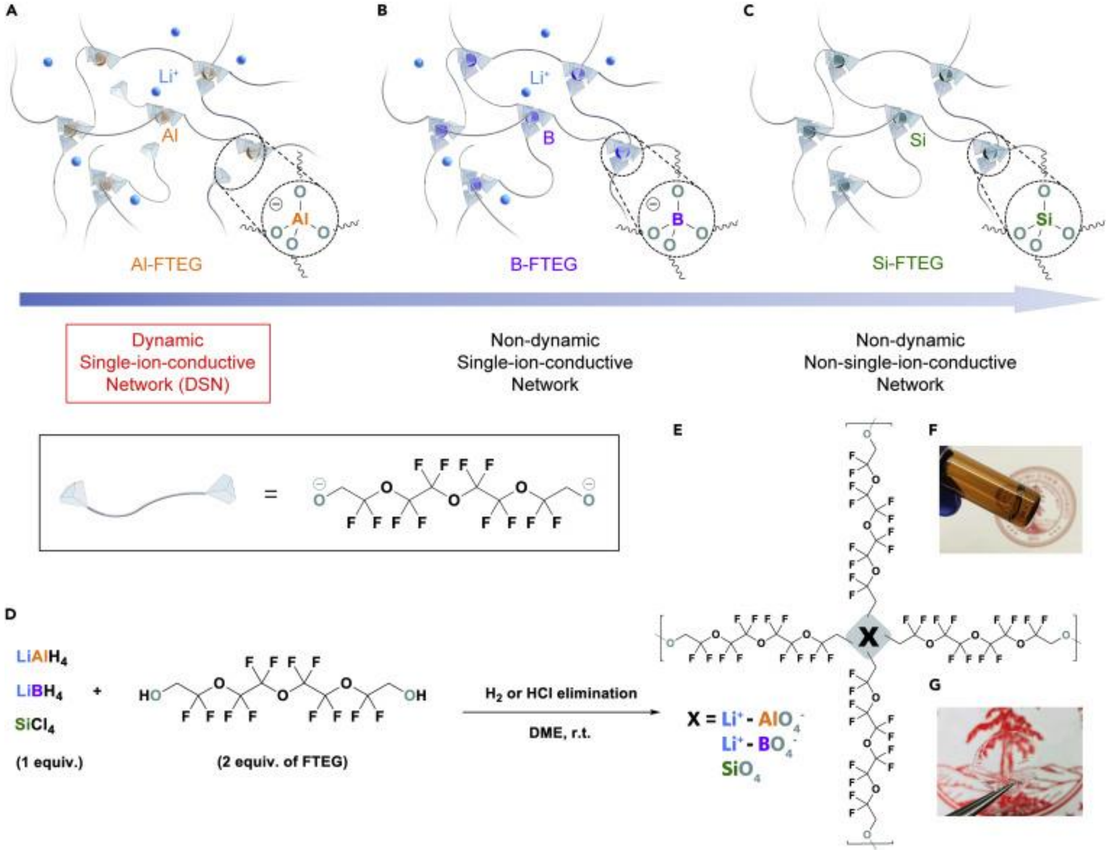

Figure 95. Molecular design and chemical structures of self-healable single-ion-conductive network (SSN) and derivatives. (a-c) Conceptual sketch of SSN (a), B-SSN (b), and Si-SSN (c). Blue spheres: Li^+; orange spheres: aluminum; purple spheres: boron; olive spheres: silicon; tetrahedra: anion centers; grey chains: soft ligands. (d) The reaction to synthesize SSN. (e) Detailed chemical structure of SSN. (f/g) Photos of an as-synthesized viscous SSN/DME solution (f) and a free-standing SSN film (g).

Highlights of Keystone Project 2

The highlights for this quarter are as follows:

- Significant advancement in understanding the form of inactive lithium with two different morphologies at nanoscale using cryo-TEM.
- For the first time, self-healability and single-ion conductivity are incorporated into one chemical structure to create an effective artificial SEI for Li-metal batteries.
- These new insights would facilitate new design approaches for creating 3D architectures that minimize the formation of inactive lithium metal as well as flowable and self-healable SEI, and therefore, will play a pivotal role in developing long-life Li-metal batteries.

Keystone Project 3: Cell Fabrication, Testing, and Diagnosis

As 250 cycles at 350 Wh/kg with less than 20% fade of a 2.5-Ah pouch cell were achieved last quarter, Keystone 3 efforts have been focusing on increasing stability of NMC-811 to stablize NMC-811 at high voltages but extend cycle life. Recent work at UW showed that with proper coating such as LiF/LiBO$_2$-coated NMC-811 cathode, higher stability can be obtained at 4.6 V cutoff to retain similar capacity as the pristine cathode (See Figure 96). The better stability of the coated NMC-811 cathode also demonstrated in the DSC experiment with smaller heat release and higher onset temperature than the pristine cathode. The conductivity measurements on the cathode materials indicated that the coating reduced the conduction on the NMC-811 surface to minimize electrolyte decomposition. The coating does not increase the polarization of the cell, thus a high specific energy could be achieved with longer cycle life.

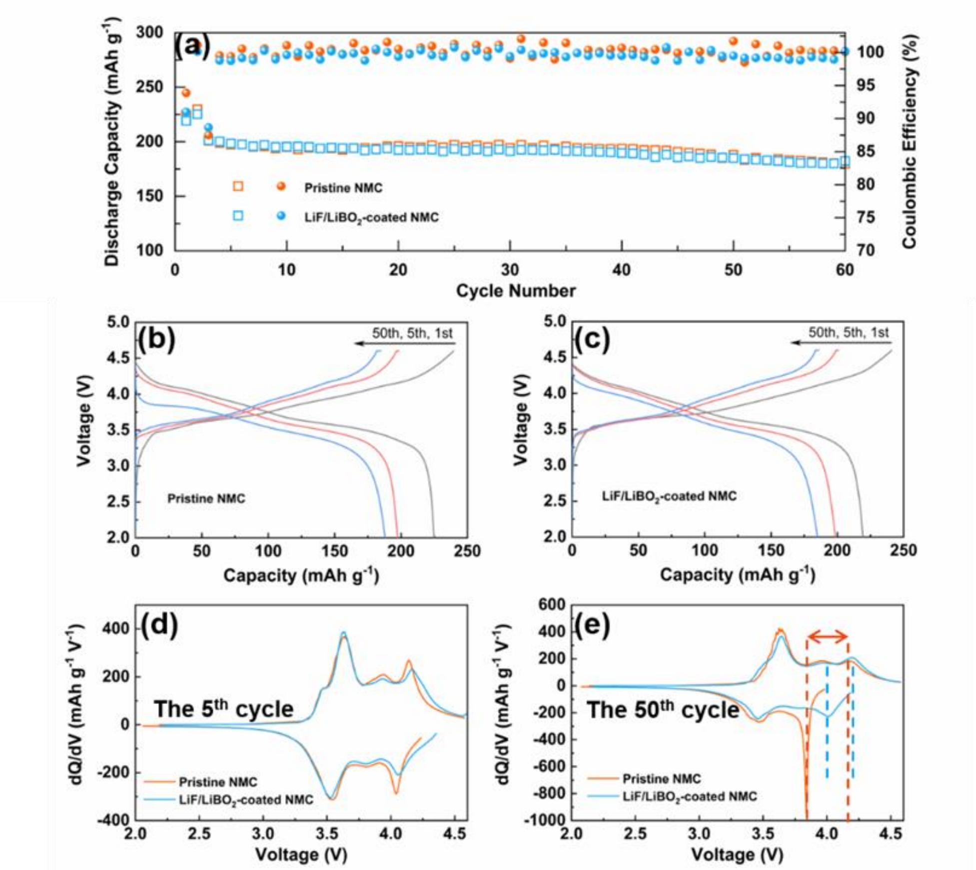

Figure 96. (a) Cycling performance of the pristine and LiF/LiBO$_2$-coated NMC-811 cathodes. Selected charge–discharge curves of (b) the pristine and (c) LiF/LiBO$_2$-coated NMC-811 cathodes. The dQ/dV plot of the pristine and LiF/LiBO$_2$-coated NMC-811 thick electrodes at the (d) 5th and (e) 50th cycles. The tests were conducted using the Battery500 testing protocol at 20°C within the voltage range of 2.8-4.4 V at C/3. There was a 4-hour rest between charge and discharge regimes during cycle aging. The formation was performed at C/10 for two cycles with 1-hour rest between charging and discharging.

Gaining a deeper understanding of the capacity fade and its attributes on cell failure has also progressed well. A novel electrochemical analytical diagnosis (eCAD) technique was developed at Idaho National Laboratory (INL) to dissect capacity fade attributes into a number of identifiable failure modes, for example, loss of active materials (LAM), artifact by IR-drop, and under-utilization of the active materials (UAM) in NMC-622; their effect and impact on cell capacity (for example, QF_{LAM}, QF_{IR}, and QF_{UAM}) can now be monitored and quantified by eCAD and using NMC-622 cathode as an internal reference. Currently, this eCAD approach has been validated with a build of 14 coin cells using lithium | standard electrolyte | NMC-622 configuration.

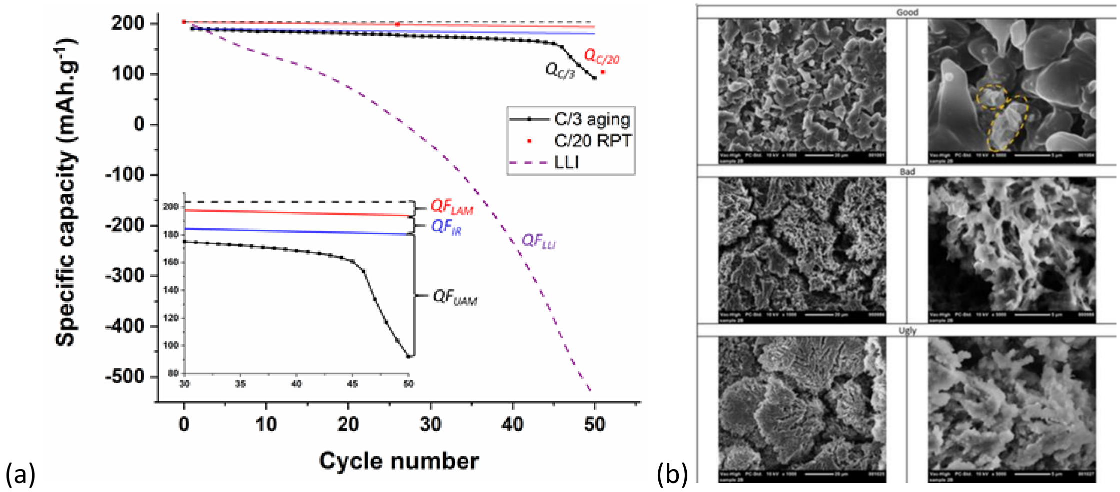

Figure 97. The electrochemical analytical diagnosis (eCAD) technique revealed (a) the attributes to the capacity fade of an early failed lithium | standard electrolyte | NMC-622 coin cell and the significant impact from loss of lithium inventory. (b) The scanning electron micrographs show the impact of the dead lithium on the lithium inventory that failed the cell.

Figure 97 shows contributions of the capacity fade attributes to the loss of active materials (QF_{LAM}), IR-drop (QF_{IR}), and under-utilization of the active materials in NMC-622 (QF_{UAM}) in the charge retention of an early failed cell during C/3 cycle aging at 25°C. The eCAD technical also allowed the team to estimate the amount of loss of lithium inventory (QF_{LLI}), as shown in Figure 97a. The revelation of the significant impact of LLI on charge retention, the inability of measuring QF_{LLI} directly by testing, and the ability to estimate such factors in quantitative detail are a critical breakthrough in diagnosis. Figure 97b exhibits the SEM micrographs of the Li-metal electrode morphology obtained from the aged cells at the end of the test. The significant amount of dead lithium on the failed cell indicates the eCAD analysis indeed revealed the correspondence of the impact from dead lithium on LLI. Protecting lithium from loss in cycle aging is key to long cycle life. The application of eCAD to other cell configurations and associated stress factors (for example, pressure on the pouch cells) is under way and will be reported in subsequent reports.

Highlights of Keystone Project 3

The highlights for this quarter are as follows:

- Demonstrated use of coating to protect NMC-811 cathode to improve stability at high voltage cutoff, retain capacity, and reduce polarization.
- At INL, developed and validated a novel eCAD technique that can conduct failure mode and effect analysis (FMEA) with a build of 14 Li || NMC-622 coin cells.
- Accomplished detailed diagnosis on capacity fade mechanism and impact from dead lithium on charge retention. Further applications to other cell types and chemistries are in progress.

Patents/Publications/Presentations

Patent

- Xiao, J., C. Niu, D. Liu, and J. Liu. "Cell Design and Fabrication of Li Metal Pouch Cells with Cell-Level Energy of 300 Wh/kg or Higher." Patent application filed by PNNL in August 2019. PNNL IPID: 31510-E.

Publications

- Zhou, H., F. Xin, B. Pei, and M. S. Whittingham.* "What Limits the Capacity of Layered Oxide Cathodes in Lithium Batteries?" *ACS Energy Letters* 4 (2019): 1902–1906. doi: 10.1021/acsenergylett.9b01236, Publication Date (Web): July 18, 2019.
- Xin, F., H. Zhou, X. Chen, M. Zuba, N. Chernova, G. Zhou, and M. S. Whittingham. "Li−Nb−O Coating/Substitution Enhances the Electrochemical Performance of the $LiNi_{0.8}Mn_{0.1}Co_{0.1}O_2$ (NMC-811) Cathode." *ACS Applied Materials & Interfaces*, 11 (2019): 34889–34894. doi: 10.1021/acsami.9b09696, Publication Date (Web): August 30, 2019.
- Omenya, F., N. Zagarella, J. Rana, H. Zhang, C. Siu, H. Zhou, B. Wen, N. Chernova, L. F. J. Piper, G. Zhou, and M. S. Whittingham. "Intrinsic Challenges to the Electrochemical Reversibility of the High Energy Density Copper (II) Fluoride Cathode Material." *ACS Applied Energy Materials* 2 (2019): 5243–5253. doi: 10.1021/acsaem.9b00938, Publication Date (Web): June 14, 2019.
- Yu, Z., D. G. Mackanic, W. Michaels, M. Lee. A. Pei. D. Feng, Q. Zhang, Y. Tsao, C. V. Amanchukwu, X. Yan, H. Wang, S. Chen, K. Liu, J. Kang, J. Qin, Y. Cui,* and Z. Bao.* "A Dynamic, Electrolyte-Blocking, and Single-Ion-Conductive Network for Stable Lithium-Metal Anodes." *Joule* (2019). doi: 10.1016/j.joule.2019.07.025, Publication Date (Web): August 26, 2019.
- Xiao, J., G. Zhou, H. Chen, X. Feng, D. Legut, Y. Fan, T. Wang, Y. Cui, and Q. Zhang. "Elaboration of Aggregated Polysulfide Phases: From Molecules to Large Clusters and Solid Phases." *Nano Letters* 19 (2019): 7487–7493. Publication Date (Web): September 11, 2019.
- Amanchukwu, C. V., X. Kong, J. Qin, Y. Cui,* and Z. Bao.* "Nonpolar Alkanes Modify Lithium-Ion Solvation for Improved Lithium Deposition and Stripping." *Advanced Energy Materials* 9, no. 41 (2019): 1902116. doi.org/10.1002/aenm.201902116, Publication Date (Web): September 23, 2019.
- Cao, X., X. Ren, L. Zou, M. H. Engelhard, W. Huang, H. Wang, B. E. Matthews, H. Lee, C. Niu, B. W. Arey, Y. Cui, C. Wang, J. Xiao, J. Liu, W. Xu,* and J-G. Zhang.* "Monolithic Solid–Electrolyte Interphases Formed in Fluorinated Orthoformate-Based Electrolytes Minimize Li Depletion and Pulverization." *Nature Energy* 4 (2019): 796–805. Publication Date (Web): September 13, 2019.
- Zhang, J-G. "Anode-less." *Nature Energy* 4, no. 8 (2019): 637–638.
- Li, S., S-J. Lee, X. Wang, W. Yang, H. Huang, D. S. Swetz, W. B. Doriese, G. C. O'Neil, J. N. Ullom, C. J. Titus, K. D. Irwin, H-K. Lee, D. Nordlund, P. Pianetta, C. Yu, J. Qiu, X. Yu, X-Q. Yang, E. Hu,* J-S. Lee,* and Y. Liu.* "Surface-to-Bulk Redox Coupling through Thermally Driven Li Redistribution in Li- and Mn-Rich Layered Cathode Materials." *Journal of the American Chemical Society* 141 (2019): 12079–12086. doi: 10.1021/jacs.9b05349, Publication Date (Web): July 9, 2019.
- Liu, S., Z. Liu, X. Shen, X. Wang, S-C. Liao, R. Yu, Z. Wang,* Z. Hu, C-T. Chen, X. Yu, X-Q. Yang, and L. Chen. "Li-Ti Cation Mixing Enhanced Structural and Performance Stability of Li-Rich Layered Oxide." *Advanced Energy Materials* 9 (2019): 1901530. doi: 10.1002/aenm.201901530, Publication Date (Web): July 15, 2019.
- Zhao, E., M. Zhang, X. Wang, E. Hu, J. Liu,* X. Yu,* M. Olguin, T. A. Wynn, Y. S. Meng,* K. Page, F. Wang, H. Li, X-Q. Yang, X. Huang, and L. Chen. "Local Structure Adaptability through Multi Cations for Oxygen Redox Accommodation in Li-Rich Layered Oxides." *Energy Storage Materials* (2019). doi: 10.1016/j.ensm.2019.07.032, Publication Date (Web): July 25, 2019.

- Deng, T., X. Fan,* L. Cao, J. Chen, S. Hou, X. Ji, L. Chen, S. Li, X. Zhou, E. Hu, D. Su, X-Q. Yang, and C. Wang.* "Designing *In-Situ*-Formed Interphases Enables Highly Reversible Cobalt-Free $LiNiO_2$ Cathode for Li-Ion and Li-Metal Batteries." *Joule* (2019). doi: 10.1016/j.joule.2019.08.004, Publication Date (Web): September 4, 2019.
- Fang, C., J. Li, M. Zhang, Y. Zhang, F. Yang, J. Z. Lee, M-H. Lee, J. Alvarado, M. A. Schroeder, Y. Yang, B. Lu, N. Williams, M. Ceja, L. Yang, M. Cai, J. Gu, K. Xu, X. Wang, and Y. S. Meng.* "Quantifying Inactive Lithium in Lithium Metal Batteries." *Nature* 572 (2019): 511–515. doi: 10.1038/s41586-019-1481-z, Publication Date (Web): August 21, 2019.
- Yang, Y., D. M. Davies, Y. Yin, O. Borodin, J. Lee, C. Fang, M. Olguin, Y. Zhang, E. S. Sablina, X. Wang, C. S. Rustomji,* and Y. S. Meng.* "High Efficiency Lithium Metal Anode Enabled by Liquefied Gas Electrolyte." *Joule* 3 (2019): 1986–2000. doi: 10.1016/j.joule.2019.06.008, Publication Date (Web): July 1, 2019.

Presentations

- Chinese Institute of Engineers (CIE) USA – Dallas Fort Worth chapter and Asian American Engineer of the Year (AAEOY) International Technology & Leadership Conference (ITLC), Dallas, Texas (August 17, 2019): "Battery Technology and Safety"; B. Liaw. Invited.
- University of Colorado, Mechanical Engineering, Boulder, Colorado (September 16, 2019): "What are the Materials Limitations to Advancing Lithium Batteries to the Next Level?"; M. S. Whittingham. Invited.
- BatteryNext, Boulder, Colorado (September 17, 2019): "Past, Present, and Future of High Energy Batteries"; M. S. Whittingham. Invited.
- Virginia Tech, Chemistry, Blacksburg, Virginia (September 20, 2019): "What are the Materials Limitations to Advancing Lithium Batteries to the Next Level?"; M. S. Whittingham. Invited.
- 5th International Conference on Energy Conversion and Storage, Beijing, China (August 15–16, 2019): "Nanomaterials Design and Interphases for Batteries"; Y. Cui. Keynote.
- International Forum on Advanced Materials 2019 (IFAM2019), Wuhan, China (September 24–26, 2019): "Nanomaterials Design for Energy and Environment"; Y. Cui. Plenary.
- 15th Asian Textile Conference (ATC-15), Hangzhou, China (September 27–29, 2019): "Fiber and Textile Materials for Energy, Environment and Electronics"; Y. Cui. Plenary.
- ACS Forum "Nanomaterials for Energy and Life Sciences," Yonsei University, Seoul, South Korea (September 30 – October 1, 2019): "Materials and Interface Design for Batteries"; Y. Cui. Invited.
- Tesla, Menlo Park, California (July 25, 2019): "High-Nickel Layered Oxide Cathodes for Lithium-Ion Batteries"; A. Manthiram. Invited.
- Institute of Chemistry, Chinese Academy of Sciences, Beijing, China (August 14, 2019): "High-Energy-Density Cathodes for Lithium-Based Batteries"; A. Manthiram. Invited.
- 2019 Lithium Battery Discussions (LiBD) Meeting, Arcachon, France (September 15–20, 2019): "High-Nickel Layered Oxide Cathodes for Lithium-Ion Batteries: Complexities and Prospects"; A. Manthiram. Invited Plenary.
- 2019 International Conference on Electrochemical Energy, Sydney, Australia (August 4–8, 2019): "Localized High-Concentration Electrolytes for Li Metal Batteries"; J-G. Zhang. Invited.
- ACS Fall National Meeting, San Diego, California (August 26, 2019): "A Monolithic SEI Layer Prevents Li Depletion and Pulverization"; J-G. Zhang. Invited.
- International Conference on Lithium-Sulfur Batteries, Beijing, China (August 12–15, 2019): "Understanding Rechargeable Lithium Sulfur Pouch Cells"; J. Liu. Invited.
- Stevens Institute of Technology (September 2019): "Clockwork Inside Cathodes – Unparalleled Insights into Defects and Inhomogeneities"; P. Khalifah. Invited.

- ACS Division of Energy & Fuels (ENFL) Conference (August 2019): "New Innovations for *Operando* Diffraction Studies of Battery Electrodes with Spatial and Temporal Resolution"; P. Khalifah. Invited.
- ACS ENFL Conference (August 2019): "Thermodynamic Relationships between Composition and Defect Concentration in NMC Cathodes Resolved Using Novel High-Precision Powder Diffraction Methods"; P. Khalifah. Invited.
- BASF Seminar, Shanghai, China (July 5, 2019): "Advanced Diagnosis and Characterization for Next Generation Energy Storage Materials"; Y. S. Meng. Invited.